

**Geology and Genesis of the
Polymetallic Ridge Zone West VHMS Deposit,
Myra Falls, Vancouver Island,
British Columbia, Canada**

by

Albert G. Chong,
P. Geo. (A.P.E.G.B.C., 1998)
B.Sc. (Major) (McMaster University, 1985)

A thesis submitted in partial fulfillment of the requirements for the degree of
Master of Science (Exploration Geoscience)



Centre for Ore Deposit Research,



University of Tasmania,

Australia

June, 2005

Statement

This thesis contains no material that has been accepted for the award of any degree or diploma at any university. To the best of the candidate's knowledge this thesis contains no copy or paraphrase of material previously written or published by another person, except where due acknowledgement is made.



Signed: Albert G. Chong

Date: June30, 2005

Authority of Access

This thesis may be made available for loan and limited copying in accordance with the

Copyright Act 1968.

ABSTRACT

The polymetallic Zn-Pb-Cu-Ba-Au-Ag-rich Ridge Zone West volcanic-hosted massive sulphide (VHMS) deposit is one of twelve known deposits in the Myra Falls property located on Vancouver Island, British Columbia, Canada. The current pre-mining geological resource estimate for the Ridge Zone West is approximately 980,000 tonnes grading 6.8% Zn, 0.8% Pb, 0.9% Cu, 2.0 g/t Au, and 72 g/t Ag. The aims of this thesis are to (1) derive a genetic model for the Ridge Zone West VHMS deposit by characterizing the geological setting and mineralization, and (2) evaluate the exploration potential of the Ridge Zone West area.

At Myra Falls, the Ridge Zone West and other VHMS deposits are located near the base of the Devonian Sicker Group, Wrangellia Terrane, of the Canadian Cordillera. The Ridge Zone West geological setting comprises from stratigraphic footwall to hangingwall: (1) the basement Price Formation basaltic andesite sequence of flows, flow breccias, and tuffaceous sediments which is conformably overlain by the Basal Conglomerate, a cobble conglomerate deposited prior to the onset of the hydrothermal system; (2) the Myra Formation H-W Horizon, a sequence of predominantly felsic, coarse to fine-grained volcano-sedimentary rocks intercalated with stacked lenses of Zn-rich mineralization; and (3) the post-mineralization Myra Formation Hangingwall Mafic flow-sill complex that is overlain or laterally equivalent to the intermediate to mafic Lower Mixed Volcaniclastic Unit consisting of graded turbidite deposits, sills, and breccias.

Rifting formed a series of restricted basins in the Myra Formation in the present Myra Falls VHMS property. A high-energy mass flow deposited the Basal Conglomerate into the basin prior to or during the early stages of the hydrothermal mineralizing event. The Ridge Zone West is located in a subordinate paleo-depression. Intermittent infill of the depression by volcanic activity is inferred from intercalated fine and coarse-grained volcano-sedimentary deposits, angular siliceous mudstone clasts, and sulphide clasts.

Following cessation of the hydrothermal system, the Hangingwall Mafic Complex (HWMC) was emplaced by intrusive and possible extrusive events excavating previously deposited, wet unconsolidated volcano-sedimentary deposits and sulphides. The Lower Mixed Volcaniclastic Unit was deposited predominantly after the HWMC.

Three post-mineralization phases of deformation are interpreted for the Ridge Zone West area and are explained in the context of the Myra Falls structural model proposed by Jones (2001). The phases are: (1) D1, a weak WNW-ESE (mine grid) striking foliation related to a Paleozoic folding event; (2) Mesozoic D3a strike-slip faults, and infrequent D3b shallow dipping striking thrust faults; and (3) Mesozoic D4 normal faults. The D4 normal faults are the most frequently occurring faults in the study area.

The footwall Price Formation and Basal Conglomerate, and hangingwall rocks in the H-W Horizon are hydrothermally altered to the same mineral assemblage sericite-quartz \pm -chlorite. Alteration intensity is weak to moderate as original textures are preserved. The footwall alteration is pervasive throughout the Basal Conglomerate, generally within the top 30 m of the Price Formation, and is observed to extend at greater depths near two faults. Hangingwall alteration of mudstones is interpreted as silicification that occur below, lateral to, and above the Zn-rich mineralization.

The Ridge Zone West VHMS deposit comprises stacked lenses of disseminated to massive mineralization associated with fine and coarse-grained volcano-sedimentary rocks. The main deposit minerals are sphalerite, pyrite, chalcopyrite, galena, tetrahedrite-tennantite, and barite. Four phases of mineralization are identified in the Ridge Zone West deposit: (1) Lower lens mineralization formed on the paleo-seafloor within fine-grained sediments during a period of quiescence and comprises disseminated and banded mineralization with pyrite framboids; (2) Main lens mineralization, the most economically significant mineralization, formed by Zn-rich fluids infiltrating and replacing permeable, dominantly coarse volcanoclastic deposits in a shallow sub-seafloor environment. Sulphide textures include anastomosing veins progressing up to massive sulphide with relic lithic clasts; (3) Upper lens mineralization deposited on the paleo-seafloor during a secondary period of quiescence and comprises sulphide bands with graded grains and soft-sediment deformation textures; and (4) Upper lens mineralization consisting of late pyrite-chalcopyrite \pm -sphalerite veins crosscutting siliceous mudstone breccias.

Based on its overall metal content, the Ridge Zone West is classified as a Zn-Pb-Cu deposit with an average Cu ratio $[100 \times \text{Cu} / (\text{Cu} + \text{Zn})]$ of 11 and an average Zn ratio $[100 \times \text{Zn} / (\text{Zn} + \text{Pb})]$ of 90. Element associations from assay data are Zn-Pb-Ag, Au-Ag \pm -Ba, and Zn-Cu. Above average Au (> 4.0 g/t) and Ag (> 150 g/t) values occur in the Lower lens and Main lens. A focused up-flow zone of hydrothermal discharge has not been identified as metal zoning patterns for Fe and the Cu ratio are broadly dispersed and unfocussed.

Exploration potential in the Ridge Zone West area includes: (1) eastward towards the Gopher lens of the Battle deposit where drill hole intersections with Zn-rich mineralization and siliceous mudstone occur; (2) below the Ridge Zone West within the footwall Basal Conglomerate; (3) north of the main study area where at least 12 drill hole intersections are up to 7.6 m in length and have Zn contents > 5%; and (4) westward for at least 200m to -250E on the mine grid, and potentially up to approximately 590 m westward to -640E where Zn-rich intersections occur in favourable host rocks similar to the Ridge Zone West.

ACKNOWLEDGEMENTS

This thesis was originally arranged by Cliff Pearson, former Chief Geologist at Myra Falls Operations, and Dr. Bruce J. Gemmell as part of a joint collaboration between Myra Falls Operations and the Centre for Ore Deposit Research (CODES). The aim was to continue improving the understanding of volcanic hosted massive sulphide deposits at Myra Falls building on the tremendous foundation established by former and current geologists. This thesis, in conjunction with two recent Ph.D. studies completed through CODES, is part of the continuing advancement of geological knowledge required for future mining and exploration at Myra Falls Operations. Ivor McWilliams and Finley Bakker, of the Myra Falls Geology department, have “unwaveringly” continued to support the completion of this project. Gratitude, appreciation, and the utmost of respect are extended to Ivor, Bruce, Cliff, and Finley. Financial support and time was provided by Myra Falls Operations. Appreciation and thanks are extended to the management at Myra Falls Operations.

Bruce Gemmell and Ron Berry are thanked for their supervision, guidance, geological expertise, critical reviews of the manuscript, and generously carving out time from their busy schedules. Briony Sinclair and Sarah Jones provided valuable insight into the numerous aspects of graduate student logistics, geological expertise, and superb dining occasions. Jocelyn McPhie, David Steele, and Ross Large are thanked for their discussions and expertise while at the University of Tasmania. Hardolph Wasteneys provided valuable editorial advice improving the final manuscript.

The Myra Falls geology department is thanked for keeping the ship running during my absences related to this project. These tremendous individuals, past and present, include Cliff Pearson, Ivor McWilliams, Finley Bakker, Rick Sawyer, Robert Baldwin, Mike Becherer, Hardolph Wasteneys, Sean McKinley, Alison Hartley, Dean Crick, and Agzim Muja.

The most important people during this whole process are my family. My wife Mia and daughter Kirsten have sacrificed countless evenings, days, and weekends without my companionship. My parents Hugh and Helen have always insisted that a strong family relationship, work ethic, and education will pave the way towards a better life. This study is dedicated to my family and the geology department at Myra Falls Operations.

Table of Contents

| | Page |
|--|-------------|
| Abstract | iii |
| Acknowledgements | vi |
| Table of Contents | vii |
| List of Figures | xiii |
| List of Tables | xvi |
| | |
| CHAPTER 1 INTRODUCTION | 1 |
| 1.1 Location | 1 |
| 1.2 Environment | 1 |
| 1.3 History | 3 |
| 1.4 Mineral Resource Estimate | 9 |
| 1.4.1 Myra Falls mineral resources | 9 |
| 1.4.2 Ore body tonnage, grade and classification | 10 |
| 1.4.3 Canadian VHMS statistics | 11 |
| 1.5 Previous Research | 12 |
| 1.6 Purpose of Thesis | 14 |
| 1.7 Methodology | 14 |
| | |
| CHAPTER 2 REGIONAL AND MYRA FALLS MINE GEOLOGY | 16 |
| 2.1 Regional Tectonics and Geology | 16 |
| 2.2 Regional Metamorphism | 19 |
| 2.3 Regional Structure | 20 |
| 2.3.1 Paleozoic Deformation (pre-accretion) | 20 |
| 2.3.2 Mesozoic Deformation (pre-accretion) | 21 |
| 2.3.3 Mesozoic Deformation (pre- to syn-collision) | 21 |
| 2.3.4 Mesozoic Deformation (syn (?) to post accretion) | 22 |
| 2.3.5 Cenozoic Deformation (post accretion) | 22 |
| 2.4 Regional Metallogeny | 23 |
| 2.5 Myra Falls Mine Geology | 24 |
| 2.5.1 Price Formation | 25 |
| 2.5.2 Myra Formation | 26 |
| 2.5.3 Thelwood Formation | 28 |
| 2.6 Geochronology | 29 |
| 2.7 Myra Falls Metamorphism | 30 |

| | | |
|------------------|---|-----------|
| 2.8 | Myra Falls Structure | 31 |
| 2.8.1 | Paleozoic Deformation (pre-accretion) | 33 |
| 2.8.2 | Mesozoic Deformation (syn (?) to post accretion) | 33 |
| 2.8.3 | Cenozoic Deformation (post accretion) | 33 |
| 2.9 | Ore Body Geometry | 34 |
| 2.10 | Ore Body Mineralogy | 37 |
| 2.10.1 | Cu-Pb-Zn-Fe rich mineral assemblage | 38 |
| 2.10.2 | Cu-rich sulphides | 39 |
| 2.10.3 | Au-Ag assemblage | 39 |
| 2.11 | Hydrothermal Alteration | 39 |
| 2.11.1 | Footwall Price Formation Alteration | 39 |
| 2.11.2 | H-W Horizon Hangingwall Alteration | 40 |
| 2.11.3 | Lynx-Myra-Price Hydrothermal Alteration | 41 |
| | | |
| CHAPTER 3 | GEOLOGY AND ALTERATION OF | |
| | THE RIDGE ZONE WEST HOST ROCKS | 42 |
| 3.1 | Introduction | 42 |
| 3.2 | Footwall Volcanic Rocks | 48 |
| 3.2.1 | Price Formation Facies | 48 |
| 3.2.2 | Basal Conglomerate Facies | 48 |
| 3.2.3 | Footwall Price Formation Andesite and Basal Conglomerate: Facies Relationships | 51 |
| 3.3 | H-W Felsic Horizon Rocks | 52 |
| 3.3.1 | Volcanic Facies | 52 |
| 3.3.2 | H-W Felsic Horizon Facies Relationships | 53 |
| 3.4 | Hangingwall Mafic Complex | 57 |
| 3.4.1 | Volcanic Facies | 57 |
| 3.4.2 | Hangingwall Mafic Complex facies relationships | 57 |
| 3.5 | Lower Mixed Volcaniclastic (LMV) | 60 |
| 3.5.1 | Volcanic Facies | 60 |
| 3.5.2 | Lower Mixed Volcaniclastic (LMV) Facies Relationships | 61 |
| 3.6 | Comparison with Myra Falls Volcanic Stratigraphy | 64 |
| 3.7 | Ridge Zone West Alteration | 65 |
| 3.7.1 | Footwall Alteration | 65 |
| 3.7.2 | H-W Horizon Alteration | 66 |
| 3.7.3 | Regional Metamorphism | 67 |
| 3.7.4 | Myra Falls Hydrothermal Alteration | 67 |
| 3.7.5 | Alteration Discussion | 70 |

| | | |
|------------------|--|------------|
| 3.8 | Geology and Alteration Summary | 71 |
| 3.8.1 | Volcanic Stratigraphy | 71 |
| 3.8.2 | General Trends | 71 |
| 3.8.3 | Geological Setting | 71 |
| 3.8.4 | Alteration Summary | 73 |
| | | |
| CHAPTER 4 | RIDGE ZONE WEST STRUCTURAL GEOLOGY | 74 |
| 4.1 | Introduction | 74 |
| 4.2 | Styles of Deformation | 75 |
| 4.2.1 | Ductile Deformation (D1-D2) | 75 |
| 4.2.2 | Brittle-Ductile Deformation (D3 to D5): Lynx 10 level map data | 80 |
| 4.2.3 | Brittle-Ductile Deformation (D3 to D5): Non-oriented drill core data | 82 |
| 4.3 | Ridge Zone West Mineralization and Major Structural Features | 85 |
| 4.4 | Comparison with the existing Myra Falls Structural Model | 87 |
| 4.5 | Summary | 91 |
| | | |
| CHAPTER 5 | RIDGE ZONE WEST MINERALIZATION | 92 |
| 5.1 | Introduction | 92 |
| 5.2 | Ridge Zone West mineralization and stratigraphy relationships | 92 |
| 5.3 | Geometry and resource estimates | 93 |
| 5.3.1 | Geometry and resource estimate methods | 93 |
| 5.3.2 | Mineralization geometry | 93 |
| 5.3.3 | Ridge Zone West Geological Inventory and Mining Reserve Estimates | 95 |
| 5.4 | Styles of mineralization and H-W Horizon volcanic facies | 96 |
| 5.4.1 | Mineralization associated with fine-grained volcanic facies | 96 |
| 5.4.2 | Mineralization associated with coarse-grained volcanic facies | 97 |
| 5.4.3 | Discussion on styles of mineralization and volcanic facies | 103 |
| 5.4.4 | Summary on styles of mineralization and volcanic facies | 105 |
| 5.5 | Ore microscopy and mineral chemistry | 106 |
| 5.5.1 | Ore microscopy and analytical methods | 106 |
| 5.5.2 | Pyrite textures | 113 |
| 5.5.3 | Pyrite chemistry | 113 |
| 5.5.4 | Sphalerite textures | 115 |
| 5.5.5 | Sphalerite chemistry | 116 |
| 5.5.6 | Chalcopyrite textures | 118 |
| 5.5.7 | Chalcopyrite chemistry | 118 |

| | | |
|------------------|---|------------|
| 5.5.8 | Galena textures | 120 |
| 5.5.9 | Galena chemistry | 120 |
| 5.5.10 | Tetrahedrite-tennantite textures | 122 |
| 5.5.11 | Tetrahedrite-tennantite chemistry | 122 |
| 5.6 | Gangue mineral microscopy and chemistry | 123 |
| 5.6.1 | Quartz textures | 123 |
| 5.6.2 | Barite textures | 124 |
| 5.6.3 | Barite chemistry | 124 |
| 5.6.4 | Muscovite textures | 125 |
| 5.6.5 | Muscovite chemistry | 125 |
| 5.6.6 | Calcite textures | 126 |
| 5.7 | Textures in metamorphosed orebodies | 126 |
| 5.8 | Chalcopyrite disease and metal zone refinement processes | 128 |
| 5.9 | Sulphide paragenesis | 129 |
| 5.10 | Comparison to other mineralogical studies at Myra Falls | 131 |
| 5.11 | Metallurgical aspects relative to ore mineralogy | 134 |
| 5.12 | Summary | 136 |
| | | |
| CHAPTER 6 | RIDGE ZONE WEST METAL ZONING | 138 |
| 6.1 | Introduction | 138 |
| 6.2 | Methods | 138 |
| 6.3 | Ridge Zone West block model metal zoning | 140 |
| 6.3.1 | Block model base metal zoning | 140 |
| 6.3.2 | Block model precious metal and sulphate zoning | 146 |
| 6.4 | Assay data metal associations | 150 |
| 6.4.1 | Assay data statistics | 150 |
| 6.4.2 | Zinc assays | 150 |
| 6.4.3 | Lead assays | 152 |
| 6.4.4 | Copper assays | 153 |
| 6.4.5 | Gold assays | 154 |
| 6.4.6 | Silver assays | 156 |
| 6.5 | Element association discussion | 158 |
| 6.5.1 | Assay data | 158 |
| 6.5.2 | Spatial distribution | 160 |
| 6.6 | Gold association | 163 |
| 6.7 | Metal ratios | 165 |
| 6.7.1 | Ridge Zone West Cu ratios | 166 |
| 6.7.2 | Ridge Zone West Zn ratios | 166 |

| | | |
|--|--|------------|
| 6.7.3 | Ridge Zone West metal ratio discussion | 169 |
| 6.8 | Property scale metal zoning | 170 |
| 6.9 | Comparison to other Myra Falls deposits | 171 |
| 6.10 | Summary and conclusions | 176 |
| CHAPTER 7 GENESIS OF THE RIDGE ZONE WEST VHMS DEPOSIT | | 177 |
| 7.1 | Introduction | 177 |
| 7.2 | Structure and synvolcanic faults | 177 |
| 7.3 | Sub-seafloor replacement | 178 |
| 7.4 | Ridge Zone West Genetic Model | 179 |
| 7.4.1 | Stage 1 (pre-mineralization basin development) | 179 |
| 7.4.2 | Stage 2 (syn-mineralization) | 181 |
| 7.4.3 | Stage 3 (post-mineralization) | 185 |
| 7.5 | Comparison to other VHMS deposits | 186 |
| 7.5.1 | Comparison to other Myra Falls deposits | 186 |
| 7.5.2 | Canadian Cordillera comparison – Tulsequah Chief | 188 |
| 7.5.3 | Modern analogue – Lau basin (Vai Lili) | 189 |
| 7.5.4 | Cambrian comparison - Que River: Gold enriched footwall stringer mineralization compared to the Ridge Zone West Basal Conglomerate | 190 |
| 7.6 | Summary of VHMS deposits for the H-W Horizon at Myra Falls | 192 |
| CHAPTER 8 SUMMARY AND RECOMMENDATIONS | | 193 |
| 8.1 | Introduction | 193 |
| 8.2 | Summary | 193 |
| 8.2.1 | Geological Setting | 193 |
| 8.2.2 | Hydrothermal Alteration | 193 |
| 8.2.3 | Structural geology | 194 |
| 8.2.4 | Mineralization | 195 |
| 8.2.5 | Metal Zoning | 196 |
| 8.2.6 | Main lens evidence for sub-seafloor replacement | 196 |
| 8.2.7 | Ridge Zone West Genetic Model | 197 |
| 8.3 | Recommendations | 198 |
| 8.3.1 | Exploration Applications | 198 |
| 8.3.2 | Ore Reserves | 199 |
| 8.3.3 | Mining Applications | 203 |
| 8.3.4 | Metallurgical Applications | 204 |
| 8.4 | Concluding Remarks | 204 |

| | |
|--|------------|
| REFERENCES | 205 |
| APPENDICES | 211 |
| Appendix 1: Drill log catalogue and selected logs | 211 |
| Appendix 2: Legend and Sample Catalogue | 224 |
| Appendix 3: Electron microprobe analytical conditions and detection limits | 232 |
| Appendix 4: Assay data conditions, block model parameters, and results | 234 |

List of Figures

| | | Page |
|------------------|---|------|
| Chapter 1 | Introduction | |
| Figure 1.1 | Myra Falls Operations location map | 1 |
| Figure 1.2 | Scenery photos of the Campbell River-Buttle Lake-Myra Falls area | 2 |
| Figure 1.3 | Location of VHMS deposits at Myra Falls Operations | 4 |
| Figure 1.4 | Geological research distribution plan | 12 |
| Chapter 2 | Regional and Myra Falls Mine Geology | |
| Figure 2.1 | Morphological belts of the Canadian Cordillera | 16 |
| Figure 2.2 | Sicker Group location map – Vancouver Island and simplified Vancouver Island stratigraphy | 18 |
| Figure 2.3 | Sicker Group stratigraphy at Myra Falls | 24 |
| Figure 2.4 | Myra Falls composite geology section | 25 |
| Figure 2.5 | Location of major faults and VHMS deposits | 31 |
| Figure 2.6 | Myra Falls deformation history and regional correlation | 32 |
| Figure 2.7 | Battle deposit – geology section 1390 E | 36 |
| Figure 2.8 | H-W deposit – geology section 3505 E | 36 |
| Chapter 3 | Geology and Alteration of the Ridge Zone West Host Rocks | |
| Figure 3.1 | Ridge Zone West geology Longitudinal section 4150 N | 43 |
| Figure 3.2 | A- Ridge Zone West geology - section -050 E B- Ridge Zone West geology – section 050 E | 44 |
| Figure 3.2 | C- Ridge Zone West geology – section 175 E D- Ridge Zone West geology – section 375 E | 45 |
| Figure 3.3 | Price Formation Andesite volcanic facies | 49 |
| Figure 3.4 | Basal Conglomerate volcanic facies | 50 |
| Figure 3.5 | H-W Rhyolite volcanic facies | 55 |
| Figure 3.6 | H-W Rhyolite volcanic facies | 56 |
| Figure 3.7 | Hangingwall Mafic Complex volcanic facies | 59 |
| Figure 3.8 | Lower Mixed Volcaniclastic Unit volcanic facies | 63 |

| | | |
|------------------|---|-----|
| Chapter 4 | Ridge Zone West Structural Geology | |
| Figure 4.1 | Structural map – Lynx 10 level | 77 |
| Figure 4.2 | S1 foliation planes – equal area pole plot | 78 |
| Figure 4.3 | S1 and S2 foliation pattern at Myra Falls | 79 |
| Figure 4.4 | Ridge Zone West geology and structure – 2990 m plan | 86 |
| Figure 4.5 | Location of major faults and VHMS deposits at Myra Falls | 89 |
| Figure 4.6 | Ridge Zone West-Myra Falls deformation history and regional correlation | 90 |
| Chapter 5 | Ridge Zone West Mineralization | |
| Figure 5.1 | Ridge Zone West mineralization - composite section | 94 |
| Figure 5.2 | Mineralization associated with fine-grained volcanic facies | 98 |
| Figure 5.3 | Mineralization associated with siliceous fine-grained volcanic facies | 99 |
| Figure 5.4 | Mineralization associated with coarse-grained volcanic facies – 1 | 100 |
| Figure 5.5 | Mineralization associated with coarse grained volcanic facies – 2 | 101 |
| Figure 5.6 | Hangingwall Mafic Complex “ore” clast breccia | 102 |
| Figure 5.7 | Pyrite facies – Lower lens mineralization in argillaceous mudstone | 107 |
| Figure 5.8 | Upper lens mineralization in mudstone | 108 |
| Figure 5.9 | Main lens mineralization in coarse-grained volcanic rocks | 109 |
| Figure 5.10 | Main lens mineralization in coarse-grained volcanic rocks – 2 | 110 |
| Figure 5.11 | Main lens mineralization in coarse-grained volcanic rocks – 3 | 111 |
| Figure 5.12 | Main lens mineralization barite-rich veining | 112 |
| Figure 5.13 | Ridge Zone West ore mineral paragenesis | 130 |
| Chapter 6 | Ridge Zone West Metal Zoning | |
| Figure 6.1 | Fe zoning | 142 |
| Figure 6.2 | Cu zoning | 143 |
| Figure 6.3 | Zn zoning | 144 |
| Figure 6.4 | Pb zoning | 145 |
| Figure 6.5 | Au zoning | 147 |
| Figure 6.6 | Ag zoning | 148 |
| Figure 6.7 | Ba zoning | 149 |

| | | |
|------------------|--|-----|
| Figure 6.8 | Zn histogram and element associations | 151 |
| Figure 6.9 | Pb histogram and element associations | 152 |
| Figure 6.10 | Cu histogram and element associations | 153 |
| Figure 6.11 | Au histogram | 154 |
| Figure 6.12 | Au associations | 155 |
| Figure 6.13 | Ag histogram and associations | 157 |
| Figure 6.14 | Lower lens mineralization metal associations | 160 |
| Figure 6.15 | Main lens mineralization metal associations | 162 |
| Figure 6.16 | Upper lens mineralization metal associations | 162 |
| Figure 6.17 | Ridge Zone West Cu ratio | 167 |
| Figure 6.18 | Ridge Zone West Zn ratio | 168 |
| Figure 6.19 | Myra Falls Cu ratio | 171 |
| Figure 6.20 | Myra Falls Zn ratio | 172 |
| Figure 6.21 | H-W geology – 3505E | 173 |
| Figure 6.22 | Battle-Gap geology – 1390E | 174 |
| Chapter 7 | Genesis of the Ridge Zone West VHMS Deposit | |
| Figure 7.1 | Genetic model stage 1: pre-mineralization | 180 |
| Figure 7.2 | A-Genetic model stage 2: Phase 1 Lower lens mineralization | 184 |
| | B- Genetic model stage 2: Phase 2 Main lens mineralization | 184 |
| | C- Genetic model stage 2: Phase 3 and 4 Upper lens mineralization | 185 |
| Figure 7.3 | Genetic model stage 3: post-mineralization | 186 |
| Chapter 8 | Summary and Recommendations | |
| Figure 8.1 | Ridge Zone West – exploration potential | 200 |

List of Tables

| | | Page |
|------------------|--|------|
| Chapter 1 | Introduction | |
| Table 1.1 | Myra Falls Operations: Exploration-Development -Mining Cycles | 5 |
| Table 1.2 | 2002 Myra Falls Operations Pre-mining Geological Resource Estimate | 9 |
| Chapter 2 | Regional and Myra Falls Mine Geology | |
| Table 2.1 | Myra Falls District: Metamorphic Mineral Assemblages | 30 |
| Table 2.2 | Myra Falls District: Deformation History | 31 |
| Table 2.3 | Myra Falls Ore Body Mineralogy | 37 |
| Chapter 3 | Geology and Alteration of the Ridge Zone West Host Rocks | |
| Table 3.1 | Descriptive names for volcanoclastic deposits | 46 |
| Table 3.2 | Grain size-based genetic nomenclature for common types of volcanoclastic deposits | 47 |
| Chapter 4 | Ridge Zone West Structural Geology | |
| Table 4.1 | Ridge Zone West structural data from non-oriented drill core | 83 |
| Chapter 5 | Ridge Zone West Mineralization | |
| Table 5.1 | Ridge Zone West selected sulphide intersections | 95 |
| Table 5.2 | Ridge Zone West geological inventory and mining reserve estimates | 95 |
| Table 5.3 | Microprobe analyses for pyrite-1 and pyrite-2 | 114 |
| Table 5.4 | Microprobe analyses for pyrite-3 | 114 |
| Table 5.5 | Microprobe analyses for sphalerite | 117 |
| Table 5.6 | Microprobe analyses for chalcopyrite | 119 |
| Table 5.7 | Microprobe analyses for galena | 121 |
| Table 5.8 | Microprobe analyses for tennantite | 123 |
| Table 5.9 | Microprobe analyses for barite | 124 |
| Table 5.10 | Microprobe analyses for muscovite | 125 |
| Table 5.11 | Ridge Zone West and Myra Falls ore body mineralogy | 133 |

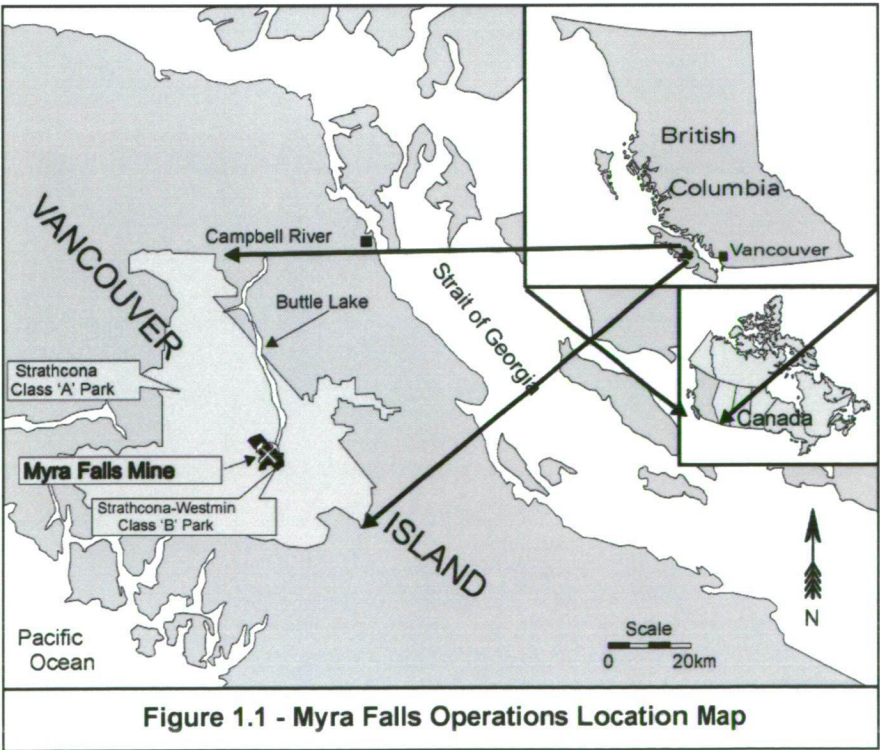
| | | |
|------------------|---|-----|
| Chapter 6 | Ridge Zone West Metal Zoning | |
| Table 6.1 | Zinc ratio of saturated solution at varying temperatures and salinities | 165 |
| Table 6.2 | Myra Falls pre-mining mineral resource estimate | 170 |
| Chapter 7 | Genesis of the Ridge Zone West VHMS Deposit | |
| Table 7.1 | Styles of VHMS deposits compared to H-W Horizon deposits | 192 |
| Chapter 8 | Summary and Recommendations | |
| Table 8.1 | Summary of averaged microprobe analyses for ore minerals | 195 |
| Table 8.2 | Summary of the Ridge Zone West genetic model | 197 |
| Table 8.3 | Selected Ridge Zone West exploration targets | 201 |
| Table 8.4 | Ridge Zone West rock quality comparison | 203 |

1.1 Location

The Ridge Zone West volcanic hosted massive sulphide (VHMS) deposit is part of the Myra Falls property, Vancouver Island, British Columbia, Canada. The property is situated within Strathcona Provincial Park at the southern tip of Buttle Lake (Fig. 1.1 and 1.2). Access is via paved highway 90 km southwest of the town Campbell River. The operation is currently owned by NVI Mining Limited, a subsidiary of Breakwater Resources Limited. The claim block measures 3,328 hectares and has dimensions of approximately 7 km long by 2 to 3 km wide on a NW to SE axis. The claim block is designated Strathcona-Westmin, Class-B Provincial Park. This special Class-B designation allows for exploration, and mining within the larger, Strathcona, Class-A Provincial Park of British Columbia and is definitely a unique working relationship between the public, free enterprise, and the government.

1.2 Environment

Terrain is mountainous having over 1,200 m of vertical relief. The steep slopes are heavily wooded with fir, hemlock, and cedar. Precipitation is typically over 250 cm per year, and may include up to 5 m of snow in winter. Temperature ranges from 32°C in summer to -18°C in winter.



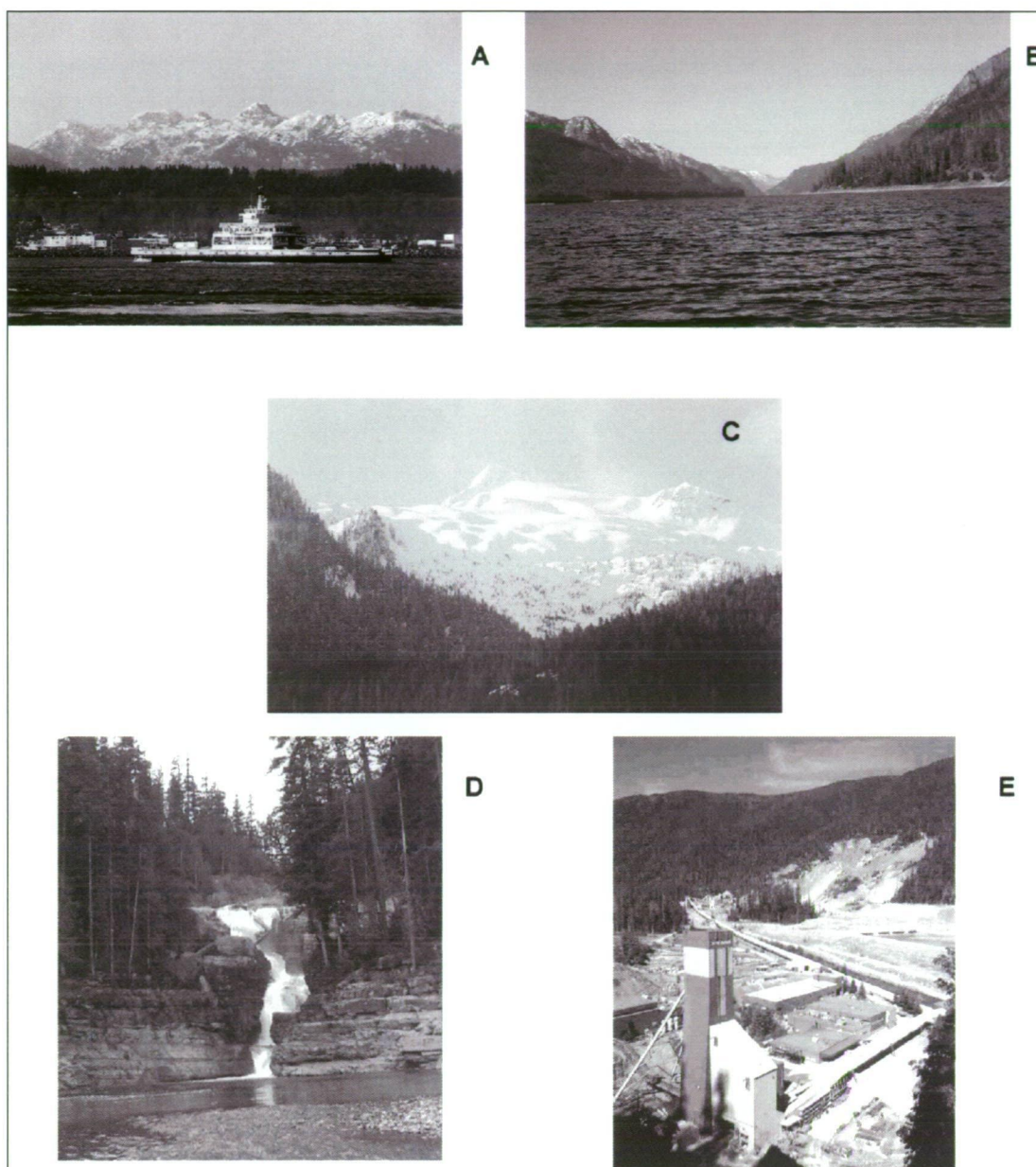


Figure 1.2: Scenery Photos of the Campbell River - Buttle Lake - Myra Falls area on Vancouver Island, British Columbia Canada

- A- The ocean-side town of Campbell River with the Vancouver Island mountain range in the background (view west).
- B- Buttle Lake bounded by the Vancouver Island mountain range (view south).
- C- Snow covered Mount Myra (1,800m elevation) at the SE end of the Myra Falls property (view SE).
- D- Myra Falls is the terminus for Myra Creek at the south end of Buttle Lake (view west).
- E- Myra Falls Operations; H-W headframe (foreground) and the concentrator are connected by a 1.4 km conveyor belt. Mining in the Lynx open pit (background) began in 1966. The H-W deposit was discovered in 1979 with mining commencing in 1985 (view WNW).

1.3 History

The Myra Falls Operations claim block has seen a constant progression of prospecting and exploration activity since 1917 as well as active mining for over three decades since 1966. Mining for the past three decades of the numerous Zn-Pb-Cu-Au-Ag rich VHMS deposits has processed 22 M tonnes of ore from four separate past and current producing mines.

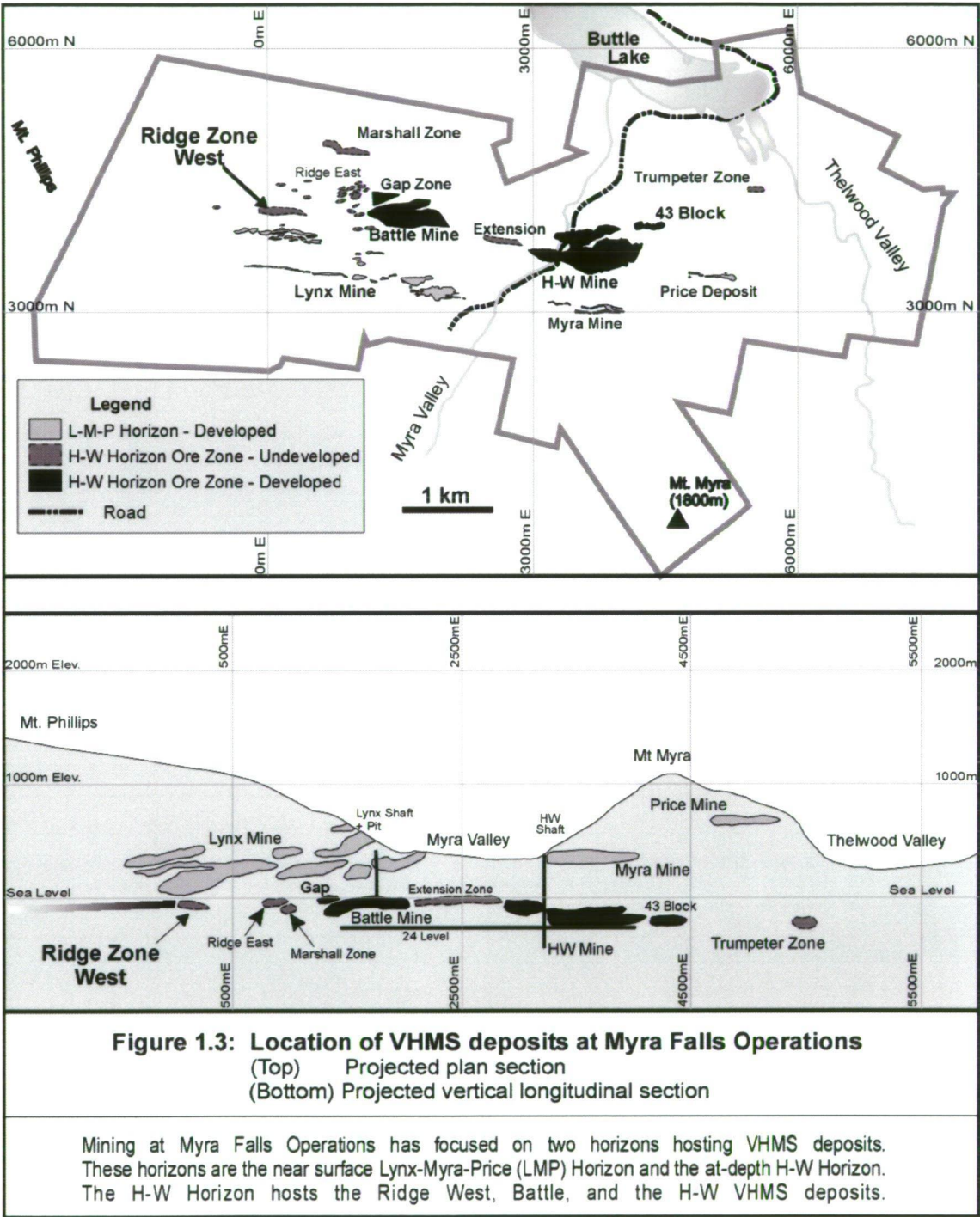
Current mine site exploration and mining activity within the Myra Falls Operations claim block has focused on two mineralized horizons, the near surface Lynx-Myra-Price (LMP) horizon and the at depth H-W horizon located 400 m below the Myra valley floor (Fig. 1.3). Although only a minor mineralized area on the property, the Ridge Zone West is currently receiving attention as a possible mining area to replace depleting resources within the mineral inventory.

The Early Days: The first documented exploration and mineral prospecting in central Vancouver Island began in 1865 with the John Buttle expedition. The expedition ventured from the west coast fishing village of Tofino, up Bedwell Sound and Bedwell River valley into what is now the southern margin of Strathcona Park. This was the first recorded sighting of what is now Buttle Lake. In 1910, the Price Ellison Expedition ventured into the Buttle Lake area. Ellison's recommendation to the provincial legislature led to the Strathcona Park Act in 1911, protecting the first and oldest provincial park in British Columbia.

Mineral prospecting and staking was opened up shortly afterwards and the first claims were staked in 1917. Claims staked by James Cross and Associates of Victoria and Paramount Mining Company of Toronto during 1917 cover the surface expressions of the Lynx, Myra, and Price deposits. Preliminary work between 1919 and 1925 was inconclusive. The Geological Survey of Canada undertook a regional study of the mineral potential around the Buttle Lake area during 1930. Gunning (1931) reported that following thorough testing, there existed the possibility of developing a large tonnage of ore with milling grade. A number of private examinations occurred on all the showings during the 1940's and 1950's, but active mineral exploration and development remained essentially dormant for the next three decades (Jeffrey, 1970).

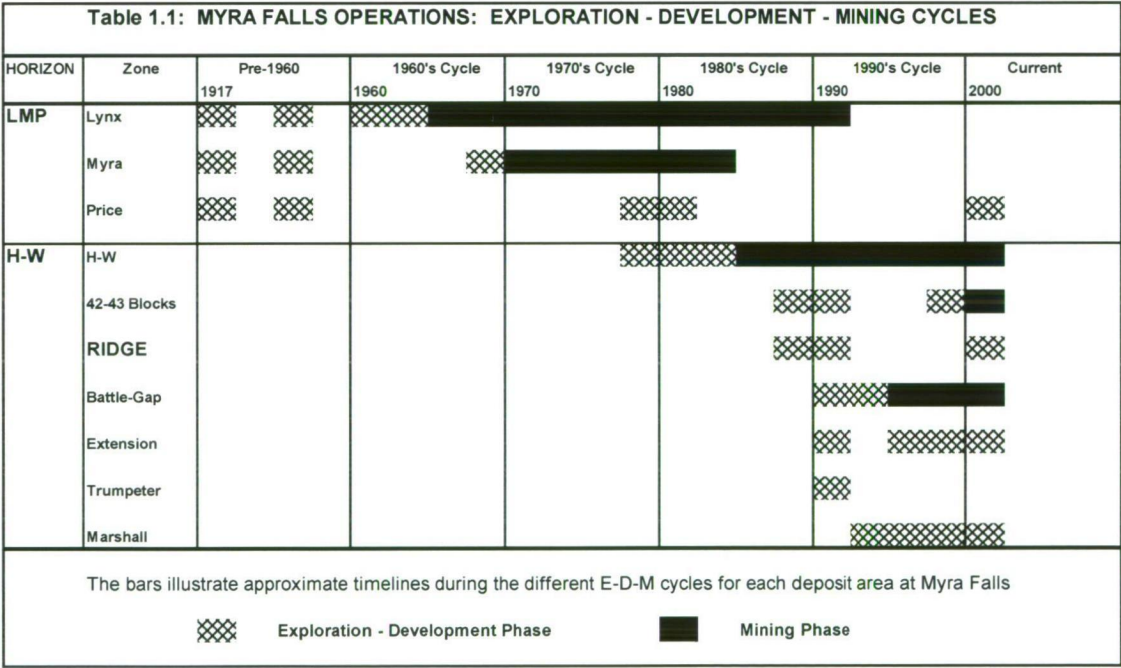
Interest in the property was revived in 1959 during the post World War II economic boom when the claims were acquired and consolidated by the Reynolds Syndicate. The new consolidated claim group was subsequently sold to Western Mines Limited of Calgary in

1961. Exploration and ore definition drill programs focused on the Lynx showings in Myra valley outlining an initial mining reserve of 1.9 M tonnes. Mining started in the Lynx open pit in 1966 and followed by underground mining.



The Exploration, Development and Mining Cycles: Since the opening of the Lynx mine in 1966, there have been four subsequent phases of exploration, development and mining (E-D-M) from four past and current producing mines. Each cycle has taken about a decade to run its course, with some minor overlap. Initiation of each cycle commenced with the need to discover new resources, as existing resources were being depleted. Much of the detailed historical information between 1966 and 1993 has been described by Pearson (1993). The following text has taken the information by Pearson (1993) and summarized it in the context of the E-D-M cycle perspective. Pre-mining mineral resource values summarized in this paper are from Bakker (2002).

The E-D-M cycles are illustrated in Table 1.1. As this is a study in exploration geoscience, some elaboration on the exploration-development-mining history deserves attention.



The 1960's

Near surface Exploration-Development-Mining (E-D-M) Cycle

(Lynx mine commissioning)

Exploration programs emphasized the near surface Lynx showings (Fig. 1.3). Development and mining began on the Lynx open pit in 1966 at a rate of 600 to 900 tonnes per day. Underground mining followed shortly thereafter, with an original mining reserve estimate of 1.9 M tonnes. Boat access to the property was upgraded with the building of a road along the east shoreline of Buttle Lake. The road connected the mine site to the town of Campbell River. Surface infrastructure facilities were constructed with much of the raw material being logged, milled, or excavated on site.

The 1970's

L-M-P Horizon E-D-M and at-depth Exploration

(Myra Deposit commissioning and H-W Horizon Discovery)

Exploration, development, and mining continued on the near surface L-M-P Horizon showings and deposits. The Lynx mine continued to operate and production began at the Myra mine during 1972 at a rate of 200 to 400 tonnes per day. Total production from the Myra mine was 1.0 M tonnes at 3.0 g/t Au, 160 g/t Ag, 1.0% Cu, 1.5% Pb, and 9.5% Zn.

In 1976, Brascan Ltd. acquired control of Western Mines Limited and formed Westmin Resources Ltd. Recognizing a decline in the mineral inventory, an aggressive exploration program was launched. The exploration program utilized recent developments in the understanding of volcanic hosted massive sulphide (VHMS) deposits from the Canadian Shield. One key development from work on Canadian Shield VHMS deposits was the understanding that deposits are hosted in relatively thick, multi-cyclic volcanic piles, and sulphide mineralization is found in the second or higher cycle, at or near the base of the host cycle (Franklin and Thorpe, 1982). The base of the host Myra Formation for the L-M-P deposits was not defined at the time. Following assessment of the property for its volcanic stratigraphy, structural deformation, style of mineralization and hydrothermal alteration, a decision to drill the north limb of the Myra anticline below the L-M-P Horizon was made. This decision was rewarded by discovery of the large tonnage H-W deposit 400 m (Fig. 1.3) below the Myra valley floor in December 1979.

The 1980's

L-M-P Horizon and H-W Horizon E-D-M

(Along strike discoveries; Commissioning of the H-W Mine)

H-W deposit delineation, development, and production were the focus in the 1980's, concurrent with exploration of both the Lynx-Myra-Price Horizon and the newly discovered H-W Horizon. Accelerated diamond drilling on the H-W deposit resulted in a positive production decision and the H-W mine was commissioned in 1985. Continued exploration led to the discovery of along strike equivalents of both mineralized horizons. On the L-M-P Horizon's Lynx deposit, discoveries were made westward in the West-G Zone and in the southerly down-dip direction for the S-Zone lenses. On the new H-W Horizon, discoveries were made immediately northeast of the H-W deposit on the 43 Block lenses (Fig. 1.3).

Approximately 3 km west of the H-W deposit, crosscuts spaced 150 m apart were driven north of the existing Lynx mine workings during 1988. These crosscuts provided diamond drill platforms to explore the newly interpreted H-W Horizon trend. Exploration diamond drill programs in 1989 and 1990, cored over fifty ore grade mineralized intersections on what is now known as the Ridge Zone West and Ridge Zone East areas (Fig. 1.3). These intersections range from 0.2-22.5 m in thickness. A preliminary mineral resource estimate of 668,000 tonnes was outlined in both the Ridge East and Ridge West Zones.

The 1990's

Continued L-M-P Horizon and H-W Horizon E-D-M

(Discovery and commissioning of the Battle-Gap deposits)

Following confirmation of strike length continuity of the H-W Horizon westward for at least 3 km and availability of new diamond drill platforms, an exploration program was launched to target the H-W Horizon between the Ridge Zones and the main H-W deposit (Fig. 1.3). In 1991, this program intersected 33.1 m of ore grade massive sulphide mineralization in the Gap lens. Subsequent discoveries of this exploration program were the Battle and the Extension deposits. Other peripheral discoveries on the H-W horizon during this time frame included the Trumpeter Zone, located approximately 1 km east of the H-W deposit. In 1995, the Marshall Zone was discovered approximately 1 km northwest of the Battle deposit lenses.

A positive production decision was subsequently made for the Battle and Gap deposits; production began in 1995. Underground production from the Lynx mine was terminated in 1993 due to poor economics, however limited access is still available for

ventilation and exploration purposes. Ownership of the property changed hands during 1998, when Boliden Limited acquired Westmin Resources Limited to form Boliden-Westmin Limited, Canada.

The Current E-D-M Cycle

(2000 to present):

Recent exploration efforts have been directed towards upgrading indicated and inferred resources of the Ridge Zone West and Marshall Zones, located 1 km west and northwest of the current infrastructure. The Price deposit, located to the east in Thelwood valley, has also been revisited. Diamond drilling for new undiscovered VHMS deposits has yet to be successful during the current E-D-M cycle. Based on financial constraints, an interim decision has curtailed development of strategically positioned underground diamond drill platforms for targets on the western and northern portions of the property. Development of diamond drill platforms is essential as the western half of the property lies under the 1,520 m high Phillips Ridge.

Definition diamond drilling is currently delineating the Extension Zone and 43 Block (Fig. 1.3). The Extension Zone is located between the H-W and Battle Zone deposits and extends over a 1 km strike length. Current pre-mining mineral resource estimate is 1.1 M tonnes. 43 Block definition diamond drilling is nearing completion; mining of initial stoping blocks on this structurally deformed lens commenced in 2001. Near surface resources of the high-grade Lynx deposit S-Zone of the L-M-P Horizon have also been outlined.

Active mining at Myra Falls Operations is currently based out of the H-W head frame and the majority of the mining activity comes from the H-W, 43 Block, and Battle-Gap deposits. Minor supplemental ore is being extracted from the Lynx open pit. Current production rates are 1.2 M tonnes annually at rates ranging between 2,800 and 3,400 tonnes per day.

During 2004, Myra Falls Operations was sold by Boliden Limited to Breakwater Resources Limited. The Myra Falls Operations are now currently owned and operated by NVI Mining Limited, a subsidiary of Breakwater Resources Limited.

1.4 Mineral Resource Estimate

1.4.1 Myra Falls Mineral Resources

Mining at Myra Falls began in 1966 with an initial mining reserve of 1.9 M tonnes at the near surface Lynx deposit. Since that time, the Myra Falls VHMS property has reached an overall pre-mining mineral resource of greater than 40 M tonnes grading 2.1 g/t Au, 49 g/t Ag, 1.8% Cu, 0.5% Pb, and 6.1% Zn (Table 1.2). To date, approximately 23 M tonnes have been mined and milled at the Myra Falls property since the beginning of production.

The Ridge Zone West accounts for approximately 983,000 tonnes of the pre-mining geological resource. The current mining reserve estimate for the Ridge Zone West is 178,000 tonnes grading 2.0 g/t Au, 65 g/t Ag, 0.9% Cu, 0.8% Pb, and 7.6% Zn.

| Table 1.2: 2004 MFO Pre-mining Geological Resource Estimate Grouped by Horizon | | | | | | | | | | |
|--|------------|----------------------|--------|--------|------|------|------|-----------------------------------|----------------------|----------------------------------|
| (modified after Bakker, 2002; Chong 2003) | | | | | | | | | | |
| Deposit | Tonnes | Average Deposit Size | Au g/t | Ag g/t | Cu % | Pb % | Zn % | Zn Ratio (1) | Cu Ratio (2) | Metal Content Classification (3) |
| lynx-mine | 5,809,000 | | 2.5 | 90 | 1.6 | 1.0 | 7.5 | 88 | 18 | Zn-Pb-Cu |
| myra | 1,037,000 | | 3.0 | 160 | 1.0 | 1.5 | 9.5 | 86 | 10 | Zn-Pb-Cu |
| price | 381,000 | | 2.1 | 73 | 1.4 | 1.3 | 9.2 | 88 | 13 | Zn-Pb-Cu |
| LMP Horizon | 7,227,000 | 2,409,000 | 2.6 | 99 | 1.5 | 1.1 | 7.9 | 88 | 16 | Zn-Pb-Cu |
| hw-mine | 22,137,000 | | 2.2 | 27 | 2.0 | 0.3 | 3.7 | 93 | 35 | Zn-Cu |
| 43-block | 971,000 | | 2.6 | 53 | 1.7 | 0.5 | 5.8 | 92 | 23 | Zn-Cu |
| trumpeter | 211,000 | | 2.4 | 58 | 3.4 | 0.3 | 3.9 | 93 | 47 | Zn-Cu |
| extension | 1,156,000 | | 1.0 | 29 | 1.4 | 0.3 | 4.5 | 94 | 24 | Zn-Cu |
| battle | 5,965,000 | | 1.4 | 53 | 1.8 | 0.7 | 12.5 | 95 | 13 | Zn-Cu |
| gap | 778,000 | | 2.0 | 121 | 2.0 | 1.0 | 13.8 | 93 | 13 | Zn-Cu |
| ridge-east | 326,000 | | 0.8 | 41 | 0.7 | 0.8 | 4.7 | 86 | 13 | Zn-Pb-Cu |
| Ridge-West | 983,000 | | 2.0 | 72 | 0.9 | 0.8 | 6.8 | 90 | 11 | Zn-Pb-Cu |
| marshall | 1,210,000 | | 1.6 | 80 | 0.5 | 0.6 | 5.3 | 89 | 9 | Zn-Pb-Cu |
| H-W Horizon | 33,737,000 | 3,749,000 | 2.0 | 38 | 1.8 | 0.4 | 5.7 | 93 | 24 | Zn-Cu |
| MFO TOTAL | 40,964,000 | 3,414,000 | 2.1 | 49 | 1.8 | 0.5 | 6.1 | 92 | 23 | Zn-Cu |
| | | | | | | | | (1) | Zn Ratio | |
| January - 2004 Diluted Mining Reserve (from Chong and Bakker, 2004) | | | | | | | | (2) | Cu Ratio | |
| MFO TOTAL | 7,747,000 | | 1.2 | 40 | 1.2 | 0.5 | 6.3 | (3) | After Solomon (1976) | |
| Ridge-West | 178,000 | | 2.0 | 65 | 0.9 | 0.8 | 7.6 | Tonnages rounded to nearest 1,000 | | |

Of significance is an increase in the geological resource estimate for the Ridge Zone West of approximately 600,000 tonnes from the original 1990 resource estimate. The change is due to a renewed exploration diamond drill program during January 2000 – 2002, this time resulting in an improved geological understanding of the area, updating of the geological interpretations, and generation of a new computerized model and mineral resource estimate based on the new interpretations. This study has contributed towards the geological understanding, interpretation, and modeling aspects of the mineral resource estimation effort.

1.4.2 Ore Body Tonnage, Grade and Classification

The Myra Falls VHMS property has 12 known deposit areas. Each deposit area represents a cluster of individual lenses. Six of the twelve known deposits have tonnages greater than 1.0 M tonnes (Table 1.2). The overall average deposit size for the Myra Falls VHMS district is 3.4 M tonnes with grades of 2.1 g/t Au, 49 g/t Ag, 1.8% Cu, 0.5% Pb, and 6.1% Zn. Deposits within the mineral resource range from 211,000 tonnes for the relatively undefined Cu-rich Trumpeter Zone to 22.1 M tonnes for the pyrite rich polymetallic H-W deposit.

The near surface L-M-P Horizon has a pre-mining 7.2 M tonne mineral resource with an average deposit size of 2.4 M tonnes. Based on their Zn and Cu ratios, the L-M-P deposits would fall under the Solomon (1976) metal content classification as Zn-Pb-Cu deposits (Table 1.2). There are an estimated 120 individual lenses within the Lynx deposit along a 2,750 m strike length. The mineralization occurs as a folded and faulted array of individual lenses varying in size from 10,000 to 150,000 tonnes. Lens dimensions range from 3 to 6 m thick, 30-60 m dip length and 90 to 120 m strike length (Becherer, 1992).

The at-depth H-W Horizon has a current pre-mining mineral resource of 33.7 M tonnes with an average deposit size of 3.7 M tonnes (Table 1.2). H-W Horizon deposits are mostly classified as Zn-Cu type (Solomon, 1976) including the H-W deposit and its adjacent lenses. Interestingly, the Battle and Gap deposits also fall within the Zn-Cu group in spite of their high Pb and Zn values relative to other deposits on the property.

Zinc-Pb-Cu deposit types in the H-W Horizon are the Ridge Zone West, Ridge Zone East, and Marshall Zones. These deposits are located approximately 1 km west of the current infrastructure (Fig. 1.3). One possible explanation for the metal content of these deposits is that these deposits may represent distal mineralization peripheral to the main hydrothermal system (Gemmell, 1998). Only wide-spaced exploration style diamond drill programs have been carried out on these deposits. Hence, the potential for discovering other Zn-Cu deposit types west of the Battle deposit still exists.

1.4.3 Canadian VHMS Statistics

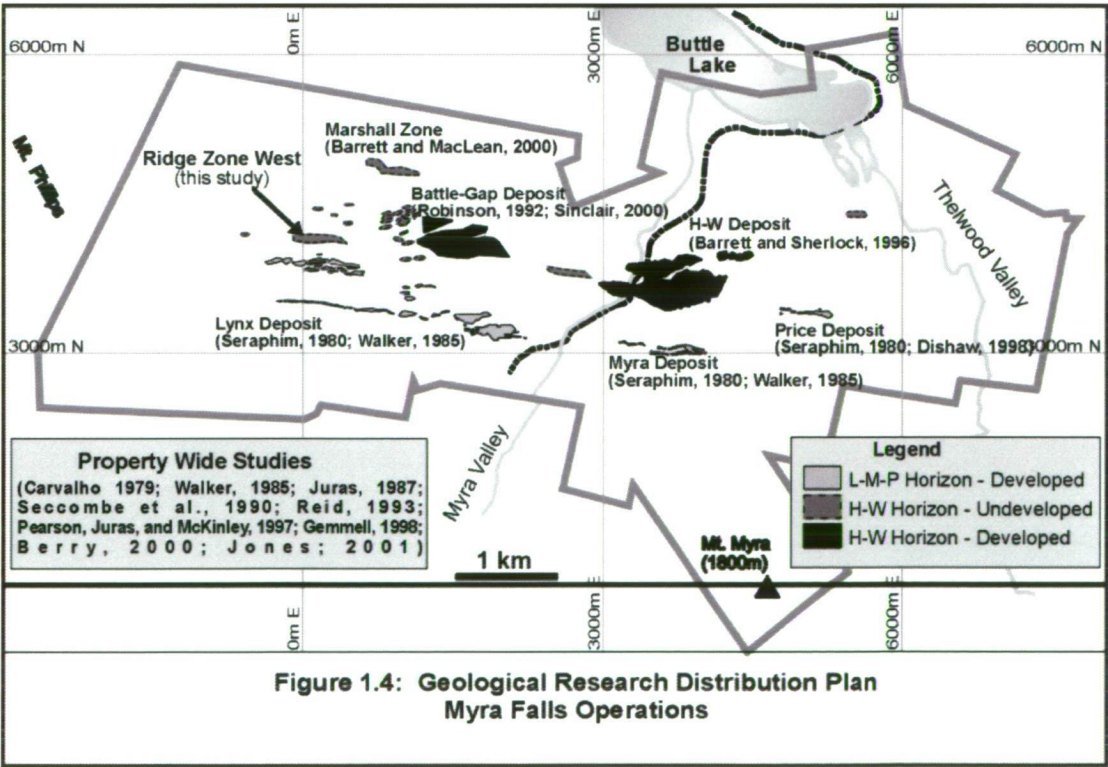
Numerous workers have conducted statistical analysis characterizing VHMS deposits and mining camps around the world. Sangster (1980) calculated the average area occupied by a cluster or mining district to be about 850 km², equivalent to a circular diameter of about 32 km and host between 4 and 20 deposits containing approximately 94 M tonnes of ore. Boldy (1977) estimated that approximately 80% of the VHMS deposits fall in the size range of 0.1 to 10 M tonnes with about 50% being less than 1.0 M tonnes for Canadian Archean VHMS deposits. Canadian deposits reviewed had a median deposit size of 1.4 M tonnes at a frequency of occurrence of 15%. Upper decile deposits contained at least 13.3 M tonnes and had a frequency of occurrence of 6.5%. From a grade perspective, Gibson and Kerr (1992) state that 88% of Canadian deposits have combined Cu+Pb+Zn grades of less than 10%.

The Myra Falls property covers an area of approximately 33 km². Compared to Sangster's (1980) estimate of 850 km² for an average VHMS district, the Myra Falls property is approximately 1/25th the size. In terms of tonnage, the 22.0 M tonne H-W deposit would be considered within the upper 10% of VHMS deposits with a significant Au content (> 1.0 M contained ounces). Though not considered large deposits, the Lynx, Myra, Price, Battle and Gap deposits have combined Cu+Pb+Zn grades greater than 10% and are considered high grade. The Ridge Zone West has a current 982,000 tonne mineral resource and is below the median deposit size of 1.4 M tonnes calculated by Boldy (1977). The current Cu+Pb+Zn grade of 8.5% for the Ridge Zone West makes the deposit area attractive from a grade perspective.

1.5 Previous Research

Many geological studies have been undertaken and completed on the Myra Falls VHMS District. Geological research has been spearheaded by the Myra Falls geological staff with in-house project reports, geological field trip guides, presentation of conference papers, hiring expert consultants, and coordinated studies with academic and government institutions. Academic institutions include the University of British Columbia (UBC), the Mineral Deposits Research Unit of UBC, the Centre for Ore Deposit Research (CODES) of the University of Tasmania, and the Masters in Mining and Exploration program of Leicester University.

Property wide geology studies since the beginning of mine production in 1966 have been by Carvalho (1979), Walker (1985), Juras (1987), Reid (1993), Pearson, Juras, and McKinley (1997), Gemmell (1998), Berry (2000) and most recently Jones (2001) (Fig 1.4). Walker (1985) and Juras (1987) focused on establishing the volcanic stratigraphy, geological setting, and general distribution of VHMS mineralization and its associated hydrothermal alteration. Juras (1987) established the overall volcanic stratigraphy of the district with emphasis on the relatively unaltered Price Mine hillside. Juras’ (1987) comparison of the Myra Falls volcanic stratigraphy with interpretations by government workers in the Cowichan-Horne Lake Uplift of the Sicker Group volcanic rocks correlates individual formations from the two areas.



Property wide structural studies by Walker (1985), Juras (1987), Reid (1993), Berry (2000) and Jones (2001) have all contributed to the evolving structural understanding of the Myra Falls district in first identifying the large scale Myra anticline and subsequent offsetting brittle-ductile structural events. Jones (2001) has taken the structural story one step further by correlating the structural model developed at Myra Falls to other regional studies on Vancouver Island. Jones (2001) also developed a pre-deformation, paleo-seafloor reconstruction identifying large-scale paleo-basins and paleo-growth faults associated with VHMS mineralization based on the isopach mapping of significant geological units, footwall contouring of the Price Andesite contact, mapping of rapid volcanic facies changes, and the deformation history of Myra Falls.

Geological research and descriptive documentation of various individual VHMS lenses and their geological settings has been ongoing since mining began in 1966. Seraphim (1980), Walker (1985) and Dishaw (1998) have studied aspects of the near surface Lynx, Myra and Price deposits and their host rocks.

For the at-depth H-W mineralized horizon, Walker (1985), Barrett and Sherlock (1996), Pearson, Juras, and McKinley (1997) and Jones (2001) have investigated various aspects of the volcanic stratigraphy, lithogeochemistry, metal zonation, and seafloor setting pertaining to the Myra Formation volcanic rocks and the 22 M tonne pyrite rich H-W orebody. Jones (2001) has proposed seafloor deposition for the H-W VHMS mound prior to influx of subsequent submarine volcanoclastic rocks based on the presence of unaltered black argillaceous sediments overlying the H-W main deposit.

Robinson (1994) and Sinclair (2000) have both researched the Battle and Gap deposits. Robinson (1994) based her study on drill core from original exploration spaced diamond drilling deriving a seafloor deposition genetic model within a submarine caldera setting for both the Battle Main Lens and Gap Lens VHMS orebodies. Sinclair (2000) on the other hand studied the Battle, Gap, Upper Zones, and the South Trough deposits of the Battle Mine area. Sinclair (2000) documented the volcanic facies architecture, massive sulphide mineralization, hydrothermal alteration and structural characteristics based on the most recent exploration and definition diamond drilling in addition to access of new underground drift exposures. Sinclair's (2000) study reevaluated the Battle and Gap deposits and proposed subseafloor replacement processes as being responsible for VHMS deposition.

Undeveloped mineralized areas west of the Battle-Gap mining area have a current geological resource of 2.4 M tonnes and are comprised of the 1.2M tonne Marshall Zone, the 0.3 M tonne Ridge Zone East, and the 0.9 M tonne Ridge Zone West (Bakker, 2002). The Marshall Zone deposit area is located approximately 1 km NW (mine grid) of the Battle-Gap deposits. Barrett and MacLean (2000) assessed the Marshall Zone area establishing a preliminary framework for the volcanic setting, stratigraphy, and alteration style based on information derived from exploration drill core interpretation and analyses.

1.6 Purpose of Thesis

The Ridge Zone West deposit area is host to a series of small, VHMS lenses within the larger Myra Falls VHMS district of British Columbia, Canada. The purpose of this study is to describe and explain the geological setting and styles of Zn-rich massive sulphide mineralization for the Ridge Zone West deposit area. Results and interpretations of the data collected have been applied to form a genetic model specific to the Ridge Zone West area.

This study is new and relevant towards the geological understanding of the Myra Falls VHMS district in that the Ridge Zone West has not been studied academically before. The study area is located 1 km west of the Battle-Gap deposit area studied by Robinson (1994) and Sinclair (2000) and is on the peripheral edge of the property wide study by Jones (2001) (Fig. 1.3). The western half of the Myra Falls property includes the Ridge Zone West area, and has a current combined geological resource of approximately 2.4 M tonnes (Bakker, 2002). Therefore, this study has relevance towards the future exploration and mining of VHMS deposits at Myra Falls. Advanced geological knowledge of the Ridge Zone West deposit and its host rocks provides the foundation for a successful mine plan.

1.7 Methodology

Data collected from detailed diamond drill core logging, photography, polished thin section and end cuts of the drill core provided the basis for this study. Information was collected from archived diamond drill core during 1999 and intermittently during 2000 to 2001 from a concurrent diamond drill program.

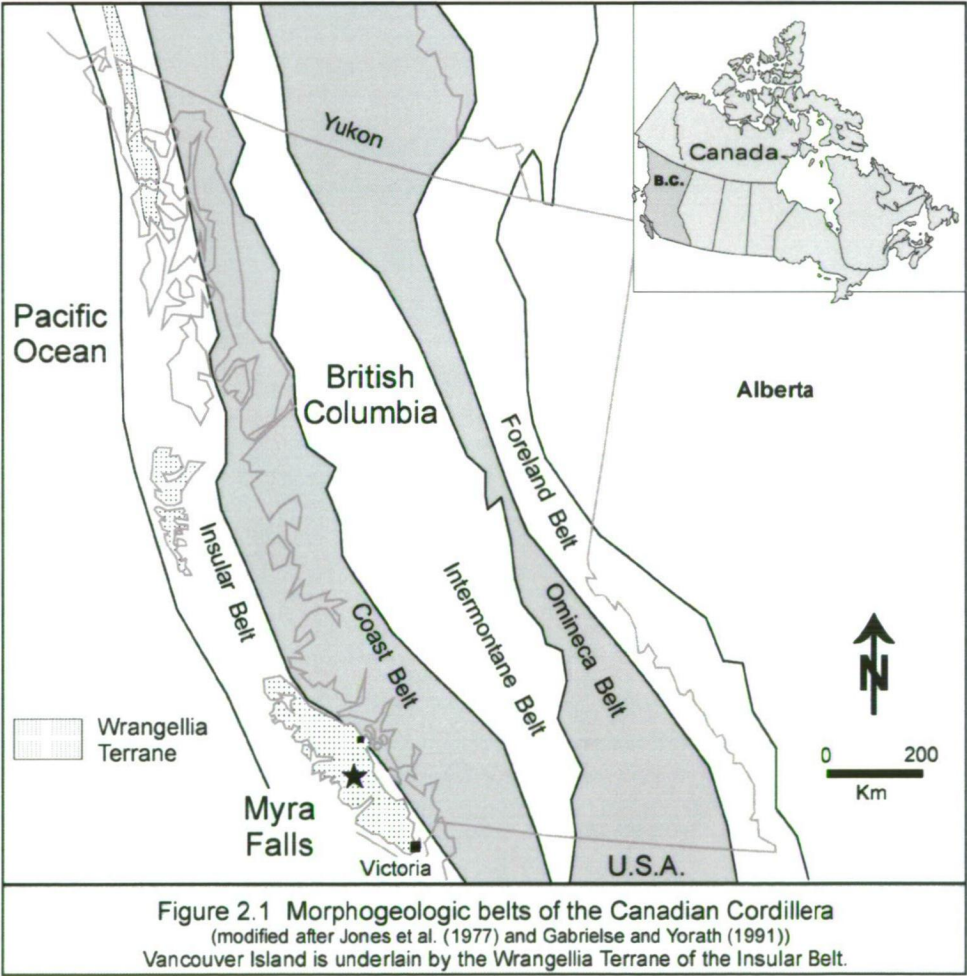
The geological setting has been interpreted by graphic logging techniques of the diamond drill core with application of volcanic facies analyses. Ore mineralization is described relative to geometry, microtextures, and associations with the host volcanic facies. The ore mineralogy is identified and quantified by optical petrography, electron microprobe analyses, and photography. An ore mineral paragenesis is proposed based on volcanic facies associations and sulphide textures.

Metal zoning of the main mineralized lenses was investigated for metal distribution. Metal ratio associations assessed relationships between the various elements. Copper and zinc ratio assessment was applied towards orebody classification and possible temperature regimes. The mineralogy work and metal zoning have direct applications towards genesis, future mining, and ore beneficiation.

The geology and mineralization are combined into a genetic model for the Ridge Zone West. Comparison of the Ridge Zone West characteristics and the interpreted genetic model has been made to other VHMS deposits of younger, similar and older age. The deposits include the modern seafloor Vai Lili hydrothermal field of the Lau Basin in the southwest Pacific, the Tulsequah Chief deposit of northern British Columbia, and the Upper Zone deposits found at Myra Falls. The Que River deposit of Tasmania, Australia is noted for possible exploration potential in the footwall rocks.

2.1 Regional Tectonics and Geology

Vancouver Island is underlain by the Paleozoic Wrangellia Terrane of the Insular Belt and is part of the Canadian Cordillera (Fig. 2.1). The Insular Belt is comprised of the Wrangellia and Alexander Terranes and is believed to have amalgamated pre-late Jurassic (Gabrielse and Yorath, 1991). The Insular Belt is sutured or welded onto the Intermontane Belt, and consequently the North American craton, by a granitic welt known as the Coast Belt. Age of accretion for the Insular Belt onto North America varies along the length of the Cordillera. Based on geologic and paleomagnetic data, accretion is possibly as early as the late Jurassic through to middle Cretaceous, and is constrained by a minimum age for the Coast Plutonic Complex (Monger et al., 1982; Gabrielse et al., 1991).



Conflicting interpretations exist as to where Wrangellia was accreted onto the North American craton and also the amount of translation involved. Paleomagnetic data from Upper Triassic Karmutsen rocks of Vancouver Island suggests their paleolatitude relative to cratonal North America; lay far to the south ($> 1,000$ and possibly up to $3,000$ km). The rock moved north due to rapid oblique subduction of the oceanic Kula Plate beneath the continental western margin of the North American Plate (Wynne et al., 1995; Irving et al., 1996). Further evidence supporting the formation of Wrangellia in more southern latitudes has been paleontological data found in limestone of the Quatsino Formation (Yorath and Nasmith, 1995). Structural geological evidence agrees in part with Late Cretaceous and Cenozoic dextral strike-slip faults aligned roughly parallel to the orogen (Gabrielse, 1992). However, direct restoration of the recognized fault systems suggests a northward translation of less than 500 km since middle Cretaceous time. This 500 km northward translation is well short of the large displacements derived by paleomagnetic data (Monger and Price, 1996).

The Wrangellia Terrane is mapped for approximately $2,000$ km from south-central Alaska to southern Vancouver Island based on similar stratigraphy, rock units, faunas, and geologic history (Jones et al., 1977) (Fig. 2.1). Wrangellian stratigraphy is characterized from oldest to youngest by Paleozoic andesitic arc rocks, Permian argillite and limestone, overlain by a thick pile of tholeiitic flows and pillow lavas capped by inner-platform carbonates (Jones et al., 1977; Muller, 1980).

Wrangellia contains three major volcano-sedimentary cycles recorded on Vancouver Island (Fig. 2.2). The volcano-sedimentary cycles are represented from oldest to youngest by the Sicker-Buttle Lake Groups, the Vancouver Group and the Bonanza Group. Plutonism is associated with each volcanic cycle. Muller (1977, 1980) documented the entire bedrock sequence on Vancouver Island while Walker (1985), Juras (1987) and Massey (1992) have revised portions of the Sicker Group stratigraphy. Subsequent erosion of Wrangellia formed, in part, Nanaimo Group sedimentary deposits during the late Cretaceous along the eastern half of Vancouver Island.

The Paleozoic Sicker Group volcanic rocks are host to the known VHMS deposits on Vancouver Island. Sicker Group rocks are exposed on Vancouver Island in several fault-bounded uplifts. The main uplifts are Buttle Lake, Cowichan-Horne Lake, Nanoose, and West Coast. The uplifts were created during the collision of Wrangellia with the North American craton. The Myra Falls VHMS deposits occur in Myra Formation rocks of the Buttle Lake uplift (Fig. 2.2).

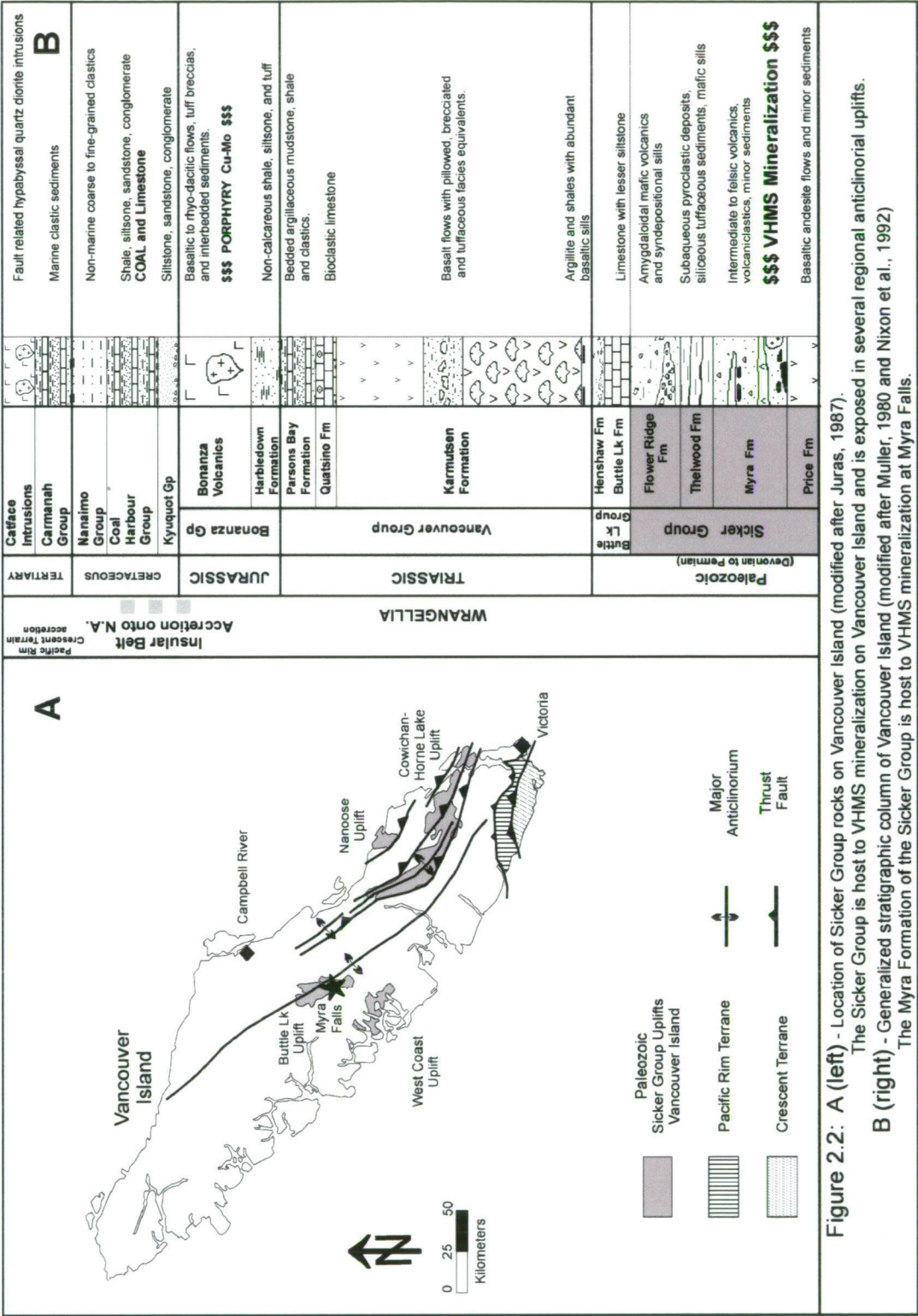


Figure 2.2: A (left) - Location of Sicker Group rocks on Vancouver Island (modified after Juras, 1987).
The Sicker Group is host to VHMS mineralization on Vancouver Island and is exposed in several regional anticlinorial uplifts.
B (right) - Generalized stratigraphic column of Vancouver Island (modified after Muller, 1980 and Nixon et al., 1992)
The Myra Formation of the Sicker Group is host to VHMS mineralization at Myra Falls.

2.2 Regional Metamorphism

Paleozoic Sicker Group rocks on Vancouver Island have been variably metamorphosed up to low-grade greenschist facies (Juras, 1987, Greenwood et al., 1991). Localized areas of higher metamorphic grade have been recognized in Sicker Group rocks in the western and southern parts of Vancouver Island and are possibly due to a deeper level of plutonic emplacement and a general increase in depth of burial (Greenwood et al., 1991).

Younger Triassic Vancouver Group rocks have been metamorphosed to very low-grade prehnite-pumpellyite to zeolite facies (Greenwood et al., 1991). Low to medium grade amphibolite facies contact metamorphism is associated with plutons of the Jurassic Island Intrusions for Sicker Group and Vancouver Group rocks (Juras, 1987, Greenwood et al., 1991, Massey, 1994). Post-Jurassic rocks on Vancouver Island are relatively unmetamorphosed with only zeolite facies assemblages related to burial (Greenwood et al., 1991; Massey 1994).

Timing of regional metamorphism is inferred from paleontological and structural evidence relative to Wrangellian stratigraphy. Conodonts progressively change color from pale yellow to black with increasing depth of burial in the Appalachian Basin (Epstein et al., 1977). Conodonts from the Permian Buttle Lake Group sediments have been compared to conodonts from the Upper Triassic Parson Bay Formation sediments (Brandon et al., 1986). The Buttle Lake Group sediments have conodont alteration indices (CAI) between 5 to 7. Based on the CAI, temperature due to burial and metamorphism is inferred to be $> 300^{\circ}\text{C}$ and is consistent with greenschist facies conditions. Comparatively, conodonts from the younger Upper Triassic Parson Bay Formation sediments have a CAI between 3 and 7 indicative of lower temperatures (Brandon et al., 1986). This paleontological evidence infers the timing of regional metamorphism on the Sicker Group rocks to be post-Permian and pre-Late Triassic.

Structural evidence regarding timing of the regional metamorphism is a variably developed penetrative foliation fabric developed in Paleozoic Sicker Group rocks. The Upper Triassic Karmutsen Formation does not have this penetrative foliation fabric. Therefore, the deformation event responsible for the penetrative fabric is reasoned to be younger than the Paleozoic Sicker Group rocks but older than the Upper Triassic Karmutsen Formation. Hence, if the deformation event responsible for the penetrative fabric discussed above is related to the regional metamorphism, then timing of the metamorphism is interpreted to be post deposition of the Permian Buttle Lake Group sediments and pre-Late

Triassic before deposition of the Karmutsen Formation (Greenwood et al, 1991). This is consistent with paleontological evidence based on the CAI as discussed above.

2.3 Regional Structure

Regional structural-tectonic studies on Vancouver Island have been centered on three areas; namely the Quatsino-Port McNeil area in northern Vancouver Island (Nixon et al., 1994), the Buttle Lake Sicker Group uplift in central Vancouver Island (Muller, 1980), and the Cowichan-Horne Lake area in southern Vancouver Island (Muller, 1980; Massey, 1994). In addition to these regional studies, structural studies at the Myra Falls property have complemented work on the Buttle Lake Sicker Group uplift (Walker, 1985; Juras, 1987; Reid, 1993; Berry, 2000; Jones, 2001).

Vancouver Island has undergone a complex history of ductile and brittle deformation along with repeated intrusion. The ductile deformation is in the form of large scale folding with variable axial planar cleavage depending on rock type competence. Multiple episodes of brittle deformation are expressed as strike-slip, normal and reverse faults. Many of the faults have been reactivated. These deformation events are interpreted to have occurred prior to, synchronous with, and post-accretion of Wrangellia onto the North American craton. The following is a summary of major deformation events on Vancouver Island and their associated structures based on observations and interpretations from the above studies. Orientations in this section are relative to true north.

2.3.1 Paleozoic Deformation (pre-accretion)

Early ductile deformation of the Sicker Group (pre-middle Triassic): Early ductile deformation produced large-scale open folds in Sicker Group volcanic rocks at the Cowichan Lake and Buttle Lake areas (Muller, 1980; Massey, 1994). In the Cowichan Lake area, the large-scale open folds formed during the Devonian to earliest Mississippian. Minimum age is based on an unconformity below the Fourth Lake Formation (Buttle Lake Formation limestone equivalent) along the SW limb of the Cowichan uplift. This unconformity reflects probable uplift and erosion during the final stages of the Sicker arc (Massey, 1994).

A second folding event affecting all Paleozoic rocks is interpreted to have occurred during the middle Permian to pre-middle Triassic, prior to deposition of the Karmutsen Formation (Massey, 1994; Muller, 1980). This folding event is characterized by a series of WNW trending, SW-verging, asymmetric folds with abundant parasitic minor folds (Muller, 1980; Walker, 1985; Massey, 1994; Jones, 2001). Regionally, the major folds plunge to the WNW (Massey, 1994).

The Myra anticline geometry at Myra Falls is an example a WNW trending, asymmetric, SW-verging fold with abundant parasitic minor folds (Muller, 1980; Walker, 1985). The Myra anticline geometry is similar to other asymmetric, W to SW verging fold structures in Sicker Group rocks around the Cameron-Nitinat area (Muller, 1980) and north of Cowichan Lake (Fyles, 1955).

2.3.2 Mesozoic Deformation (pre-accretion)

Crustal extension during Karmutsen Formation deposition and intrusion (late Triassic): Extensive crustal dilation accompanied the effusion of Karmutsen Formation lavas (Fig. 2.2) and intrusion of the Mt. Hall gabbro (Massey, 1994). Structures have not been documented for this event.

2.3.3 Mesozoic Deformation (pre- to syn-collision)

Regional-scale uplift of Wrangellia (early to middle Jurassic): Pre-Nanaimo Group deformation resulted in regional scale warping of Vancouver Group rocks, producing major geanticlinal uplifts cored by Sicker Group rocks (Muller, 1980; Massey, 1994). The Cowichan-Horne Lake and Buttle Lake uplifts are two examples of major geanticlinal uplifts on Vancouver Island (Fig. 2.2). Faulting is axial to the regional scale folding (Massey, 1994). Nixon et al. (1994) infer N to NE directed compression for this deformation based on cleavage orientations. Uplift and erosion followed this deformational phase, establishing the pre-Nanaimo Group topography (Massey, 1994).

Muller (1980) inferred this regional scale warping of Wrangellia to be concurrent with Jurassic plutonism. Regionally, the plutons show little or no deformation suggesting syntectonic to post-deformation timing (Massey, 1994). Timing of the regional scale warping is possibly related to the collision and accretion of the Wrangellia and Alexander Terranes to form the Insular Belt during the late Jurassic (Monger et al., 1982). Subsequent accretion of the Insular Belt onto North America is interpreted to have occurred by the middle Cretaceous (Monger et al., 1982; Monger et al., 1985; Gabrielse and Yorath, 1991).

2.3.4 Mesozoic Deformation (syn (?) to post accretion)

NW and NE trending faults (post middle Cretaceous): This deformation episode postdates deposition of middle Cretaceous Coal Harbour Group sediments and may predate deposition of the Upper Cretaceous Nanaimo Group (Nixon et al., 1994) (Fig. 2.2). This episode is characterized by intense strike-slip faulting and lesser thrusting, that resulted from north directed compression (Nixon et al., 1994).

Faults formed during this episode are dominantly NW trending structures in northern Vancouver Island and have produced significant drag folding, particularly where adjacent units are well bedded. The most obvious of these are NW striking, high-angle oblique slip faults that have a right-lateral and south-up sense of motion. NE trending antithetic faults are also common and exhibit sinistral, NW side up displacement. Minor NW trending thrust faults have a south side up sense of motion (Nixon et al., 1994).

2.3.5 Cenozoic Deformation (post accretion)

Extension and reactivation (post late Cretaceous): In northern Vancouver Island, the youngest phase of deformation is represented by NW to NNW directed extension. This phase is characterized by minor NE to ENE striking normal faults that affect Upper Cretaceous and older strata (Nixon et al., 1994). Reactivation of pre-existing strike-slip faults is rare.

Timing of this phase of extension is unclear based on regional data. Within Sicker Group rocks at Myra Falls in central Vancouver Island, Jones (2001) describes normal faults with similar orientations noted by Nixon et al. (1994). The normal faults at Myra Falls consistently postdate a deformation event with two-stages of strike-slip and thrust faults similar to those interpreted as post middle Cretaceous by Nixon et al., (1994). Jones (2001) also notes that the normal faults at Myra Falls are consistently crosscut by NW trending gouge-rich, thrust faults with coeval ENE-WSW trending strike-slip faults and correlates these thrust faults to the large scale, late Eocene (?) thrust faults observed by Muller (1980), England and Calon (1991) and Massey (1994).

NW trending thrust faults (late Eocene (?)): This deformation is characterized by large-scale W-NW trending, SW verging linked thrust systems of the Cowichan fold and thrust system formed by crustal contraction involving the Upper Cretaceous Nanaimo Group and older Wrangellian rocks (Muller, 1980; England and Calon, 1991; Massey, 1994). These

faults postdate the Nanaimo Group sediments and are indirectly dated as late Eocene (England and Calon, 1991).

Where exposed, these faults are high-angle reverse faults that dip between 45–90 degrees to the N-NE, paralleling the earlier axial foliation in Paleozoic rocks. Horizontal displacements along fault planes are unknown but are inferred between 1 and 10 km. Vertical displacements are constrained by balanced sections to be about 1 to 2 km (England and Calon, 1991; Massey, 1994). The regional map pattern suggests movement along the faults was directed to the W-SW, although slickensides on fault planes indicate the latest movement was horizontal and westerly directed.

NE trending faults (Late Eocene (?)): Several N-NE trending vertical cross-faults, offset the large-scale Cenozoic thrusts with apparent sinistral sense in the Cowichan fold and thrust system (England and Calon, 1991; Massey, 1994). The age of faulting is unknown but may be a late stage of the Eocene contractional event. Similarly, NE striking strike-slip faults on southern Vancouver Island are early Miocene in age and have dextral offsets (Massey, 1994).

Late Eocene thrust faulting is postulated by England and Calon (1991) to have resulted from the collision and accretion of the Pacific Rim and Crescent Terranes with North America during late Eocene time. Transcurrent faults are interpreted to be the result of NW movement of the Pacific plate relative to the North American plate.

2.4 Regional Metallogeny

On Vancouver Island, two major metallogenic groups were classified by Northcote and Muller (1972), volcanic and plutonic. Massey (1992) has further subdivided the two groups based on timing relative to pre and post accretion. The plutonic group deposits are skarn, vein, Sooke-type Cu and porphyry Cu. Intrusions are typically Jurassic or Tertiary in age.

Two main VHMS areas occur on Vancouver Island. They are centered about the past producing Twin J mine in the Cowichan-Horne Lake Sicker Group uplift and the Myra Falls deposits in the Buttle Lake Sicker Group uplift. These deposits have been compared to the Kuroko type deposits of Japan, which are considered to have resulted from volcanic exhalative processes (Northcote and Muller, 1972; Hoy, 1991).

2.5 Myra Falls Mine Geology

The Myra Falls VHMS deposits occur at or near the base of Paleozoic Sicker Group rocks within the Buttle Lake uplift and are associated with the first phase of volcanism on Vancouver Island (Fig. 2.3). Mine sequence geology in the Ridge Zone West area from oldest to youngest is the Price Formation, the Myra Formation, and the Thelwood Formation, as established by Juras (1987). The following is a summary of work by Walker (1985), Juras (1987), Pearson (1993), Barrett and Sherlock (1996) and Sinclair (2000) pertaining to mine sequence rocks (Figs. 2.3 and 2.4).




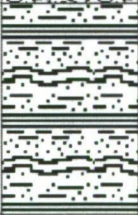
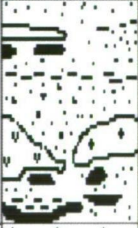

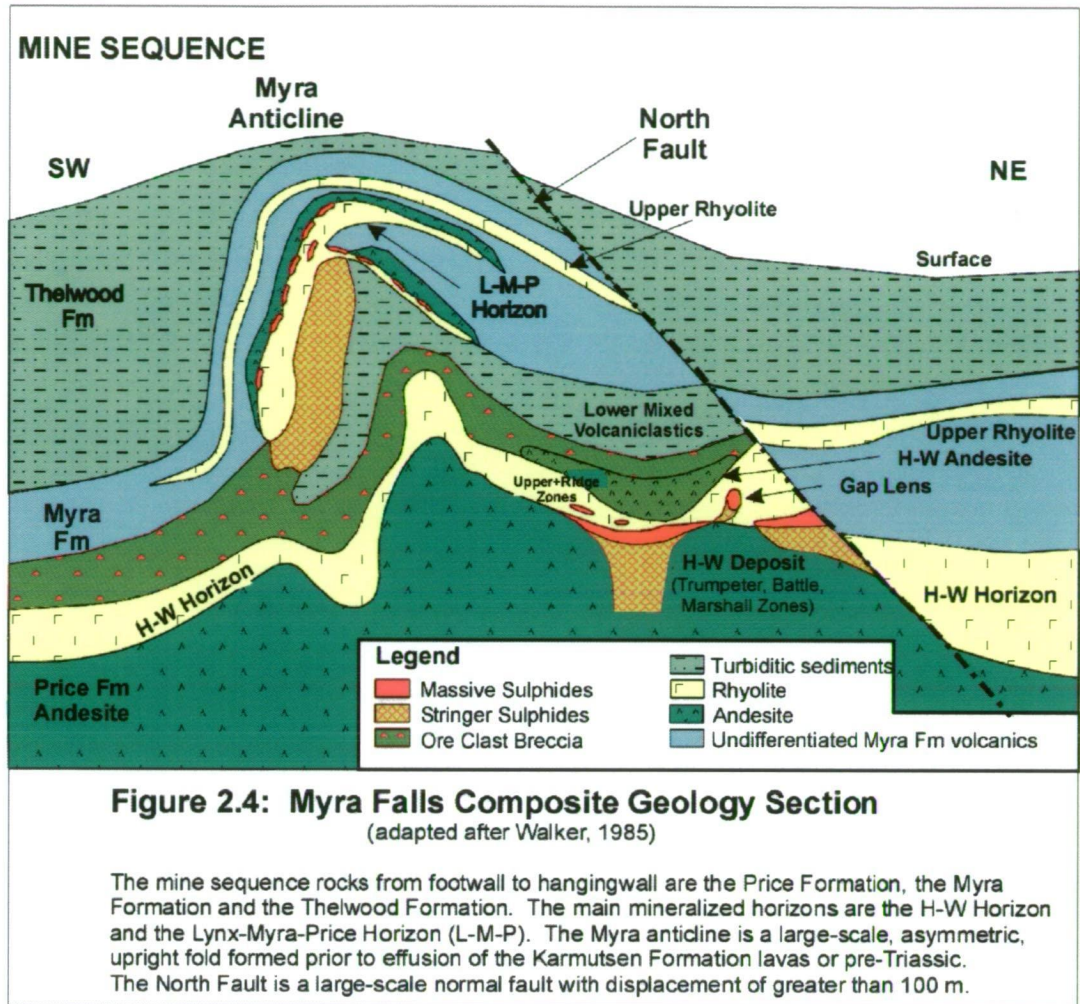
| | | | | | |
|-------------------|---------------------------------|------------------------|---|---|--|
| Buttle Lake Group | Early Permian (?) | Henshaw Formation |  | <100m | Conglomerate, epiclastic deposits, and vitric tuff |
| | Early Permian to Pennsylvannian | Buttle Lk Formation |  | 300m | Crinoidal limestone |
| Sicker Group | Pennsylvannian or Mississippian | Flower Ridge Formation |  | 650m+ | Amygdaloidal mafic lapilli tuff, tuff breccia, intercalated tuffs and flows |
| | Mississippian(?) | Thelwood Formation |  | 270-500m | Subaqueous pyroclastic deposits, siliceous tuffaceous sediments, and mafic sills |
| | Late Devonian | Myra Formation |  | \$\$\$ VHMS Mineralization (L-M-P Horizon) \$\$\$ 310-440m | Intermediate to felsic volcanics, volcaniclastics, and sediments. |
| | Late Devonian or Earlier | Price Formation |  | \$\$\$ VHMS Mineralization (H-W Horizon) \$\$\$ 300m + | Andesite flows, flow breccias, and pyroclastic deposits |

Figure 2.3 Sicker Group Stratigraphy, Myra Falls, Vancouver Island (Adapted from Juras, 1987)
The Myra Formation hosts two main VHMS horizons, the L-M-P and H-W Horizons.



2.5.1 Price Formation

The Price Formation is the oldest exposed unit within the Buttle Lake uplift and is at least 300 m thick consisting of feldspar +/- pyroxene porphyritic basaltic andesite flows and flow breccias with lesser volcaniclastic deposits. Rocks from this unit are moderate to strongly altered with chlorite + epidote + albitic plagioclase +/- actinolite assemblages.

A conspicuous feature of this formation is the presence of medium to very coarse grained, black to dark green, pyroxene phenocrysts pseudomorphed by actinolite. However, the presence of pyroxene grains is not diagnostic of the Price Formation as pyroxene phenocrysts and crystals occur within overlying formations. The top of the Price Formation is defined as the lower contact of the first, widespread rhyolitic volcanic rocks of the overlying Myra Formation. Juras (1987) postulates that the Price Formation formed in an early phase of island arc volcanism in a marginal basin or volcanic arc setting.

2.5.2 Myra Formation

The Myra Formation is 310 to 440 m thick and conformably overlies the Price Formation (Pearson, 1993). The Myra Formation consists of rhyolitic volcanic flows, volcaniclastic, and intrusive rocks with lesser sedimentary units. The volcanic rocks are predominantly intermediate in composition, consisting of flows and flow breccias, and subaqueous volcaniclastic rocks emplaced by sediment gravity flow processes. Sedimentary units include heterolithic volcaniclastic breccia and lesser sandstone, siltstone, argillite, and chert. Individual units are continuous on a northwest to southeast trend but have abrupt facies changes on a northeast to southwest orientation (Walker, 1985). The Myra Formation hosts the VHMS mineralization (Figs. 2.3 and 2.4).

Juras (1987) postulates that the Myra Formation represents a phase of island arc rifting and basin development reflected by three general geologic settings. The three settings are: a volcanic arc setting consisting of andesite to rhyolite flows and volcaniclastic deposits; a rift basin setting comprising volcanogenic sediments, pelagic deposits, hydrothermal mineralization, and intermediate volcanic flows; and lastly, an intra-arc or back-arc rift setting consisting of mafic flows and volcaniclastic deposits.

The Myra formation has been subdivided into ten stratigraphic units based on surface outcrop mapping of the Price hillside located towards the southeast end of the property (Juras, 1987). These units from oldest to youngest are: the H-W Horizon, H-W Hangingwall Andesite, Ore Clast Breccia, Lower Mixed Volcaniclastic Rocks, Upper Dacite / SE Andesite; Lynx-Myra-Price Horizon, G-Flow, Upper Mixed Volcaniclastic rocks, Upper Rhyolite, and, the Upper Mafic Unit.

The H-W Horizon, Hangingwall Andesite, Ore Clast Breccia, and Lower Mixed Volcaniclastic rock descriptions are described below due to their relevance to this study.

H-W Horizon:

H-W Rhyolite Facies: The volcaniclastic rocks range from autoclastic breccias, to resedimented syn-eruptive mass flow deposits and mudstones. These rocks grade from proximal coarse volcaniclastics and lavas in the northeast to volcanic sandstones and intercalated sedimentary deposits toward the southwest (Pearson, 1993; Sinclair, 2000).

H-W Sulphide Facies: The majority of the massive sulphide mineralization was deposited at the base of the Myra Formation within what is known in mine terminology as the H-W

Horizon. The H-W Horizon is either immediately above the mafic Price Formation, or in felsic volcanoclastic rocks in the lowermost part of the Myra Formation. H-W Horizon mineralization is represented by H-W Main Lens, H-W North Lenses, Extension Zone, and the Battle Lenses (Fig. 2.4).

Stratigraphically higher in the H-W Horizon is the Upper Zone and Gap Zone massive sulphides, located 10 to 40 m above the H-W and Battle Zone lenses. The Upper Zone and Gap Zone lenses consist of small Au+Ag+Pb+Ba-rich polymetallic ore zones. Previous work documented the Ridge Zone area to be at an even higher stratigraphic position within the H-W Horizon known as the Hangingwall Zone (Juras, 1987; Pearson, 1993). Current mine terminology would equate this to Upper Zone stratigraphic position.

Hangingwall Andesite Unit:

Hangingwall Andesite Coherent-Autoclastic Facies: The middle portion of the Myra Formation is commonly occupied by this massive, coherent, pyroxene phyric mafic facies. Facies thicknesses are up to 100 m. Facies transitions include thick zones of in-situ quench breccia and peperitic interaction textures around its margins. Geochemical composition is interpreted as basaltic andesite (Juras, 1987; Barrett and Sherlock, 1996).

Ore Clast Breccia Unit:

The Ore Clast Breccia facies is an autobrecciated to autoclastic mafic unit characterized by subangular massive sulphide clasts ranging from 1 cm to 1.5 m. The clasts are typically not concentrated enough to make ore grade. Also present are syn-eruptive mafic and felsic volcanoclastics, post-eruptive mafic and felsic volcanogenic sedimentary deposits. In-situ quench breccia and peperitic interaction textures also exist in this unit (Juras, 1987; Sinclair, 2000). The Ore Clast Breccia occurs both laterally equivalent to and overlying the Hangingwall Andesite (Fig. 2.4).

Juras (1987) and Pearson (1993) previously described the Ore Clast Breccia unit as a series of volcanoclastic submarine debris flows and subordinate subaqueous pyroclastic deposits up to 90 m thick. Further work by Barrett and Sherlock (1996) and the geology department staff at Myra Falls has modified this interpretation such that many occurrences of the Ore Clast Breccia are interpreted to be lateral facies equivalents of Hangingwall Andesite flows or sills interacting with adjacent felsic volcanoclastic and sulphide-bearing host rock. This modified interpretation appears to be applicable to the Ridge Zone West area (see Chapter 3).

Lower Mixed Volcaniclastic Unit:

The Lower Mixed Volcaniclastic Unit typically overlies the Hangingwall Andesite and the Ore Clast Breccia but has also been noted to be laterally equivalent to both units. It is up to 90 m thick and composed of andesitic volcaniclastic deposits, ranging from breccias to mudstones. These rocks are thickest to the southeast and thin to the northwest (Lynx mine area). Toward the southwest, the unit merges with both the Hangingwall Andesite and the Ore Clast Breccia Unit forming an andesitic volcaniclastic unit with minor dacite and trace rhyolite components (Juras, 1987).

The Lower Mixed Volcaniclastic Unit marks the beginning of the upper sequence of mafic and felsic volcano-sedimentary rocks for the Myra Formation. The upper sequence is host to the Lynx-Myra-Price (L-M-P) Horizon.

2.5.3 Thelwood Formation

The Thelwood Formation conformably, and in places unconformably, overlies the Myra Formation. The Thelwood Formation is 270 to 500 m thick and is characterized by thin-bedded, fine-grained mafic volcaniclastic turbidites, tuffs, volcaniclastic debris flows, and penecontemporaneous mafic sills. Turbidite beds are 5 to 30 cm thick and grade upward from coarse-grained crystal-lithic mafic sandstone to pale green, laminated siltstone-mudstone. Volcanic debris flows are 1 to 10 cm thick, moderately well sorted, crudely stratified, and consist mainly of gravel to pebble-sized mafic clasts. Mafic sills are 1 to 10 m thick (Walker, 1985; Juras, 1987).

2.6 Geochronology

Juras (1987), Parrish and McNicoll (1992), and Barrett and Sherlock (1996) report U-Pb zircon age determinations on rhyolite from the Myra Formation. Juras (1987) sampled a rhyolite unit in the upper part of the Myra Formation and he estimates an age of $370 \pm 18/-6$ Ma for the upper rhyolite unit. Parrish and McNicholl (1992) sampled a rhyolite from the lower part of the Myra Formation and estimate a minimum age of 366 ± 4 Ma for the Myra Formation, interpreted as the probable age of crystallization of the rhyolite. Barrett and Sherlock (1996) sampled felsic volcanic strata near the H-W deposit and reported an age estimate of 365 ± 4 Ma (weighted mean age of 5 fractions) or $369 \pm 12/-7$ Ma (best fit line) that confirmed the work of Parrish and McNicholl (1992). These dates indicate a Late Devonian to Early Mississippian age.

Jones (2001) identified radiolaria in the sediments immediately overlying the H-W and Battle deposits. Muller (1980) identified radiolaria in a sediment-sill unit at the top of the Myra Formation. Radiolaria from both locations indicate an Early Mississippian age.

2.7 Myra Falls Metamorphism

The most extensive work on metamorphism in the Buttle Lake uplift was by Juras (1987). Regional metamorphism in the Buttle Lake uplift is lower greenschist facies in the Price and Myra Formations and lower greenschist to subgreenschist pumpellyite-actinolite in the younger Thelwood and Flower Ridge Formations, respectively. Metamorphic mineral assemblages are diverse, reflecting the original bulk composition of rock types present (Table 2.1). In the Thelwood Formation, Juras (1987) attributes silicification to alteration from the penecontemporaneous emplacement of thick mafic sills. Moderate to strong irregular veining and disseminations of epidote is attributed to hydrothermal activity.

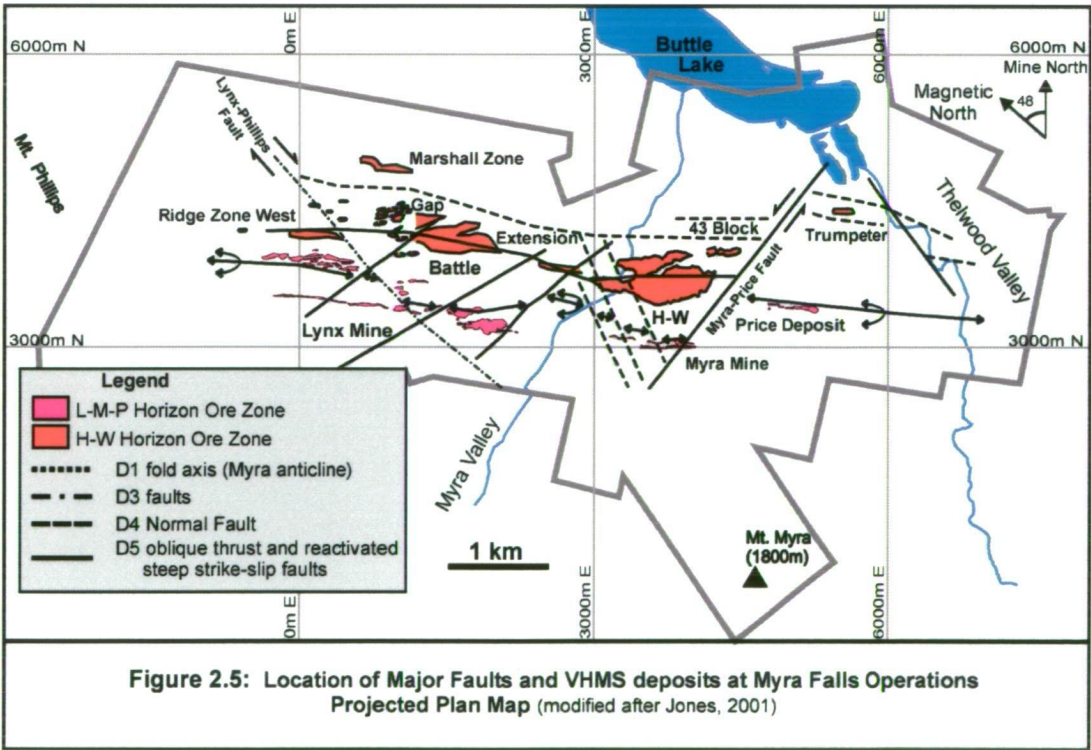
Early Mesozoic metamorphism was caused by burial. This interpretation is based on the resetting of K-Ar and Rb-Sr isotopic dates during emplacement of the Early Jurassic Island Intrusions (Walker, 1985; Juras, 1987). Phyllosilicate phases have been recrystallized to coarser grain sizes and there is some pressure shadow development. These effects are most pronounced in the hinge areas of Mesozoic structures and in schist zones related to faulting.

| Table 2.1: Myra Falls District: Metamorphic Mineral Assemblages (from Juras, 1987) | | |
|---|---|---|
| Price Fm | Basaltic andesite, andesite (mid-ocean ridge analogy) | chl+ep+ap+q+cc+/-act |
| Myra Fm | High MgO basalt | act+chl+ab+ep chl+cc+ser+hem |
| Basalt | | chl+q+ab chl+ep+ab+q+/-act+/-cc ep+q+ab+cc+/-act |
| Basaltic andesite, andesite | | ep+ab+q+/-chl+/-cc+/-act chl+ab+q+/-ep+/-cc |
| Feldspar porphyritic felsic volcanic | | ab+q+ep+ser+/-chl+/-hem |
| Quartz feldspar porphyritic rhyolite | | ser+q+ab+/-chl |
| Thelwood Formation | Intermediate tuffs Mafic sills | chl+ep(+/-clz)+q+ab chl+ab+ep |
| Flower Ridge Formation | basalt | chl+ep(+/-clz)+ab+q+act+/-cc+/-pp chl+ep(+/-clz)+ab+q+act+/-cc |
| Actinolite - act; Albite - ab; Apatite - ap; Calcite - cc; Chlorite - chl; Clinozoisite - clz; Epidote - ep; Hematite - hem; Prehnite-pumpellyite - pp; Quartz - q; Sericite - ser | | |

2.8 Myra Falls Structure

Five phases of deformation have been interpreted at Myra Falls. Walker (1985) and Juras (1987) document two early ductile deformation events (Figs. 2.4 and 2.5); a large scale, upright, open fold referred to as the Myra anticline; and a ductile event that has resulted in broad zones of shearing. Reid (1993), Berry (2000), and Jones (2001) focused on subsequent property wide brittle deformation events. Berry (2000) and Jones (2001) propose a five stage structural history for Myra Falls as outlined in Table 2.2 and Fig. 2.5. Orientations noted in Table 2.2 and the following text are relative to true north, thus facilitating correlations between both property and regional scale observations.

| Table 2.2: Myra Falls District: Deformation History (Berry, 2000; Jones, 2001) | |
|--|--|
| Event | General Description |
| D ₀ | Early extension and formation of syn-depositional growth faults. |
| D ₁ | NE-SW compression; folding and development of an NW-SE foliation; shallow plunges to the NW and SE. |
| D ₂ | Shear zones. |
| D ₃ | NE-SW compression; a two-stage generation of steep strike-slip faults; followed by shallow-dipping NE-SW dipping thrust faults. |
| D ₄ | Extension with planar normal faults. |
| D ₅ | NE-SW compression resulting in NE-SW dipping gouge-rich thrust faults and coeval, steep E to SE trending sinistral strike-slip faults. |



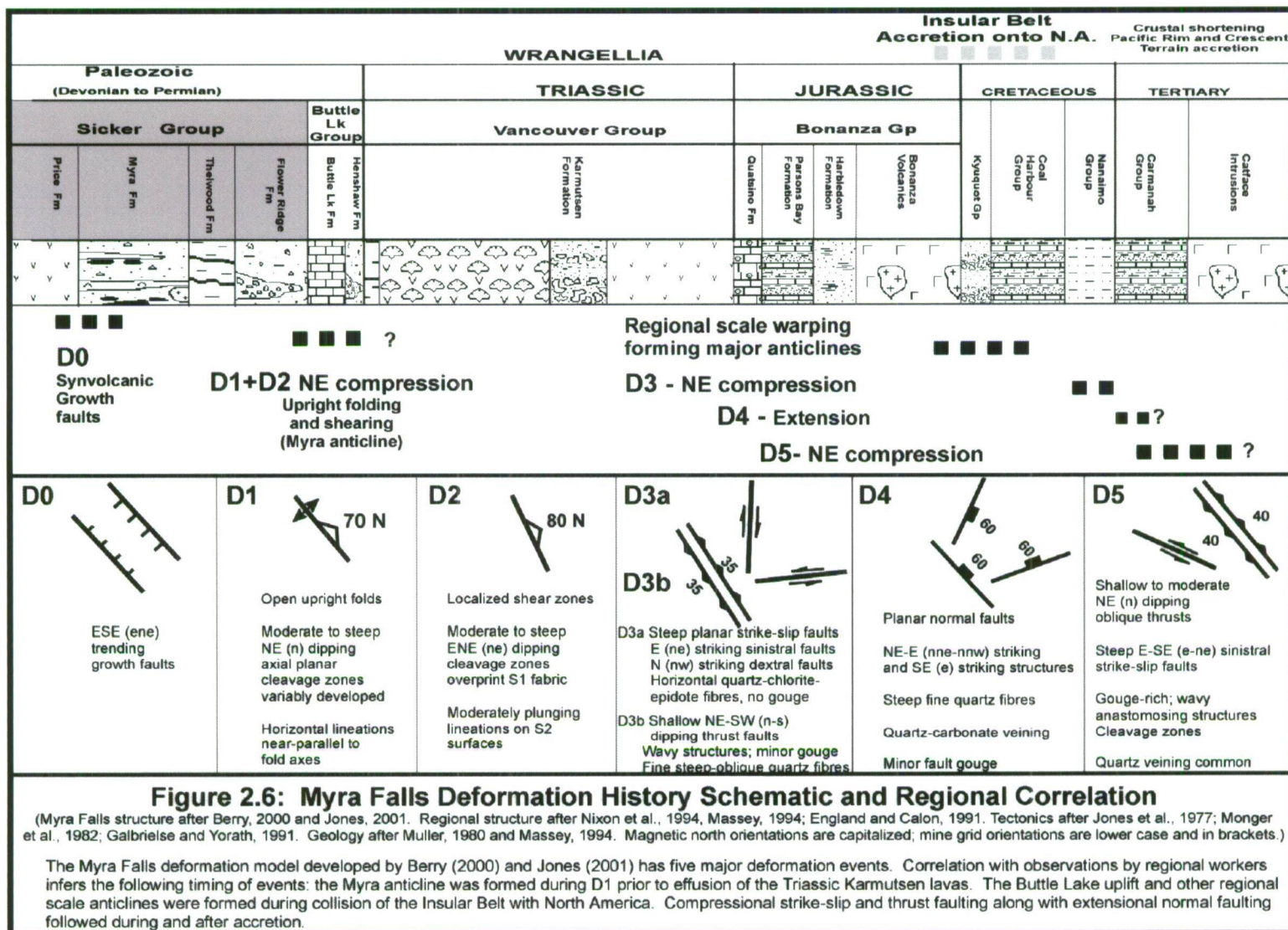


Figure 2.6 is a schematic representation reflecting the Myra Falls deformation model and regional correlation as interpreted by Berry (2000) and Jones (2001). Timing of the five main deformation events is inferred from regional structural studies in northern Vancouver Island around the Quatsino-Port McNeill area (Nixon et al., 1994), central Vancouver Island (Muller, 1980), and south Vancouver Island around the Cowichan Uplift (England and Calon, 1991; Massey, 1992; Yorath et al., 1999).

2.8.1 Paleozoic Deformation (pre-accretion)

Early ductile deformation of the Sicker Group (pre-middle Triassic): Jones (2001) conclude that the ductile D1 folding and D2 shearing is a result of NE-SW compression. These events formed the asymmetric, SW verging, large-scale Myra anticline and its parasitic folds (Figs. 2.4, 2.5, and 2.6). Structures resulting from this event have been mapped in Sicker Group rocks throughout Vancouver Island. The D1 folding and D2 shearing events are believed to have occurred within the Wrangellia Terrane prior to collision with the ancient North American craton.

2.8.2 Mesozoic Deformation (syn (?) to post accretion)

NW and NE trending faults (post middle Cretaceous): The D3 faults at Myra Falls result from a two-stage evolution of strike slip and thrust faults (Berry, 2000; Jones, 2001) (Figs. 2.5 and 2.6). A similar two-stage strike-slip and thrust-faulting event has been documented in northern Vancouver Island and it is believed to have occurred during the post middle to pre-late Cretaceous time (Nixon et al., 1994).

2.8.3 Cenozoic Deformation (post accretion)

Extension and reactivation (post late Cretaceous): The D4 normal faults at Myra Falls consistently postdate a deformation event with two-stages of strike-slip and thrust faults similar to those interpreted as post middle Cretaceous by Nixon et al., (1994) (Berry, 2000; Jones, 2001) (Figs. 2.5 and 2.6). Timing of the D4 faults is unclear. Jones (2001) notes that small-scale normal faults at Myra Falls with displacements less than 15 m are consistently crosscut by NW trending gouge-rich, thrust faults with coeval ENE-WSW trending strike-slip faults and correlates these thrust faults to the large scale, late Eocene (?) thrust faults observed by Muller (1980), England and Calon (1991) and Massey (1994). Berry (2000) notes that the large-scale, gouge-rich North Fault, with interpreted normal displacement of greater than 100 m, is possibly post Cenozoic thrust faulting or reactivated during D5.

NW trending thrust faults (late Eocene (?)): Large scale, gouge-rich D5 thrust faults at Myra Falls are likely related to the large NW oriented thrust faults that dominate the structural fabric of Vancouver Island (Berry, 2000; Jones, 2001) (Figs. 2.5 and 2.6). These

A. Chong, 2005: Geology and genesis of the polymetallic Ridge Zone West VHMS deposit

thrust faults may be correlated to north dipping thrust faults in the Cowichan Uplift of southern Vancouver Island documented by England and Calon (1991), Massey (1992), and Yorath et al. (1999). The faults are inferred to have developed during crustal shortening caused by the collision and accretion of Wrangellia, Pacific Rim and Crescent Terranes onto North America. Strike slip components of the D5 faults are due to NW movement of the Pacific Plate relative to the North American plate.

2.9 Ore Body Geometry

The following discussion on ore body geometry is taken directly from Chong (2003). The ore lenses at Myra Falls have been modified by varying degrees of deformation. Deposits such as the Lynx and Myra (Fig. 2.4 and 2.5) have been substantially folded making derivation of primary geometry difficult. Other lenses such as 43 Block (Fig. 2.5) have had at least 3 phases of brittle-ductile deformation, also making derivation of primary geometry difficult. Even though the Battle, Gap, and H-W deposits (Fig 2.5) have had many phases of brittle and ductile deformation superimposed on their original geometries, the current gross overall geometries and thickness variations appear to be reasonably similar to their inferred original geometries prior to deformation. Therefore, a review of the ore body geometries of the Battle, Gap, and H-W deposits would be useful as a general guideline to the variety of deformed geometry types for the H-W Horizon at Myra Falls.

Aspect ratios are typically calculated for primary undeformed lens geometries by the following formula: thickness / length. For purposes of discussion, the aspect ratios used in this document are for deformed, secondary aspect ratios. Lengths used are for N-S minor axis dimensions as this perspective provides the greatest variation for massive sulphide geometry.

The Battle main lens has a sheet style geometry measuring approximately 900 m long by 250 m wide by 3 to 30 m thick and has an aspect ratio below 0.2 (Figs. 2.5 and 2.7). The Gopher lens (approximately 1.0 M tonnes) appears to have an asymmetric mound geometry with an aspect ratio of approximately 1.0 at its thickest part on a N-S cross-section perspective. The Upper Zones, located 10 to 70 m above the main lenses are polymetallic disseminations, stockwork veins, and massive sulphide lenses with low aspect ratios. The Gap lens has a high aspect ratio of 2 and measures at least 330 m long by 30 m wide by 3 to 45 m thick. Sinclair (2000) documented the Gap lens as having a pipe shaped geometry.

The H-W main lens appears to have an asymmetric mound geometry at its thickest accumulation measuring 950 m long by 450 m wide by 1 to 60 m thick (Figs. 2.5 and 2.8).

Further to the east at 3750E, the H-W main lens thins out and has low-aspect sheet geometry. The North lens appears to be a low aspect ratio mound or sheet style deposit on 3750E. Upper Zone style mineralization of disseminated to massive replacement style vein mineralization is prominent above the polymetallic southern fringe of the H-W main lens.

Based on the above discussion, there are currently four main types of ore lens geometries for the H-W Horizon at Myra Falls. These geometries are:

- (1) Low aspect asymmetric mound deposits ranging between 1.0 to 10.0 M tonnes,
- (2) Low aspect sheet (lens) deposits ranging between 0.01 to 6.0 M tonnes,
- (3) Upper Zone disseminated to replacement vein and lens style mineralization,
- (4) High aspect pipe shaped deposits as per the Gap deposit, with tonnage potential of at least 700,000 tonnes.

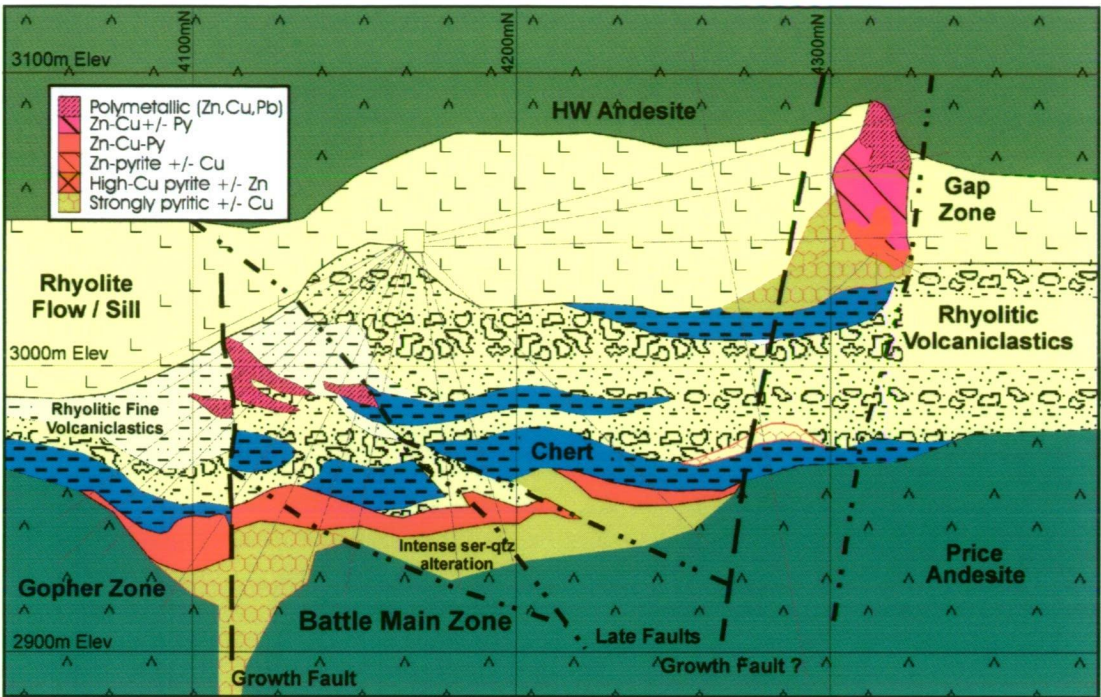


Figure 2.7: Battle Deposit - Geology Section 1390 E

(modified after Chong (2003))

Ore body geometry for the Battle Main lens is a low aspect sheet geometry, the Gopher lens a low aspect asymmetric mound and the Gap lens a high aspect ratio pipe geometry. Footwall alteration below the Battle deposit is diffuse, semi-concordant and within 30 m of the main sheet. Hydrothermal alteration below the Gap lens, and possibly the Gopher lens, is a focused pipe geometry. Hangingwall alteration of the Gopher and Battle Main lenses is unfocused, diffuse and forms the footwall alteration for the Upper Zone and Gap lenses.

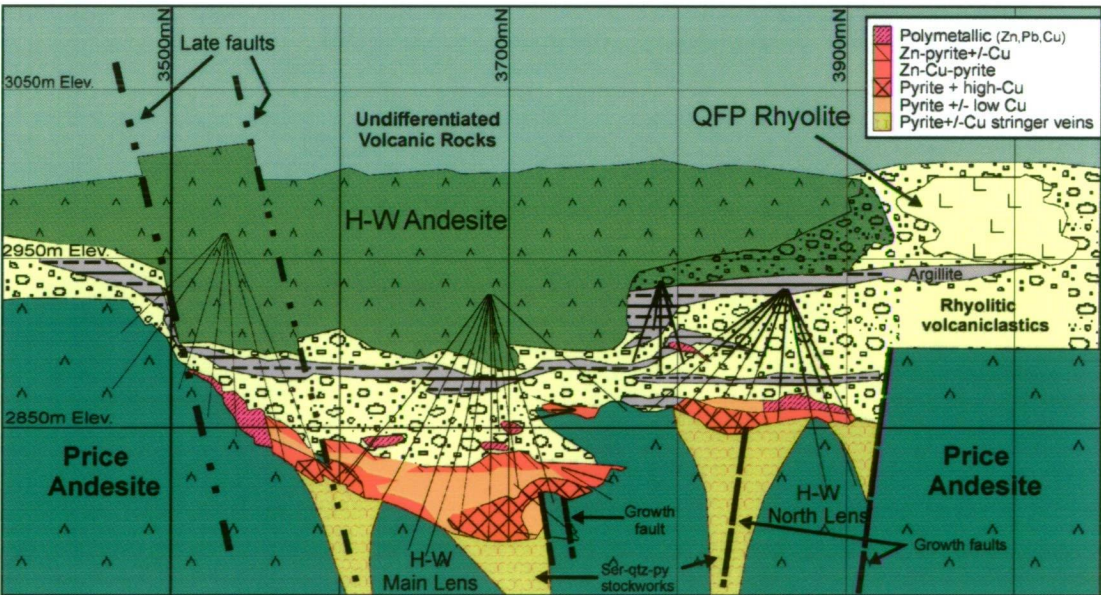


Figure 2.8: H-W Deposit - Geology Section 3505 E

(modified after McKinley et al., 1997)

The deformed ore body geometry for the H-W lens is a low aspect sheet but is asymmetric at its thickest accumulation. Hydrothermal alteration below the H-W deposit is at least 80 m below the paleoseafloor and is interpreted to have focused pipe shaped geometries.

2.10 Ore Body Mineralogy

The following discussion on ore body mineralogy is taken directly from Chong (2003) based on work by Walker (1985), Robinson (1994), Wilson (1993), and Sinclair (2000). Sulphide mineralogy at Myra Falls is typical of most VHMS deposits. The common sulphide minerals present in order of decreasing abundance are pyrite, sphalerite, chalcopyrite, and galena. Less common sulphides are pyrrhotite, arsenopyrite (Walker, 1985) and the Cu-rich sulphides bornite, renierite, and anilite (Robinson, 1994; Sinclair, 2000). Common sulfate and sulphosalt minerals present are barite and tennantite, respectively. A late stage Ag-Au rich mineral assemblage includes stromeyerite and electrum (Sinclair, 2000). Table 2.3 lists the orebody minerals present at Myra Falls, their general chemical formulas, and some of the more significant elemental associations.

| Assemblage | Type | Mineral | General Formula | Other elements | Inclusions - Impurities |
|-----------------|-----------------|---------------|---|----------------|----------------------------|
| Cu-Pb-Zn-Fe | Sulphides | Pyrite | FeS ₂ | Ni, As | Zn, Cd, Cu, Pb, As, Mn, Au |
| | | Sphalerite | ZnS | Fe, Cd, Mn | Cu |
| | | Galena | PbS | Se, Te | Zn, Fe, Cu |
| | | Chalcopyrite | CuFeS ₂ | Se, In | Ba, Zn, Au |
| | | Pyrrhotite | Fe _{1-x} S | | |
| | | Arsenopyrite | FeAsS | | |
| | Sulphosalts | Tennantite | (Cu ₁₀ Ag) Zn ₂ Fe(As ₃ , Sb) ₃ S ₁₂ | Fe, Se, Cd | |
| | Trace Minerals | Rutile | TiO ₂ | | Si, Al, Fe |
| | | Colusite | Cu ₃ (As, Ge, V) ₄ S ₄ | Ba, Sb | Ag, Mo, Zn, Fe |
| | Tellurides | Altaite | PbTe | | |
| | | Hessite | Ag ₂ Te ₃ | | |
| | | Pilsenite | Bi ₂ Te ₃ | | |
| Cu-Rich | Sulphides | Bornite | Cu ₅ FeS ₄ | Ag, Ba | Zn, Cd |
| | | Covellite | CuS | | |
| | | Renierite | Cu ₁₀ (Zn _{1-x} Cu)Ge _{2-x} As _x Fe ₄ S ₁₆ | V, Sb, Ba | |
| | | Anilite | Cu ₂ (Ag)S | Ag, Ba | |
| Late Ag-Au Rich | Sulphides | Stromeyerite | CuAgS | Fe | |
| | Precious metals | Electrum | AuAg | | |
| | | Native silver | Ag | | |
| Gangue | | Barite | BaSO ₄ | | |
| | | Quartz | SiO ₂ | | |
| | | Muscovite | K ₂ Al ₄ (Si ₈ Al ₂ O ₂₀)(OH, F) ₄ | | |
| | | Chlorite | (Mg, Fe) ₃ (Si, Al) ₄ O ₁₀ (OH) ₂ (Mg, Fe) ₂ (OH) ₆ | | |
| | | Epidote | Ca ₂ (Al, Fe) ₃ Si ₃ O ₁₂ (OH) | | |
| | | Calcite | CaCO ₃ | | |
| | | Gypsum | CaSO ₄ ·2H ₂ O | | |
| | | Anhydrite | CaSO ₄ | | |
| | | Jasper | SiO ₂ | | |
| | | Specularite | Fe ₂ O ₃ | | Fe |
| | | Smithsonite | ZnCO ₃ | | |

Data after Robinson (1992), Wilson (1993), Sinclair (2000), and M. Becherer (pers. comm., 2003)

Assemblages adapted from Battle-Gap study by Sinclair (2000)

Sinclair (2000) has identified three main mineral assemblages. These are a Cu-Pb-Zn-Fe rich mineral assemblage, a Cu-rich mineral assemblage, and a late stage Ag-Au rich assemblage for the Battle deposit. Since the Battle deposit has similar but enhanced sulphide mineralogy relative to other deposits at Myra Falls, the assemblages outlined by Sinclair (2000) will be used to discuss the orebody mineralogy.

2.10.1 Cu-Pb-Zn-Fe rich mineral assemblage

Common minerals for the Cu-Pb-Zn-Fe rich assemblage are pyrite, sphalerite, galena, chalcopyrite, and tennantite. Pyrite has a wide range of textures ranging from microscopic framboids, ring structures, fine-grained disseminated euhedra, fine-grained spongy pyrite, and annealed coarse-grained porphyroblasts (Robinson, 1994; Sinclair, 2000). The framboids, ring structures, and fine-grained spongy pyrite are interpreted as primitive textures formed during VHMS mineral deposition (Sinclair, 2000). Coarse-grained porphyroblasts and cataclastic textures are interpreted to be the result of metamorphism and deformation. Pyrite has Au and As associations identified by ion microprobe (Wilson, 1993) with Au values between 25-1000 ppb.

In the Battle-Gap deposit and Upper Zone areas, much of the sphalerite is a low-Fe variety averaging approximately 0.6 wt% FeO (Robinson, 1994; and Sinclair, 2000) and is commonly referred to as “honey” sphalerite. In the H-W and Lynx deposits, the sphalerite is darker grey in colour due to a relatively higher Fe content (pers. comm. M. Becherer, 2003). In thin section, sphalerite crystals exhibit textures resulting from metamorphism. These textures include coarsening of individual crystals, 120° triple points between sphalerite crystals, and the migration of chalcopyrite to triple point junctions and grain boundaries (Sinclair, 2000).

Galena at Myra Falls occurs as recrystallized anhedral masses and grains interlocked with tennantite and barite. Chalcopyrite is generally remobilized. The sulphosalt present is the As-rich end member tennantite.

Trace minerals are rutile, tellurides and colusite. The tellurides of altaite, hessite, and pilsenite commonly occur as microscopic inclusions in tennantite and galena. Colusite occurs exclusively in the Gap and Upper Zone ores as rounded blebs in sphalerite, pyrite, and bornite (Sinclair, 2000).

2.10.2 Cu-rich sulphides

Bornite is common within the Gap deposit, Upper Zone mineralization, the Bornite lens and the NE portion of the H-W Main lens. Renierite, also known as orange bornite, occurs as rounded grains in bornite, or in sphalerite where bornite is abundant. Anilite is a “blue” copper rich sulphide that is part of the chalcocite group (Robinson, 1994; Sinclair, 2000).

2.10.3 Au-Ag assemblage

Gold within the Gap and Upper Zone mineralization above the Battle deposit occurs as submicroscopic inclusions at grain boundaries and scattered grains of gold or electrum (Sinclair, 2000). In 2000, a mine geology staff member observed a 1 m thick gold enriched barite bed with stromeyerite-tennantite-electrum (+/-manganese?) veining located in the immediate hangingwall to the polymetallic Zn-Pb-Cu-Ba enriched portion of the H-W deposit. This baritic bed sample had an outstanding total metallic precious metal assay of 5,000 g/t Au and 5,379 g/t Ag.

2.11 Hydrothermal Alteration

The following discussion on hydrothermal alteration is taken directly from Chong (2003). The alteration mineralogy at Myra Falls includes sericite and silica with subordinate chlorite, albite, and carbonate. Sulphide mineralogy of pyrite+/-chalcopyrite+/-sphalerite+/-galena+/-tennantite is also present in varying modal percentages as disseminations and veinlets. The overall depth and lateral distribution of the hydrothermal system for the Myra Falls deposits has not yet been defined. Zones of pyrite stringer mineralization have been observed to underlie the H-W, Battle, Lynx and Myra deposits. A majority of the following discussion is based on hydrothermal alteration studies for deposits on the H-W Horizon, as little has been written about the L-M-P Horizon on this topic.

2.11.1 Footwall Price Formation Alteration

Alteration within the Price Formation andesite is not well defined at depth beneath the mineralized zones as diamond drill coverage is typically designed to define the ore bodies. The most common alteration immediately below the ore lenses in the Price Formation andesite is a texturally destructive intense sericite-quartz-pyrite alteration. Hydrothermal alteration has been observed in the Price Formation andesite to depths of at least 80 m below the H-W deposit (Barrett and Sherlock, 1996) (Fig. 2.7). A zone of albite-quartz+/-sericite+/-chlorite alteration flanks the main hydrothermal alteration feeder system in the footwall of the H-W deposit (Juras, 1987).

The largest zone of hydrothermal pyrite stringer mineralization at Myra Falls underlies the H-W deposit (Walker, 1985), where the pyrite content ranges from 5 to > 30% (Fig. 2.7). The pyrite is coarsely crystalline (3 to 10 mm) in contrast to the overlying, typically fine-grained, massive pyrite. Individual pyrite and quartz stringers range up to 1 m thick (Walker, 1985) and have steep dips. Generally, pyrite stringer mineralization is not economic.

Immediately below the Battle deposit, a similar texturally destructive intense sericite-quartz-pyrite alteration system exists (Fig. 2.6). Localized intense Mg-chlorite alteration is also present within the sericite-quartz-pyrite alteration below the Battle deposit (Robinson, 1994; Sinclair, 2000). Thirty meters below the Battle deposits a sericite-chlorite-pyrite alteration assemblage becomes dominant (Sinclair, 2000).

A semi-conformable pyrite stringer mineralized zone has been observed to underlie the Battle Main lens for a few meters into the footwall rocks. A more extensive pyrite stringer zone with intense sericite-quartz alteration is spatially associated with an interpreted synvolcanic fault between the Gopher and Battle Main lenses. This Gopher-Battle Main stringer zone appears to have a subvertical orientation, possibly representing an alteration pipe (Fig. 2.6). Below the Battle-Gopher-South Trough lenses, are disseminated to veined coarse-grained pyrite stringer zones.

2.11.2 H-W Horizon Hangingwall Alteration

Juras (1987) noted that at the property scale, felsic volcanic rocks in the Myra Formation form numerous mineral assemblages. Hydrothermal metamorphism of feldspar porphyritic felsic volcanic rocks yields the assemblage albite-quartz-epidote-sericite+/-chlorite+/-hematite. Quartz-feldspar porphyritic rhyolite has an alteration mineral assemblage of sericite-quartz-albite+/-chlorite.

The hangingwall alteration in felsic volcanic rocks above the Battle deposit area is typically diffuse and unfocussed, but can be well developed in areas with Upper Zone style mineralization. The most common alteration minerals are a pervasive sericite-quartz assemblage. Intense hydrothermal silicification of fine-grained volcanoclastic deposits immediately above massive sulphide mineralization commonly produces a lithology referred to as “chert” in mine terminology (Jones, 2001). Dolomite, barite, and disseminated to veinlet style sulphides are present. The dolomite alteration occurs as texturally destructive blebs and rhombs up to 2 cm in diameter. It has a restricted distribution and is proximal to the peripheral edge of the hydrothermal system (Sinclair, 2000).

The current understanding is that much of the hangingwall alteration is footwall alteration to the Upper Zones and Gap deposit (Robinson, 1994; Sinclair, 2000). Underlying the Gap lens is a massive, well-defined, focused, massive pyrite-rich stringer zone below the Gap lens with a pipe-shaped geometry (Fig. 2.6).

2.11.3 Lynx-Myra-Price Hydrothermal Alteration

The following discussion on L-M-P hydrothermal alteration is from Walker (1985). Ore-related alteration has been metamorphosed and is now manifested by broad zones of pyrite-sericitic schist. Within the more extensive sericite schists, which contain a few percent disseminated pyrite, two separate zones of pyrite stringer mineralization have been recognized along the Lynx-Myra-Price Horizon. These pyrite stringer zones underlie the Lynx and Myra deposits. The Lynx deposit pyrite stringer zone conformably underlies the S-Zone lenses (Fig. 2.4).

A relatively smaller pyrite stringer zone underlies the Myra deposit. The Myra pyrite stringer zone has elevated Cu values, which have locally attained economic Cu concentrations sufficient to allow mining. Smaller zones of galena and sphalerite-bearing stringer mineralization are recognized peripheral to or away from the major pyrite stringer zones mentioned.

Chapter 3 Geology and Alteration of the Ridge Zone West Host Rocks

3.1 Introduction

This chapter describes the volcanic setting of the Ridge Zone West host rocks using volcano-sedimentary facies analyses and interpretation starting with the footwall Price Formation, passing up through the H-W Horizon, and ending up-stratigraphy with the Lower Mixed Volcaniclastic unit of the Myra Formation. Following the descriptive portion of the chapter, a discussion examines the volcanic stratigraphy for the Ridge Zone West deposit area and compares it to the property wide volcanic stratigraphy. Alteration of the Ridge Zone West host rocks is briefly discussed based on drill core observations and section interpretations.

Approximately 4,000 m of core from 11 drill holes was graphic logged in detail by the author during the years 2000 and 2001. These drill holes have been interpreted on sections 4150N, -050E, 050E, 175E, and 375E (Fig. 3.1, 3.2a-d) covering an area of approximately 650 m by 200 m. Other drill holes from the Myra Falls database adjacent to the sections have been incorporated to complement geological interpretation.

The host rock naming classifications used in this study are after McPhie et al. (1993) (Tables 3.1 and 3.2). The non-genetic classification scheme is used to avoid any genetic inferences in the descriptive portion of the facies analyses. Barrett and Sherlock (1996) as well as Sinclair (2000) have used a similar volcanic facies naming convention in their studies of the H-W and Battle-Gap deposits respectively. All references to orientation in this chapter are relative to mine grid north. Mine grid north is rotated 48° east of true north.

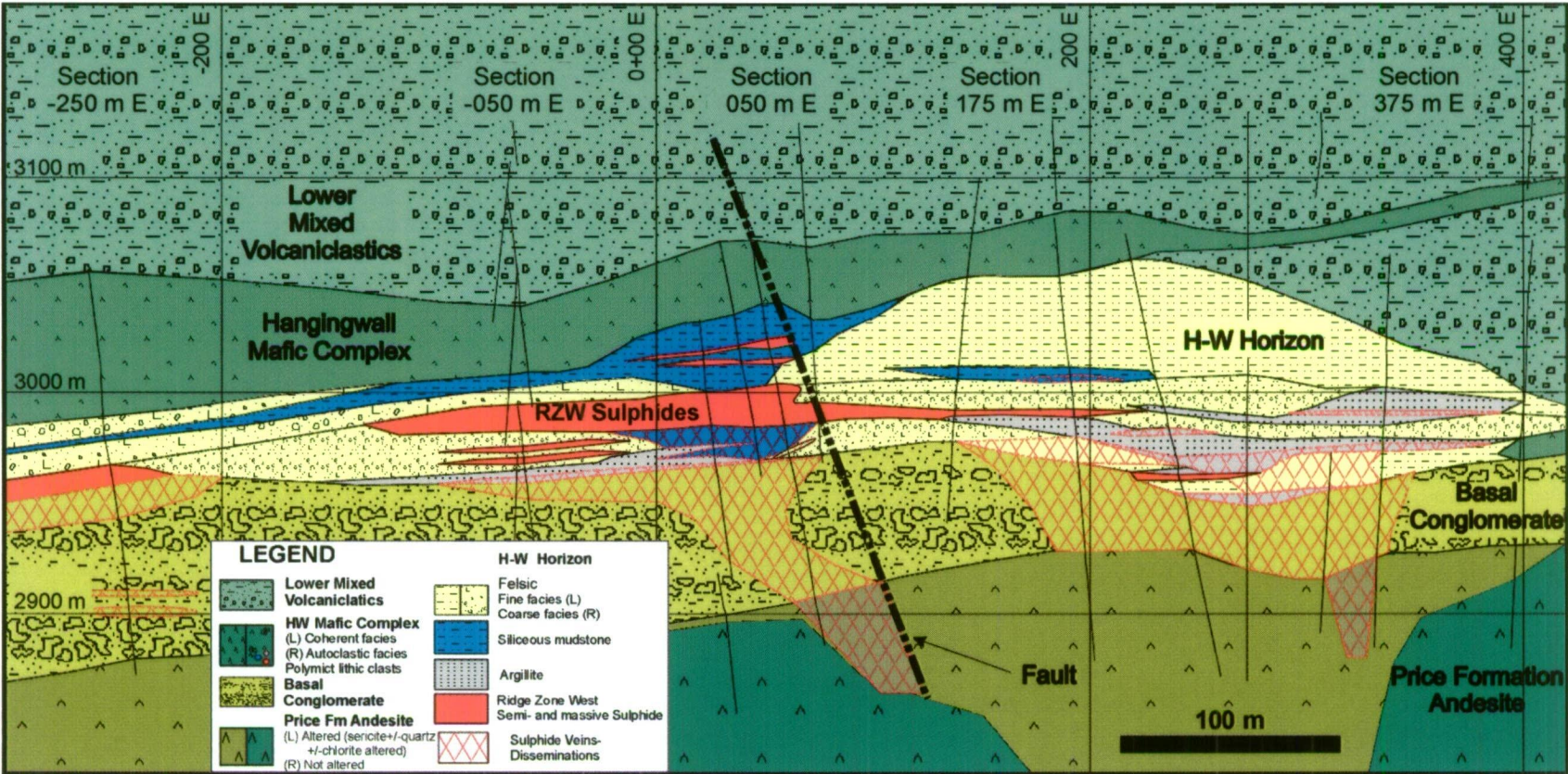


Figure 3.1: Ridge Zone West Geology - Longitudinal Section 4150 m N

Observations and data for this study are from sections -250 m E, -50 m E, 50 m E, 175 m E, and 375 m E. The main units from stratigraphic footwall to hangingwall are: the Price Formation andesite, the Basal Conglomerate, the H-W Horizon, the Hangingwall Mafic Complex, and the Lower Mixed Volcaniclastics. The H-W Horizon is composed of fine to coarse volcaniclastic rocks, sediments, and sulphide mineralization. Sulphide disseminations and stringers are the dominant styles of mineralization between 175 m E to approximately 400 m E. The best mineralization for the Ridge Zone West is located between -50 m E and 50 m E. Significant sulphide mineralization is located at section -250 m E and the zone is open westward. Footwall vein and disseminated mineralization continuing off-section 4150N have been included for interpretive purposes.

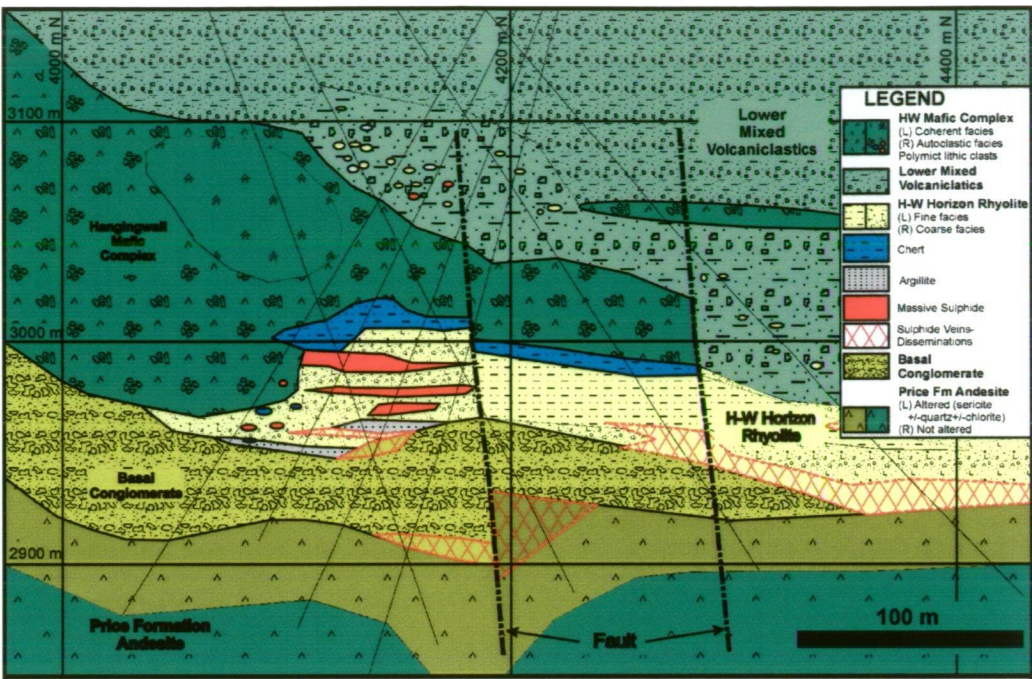


Figure 3.2a: Ridge Zone West Geology - Section -50 m E (view west)

Section -50E is the western extent of the best mineralization discovered to date. Footwall alteration in the Price Formation andesite is characterized by weak to moderately developed sericite +/- quartz +/- chlorite. The Basal Conglomerate is altered by pervasive quartz + sericite +/- chlorite alteration. Disseminated and vein style sulphide mineralization in the footwall is typically pyrite +/- sphalerite +/- chalcopyrite. Section influence is +/- 15 m.

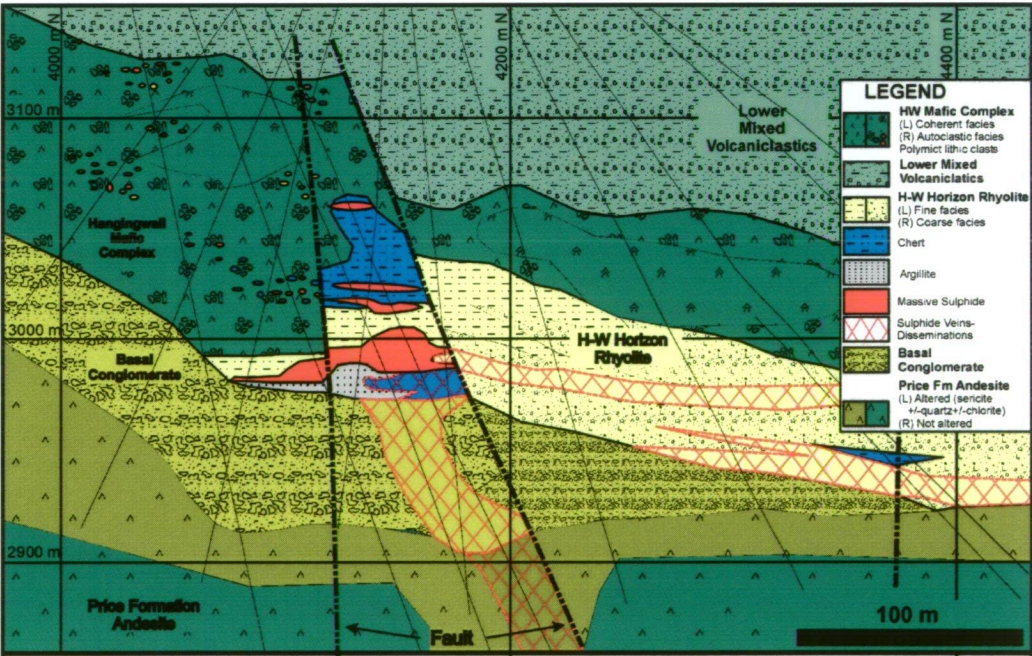


Figure 3.2b: Ridge Zone West Geology - Section +50 m E (view west)

Section 50 m E is the most mineralized area of the Ridge Zone West discovered to date. Stacked lenses are hosted by fine sediments and volcaniclastic deposits of the H-W Horizon. Sulphide clasts occur as components within H-W Horizon volcaniclastic rocks as well as within autoclastic facies of the Hangingwall Mafic Complex. Section influence is +/- 15m.

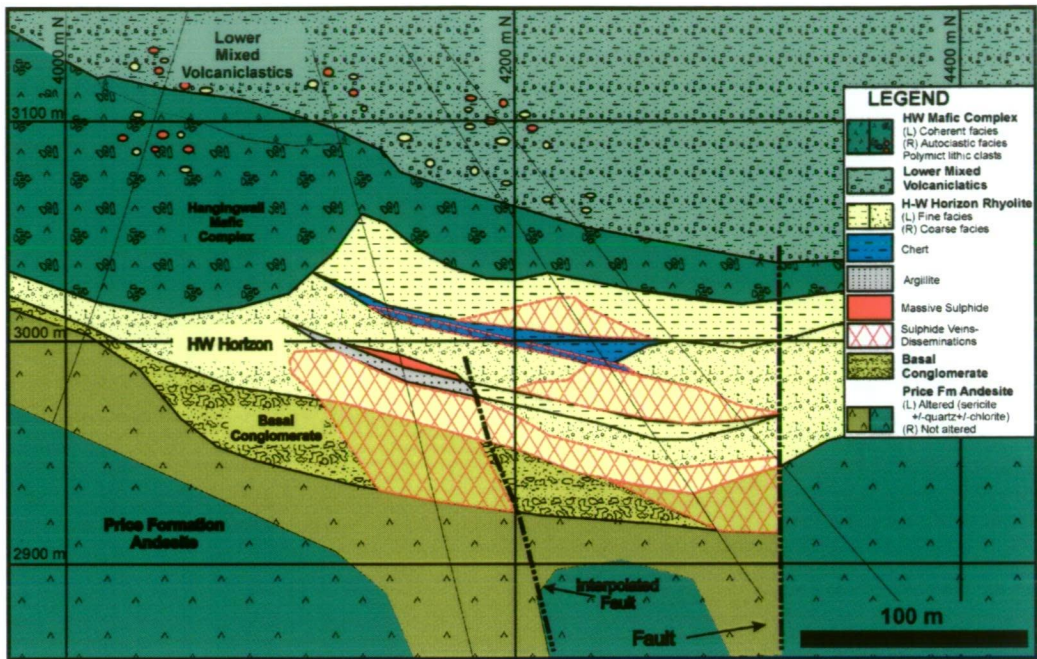


Figure 3.2c: Ridge Zone West Geology - Section +175 m E (view west)

Section 175 m E is a poorly mineralized area of the Ridge Zone West. Zinc-rich semi-massive sulphide mineralization is hosted by coarse volcaniclastic rocks overlying argillaceous fine-grained sediments. Section influence is +/- 50 m.

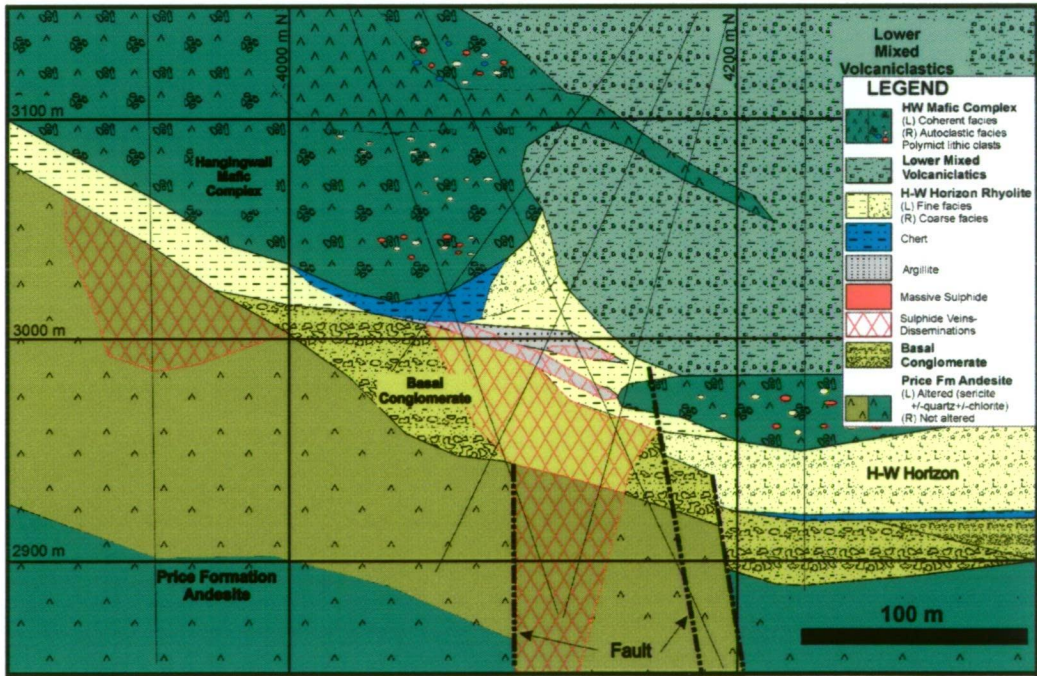


Figure 3.2d: Ridge Zone West Geology - Section +375 m E (view west)

Section 375 m E is the eastern extent of diamond drill coverage assessed for this study. Sulphide mineralization occurs as sulphide veins and disseminations associated with fine facies argillaceous mudstone of the H-W Horizon. Section influence is +/- 50 m.

Table 3.1: Descriptive names for volcanoclastic deposits.
(from McPhie et al., 1993)

| Ideal combination: ④ + ③ + ② + ① | | | | |
|----------------------------------|------------|---|--|--|
| | alteration | | lithofacies term | components |
| | e.g. | chloritic-pyritic, very thickly bedded, volcanic lithic breccia | | |
| | | thinly interbedded, shard-rich mudstone and crystal-rich sandstone | | |
| Minimum: | ② + ① | e.g. | crystal-rich sandstone; pumice granule breccia | |
| | ③ + ① | e.g. | laminated mudstone; poorly sorted, massive breccia | |
| | ④ + ① | e.g. | pyritic sandstone; chloritic breccia | |
| ① GRAIN SIZE | | | | |
| | | mud/mudstone | | < 1/16 mm |
| | | sand/sandstone | | 1/16–2 mm |
| | | gravel/conglomerate or breccia: | granule | 2–4 mm |
| | | | pebble | 4–64 mm |
| | | | cobble | 64–256 mm |
| | | | boulder | >256 mm |
| ② COMPONENTS | | | | |
| | | • crystals, crystal fragments: <i>crystal-rich</i> ... | | • shards: <i>shard-rich</i> ... |
| | | • lithic fragments: <i>lithic-rich</i> ... | | • accretionary lapilli: <i>accretionary lapilli-rich</i> ... |
| | | • volcanic or non-volcanic, polymict or monomict | | • vitriclasts: <i>vitriclast-bearing</i> ... |
| | | • pumice or scoria: <i>pumiceous</i> ..., <i>scoriaceous</i> ... | | • flame: <i>flame-bearing</i> ... |
| | | | | • cement: <i>siliceous</i> ..., <i>carbonate</i> ..., <i>zeolite</i> ... |
| ③ LITHOFACIES | | | | |
| | | • massive (non-bedded) or stratified (bedded) | | |
| | | • bedding: laminated < 1 cm | | • equal or unequal thickness |
| | | very thinly bedded 1–3 cm | | • laterally even or uneven thickness |
| | | thinly bedded 3–10 cm | | • laterally continuous or discontinuous |
| | | medium bedded 10–30 cm | | • cross-bedded, cross-laminated |
| | | thickly bedded 30–100 cm | | |
| | | very thickly bedded > 100 cm | | |
| | | • massive (non-graded) or graded: normal ↑, reverse ↓ | | |
| | | | normal–reverse ↓, reverse–normal ↑ | |
| | | • fabric: clast-supported or matrix-supported | | |
| | | poorly sorted, moderately sorted, well sorted | | |
| | | • jointing: blocky, prismatic, columnar, platy | | |
| ④ ALTERATION | | | | |
| | | • mineralogy: chlorite, sericite, silica, pyrite, carbonate, feldspar, hematite ... | | |
| | | • distribution: disseminated, nodular, spotted, pervasive, patchy ... | | |

Table 3.2: Grain size-based nomenclature for common types of volcanoclastic deposits.
(from McPhie et al., 1993)

| GRAIN SIZE | VOLCANICLASTIC DEPOSITS IN GENERAL and VOLCANOGENIC SEDIMENTARY DEPOSITS | AUTOCLASTIC DEPOSITS | | | RESEDIMENTED AUTOCLASTIC DEPOSITS |
|------------|--|--|---|---|---|
| | | Hyaloclastite | Autobreccia | Mixture or uncertain origin | |
| < 1/16 mm | volcanic mudstone | fine hyaloclastite | ? | autoclastic mudstone | resedimented fine hyaloclastite , resedimented autoclastic mudstone |
| 1/16-2 mm | volcanic sandstone | hyaloclastite sandstone | | autoclastic sandstone | resedimented hyaloclastite sandstone, resedimented autoclastic sandstone |
| 2-4 mm | volcanic conglomerate, volcanic breccia | granular hyaloclastite | granular autobreccia | granular autoclastic breccia | resedimented granular hyaloclastite, resedimented granular autobreccia, resedimented granular autoclastic breccia |
| 4-64 mm | | hyaloclastite breccia | autobreccia | autoclastic breccia | resedimented hyaloclastite breccia, resedimented autobreccia, resedimented autoclastic breccia |
| > 64 mm | | coarse hyaloclastite breccia | coarse autobreccia | coarse autoclastic breccia | resedimented coarse hyaloclastite breccia, resedimented coarse autobreccia, resedimented coarse autoclastic breccia |
| | | | | | |
| GRAIN SIZE | PYROCLASTIC DEPOSITS | | PYROCLAST-RICH DEPOSITS | | |
| | Unconsolidated tephra | Consolidated pyroclastic rock | RESEDIMENTED SYN-ERUPTIVE | Post-eruptive resedimented or reworked, or uncertain origin | |
| < 1/16 mm | fine ash | fine tuff | resedimented ash-rich mudstone | tuffaceous mudstone | |
| 1/16-2 mm | coarse ash | coarse tuff | resedimented ash-rich sandstone | tuffaceous sandstone | |
| 2-64 mm | lapilli tephra | lapillistone (or lapilli tuff or tuff-breccia) | resedimented pyroclast-rich lapillistone, resedimented pumice lapillistone, resedimented pumice and lithic lapillistone | tuffaceous conglomerate, tuffaceous breccia | |
| > 64 mm | bomb (fluidal shape) tephra, block (angular) tephra | agglomerate (bombs present), pyroclastic breccia | resedimented pyroclast-rich breccia, resedimented pumice breccia, resedimented pumice and lithic breccia | | |

3.2 Footwall Volcanic Rocks

3.2.1 Price Formation Facies

Monomict, autoclastic andesite facies

This facies is dominantly a monomict, fragmental facies with up to 50% feldspar porphyritic andesite clasts associated with the massive, coherent andesite facies (Fig. 3.3A). Clasts are typically subangular but can be locally subrounded. Sericite-altered fragments with curvilinear forms and altered hyaloclastite textures are also observed. Sand to granule sized matrix supports coarse monomict angular fragments. This facies is up to 18 m thick and is intercalated with the massive coherent facies throughout the study area.

Massive coherent andesite facies

This facies is typically a weak to moderate chlorite+sericite altered, <5% feldspar +/-pyroxene phyric, massive coherent amygdaloidal andesite (Fig. 3.3B, C). Amygdules are filled with silica+/-epidote+/-chlorite+/-calcite+/-pyrite and are up to 2 mm diameter. This facies is found throughout the study area and is the major facies type of the Footwall Andesite.

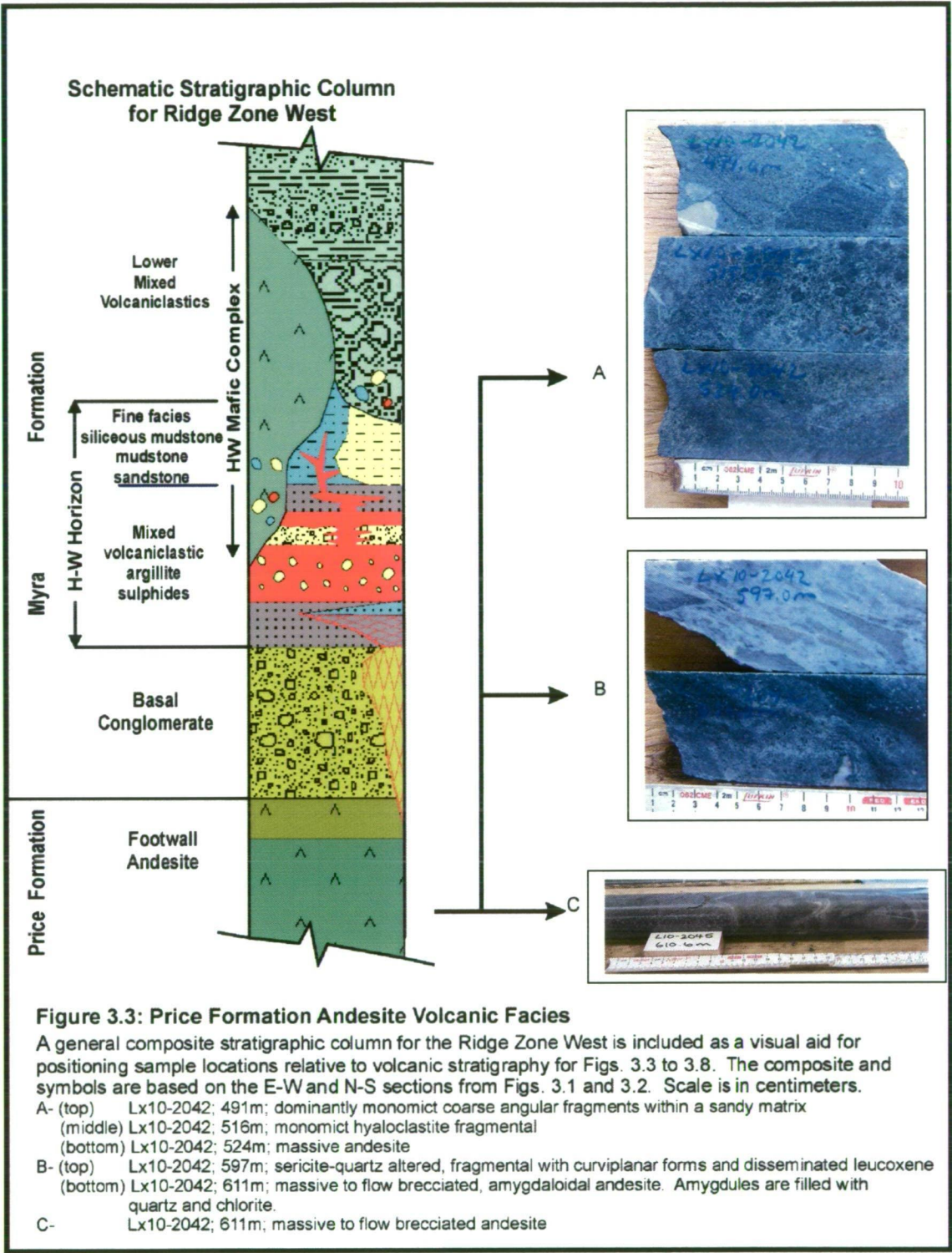
3.2.2 Basal Conglomerate Facies

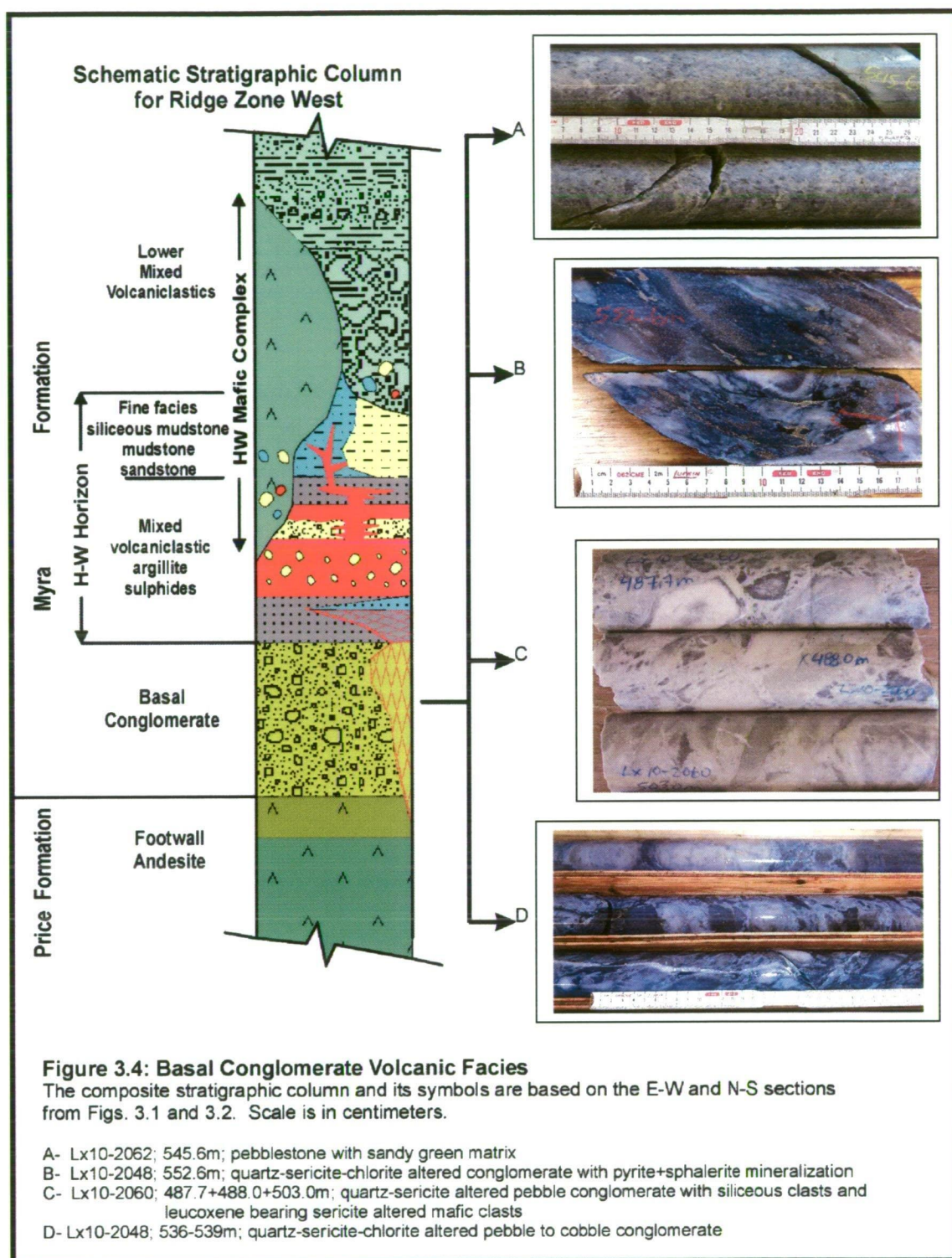
Polymict pebble bearing sandstone facies

The polymict pebblestone is spatially associated with an unsorted, monomict coarse cobblestone (Fig 3.4A). This facies is volumetrically less than the underlying polymict pebble conglomerate. Components are massive, coherent, mafic to intermediate in composition, with up to 5% angular siliceous pebbles within a green, sandstone matrix.

Polymict, pebble to cobble conglomerate facies

The basal pebble conglomerate facies is a polymict pebblestone with a quartz-sericite+/-chlorite altered sandstone matrix (Fig. 3.4B, C, D). The pebbles consist of reworked, subrounded siliceous clasts, subrounded to subangular leucocrystalline-bearing mafic clasts, and minor quartz+pyroxene phyric clasts. This volcanoclastic facies is either clast or matrix supported and is normally graded. On section 4150 N (Fig. 3.1) thickness ranges between 30 m at the east end of the study area increasing to 90 m towards the western end. The north-south extent of the facies appears to be at least 400 m trending beyond the limits of the study area (Fig. 3.2A-D). Greatest thickness appears to be below the mineralized lenses (Fig. 3.2A-B) with thinning to the north and south.





3.2.3 Footwall Price Formation Andesite and Basal Conglomerate:

Facies Relationships

Massive coherent andesite is the dominant footwall lithology in the Ridge Zone West area. Where this facies occurs, there is no difficulty defining the footwall of the H-W Horizon. The massive, feldspar and pyroxene-phyric, amygdaloidal andesite is interpreted to be a coherent flow with autoclastic breccias at the flow margins. Breccia components observed are monomict, fine to coarse, poorly sorted, mafic fragments with globular and angular curvilinear forms. Local angular coarse fragmental rocks with a sandy, mafic matrix may be either autobrecciated margins of a flow or possible volcanoclastic deposits (Fig. 3.3A). The setting is interpreted to be subaqueous based on the angular curvilinear quench textures of the autobrecciated margins. Absolute water depth is not constrained by the presence of amygdaloids and the textures described above.

The Basal Conglomerate (polymict conglomerate facies) is found in paleo-depressions where coarse, subrounded to subangular clasts of variable provenance have been deposited. Figs. 3.1 and 3.2 show that the Basal Conglomerate overlies massive coherent and autobrecciated andesite flows of the Price Formation. Subrounded, cobbles-sized, polymict clasts suggest mechanical abrasion and transport by gravity mass flow processes. The unsorted nature and size distribution of clasts within the conglomerate implies a process that would have occurred during one or more high-energy mass flow events within a short time span.

The polymict components for the Basal Conglomerate are of variable provenance. Based on section 4150 N (Fig. 3.1) provenance, or source direction, appears to be from the west as the greatest overall unit thickness is west with relative thinning eastward. This is supported by inference, as the Basal Conglomerate does not occur within the Battle and H-W deposit volcanic sequences located to the east.

The greatest apparent thickness of the Basal Conglomerate underlies sulphide mineralization between -050E to 050E, suggesting a paleo-basin within the Price Formation andesite or thickening due to structural folding. The upper contact of the Basal Conglomerate is interpreted to represent the paleo-seafloor prior deposition of fine facies rocks for the H-W horizon and the Ridge Zone West sulphide lenses.

3.3 H-W Felsic Horizon Rocks

3.3.1 Volcanic Facies

Coarse facies felsic pebbly sandstone facies

The felsic pebbly sandstone facies is a sericite-altered, matrix supported, polymict, pebbly sandstone. Clasts make up 10-15% of the overall facies by volume. The clasts are subrounded to subangular and are composed of either silica-altered or sericite+/-chlorite-altered mafic clasts. Siliceous clasts are the dominant clast type present and vary between 15-35 mm. There are minor (<3%) reworked, sericite-altered pumice-scoria fragments with silica filled vesicles. The matrix consists of massive, intermediate to felsic sericite-altered sandstone and granulestone. The sandstone-granulestone matrix has up to 7% of 0.5 mm quartz grains (Fig. 3.5A, B). This facies volumetrically makes up the majority of H-W Horizon rocks and is spatially associated with the known mineralization.

Fine facies felsic massive granulestone to sandstone facies

This facies is pale grey-white, massive to diffusely bedded granulestone to sandstone intercalated with other facies of the H-W Horizon. Siliceous granules are subangular to subround. Subrounded reworked quartz grains make up 3-5% of the facies and are up to 1.5 mm in size. Weak to moderate pervasive sericite alteration is typical for this facies (Fig. 3.5A).

Fine facies argillite facies

The argillite facies is black, massive, weakly foliated fine-grained sediment with 5-7% fine-grained disseminated pyrite and local disseminated fine-grained sphalerite and galena. The argillite facies overlies the Basal Conglomerate and is in contact with sulphide mineralization, unsorted polymict pebblestone, and siliceous mudstone breccias (Fig. 3.5C).

Fine facies siliceous mudstone facies (Chert)

This facies is a pale white to grey, very fine-grained, mudstone with diffuse bedding and laminations (Fig 3.6B, C). The mudstone is intercalated with narrow quartz+sericite altered pebblestone as well as unsorted mudstone breccia (Fig 3.6A). Individual mudstone breccia fragments have inconsistent bedding orientations relative to drill core orientation. This facies has a weak to moderate pervasive sericite alteration and 10-15% quartz+sericite+/-pyrite veins. This facies is known as “chert” in mine terminology at Myra Falls.

Mafic intrusion

The mafic intrusion has very fine-grained, coherent andesite dykes and sills with variable widths in drill core between 0.1-2.0 m. The intrusions typically have sharp contacts and chilled margins up to 2.0 mm wide. Quartz and carbonate occurs in randomly oriented fracture veinlets and tension gash fillings. The mafic intrusion has up to 7% disseminated 1.0 mm size pyroxene phenocrysts.

Quartz porphyritic rhyolite

This facies is a light grey, massive, quartz phyric rhyolite and is observed adjacent to faults and between or within andesite flows. Thickness is up to 1 m wide in drill core and contacts are gradational. Due to the narrow thicknesses, poor contact relationships, proximity to faults and andesite flows, this facies may be an altered lithic component emplaced adjacent to a synvolcanic fault or between andesite flows.

3.3.2 H-W Felsic Horizon Facies Relationships

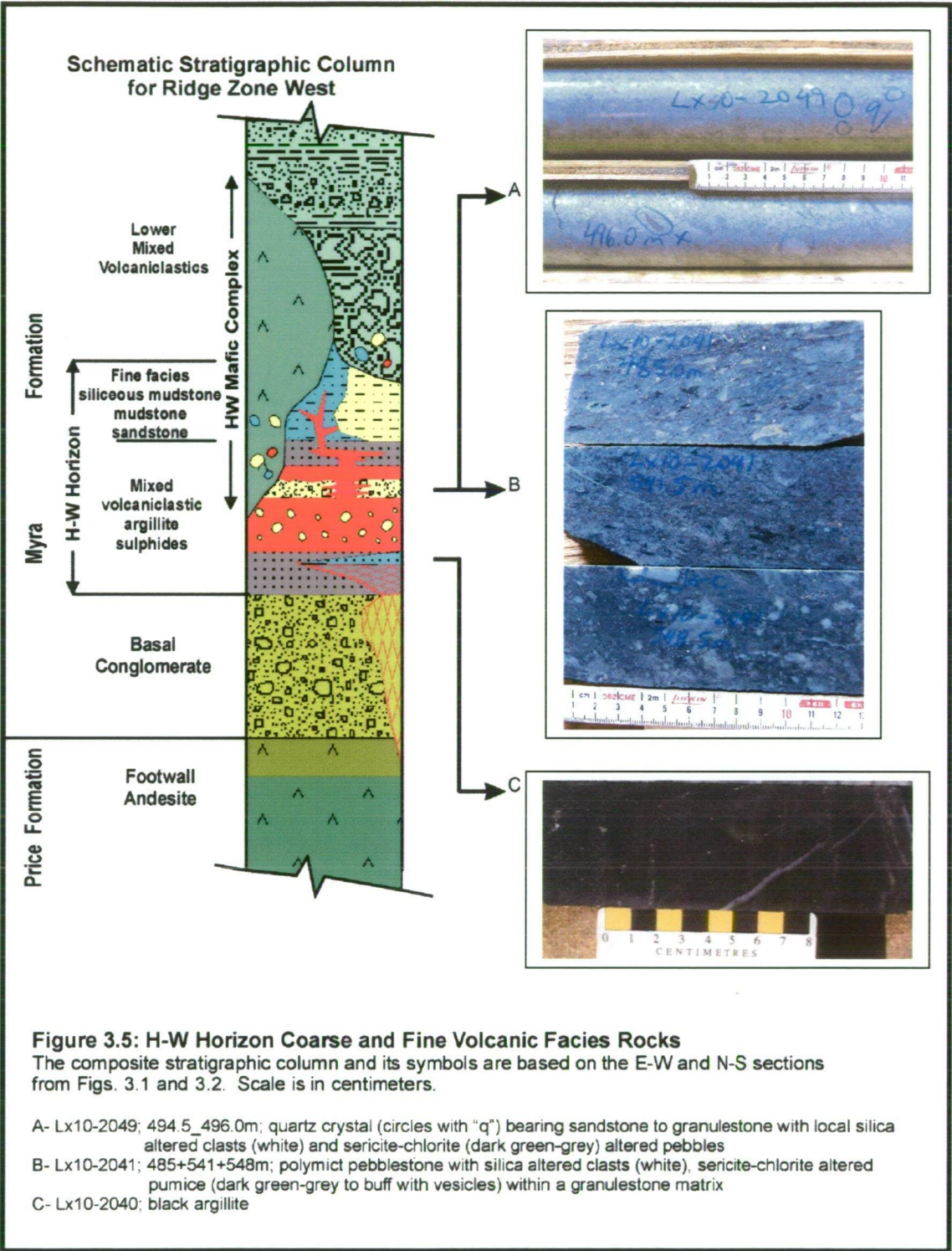
The coarse-grained volcanoclastic facies of the H-W Horizon are interpreted to be a series of poor to moderately sorted, high concentration sediment gravity flows (mass flows) with components of variable provenance. The subrounded siliceous pebbles+/-cobbles are reworked lithic clasts. Abrasion of the clasts may have been due to erosion with subsequent transportation to the site of deposition or from mass flow transport and abrasion. Lithic clasts of mudstone origin must have formed below wave base implying transport and re-deposition by the host gravity flow.

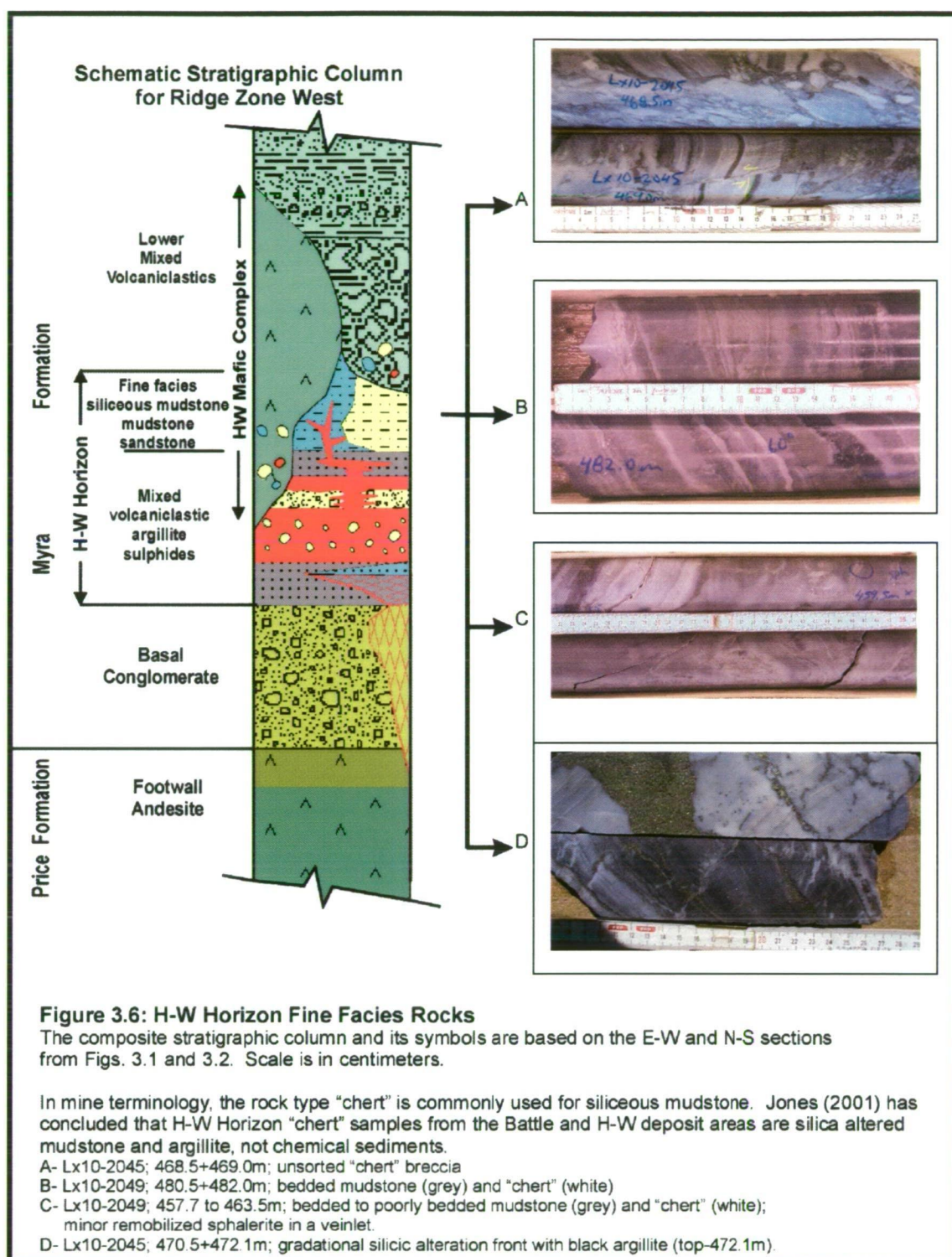
Fine-grained volcanic facies massive sandstone-granulestone is a minor component of the H-W Horizon. It typically occurs between two pebbly sandstone intervals and is 1-5 m thick. Greater thickness of up to 22 m are observed where pebbly sandstone facies are normally graded up to a sandstone-granulestone facies, and subsequently overlain by a diffuse or laminated mudstone facies.

Diffuse and laminated mudstone is typically located towards the upper portion of the H-W Horizon. The facies represents either a pale grey-white, silicified mudstone or volcanic ash from suspension sediments (Allen, 1993). Jones (2001) concluded that “chert” samples around the Battle and H-W deposits at Myra Falls are silica-altered mudstones, not chemically derived sediments.

Mudstone and siliceous mudstone is spatially associated with the massive sulphide mineralization, particularly where the facies becomes brecciated or interbedded with pebble breccias. Bedding angles are highly variable and some beds are folded in core. The breccia mudstone fragments are interpreted to be clasts. Folded beds may be formed by syndepositional soft sedimentary deformation or by subsequent post-lithification deformation.

Subordinate intervals of black, pyritic mudstone/argillite are also observed. Spatially, the argillite occurs at a lower stratigraphic horizon and is more dominant volumetrically in the eastern half of the study area (Fig 3.1). Fine facies mudstone and argillite are submarine rock types formed below wave base, commonly within restricted basins. The limited N-S extent of the argillaceous mudstone suggests a narrow, elongate, paleo-depression for the sulphide mineralization. The occurrence of intercalated volcanoclastic pebblestone with these fine sediments implies influx of synchronous, intermittent volcanoclastic deposits during their formation.





3.4 Hangingwall Mafic Complex

3.4.1 Volcanic Facies

Massive, coherent andesite facies

The massive, coherent andesite facies of the Hangingwall Mafic Complex has both domed and sheet geometries. It is pyroxene-phyric and contains up to 7% anhedral plagioclase phenocrysts towards the base of the facies (Fig. 3.7C). The basal contacts are sharp or have 0.1-1.0 m intervals with intermixed siliciclastic sediments possibly excavated from the substrate. Individual units are up to 10 m thick.

Monomict, autoclastic andesite facies

The autoclastic andesite facies has 75% subangular to subrounded blocky, mafic breccia components (Fig. 3.7C) and less common angular, fine to coarse-grained, jigsaw fit autoclasts with curvilinear margins (Fig. 3.7B). Individual unit thickness is up to 8.0 m. This facies is typically found at or proximal to the margins of a massive coherent facies.

Polymict Breccia facies

This facies has 20% subangular to subrounded, pyroxene phyric clasts of andesite 10 to 30 mm in diameter, supported by a green, fine sand matrix. Minor felsic clasts are observed towards the base of the facies. The basal part of this facies is massive to texturally chaotic grading up into thinly bedded volcanic sandstone. This facies is commonly located at the margins of the massive coherent and autoclastic mafic facies in transition with laterally equivalent polymict pebblestone (Fig. 3.7A, D).

3.4.2 Hangingwall Mafic Complex facies relationships

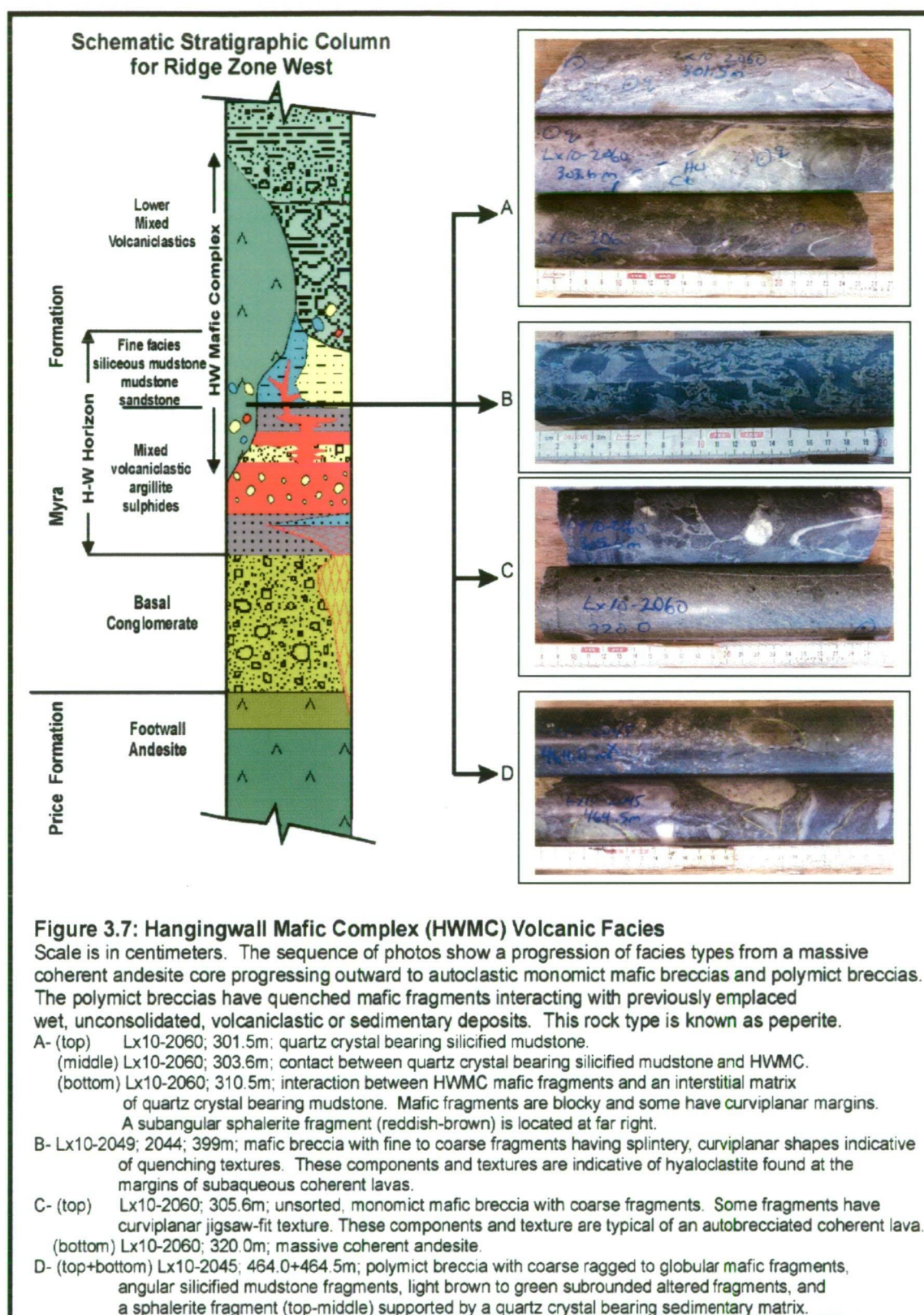
The Hangingwall Mafic Complex flow-sill unit appears to be a concordant, pyroxene phyric, massive, coherent, andesite unit with its thickest accumulation centered about 4025N / 3050m elevation. The complex thins northward and has a sheet-shaped geometry. This unit is continuous over the entire 650 m strike length of the current drill coverage. The sheet geometry in the north half of the study area is partly disrupted and has varying elevations within the stratigraphic pile.

Autoclastic breccia margins have coarse, blocky, subrounded to subangular, monomict, jigsaw-fit fragmentation and are interpreted to be the result of autobrecciation. Autobreccia is formed by non-explosive fragmentation of cooler, more viscous, lava at the margins of a flow or intrusion (McPhie et al., 1993). The jigsaw-fit nature of the fragments implies in-situ fragmentation.

Fine to coarse-grained hyaloclastite breccia is observed with individual fragments having glassy, angular, jigsaw fit, and curvilinear quench textures. Hyaloclastite breccia is formed by non-explosive fracturing and disintegration of quenched lavas and intrusions (McPhie et al., 1993). Fragmentation is due to thermal stress, built up during rapid cooling, and stress imposed on chilled outer parts of lava flows and intrusion by continued movement of the ductile interior (Kokelaar, 1986). The jigsaw-fit nature of the fragments is characteristic of an in-situ hyaloclastite rather than a resedimented hyaloclastite.

Facies transition from monomict mafic autoclastic facies to polymict volcanic breccias is found at the interface between polymict pebblestone and the Hangingwall Mafic Complex. Mafic fragments are coarse with ragged, angular curvilinear and globular form. The mafic fragments are supported by a matrix of the surrounding volcanoclastic deposits (Fig. 3.7A, D). Hangingwall and lateral contacts are gradational into the matrix supported, polymict breccia. The textures of the mafic fragments interacting with the adjacent volcanoclastic deposits, the spatial association to the coherent and brecciated margins of a mafic flow-intrusion is commonly observed for a volcanic rock known as peperite. Peperite is a rock generated by the mixing of coherent lava or magma with unconsolidated wet sediment (Williams and McBirney, 1979). It commonly occurs at the contacts between intrusions and wet sediments, and along basal contacts of lava flows that override or burrow into unconsolidated sediments (Schmincke, 1967).

Based on the above observations, the Hangingwall Mafic Complex is a mafic flow or sill with a massive coherent core. The core has a dominantly mafic autoclastic carapace grading out into a polymict breccia intermixed with wet, unconsolidated, volcanoclastic deposits. Hence, the Hangingwall Mafic Complex is a synvolcanic flow or sill deposited after H-W Horizon rocks. The unaltered nature of the unit suggests emplacement after the main mineralizing event responsible for forming the Ridge Zone West lenses.



3.5 Lower Mixed Volcaniclastic (LMV)

3.5.1 Volcanic Facies

Volcanic Mudstone Facies

This facies is green to grey and ranges between 1 to 3 m thick with individual beds up to 1 cm thick. Mudstone intervals are typically at or near the top of a coarse to fining up sequence (Fig. 3.8 A). Contorted, soft sediment deformed beds of the mudstone is rare.

Pebbly Sandstone Facies

The pebbly sandstone facies is a medium green, diffusely bedded to massive green sandstone supporting 5 to 20% subangular pale yellow-green to yellow-white altered pebble clasts of intermediate composition. Beds between 1 to 3 m thick are normal and / or reverse graded (Fig. 3.8B). Massive sequences of pebbly sandstone with no apparent grading have thicknesses up to 20 m.

Polymict Pebblestone Facies

The polymict pebblestone facies of the LMV have subangular to angular pebble size andesite clasts comprising 90 to 95% of the facies and 5% yellow-white altered intermediate-felsic clasts (Fig. 3.9B). Some intermediate-felsic clasts have relict textures that may have been either bedding or flow banding. Occasional subrounded, pale white siliceous clasts are quartz phyric. This facies is clast supported with minor interbedded volcanic sandstones. Individual bedding laminations are up to 3 mm thick. Weak to moderate patchy epidote+quartz veinlets occur throughout the unit.

Massive Coherent Andesite Facies

This facies is a medium green, massive, coherent andesite with trace to 3% anhedral to subhedral feldspar phenocrysts and is gradational into the andesite breccia facies (Fig. 3.8C). Quartz+carbonate veining can produce pseudo fragmental texture.

Andesite Breccia Facies

This facies is a massive andesite with 5 to 20% monomict autobrecciated fragments (Fig. 3.8D). Hyaloclastite breccia has fine to coarse, monomict, angular andesite fragments with curvilinear margins and jigsaw-fit texture. This facies is up to 10 m thick with contacts subparallel to bedding in adjacent facies. Contacts are typically autobrecciated with some minor quench textures.

3.5.2 Lower Mixed Volcaniclastic (LMV) Facies Relationships

The LMV has thick sequences of polymict pebblestone intercalated with intervals of normal to reverse graded pebbly sandstone and thickly bedded to laminated sandstone. Bedded mudstone is also noted at the top of fining up sequences (Fig. 3.8A). Fining up sequences are 1 to 5 m thick. Some isolated mudstone intervals have deformed bedding laminae in contrast to non-deformed adjacent units. This texture is commonly associated with soft sediment deformation due to the rapid accumulation and loading by subsequent overlying deposits prior to lithification.

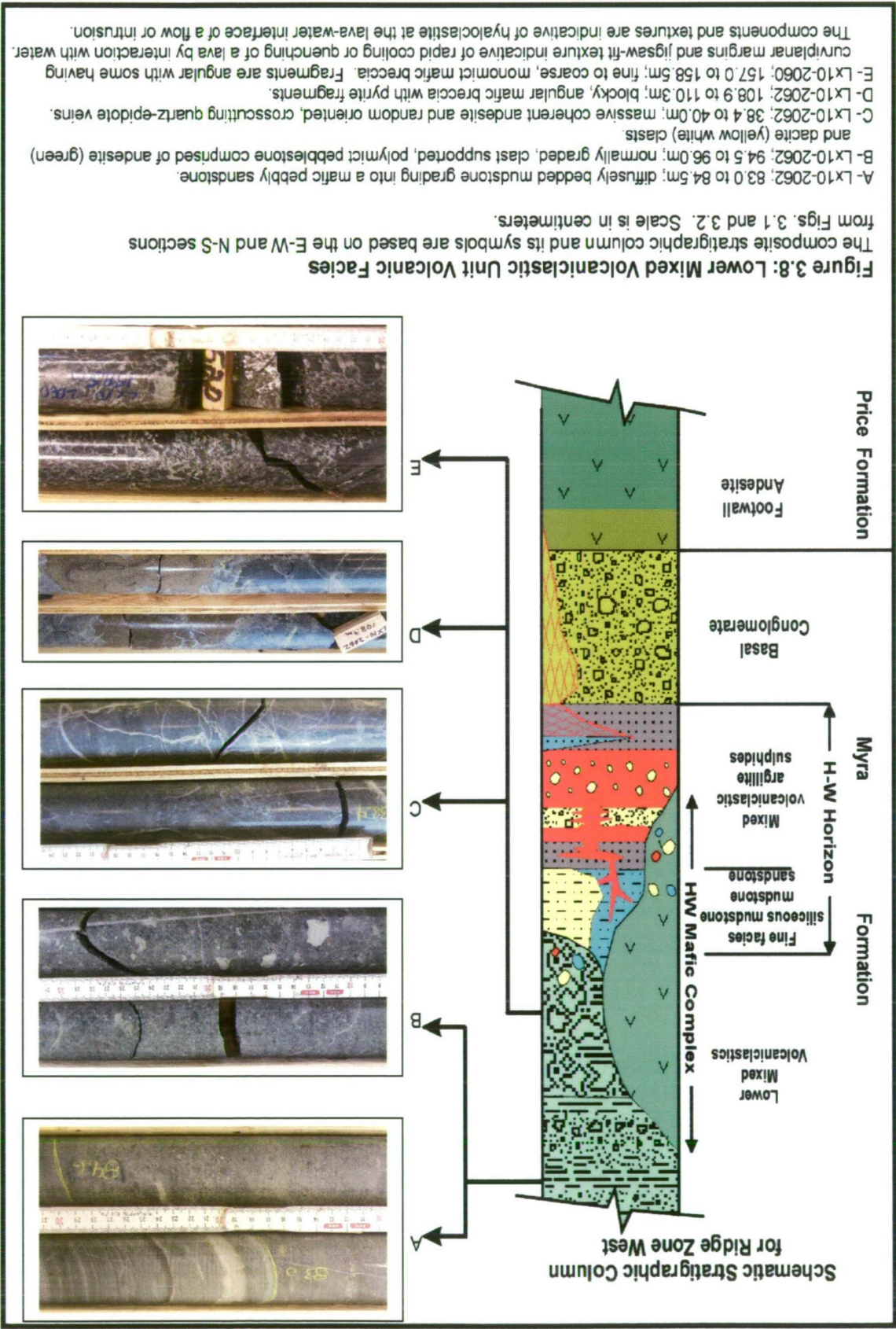
Massive, thick sequences of polymict pebblestone and pebbly sandstone indicate an accumulation of reworked proximal, angular to subangular mafic clasts with subordinate altered intermediate-felsic clasts. Intervals have up to 15% pebble-size clasts (Fig. 3.8B).

Repeated fining upward sequences of pebbly sandstone to diffuse and bedded sandstones and mudstone for the LMV is interpreted to be the product of both high and low-density turbidity currents. Gravelly high density currents can carry up to 15% pebble and cobble size particles, together with clay to coarse sand, supported by a combination of dispersive pressure and matrix buoyant lift (McPhie et al., 1993). Sandy high-density currents are dominated by sand size particles with minor granules or pebbles. Particles are supported mainly by turbulence (McPhie et al., 1993). Reverse graded sequences represent traction-carpet deposits (Lowe, 1982). Normally graded sandstones are deposited directly and rapidly from dense suspension (Lowe, 1982). Sandy high-density turbidity currents occur progressively from the base up in stages that reflect increasing flow unsteadiness and decreasing flow competence (McPhie et al., 1993).

For sandy high-density turbidite sequences, normal to reverse graded pebbly-sandstone to sandstone sequences often overlie traction structures such as plane laminations and cross stratification found at the base of a sequence (Lowe, 1982). These bed forms are not common in the LMV within the Ridge Zone West area.

Minor coherent to brecciated andesite flows and / or sills appear to have similar dips to beds in adjacent units. Fine-grained, coherent andesite lavas occur as massive flow-sills or as blocky breccias with local occurrences of medium grained pebble size pyrite clasts (Figs. 3.8C and D). Fine, monomict, autoclastic mafic breccia have jigsaw-fit fragments with curvilinear margins indicative of hyaloclastite quench texture due to the

interaction of a hot lava with cold seawater (Fig. 3.8E). Late quartz-carbonate-epidote veining is common and probably due to regional metamorphism.



3.6 Comparison with Myra Falls Volcanic Stratigraphy

The general volcano-sedimentary stratigraphic sequence for the Ridge Zone West study area is similar to that recorded for other areas at Myra Falls such as the Battle and H-W deposit areas, and the Price Hillside area (Walker, 1985; Juras, 1987; Robinson, 1994; Pearson 1993; Barrett and Sherlock, 1996; Sinclair, 2000; and Jones, 2001). This lithofacies correlation is based on volcanic stratigraphy for each of the main formations found on the property and their subordinate sub-units; namely the footwall Price Formation andesite and the Myra Formation's, mineralized H-W Horizon, hangingwall mafic flow-sill units and the overlying Lower Mixed Volcaniclastic unit (Figs. 2.4 and 3.1).

The existence of the same general volcanic stratigraphy, including the mineralized H-W Horizon establishes continuity for at least 5 km along strike (sections –250 E to 4800 E) and the potential for massive sulphide mineralization is open westward (Fig. 2.5). Exploration diamond drill programs have traced the H-W Horizon for at least 1 km north of the Ridge Zone West. This is where the recently discovered Marshall Zone lenses are located (Fig. 2.5). Mine grid N-S extent of the H-W Horizon is at least 1 km but the limits have not been found.

An exception to the general volcanic stratigraphy at Myra Falls is the Basal Conglomerate. In the Ridge Zone West area, immediately overlying the basement Price Formation andesite is the Basal Conglomerate (Figs. 3.1 and 3.2a-d). Overlying the Basal Conglomerate are volcano-sedimentary rocks and massive sulphide mineralization (Ridge Zone West) of the H-W Horizon. The Basal Conglomerate does not occur within the Battle and H-W deposit volcanic sequences 1 to 3 km to the east. In these areas, immediately overlying the Price Formation andesite is the H-W Horizon (Figs. 2.7 and 2.8). These observations support the interpretation of a western provenance for the Basal Conglomerate.

The Basal Conglomerate occurs stratigraphically below massive sulphide mineralization for the Ridge Zone West. The main massive sulphide lenses for the Battle and H-W deposits occur either at or proximal to the Price Formation andesite contact. Timing of deposition for the Basal Conglomerate is therefore interpreted to be during a short time span, prior or possibly partially synchronous with the main mineralizing event(s) responsible for forming the Ridge Zone West, Battle and H-W deposits.

The geology at Myra Falls is continuous on a mine grid E-W trend but has abrupt facies changes in the N-S orientation (Walker, 1985) (mine grid north is rotated 48 degrees

east of true north). Volcanic facies in the Ridge Zone West study area have similar characteristics for the major units with good continuity E-W (Figs. 3.1 and 3.2a-d) and rapid facies changes in the N-S orientation (Figs. 3.2a-d).

3.7 Ridge Zone West Alteration

The following is a brief discussion on the spatial distribution of the alteration mineral assemblages based on drill core observations, historical drill log descriptions, and section interpretations. An in-depth study of the alteration will not be presented as the emphasis for this study is on the Zn-rich polymetallic mineralization.

3.7.1 Footwall Alteration

The footwall alteration is semi-conformable with the upper contact of the Price Formation andesite and the overlying Basal Conglomerate. The extent of the alteration system has not been defined in the N-S or E-W directions. Alteration within the Price Formation andesite comprises the mineral assemblage sericite-quartz-chlorite and is weak to moderately developed (Fig. 3.3). The alteration is generally semi-conformable and within 30 m of the upper contact of the Price Formation (Figs. 3.1 and 3.2).

Alteration within the Price Formation andesite is only observed at depths greater than 30 m relative to the upper contact in three locations: (1) proximal to ESE-WNW trending, steep north dipping faults located north and south of the Ridge Zone West mineralization (Figs. 3.2a-d), (2) section 375E, approximately 150 m south of the Zn-rich mineralization where moderate quartz-sericite+/-chlorite alteration is observed down to approximately 130 m vertical below the upper contact in drill hole LX10-2062 (Fig. 3.2d), and (3) an area in the vicinity of -250E located below significant Zn-rich polymetallic mineralization (Fig. 3.1). The lower limit of alteration depth for areas (1) and (3) has not been defined. Sulphide mineralization associated with footwall alteration comprises up to 3% pyrite+/-sphalerite+/-chalcopyrite disseminations and veins. The sulphide disseminations and veins are most common near the ESE-WNW trending faults. Drill hole LX10-2062 on section 375E has up to 3% pyrite+/-chalcopyrite+/-sphalerite veins within 50 m of the upper Price Formation contact.

The Basal Conglomerate is pervasively altered by quartz-sericite+/-chlorite and is dependent on the primary composition of the clasts and matrix. The unit has a characteristic pale white colour and original clast shapes are preserved (Fig. 3.4). Siliceous, pebble and cobble-size clasts have dark grey and white internal zonation. Sericite altered clasts commonly have relict leucoxene. Sulphide mineralization associated with the

hydrothermal alteration has up to 5% sphalerite-pyrite+/-chalcopyrite+/-galena disseminations and veins (Fig. 3.4b) with trace to 2% occurrences most common. Sericite-quartz+/-chlorite alteration, and associated sulphide mineralization near faults below the Zn-rich polymetallic mineralization, is interpreted to have steep orientations (Figs. 3.2a-d).

3.7.2 H-W Horizon Alteration

Alteration in the H-W Horizon is weak to moderate with original textures preserved. The alteration assemblage is sericite-quartz. Fine-grained siliceous mudstone, or chert in mine terminology, is a quartz-sericite altered facies located stratigraphically below and above the Ridge Zone West mineralization. The most prominent occurrence of siliceous mudstone is on section 50E (Fig. 3.1 and 3.2b) and is spatially associated with the most significant Zn-rich, polymetallic mineralization of the Ridge Zone West. Other areas with siliceous mudstone in the stratigraphic hangingwall to the Ridge Zone West mineralization are sections on -250E, -50E, and 175E.

Jones (2001) investigated the origin of the siliceous “cap” rocks at Myra Falls. The Battle deposit cherts are characterized by many features suggesting replacement of the pre-existing sediments rather than as a primary accumulation of amorphous silica. Some of the features described by Jones (2001) include:

- Sedimentological and petrological similarities to adjacent fine-grained sediments such as fine laminations, soft-sediment deformation, interbedded turbidites, and the presence of radiolarians.
- Argillite and chert occur at the same stratigraphic level.
- Silica alteration fronts gradationally separate chert from mud.
- The microcrystalline groundmass overprints earlier lithological variations such as increase in grain size of detrital elements.
- Diffuse contacts between the argillite, black chert and pale-grey mudstones.
- Similar immobile element signature of chert and adjacent argillite.
- The Battle chert samples plot in the non-hydrothermal or terrigenous field on the Al-Fe-Mn ternary Bostrom plot.
- Enrichment in the metals Zn, Cu, Pb, Cd, As, S, U and V suggest a hydrothermal component.
- Mass balance relationships between the Battle chert and unaltered argillite indicate the addition of up to 200% SiO₂ for white chert.
- A distinct shift from light $\delta^{34}\text{S}$ values in unaltered argillite, to heavier $\delta^{34}\text{S}$ values in black chert reflecting input of hydrothermal sulphur into seafloor sediments.

Observations suggesting the Ridge Zone West siliceous sediments are possibly related to hydrothermal alteration are:

- The siliceous sediments occur at the same stratigraphic position as argillaceous mudstones (Figs. 3.1 and 3.2).
- The siliceous sediments occur at varying elevations within the stratigraphic sequence proximal and coincident with sulphide mineralization (Figs. 3.1 and 3.2b).
- Silica alteration fronts recognized between siliceous mudstone and adjacent argillaceous mudstone (Fig. 3.6d).

3.7.3 Regional Metamorphism

Regional alteration mineralogy has been characterized by Juras (1987) and Sinclair (2000). Price Formation andesite is characterized by the metamorphic mineral assemblage chlorite-epidote-albite-carbonate. This low grade metamorphism is not texturally destructive. Regional alteration for H-W Horizon volcanoclastic rocks is pervasive, texturally non-destructive, and has the mineral assemblage albite-quartz-epidote-sericite+/-chlorite+/-hematite for feldspar porphyritic felsic volcanic rocks (Juras, 1987; Sinclair, 2000). Quartz-feldspar porphyritic rhyolite has the metamorphic assemblage sericite-quartz-albite+/-chlorite (Juras, 1987).

3.7.4 Myra Falls Hydrothermal Alteration

Price Formation Footwall Alteration:

Footwall alteration in the Price Formation andesite can be traced discontinuously along inferred fissure systems associated with subparallel graben systems over at least 3 km. The most intense alteration is centred below several major deposits. Hydrothermal alteration within the footwall Price Formation is typically intense and texturally destructive when proximal to massive sulphide mineralization. Hydrothermal alteration mineral assemblages are sericite-quartz-pyrite+/- Mg-chlorite for the H-W, Extension and Battle deposits.

The H-W deposit is an asymmetric, low aspect ratio polymetallic massive sulphide deposit formed on the seafloor (Barrett and Sherlock, 1996; Jones, 2001). The footwall alteration geometry is pipe shaped located immediately below the deposit. Barrett and Sherlock (1996) noted strong sericite-pyrite+/-silica alteration for about 30 m below the deposit with chemical evidence extending at least to twice that depth. An additional flanking zone consists of moderate to strong albitization and silicification yielding an assemblage of albite-quartz+/-sericite+/-chlorite (Juras, 1987; R. Sawyer, pers. comm.).

Associated sulphide mineralization includes sub-economic disseminated to massive veins of coarse-grained recrystallized pyrite, disseminated to stockwork style veinlets of chalcopyrite and sphalerite.

Battle area deposits are interpreted to be low aspect ratio sheet style lenses, possibly formed by a series of coalescing mounds at or below the seafloor (Robinson, 1994; McKinley, 1997; Sinclair, 2000). Footwall alteration has the appearance of a stratabound blanket of intense muscovite-quartz-pyrite alteration with an approximate thickness of 20 to 30 m and an unknown lateral extent Sinclair (2000). Mine geologists have traced the intense footwall alteration for at least 700 m along strike. Below 30 m, a less intense zone of sericite-chlorite-pyrite alteration occurs to a much greater, undefined depth.

The main Battle area footwall alteration is intense, texturally destructive and has a mineral assemblage of coarse muscovite-quartz-pyrite+/-Mg-chlorite+/-calcite+/-rutile with sub-economic pyrite+/-chalcopyrite+/-sphalerite+/-galena disseminations and stringers (Robinson, 1994 and Sinclair, 2000). Mg-chlorite alteration occurs in small, discontinuous, sub-horizontal patches on centimeter to meter scale domains within the sericite-pyrite alteration (Sinclair, 2000)

Of note are two subparallel fissures interpreted from diamond drilling and drift mapping by mine geologists that partition the Battle deposit area into south, central, and north portions. The interpreted fissures appear to have feeder systems with a greater vertical component than indicated by Sinclair (2000).

Hangingwall Alteration in Felsic H-W Horizon rocks:

Hangingwall alteration in VHMS systems is typically less intense than footwall alteration and commonly lacks sulphide minerals (Large, 1992). The typical hangingwall mineral assemblage found at Myra Falls is white mica-quartz+/-chlorite (Jones, 2001). Chlorite is present as a minor component and more prevalent in the dacitic and andesitic lithologies.

Hangingwall alteration for the Upper Zones above the Battle Zone is interchangeably categorized as footwall alteration for Upper Zones in the Battle deposit area. Sinclair (2000) has noted three overlapping styles with the mineral assemblage sericite-quartz-pyrite+/-dolomite:

- Sericite alteration intimately associated with the felsic volcanoclastic rocks weakening with increasing distance from the massive sulphide lenses
- Silicification that post dates the sericite alteration, and
- Dolomite alteration as discrete zones at the top of the H-W Rhyolite peripheral to Upper Zone mineralization.

The sericite alteration is pervasive and texturally destructive and the quartz alteration is heterogeneous and non-destructive. Each style of alteration has mass gains of Cu, Pb, Zn, Ba, As, and Ni presumably due to the mineral assemblage chalcopyrite-galena-sphalerite-barite-tennantite (Sinclair, 2000). Aside from the Gap deposit, Upper Zone lenses do not have focused pyrite-rich feeder systems.

Localized alteration zones in the hangingwall rocks above the H-W deposit most likely represented feeder zones for the Upper Zones (Jones, 2001). In comparison, the hangingwall rocks above the Battle orebody are more strongly altered due to hot hydrothermal fluids migrating up through a pre-existing volcanoclastic pile and acting as a diffuse, unfocused feeder (Robinson, 1994; Sinclair, 2000; Jones, 2001).

3.7.5 Alteration Discussion

The style of alteration for the Ridge Zone West has similarities to regional metamorphism and the diffuse hydrothermal alteration below the Upper Zone lenses. The non-destructive nature of the alteration can be attributed to either regional alteration or hydrothermal alteration. Observations suggesting that the footwall alteration is at least partially formed by hydrothermal alteration are:

- The semi-conformable nature of the quartz-sericite+/-chlorite alteration associated with the Basal Conglomerate and the upper 30 m of the Price Formation andesite.
- Spatially associated pyrite-sphalerite+/-chalcopyrite+/-galena mineralization and quartz-sericite+/-chlorite alteration extending to depth near steep dipping faults.
- Proximity to Zn-rich polymetallic mineralization.
- The absence of epidote in the Price Formation andesite but presence within the unaltered Lower Mixed Volcaniclastic rocks.

Based on the above observations, the texturally non-destructive footwall alteration within the Basal Conglomerate and Price Formation andesite is suggested to be a weak, diffuse, unfocussed, alteration system derived at least in part by hydrothermal mineralizing fluids. The style of footwall alteration for the Ridge Zone West is similar to the footwall alteration associated with Upper Zones above the Battle Main lens.

The footwall alteration assemblage sericite-quartz+/-chlorite and associated pyrite-sphalerite+/-chalcopyrite+/-galena mineralization is not texturally destructive. Sulphide mineralization contains only trace to 5% disseminations and veins. A significant pyrite-rich feeder system or alteration pipe is not observed.

Hangingwall alteration is characterized by sericite-quartz+/-chlorite alteration. Textural and spatial associations infer possible silica replacement of previously deposited fine-grained sediments similar to the processes that formed the Battle area chert.

The steep, north dipping faults are suggested to have some spatial influence on the hydrothermal mineralizing fluids based on the proximity of pyrite-sphalerite-chalcopyrite+/-galena mineralization and the distribution of sericite-quartz+/-chlorite alteration.

3.8 Geology and Alteration Summary

3.8.1 Volcanic Stratigraphy

The major rock formations for the Myra Falls property and the Ridge Zone West area are the Price Formation andesite and the Myra Formation. The Myra Formation comprises intermediate to felsic volcano-sedimentary rocks and sulphide mineralization of the Ridge Zone West deposit. The main rock units observed in the Ridge Zone West area from stratigraphic footwall to hangingwall are: the basement Price Formation andesite, the footwall Basal Conglomerate, the H-W Horizon, the Hangingwall Mafic Complex and the Lower Mixed Volcaniclastic rocks.

3.8.2 General Trends

The main geological rock formations have good E-W continuity for at least 5 km from the Ridge Zone West eastward to the H-W deposit area. Facies variation is rapid in the N-S orientation making geological interpretation for individual volcano-sedimentary deposits difficult on a property scale.

The geological units are generally flat lying with an overall 4° dip westward. The significance of the westerly dip is unclear but is possibly related to a regional westerly dip across the property (Walker, 1985). On N-S section, the volcanic stratigraphy is generally flat lying except for a relatively sharp increase in elevation for most of the units at the south portion of the study area (Figs. 3.2a-d). The increase in dip at the south portion of the study area is probably related to D1 folding associated with the large-scale, asymmetric, upright Myra anticline as defined by Walker (1985), Berry (2000), and Jones (2001). The folding inference is based only on general location of the anticlinal axis relative to the study area and general dip of the volcano-sedimentary units.

3.8.3 Geological Setting

Footwall Rocks

The Price Formation andesite is weak to moderately sericite-quartz+/-chlorite altered, massive, coherent, feldspar+/-pyroxene phyric, amygdaloidal andesite. The coherent rocks have local monomict to polymict intervals of autobrecciated and volcaniclastic rocks. The setting is interpreted to be subaqueous based on the angular curvilinear quench textures of the autobrecciated margins. Absolute water depth is not constrained. The Price Formation andesite is the stratigraphic basement.

A quartz-sericite+/-chlorite altered, coarse cobble conglomerate conformably overlies the Price Formation andesite. This unit has been named the Basal Conglomerate. The Basal Conglomerate has E-W strike continuity but significant thickness variation. The Basal Conglomerate is interpreted to have a westerly provenance based on a general westward thickening of the unit on section 4150N and its absence from volcanic sequences for the Battle and H-W deposit areas. Deposition is by mass flow processes during a very short time span, either prior to or during the initial stages of sulphide mineralization. The upper contact of the Basal Conglomerate is interpreted to represent the paleo-seafloor prior deposition of fine facies rocks for the H-W Horizon and the Ridge Zone West sulphide lenses.

Host Rocks

The H-W Horizon is a sequence of argillite, sulphide mineralization, and felsic coarse to fine volcanoclastic rocks. The H-W Horizon is up to 100 m thick between sections 200 E to 370 E, but thins to 25 m thickness on section –250 E. Fine facies rocks such as argillite and mudstone infer a below wave-base restricted basin setting. The limited N-S extent of the argillaceous mudstone suggests a narrow, elongate paleo-depression for the sulphide mineralization. This observation is supported by the Basal Conglomerate having its greatest apparent thickness below sulphide mineralization, implying a possible paleo-depression.

Hangingwall Rocks

The Hangingwall Mafic Complex is a mafic flow or sill with a massive coherent core. The core has a dominantly mafic autoclastic carapace grading out into a polymict breccia intermixed with wet, unconsolidated, volcanoclastic deposits including peperite textures. Hence, the Hangingwall Mafic Complex is a syn-volcanic flow or sill deposited after H-W Horizon rocks but prior to consolidation. The relatively unaltered nature of the unit suggests emplacement after the main mineralizing event responsible for forming the Ridge Zone West ore lenses.

The Lower Mixed Volcanoclastic Unit is dominated by repeated fining upward sequences of pebblestone to sandstone. The sequences are interpreted to be the product of both high and low-density turbidity currents. Minor coherent to brecciated andesite flows and / or sills are intercalated with the turbidite sediments. Jigsaw-fit fragments with curvilinear margins are indicative of hyaloclastite quench texture related to the interaction of hot lava with cold seawater in a subaqueous setting.

3.8.4 Alteration Summary

The texturally non-destructive footwall alteration within the Basal Conglomerate and Price Formation andesite is suggested to be a weak, diffuse, unfocussed, alteration system derived at least in part by hydrothermal mineralizing fluids. The style of footwall alteration for the Ridge Zone West is similar to the footwall alteration associated with Upper Zones above the Battle Main lens. The footwall alteration assemblage sericite-quartz+/-chlorite and associated pyrite-sphalerite+/-chalcopyrite+/-galena mineralization is not texturally destructive.

Hangingwall alteration is characterized by sericite-quartz+/-chlorite alteration. Textural and spatial associations infer possible silica replacement of previously deposited fine-grained sediments similar to the processes that formed the Battle area chert.

The steep, north dipping faults are suggested to have some influence on the hydrothermal mineralizing fluids based on the spatial association with pyrite-sphalerite-chalcopyrite+/-galena mineralization and the increase in width and depth of sericite-quartz+/-chlorite alteration near these faults.

4.1 Introduction

The purpose of this chapter is to characterize the styles of deformation, assess possible timing relationships, and interpret how these features pertain to the Ridge Zone West host rocks and the property wide structural model. Structural information for this portion of the study is from three sources; structural mapping of the Lynx 10 level drift, structures observed in non-oriented core from the diamond drill holes, and sectional interpretations from diamond drill hole data.

Structural mapping of Lynx 10 level was by the author and occurred during one mapping session during 2001 (Fig. 4.1). The mapped drifts are located approximately 450 m above the Ridge Zone West polymetallic sulphide mineralization and the rocks are considered part of the Myra Formation. The Myra Formation was deposited during the late Devonian (Juras, 1987). All of the deformation phases outlined by Berry (2000) and Jones (2001) are interpreted to have occurred after deposition of the Myra Formation. The various deformation events described by Berry (2000) and Jones (2001) are a Pre-Permian compression event (D1 folding and D2 shearing), Mesozoic era compression concurrent with accretion of the Insular Belt onto the North American plate (D3 brittle-ductile faulting), extension (D4 normal faulting) and post-accretion Cenozoic era compression (D5 brittle-ductile faulting) (Fig. 2.6). Therefore, structural mapping on Lynx 10 level has relevance towards developing the structural history of the Ridge Zone West as the rocks have been deformed by the same events.

The structural data has been grouped by structural style. Timing and naming of the various events is relative to observations from this study and inferences using the model developed by Berry (2000) and Jones (2001). Interpretation of the sectional and drift mapping data is combined to generate a geology plan view map at the 2990 m elevation showing major geologic units, location of the polymetallic sulphide mineralization, and pertinent structures for the Ridge Zone West area. All measurements are relative to mine grid north (48° east of true north).

4.2 Styles of Deformation

4.2.1 Ductile Deformation (D1-D2)

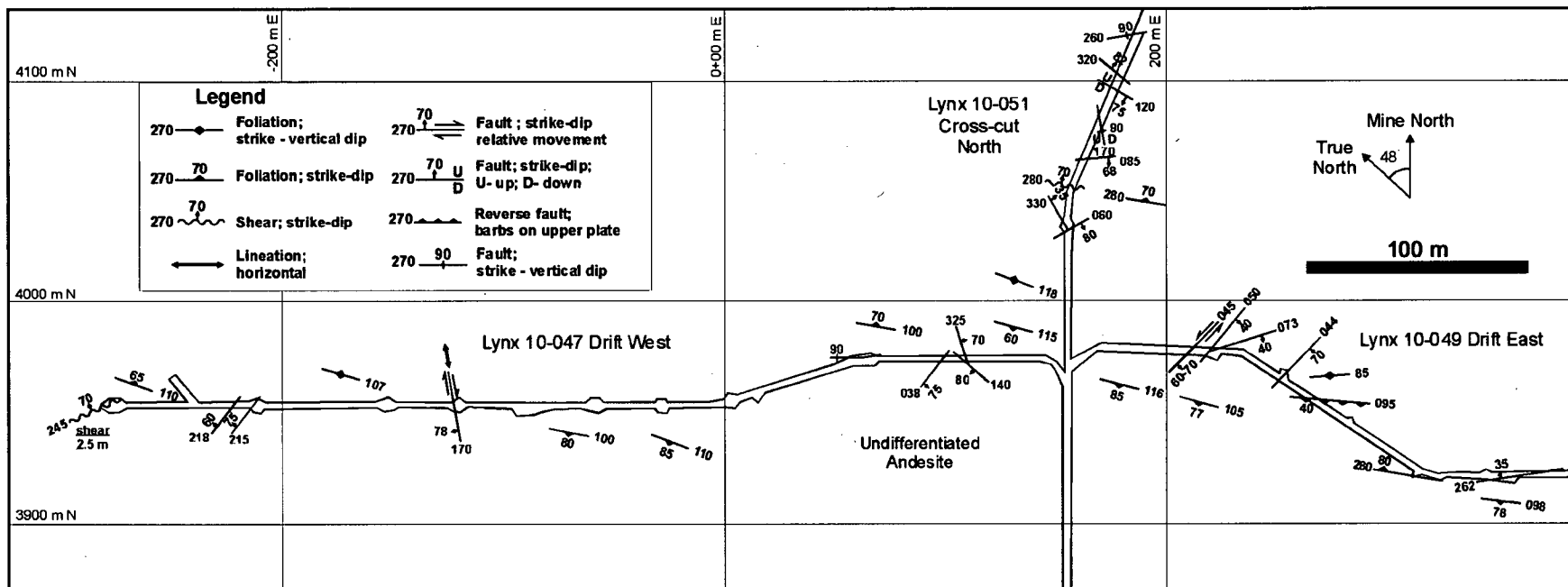
A penetrative foliation is observed in both diamond drill core and drift mapping. From diamond drill core, the foliation is weak to moderately developed where the presence of sericite and chlorite occur within the Price Formation andesite rocks and the H-W Horizon rocks. Rock units overlying the H-W Horizon such as the Lower Mixed Volcaniclastic unit have a weak foliation (Fig. 3.8). Unaltered, coherent rock types such as Hangingwall Mafic Complex have a poor to indistinguishable foliation (Fig. 3.7).

Lynx 10 level drift mapping of the structures provide a small data set of thirteen foliation measurements to assess (Fig. 4.1). The data is plotted on an equal area stereonet (Fig. 4.2). The foliation planes measured have a consistent azimuth with a mean orientation of $105^{\circ} / 87^{\circ}$ S. Foliation plane dips vary from steep south or steep north with 75% of the planes dipping south. One foliation plane at the east end of the map area had an orientation of $280^{\circ} / 80^{\circ}$ N with a mineral lineation plunging 10° west. Regardless of the variable dip, the strike is consistent at ESE-WNW.

The Ridge Zone West foliation is crosscut by, and dragged into the plane of later brittle-ductile structures. Therefore, the penetrative foliation pre-dates the brittle-ductile structures observed and represents an earlier phase of deformation. This observation is typical of the Myra Falls property based on observations by the author in the Battle and H-W deposit areas as well as the structural model developed by Berry (2000) and Jones (2001). Mesoscopic folding of bedding planes was not observed in drift mapping.

Two predominant foliations have been recognized in rocks at the Myra Falls property. The foliations are related to the Myra anticline forming ductile D1 event (Jones, 2001). The property-wide penetrative S1 foliation has an E-W trend with an average orientation of $267^{\circ} / 68^{\circ}$ N, moderate to steep north dipping axial planar cleavage, and sub-horizontal mineral lineations (Jones, 2001). The property wide S2 foliation is developed in localized shear zones and has an ESE-WSW trend with steep northeast dipping cleavage zones that overprint S1 (Jones, 2001). Mineral lineations for the S2 foliation have a moderate WSW plunge. Jones (2001) suggests that the S2 foliation developed during the late stages of ductile deformation possibly by an increase in the strain partitioning and/or a slight rotation in the principle strain axes.

The foliation for the Ridge Zone West area on Lynx 10 level is most consistent in character with the property wide S1 cleavage based on its widespread nature, weak developed fabric, and pre-D3 timing. The ESE-WNW trend is most similar with S2 orientations but the foliation is not related to shearing. This could be related to a slight rotation in the regional strike between the Battle deposit area and the Ridge Zone West (Berry, pers. comm.). Proximity of the Myra anticline fold axis relative to the study area may also be a factor (Fig. 4.3). Based on the general ESE-WNW trend with steep dip of the foliation for the Ridge Zone West area and the structural model developed by Jones (2001), the foliation will be referred to as an S1 foliation for future purposes. The regional strike was assumed to be mine grid EW by the author and other company geologists during the diamond drill campaign. Hence, a characterization study is necessary prior to making preliminary assumptions for orienting structures in diamond drill core relative to the S1 foliation.



Lynx 10 level drifting is the diamond drill platform located approximately 450 m higher in elevation than the Ridge Zone West mineralization and is considered part of the Myra Formation rocks. All of the deformation outlined by Berry (2000) and Jones (2001) is interpreted to have occurred after deposition of the Myra Formation (D1 folding), during and after the Mesozoic accretion of the Insular Belt onto the North American plate (D3-D5). Therefore, structural mapping on Lynx 10 level can enhance the geological interpretation of the Ridge Zone West. On Lynx 10 level, there is a weakly developed ESE foliation with mostly southerly dips; one NE-SW trending shear; two translational faults with NE-SW and NNW-SSE trends; two normal faults with N-S and NW-SE trends; and one reverse fault trending E-W. Several structures did not have kinematic indicators but have been included with fault symbols without relative movement. All orientations are relative to mine grid coordinates rotated 48 degrees east of true north.

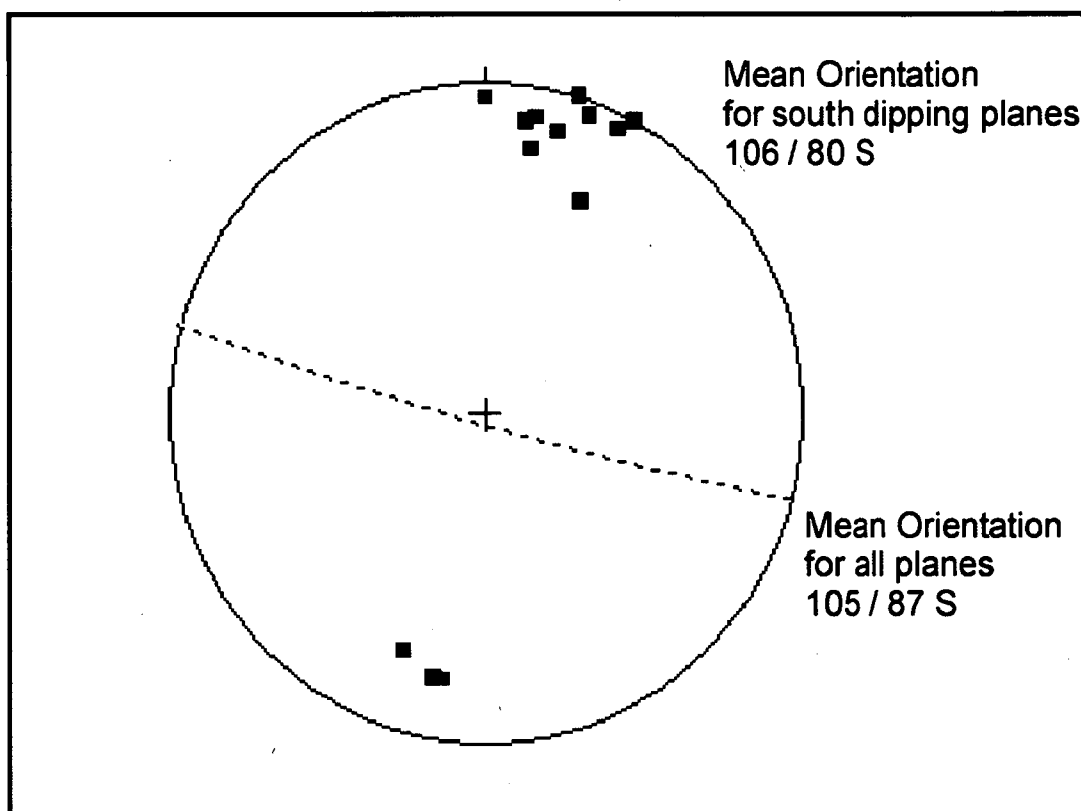
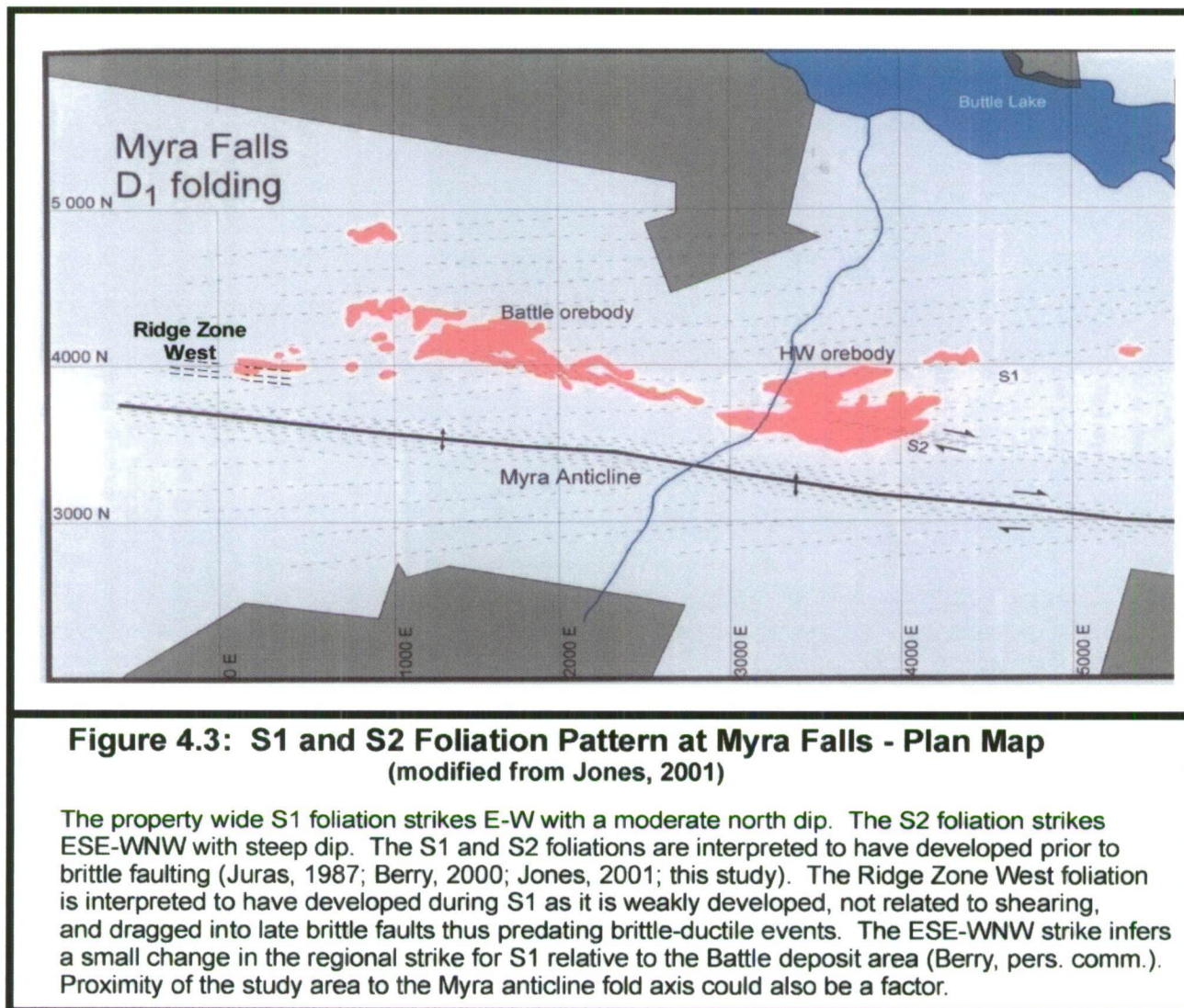


Figure 4.2: S1 foliation planes - Equal area pole plot.

The equal-area stereonet plot shows the poles of foliation planes from Lynx 10 level drift mapping. A total of 13 planes were measured. A potential for two populations exist with similar azimuths trending ESE but differing dips at moderate to steep south dip or moderate north dip. The mean orientation for all the foliation planes measured is 105 / 87S. The mean orientation for just the south dipping planes is 106 / 80S. Data is plotted using Georient version 9 software by R. Holcombe.



4.2.2 Brittle-Ductile Deformation (D3 to D5): Lynx 10 level map data

Kinematic indicators observed on some brittle-ductile structures from the Lynx 10 level mapping allowed some inferences towards characterizing the styles of faulting present (Fig. 4.1). The kinematic indicators observed were striations, grooves, plane roughness, quartz slickenfibres, and foliation drag. Lynx 10 level drift mapping had the following structures with discernable kinematic indicators.

D3a strike-slip faults: One style of faulting is translational strike-slip. Two faults of this type are noted on Fig. 4.1, one dextral fault and one suspect sinistral fault. The dextral fault has a NNW-SSE strike, steep SW dip, and weak quartz-sericite veining over 2-10 cm widths. Kinematic indicators include horizontal mineral lineations and plane roughness. This fault post-dates S1 and an ENE-WSW trending, south dipping structure without any observed kinematic indicators.

A NE-SW striking, moderate SE dipping fault has up to 10% quartz-carbonate veins+/- gouge. Fault drag folding of S1 indicates a possible sinistral sense of movement in the plane of the drift back. The sense of displacement is considered suspect as fault drag folds can only be used for strike-separation in map view and dip-separation in vertical section (Ragan, 1973). This fault post-dates S1 and an ENE trending fault. The translational strike-slip faults are similar in character to the D3a event proposed by Berry (2000) and Jones (2001).

At the western end of 10-047 DW, a single NE-SW trending, moderate NW dipping shear zone has moderate to strong cleavage over a 2.5m width. This shear zone has up to 5% quartz-sericite-chlorite veining. No discernable kinematic indicators were observed. Timing of this structure is not clear due to the lack of crosscutting evidence with other structures. Compared to the Myra Falls structural model proposed by Berry (2000) and Jones (2001), steep E to NE trending, gouge rich faults with wavy anastomosing structures, strong cleavage zones, and quartz veining are characteristic of the D5 compression event. Based on drift mapping, it is not clear whether the NE-SW trending structure is part of the D3a or the D5 event. This structure is described with the D3a structures based on diamond drill data described later in section 4.2.3.

D3b reverse faults: A second style of faulting is reverse faulting. One E-W striking, moderate south dipping reverse fault has a 2.0 m wide cleavage zone. Centimeter scale quartz slickenfibres observed on the fault plane along the drift back are the only discernable kinematic indicators. This style of faulting is comparatively similar to flat faulting associated with NE-SW compression of either the D3b or the D5 events proposed by Berry (2000) and Jones (2001). The D3b event is favoured for the reverse fault observed as no strike-slip component was observed.

D4 normal faulting: A third style of faulting noted in Fig. 4.1 is normal faulting. Two normal faults have NW-SE and N-S trends with steep to subvertical dip. Kinematic indicators are fault plane striations, grooves, and quartz slickenfibres. Timing with other structures is unclear. Compared to the Myra Falls structural model developed by Berry (2000) and Jones (2001), this style of normal faulting is similar to NW-SE trending reactivated normal faults such as those found at the western end of the H-W and 43-Block deposits located 3.0 to 4.0 km east. Displacements observed for normal faults with NW-SE and N-S trending normal faults at Myra Falls are typically less than 10 m and spaced 5 to 10 m apart even though large scale normal structures have displacements greater than 100's of meters (eg. the North Fault Zone). The normal faulting is possibly related to the D4 extensional, normal faulting event proposed by Berry (2000) and Jones (2001).

4.2.3 Brittle-Ductile Deformation (D3 to D5): Non-oriented drill core data

Structural data from the non-oriented drill core is noted in Table 4.1. This data was collected by the author and company geologists from diamond drill holes used to generate the geology sections for Chapter 3, Fig. 3.2a-d. The structures were measured relative to the core long axis and the S1 foliation where applicable.

Calculating orientations of structures in drill core relative to an assumed known plane such as the S1 foliation is a method described and calculated by software programs (Holcombe, 2004; Scott and Berry, 2003). This method is not used for the study due to variable north and south dips of the S1 foliation and inconsistent methods of recording structural data by the author and company geologists. Instead orienting structures in diamond drill core used the following references for qualitative dip-slip or strike-slip inferences:

- orientation of the drill hole based on down-hole surveys
- angle of the structure's plane relative to the core long axis for apparent dip possibilities
- an inferred ESE-WNW strike for the S1 foliation
- where available, the general trend (dip-slip or strike-slip) of any kinematic indicators are relative to the down-hole end for the long axis of the structure's elliptical section; looking down-hole, in the plane perpendicular to the core axis.

Qualitative general trends noted in Table 4.1 such as S1 parallel, NE-SW strike, strike-slip or dip-slip displacement, have been noted for structures with kinematic indicators. Drill core structural data noted in Table 4.1 notes several styles of brittle-ductile fault structures for the Ridge Zone West area. Timing for the styles of faulting draws from both the Lynx 10 level mapping and the Myra Falls structural model (Berry, 2000 and Jones, 2001).

TABLE 4.1: RIDGE ZONE WEST STRUCTURAL DATA FROM NON-ORIENTED DIAMOND DRILL CORE

| DDH | Depth from m | Depth to m | Section | MFO Deformation Event | Displacement | Orientation | Kinematic Indicators | Gouge Clay Breccia | Broken Core Cleavage | Vein Minerals |
|----------|--------------------|------------------|---------|-----------------------------|----------------------|---|---------------------------|--------------------------|----------------------------|------------------|
| L10-2049 | 208 | 209 | 300E | D3a | strike-slip | S1 II; steep dip | slickenside; qt fibres | | | |
| L10-2049 | 371 | 372 | 300E | D3a | strike-slip | strike-slip; NW or NE trend; steep dip | slickenside; qt fibres | | | |
| L10-2049 | 596 | 603 | 300E | D3a | strike-slip | NE-ESE or NW-WNW trend | striations | clay | bc | qt-cb |
| L10-2049 | 606 | 606 | 300E | D3a | strike-slip | S1 II; steep dip | striations | clay | | qt-cb |
| L10-2049 | 656 | 656 | 300E | D3a | strike-slip | S1 II; steep dip | slickenfibres; striations | clay | | |
| L10-2054 | 569 | 570 | -250E | D3a | strike-slip | S1 II; steep dip | slickensides; qt fibres | wk gg | bc | |
| L10-2041 | 284 | 296 | -050E | D3a+D4 | strike-slip+dip-slip | S1 II; steep dip | foliation drag; roughness | 3 cm gg | bc | qt-cb; chl-ser |
| L10-2041 | 403 | 417 | -050E | D3a+D4 | strike-slip+dip-slip | S1 II; steep dip | striations | 20 cm gg | | qt-cb; chl-ser |
| L10-2054 | 1 | 23 | -250E | D3a+D4 | strike-slip+dip-slip | mapped NE trend; mod NW dip | slickenfibres; striations | minor gg | bc; cleav / 2.5m | qt-cb-epi |
| L10-2054 | 84 | 145 | -250E | D3a+D4 | strike-slip+dip-slip | steep to mod dip; low angle to drill hole | slickenfibres; striations | wk-mod gg | str cleavage | qt-cb-chl |
| L10-2045 | 457 | 457 | 0+00E | D3b | dip-slip | FF; N-NW dip | striations | wk gg; bx | | |
| L10-2041 | 300 | 300 | -050E | D4 | dip-slip | steep dip | dip-slip striations | | | qt-cb |
| L10-2041 | 325 | 325 | -050E | D4 | dip-slip | steep dip | lineation; grooves | gg seams | bc | |
| L10-2042 | 381 | 391 | -050E | D4 | dip-slip | S1 II; steep dip | dip-slip striations | gg | bc | qt-cb |
| L10-2048 | 214 | 215 | +050E | D4 | dip-slip | steep dip | striations; qt fibres | | | |
| L10-2048 | 357 | 359 | +050E | D4 | dip-slip | S1 II; steep dip | dip-slip striations | | bc | qt-cb |
| L10-2048 | 416 | 419 | +050E | D4 | dip-slip | S1 II | dip-slip striations | 60 cm gg | | |
| L10-2048 | 467 | 468 | +050E | D4 | dip-slip | steep dip | dip-slip striations | | bc | |
| L10-2048 | 543 | 543 | +050E | D4 | dip-slip | S1 II; steep dip | slickenside | | bc | |
| L10-2049 | 20 | 27 | 300E | D4 | dip-slip | moderate or steep | striations; qt fibres | | bc | |
| L10-2049 | 169 | 172 | 300E | D4 | dip-slip | S1 II; mod dip | dip-slip striations | 2 cm gg | | |
| L10-2049 | 187 | 187 | 300E | D4 | dip-slip | NNE or NNW trend; steep or mod dip | dip-slip striations | 10cm gg | | |
| L10-2049 | 248 | 248 | 300E | D4 | dip-slip | S1 II; steep or mod dip | dip-slip striations | | | qt-cb-hem |
| L10-2049 | 260 | 261 | 300E | D4 | dip-slip | S1 II; steep dip | dip-slip striations | strong gg | | |
| L10-2049 | 319 | 320 | 300E | D4 | dip-slip | NW trend; steep dip | dip-slip striations | | bc | qt-cb |
| L10-2049 | 527 | 529 | 300E | D4 | dip-slip | S1 II | dip-slip striations | 10 cm gg | bc | qt-cb-py-ser |
| L10-2049 | 534 | 561 | 300E | D4 | dip-slip | S1 II | dip-slip striations | 10 cm gg | bc | qt-cb-py-ser |
| L10-2049 | 575 | 576 | 300E | D4 | dip-slip | NW or NE trend; steep dip | dip-slip striations | | | cb |
| L10-2049 | 614 | 615 | 300E | D4 | dip-slip | S1 II; steep dip | striations | clay | bc | |

Fault orientation is interpreted using the core angle with the drill hole and the relative orientation of an assumed ESE-WNW striking S1 foliation as references. Because of the variable dip and moderate difficulty in recognizing the S1 fabric in some rock types, only strike-slip and dip-slip displacement inferences have been made. The Myra Falls Operations deformation model is after Berry (2000) and Jones (2001) noted in Chapter 2, section 2.8

Abbreviations: Mineralogy: cb - carbonate; chl - chlorite; epi - epidote; hem - hematite; py - pyrite; qt - quartz; ser - sericite
S1 II - S1 foliation parallel; flat fault - FF; gouge - gg; wk - weak; mod - moderate; str - strong

D3a strike-slip faults: From Table 4.1, strike-slip faults have two general orientations; subparallel to ESE-WNW trending S1 foliation and conjugate NW-WNW or NE-ENE trending structures. Kinematic indicators include striations, roughness, quartz slickenfibres and foliation drag. These fault types are accompanied by quartz-carbonate veins, clay and broken core. Four S1 parallel strike-slip faults have been reactivated with dip-slip movement in L10-2054 on section -250 E and L10-2041 on section -50 E.

The ESE-WNW trending, S1 parallel, strike-slip faults have similar characteristics to both the D3 and the D5 events proposed by Berry (2000) and Jones (2001). Reactivation by later dip-slip movement implies that at least some of the strike-slip faults are formed by a deformation event prior to the D4 extensional normal faulting episode. The style of faulting discussed for D3a structures typically do not have gouge-rich, wavy anastomosing structures with strong cleavage zones and abundant quartz veining characteristic of the D5 event characterized by Berry (2000) and Jones (2001). Therefore, at least some of the ESE-WNW trending, S1 parallel, strike-slip faults are associated with the D3 compression event based on reactivation by D4 indicators and a lack of D5 diagnostic features.

D3b flat faults: One flat dipping fault is listed for L10-2045 on section 0+00 E. This flat fault has weak gouge, some fault breccia and an apparent dip-slip sense of displacement based on slickensides and striations. Berry (2000) and Jones (2001) describe two episodes involving flat faults. These are the D3b and the D5 compression episodes. The D3b episode is characterized by shallow N and S dipping thrust faults, wavy structures, minor gouge, and fine steep to oblique quartz fibres. The D5 episode is gouge-rich, has wavy anastomosing structures, strong cleavage zones, and quartz veining. Therefore, the flat structure observed in L10-2045 is interpreted as part of the D3b event based on the weak gouge, apparent dip-slip quartz slickenfibres and a lack of a strong, wavy anastomosing cleavage zone.

D4 normal faults: Normal dip-slip faults are the most abundant faults listed in Table 4.1. The normal faults have a range of trends with the most common orientation trending subparallel to the S1 foliation with steep dip. Other orientation trends include NNE-SSW and NW-SE with steep to moderate dip. Kinematic indicators include striations, quartz slickenfibres, roughness and grooves. Gouge, clay and broken core are common. The normal faults are accompanied by quartz-carbonate+/-hematite and quartz-sericite veining. This style of faulting is observed in all the diamond drill sections and is most common north of the Ridge Zone West mineralization.

Timing of normal dip-slip faults is not clear from either Lynx 10 Level drift mapping or drill core. From drill core the normal faults post-date at least one S1 parallel, strike-slip fault. More evidence is required to verify the timing of this style of faulting. Based on the above observations, the normal faulting observed in diamond drill core is interpreted to be part of a D4 extensional event proposed by Berry (2000) and Jones (2001). This event is characterized by planar normal faulting, with NNE-SSW, NNW-SSE, and E-W trends, steep fine quartz slickenfibres, quartz-carbonate veining, and minor fault gouge.

4.3 Ridge Zone West mineralization and major structural features

The Ridge Zone West mineralization is mainly deformed by the S1 foliation, strike-slip faults of the D3 event, and D4 normal faults. The most common faults observed are D4 normal faults. To best illustrate and synthesize the geological cross-sections of Figs. 3.2a-d, a geological plan map has been constructed by orthographic projection to the 2990 m elevation (Fig. 4.4). The 2990 m elevation represents an approximate mid-elevation for the mineralization. From Fig. 4.4, the most significant structural feature(s) observed during the study is a series of D4 normal faults located at the northern edge of the mineralization. This fault system is also sub-parallel to the ESE-WNW S1 foliation.

The D4 normal faults located immediately north of the Ridge Zone West mineralization are ESE-WNW trending, steep dipping, and spaced up to 10 m apart over 40 m cumulative widths. These faults are characterized by quartz slickenfibres and striations sub-perpendicular to S1, quartz-carbonate veining, broken core, minor clay and gouge. Minor, weak strike-slip striations subparallel to S1 indicate possible reactivation of previous D3 structures or later reactivation by the D5 event. The lack of well developed, anastomosing cleavage zones lead the author to favour reactivation of D3 strike-slip structures by the D4 event, or accommodation.

A NE-SW trending sheared D3 strike-slip fault has been extrapolated from Lynx 10 level mapping as it is the most significant feature mapped. Another purpose for highlighting these structures is that they represent potential poor ground conditions for future mining scenarios.

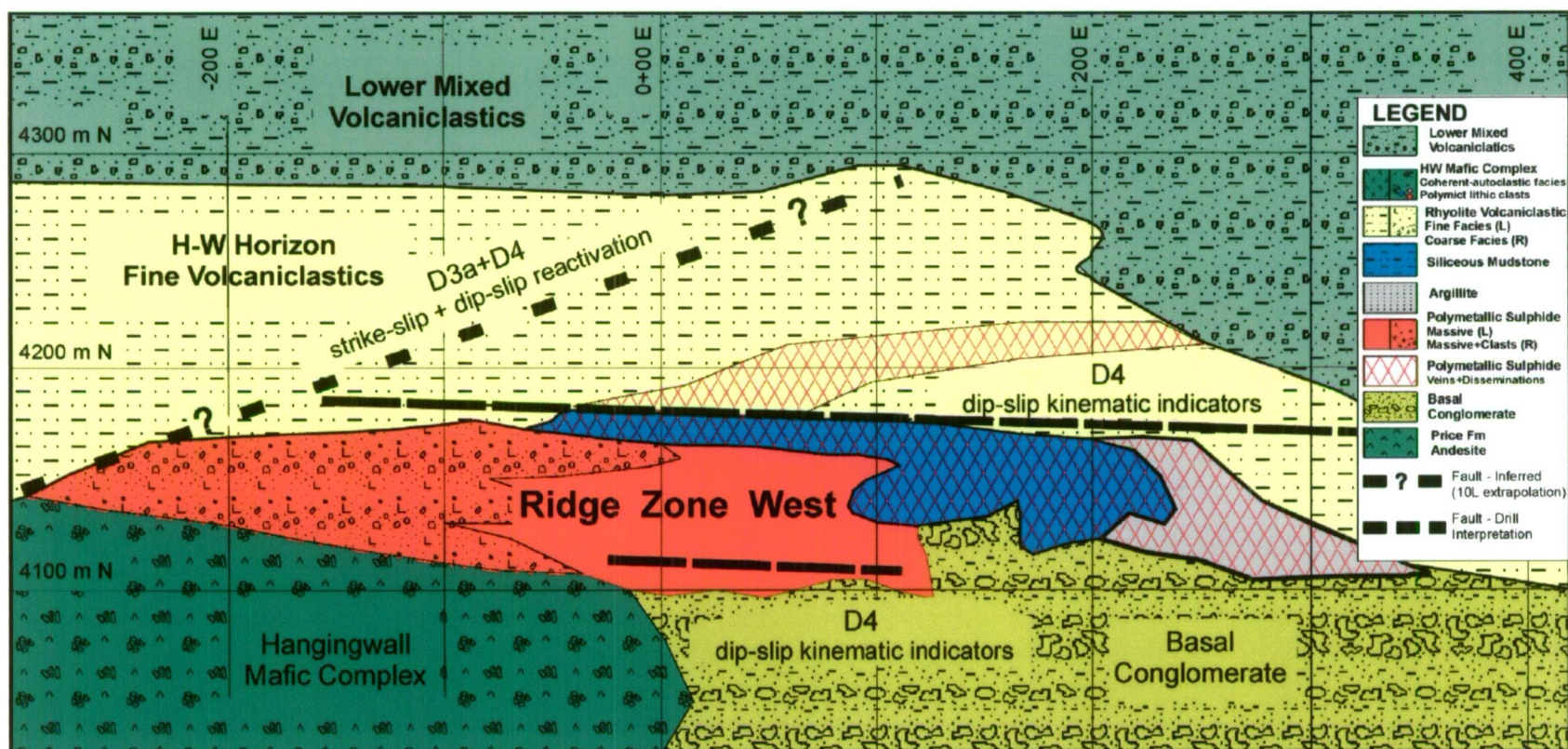


Figure 4.4: Ridge Zone West Geology and Structure- 2990 m plan map

The 2990 m elevation represents the approximate mid-elevation for the main mineralized lens of the Ridge Zone West. Structures with continuity or relevance to future mining have been added to the map. A NE-SW, strike-slip fault with minor dip-slip reactivation is extrapolated from Lynx 10 level. This structure is not confirmed by drilling but is included due to the amount of associated shearing. The sheared nature of the structure could lead to significant ground control issues during future mining scenarios. The ESE-WNW striking structure north of the main mineralization represents a number of dip-slip faults with occasional strike-slip indicators. These faults are spaced up to 10 m apart over 40 m cumulative widths. The faults are interpreted to be part of the D4 extensional event with possible D3a reactivation. D4 normal faults are the most common faults observed from diamond drilling.

4.4 Comparison with the existing Myra Falls Structural Model

Based on observations from mapping structures in Lynx 10 level drifts, non-oriented diamond drill core, and timing inferences, the following structural summary for the Ridge Zone West area is compared to the existing Myra Falls structural model developed by Berry (2000) and Jones (2001) (Figs. 4.5 and 4.6).

D1 – Ductile deformation: This event is interpreted as a major folding event responsible for forming the large-scale, open, upright, asymmetric Myra anticline (Berry, 2000; Jones, 2001). Parasitic folds have been observed for both the north and south limbs of the anticline (Walker, 1985; Juras, 1987; Sinclair, 2000; Jones, 2001). No large or small scale folding was definitively observed in either drift mapping or diamond drill core for this study. Insufficient data and location of the Ridge Zone West with respect to the Myra anticline fold axis are both possible explanations for the apparent lack of folding in the rocks (Fig. 4.5).

This event is characterized by a weak penetrative foliation fabric developed in rocks with phyllosilicate minerals. The foliation has an ESE-WSW trend with variable moderate to steep south and north dip. The study area foliation is weakly developed and contrasts with the strongly developed D2 foliation. The level of confidence for this style of deformation is low to moderate due to the small population of readings from drift mapping and the non-oriented nature of the diamond drill core. The Ridge Zone West foliation compares most favourably with the D1 orientation of the Myra Falls model.

D2 – Ductile deformation: This event was not recognized in the drift mapping or the diamond drill core.

D3a – Brittle-ductile strike-slip faults: The D3a faults are characterized by S1 parallel, steeply dipping strike-slip faults, NW-WNW dextral and NE-ENE trending sinistral faults with steep to moderate dip. Kinematic indicators include roughness, foliation drag, striations, and slickensides with quartz fibres. Other diagnostic features include clay, broken core, quartz-carbonate+/-chlorite+/-epidote veining and chlorite-sericite mineralogy.

The strike-slip faults observed from Lynx 10 level mapping have orientations and displacements consistent with the Myra Falls model. The large scale D3 Lynx-Phillips fault interpreted by former company geologists was not observed or inferred from diamond drill

data during the study (Fig. 4.5). It is probably located east of the drifts mapped and the sections logged in this project.

D3b – Brittle-ductile flat faults: The D3b flat faults are characterized by E-W trending south dipping flat faults with weak gouge. Dip-slip kinematic indicators include striations and slickensides with quartz fibres. This style of faulting is observed in one Lynx 10 level structure and one occurrence in diamond drill core. The small number of D3b flat faults observed suggests this event is not important in the Ridge Zone West area.

D4 – Normal faulting: The most common orientation trends subparallel to the S1 foliation with steep dip. Other orientation trends include NW to NNW and NE to NNE with steep to moderate dip. Kinematic indicators include striations, quartz slickenfibres, roughness and grooves. Gouge, clay and broken core are common. The normal faults are accompanied by quartz-carbonate+/-hematite and quartz-sericite veining.

This is the most common fault type observed from diamond drill core. The orientations, kinematic indicators and other characteristics are consistent with the Myra Falls model. The D4 fault system located north of the mineralization has been modified to reflect the observations of this study (Fig. 4.5). The presence of hematite with the quartz-carbonate veining appears to be a variation from the observations of Jones (2001) (Fig. 4.6).

D5 – Reactivation and oblique thrust faulting: This style of faulting was not observed during drift mapping or diamond drill core. Key diagnostic features observed by Berry (2000) and Jones (2001) include shallow to moderate N dipping oblique thrusts with top to the west displacement and steep E-NE sinistral strike-slip faults. These faults are characterized by strong gouge, wavy anastomosing structures, cleavage zones, fault striations as fine grooves in gouge and quartz veining. Even though many structures in the study area have strong gouge, other diagnostic features required for this event were not observed.

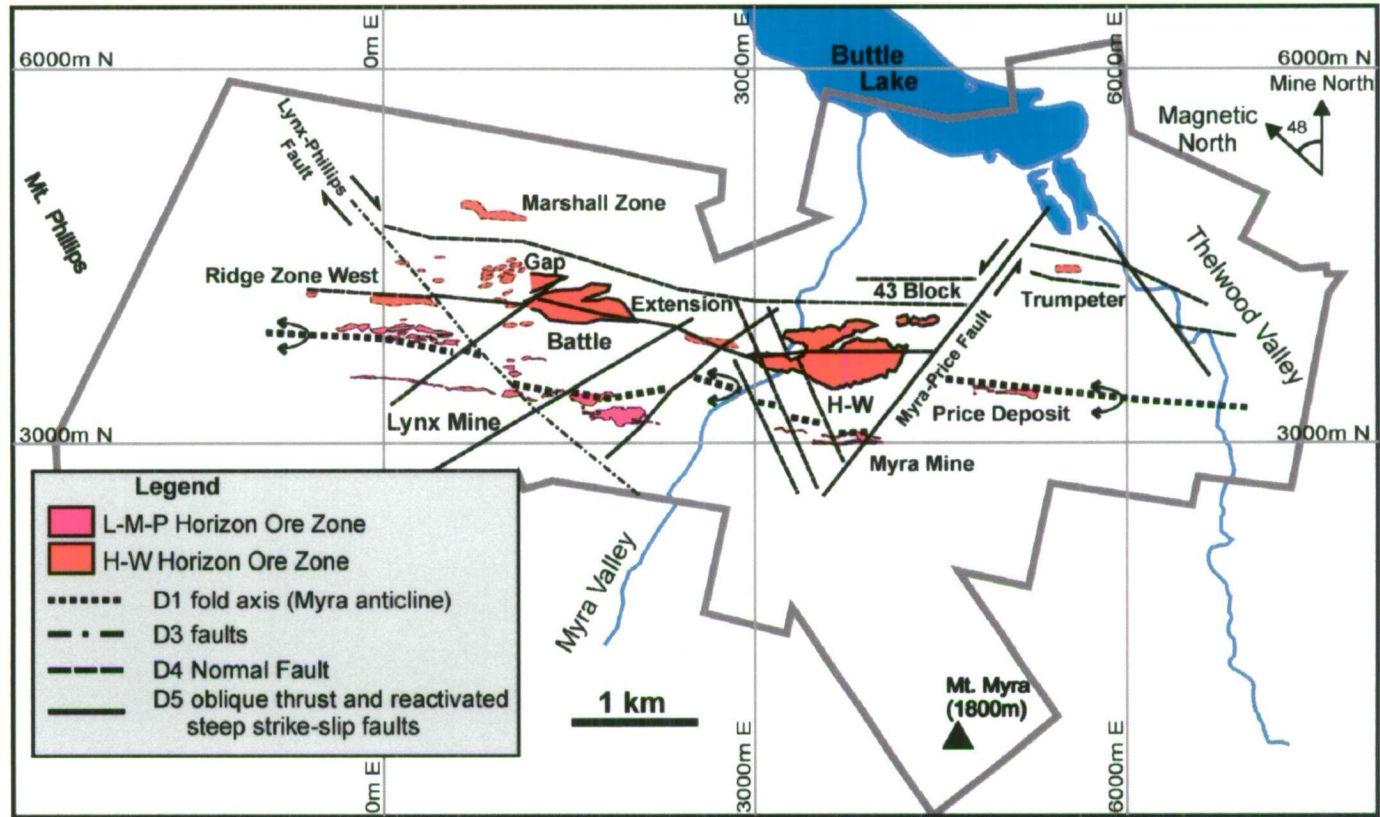
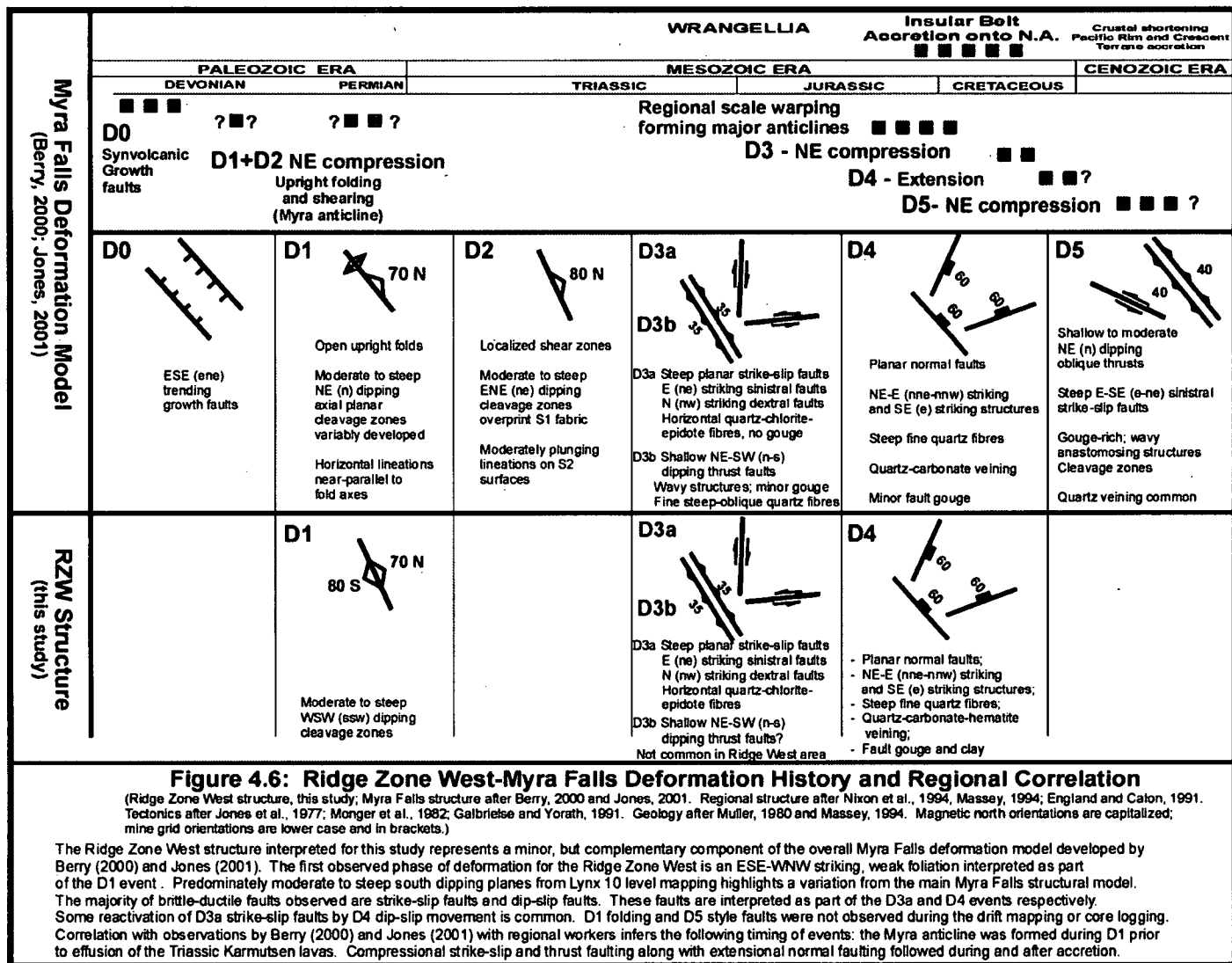


Figure 4.5: Location of Major Faults and VHMS deposits at Myra Falls Operations
Updated Projected Plan Map (this study and modified after Jones, 2001)

The main styles of deformation observed for the Ridge Zone West area are a weak S2 ESE-WNW trending foliation fabric and brittle-ductile faulting. The most common style of brittle-ductile faulting are steep dipping D4 normal faults located north of the Ridge Zone West mineralization. Minor strike-slip kinematic indicators on the D4 normal faults imply reactivation. Large and small scale folding is not a characteristic style of deformation for the Ridge Zone West. The NW trending Lynx-Phillips fault was not observed. The property-wide structural plan map derived by Jones (2001) has been updated to show the D4 normal fault(s) north of the Ridge Zone West mineralization observed by this study. Faults in this location were previously shown as D5 reactivated strike-slip faults by Jones (2001).



4.5 Summary

Preliminary data from drift mapping and diamond drill core indicate that the styles of structural deformation are similar to the ductile D1 event and the brittle-ductile D3 and D4 events proposed by Berry (2000) and Jones (2001) for the Myra Falls property. No folding is observed for the Ridge Zone West area. The penetrative foliation for the Ridge Zone West has an ESE-WNW orientation. Strike-slip and dip-slip faults are common for the Ridge Zone West area. The most significant faults are a series of ESE-WNW trending, steep dipping normal faults located north of the Ridge Zone West mineralization.

5.1 Introduction

This chapter describes and discusses the association of mineralization with volcanic stratigraphy, orebody geometry, mineral resource and mining estimates, styles of mineralization, ore mineralogy and mineral chemistry. An interpretation on the controls of sulphide deposition is based on observations from drill core and thin section. Finally, sulphide mineralization of the Ridge Zone West is compared to mineralization found elsewhere at Myra Falls. All references to orientation in this chapter are relative to mine grid north. Mine grid north is rotated 48° east of true north.

5.2 Ridge Zone West mineralization and stratigraphy relationships

Massive sulphide mineralization at Myra Falls is found along multiple stratigraphic positions within the Myra Formation. The H-W Horizon and Lynx-Myra-Price Horizon are the main host horizons for massive sulphide mineralization. Within the H-W Horizon, the most common stratigraphic positions hosting massive sulphide mineralization are known as the Contact Zone and the Upper Zones in mine terminology. Contact Zone mineralization is located near or at the interface between the footwall Price Formation andesite and the overlying H-W Horizon (Juras, 1987; Pearson, 1993). The Battle and H-W deposits are two examples of Contact Zone mineralization. Upper Zone lenses are polymetallic Zn-Pb-Cu-Ba[±]-Au[±]-Ag[±]-rich mineralization located up to 70 m stratigraphically above Contact Zone mineralization within volcano-sedimentary rocks of the H-W Horizon. The Gap lens and the Upper Zone lenses are two examples of Upper Zone mineralization.

Ridge Zone West mineralization does not occur at or near the upper contact of the Price Formation andesite. Instead, the main Ridge Zone West mineralization occurs at varying stratigraphic positions within the H-W Horizon. The Ridge Zone West mineralization is interpreted to have a similar stratigraphic position as the Upper Zone lenses that are located stratigraphically above the Battle and H-W deposits.

5.3 Geometry and resource estimates

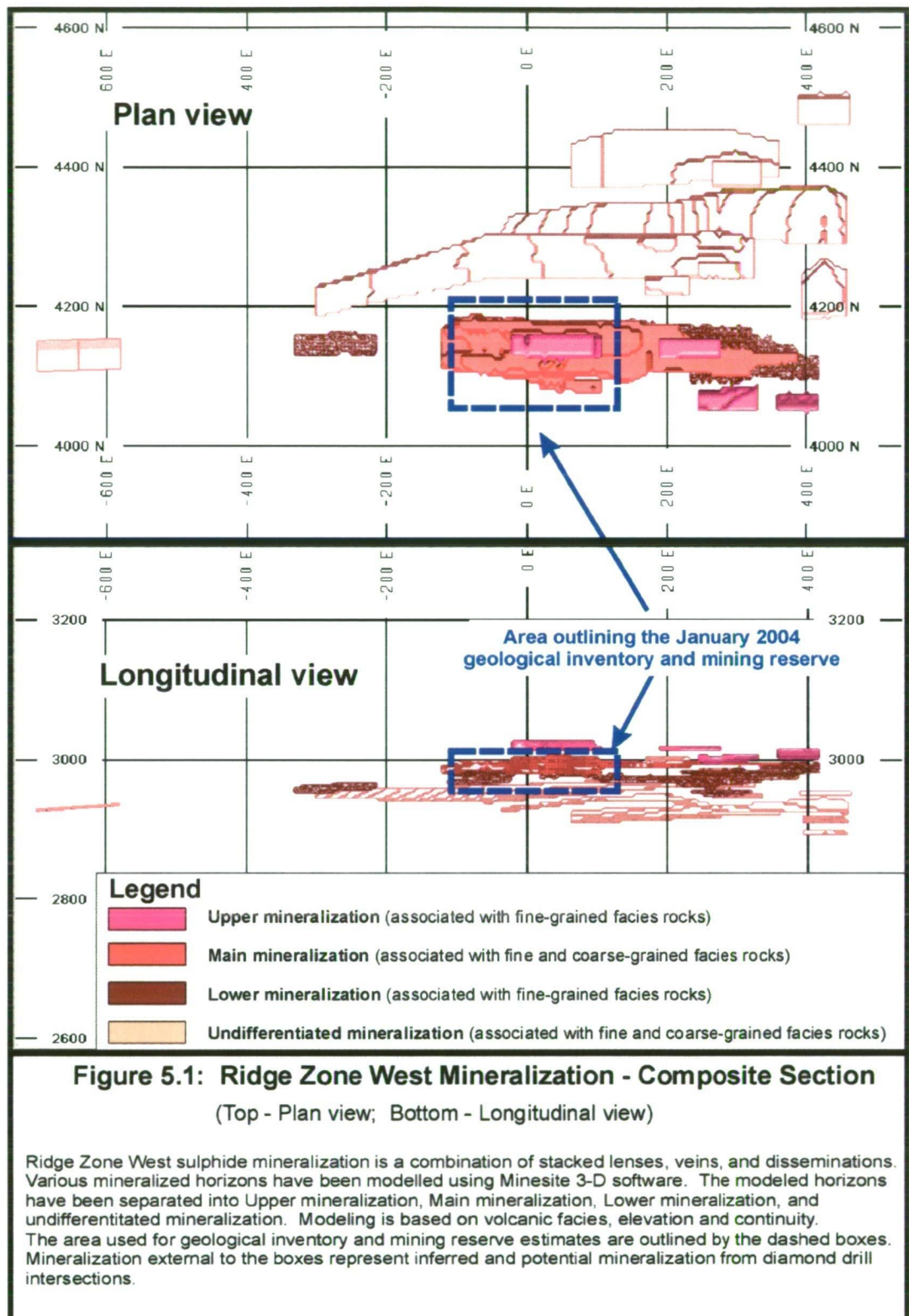
5.3.1 Geometry and resource estimate methods

Mineralization geometry, tonnage and grade values are from diamond drill section interpretations and computerized modeling of Ridge Zone West. The computer modeling was completed by the author during 2002 and 2004 using Compass and Minesite 3-D mining software. The modeling applied geology and assay information from recent and historical drill holes.

The resource estimate is based on a block model using an inverse distance cubed algorithm. The grade for a specific block is estimated using the nearest eight samples within a search ellipsoid applying the inverse distance cubed algorithm. Individual blocks are 5 m E-W, 5 m N-S, and 4 m high. The search ellipsoid has dimensions of 50 m E and W, by 25 m N and S, by 15 m vertically above and below the block. The block model parameters described above are the same parameters used for the global ore reserve estimation at Myra Falls. The inverse distance cubed algorithm closely replicates tonnage and grade estimations produced by classical sectional polygonal methods for a portion of the H-W deposit North lens.

5.3.2 Mineralization geometry

Zinc-rich massive lenses, veins and disseminations of sulphide mineralization for the Ridge Zone West occur over an area measuring approximately 1,000 m E-W along strike, 450 m N-S across strike and are up to 70 m vertical (Fig. 5.1). The most economically significant mineralized lenses discovered to date are centered about section 0+00E. The current known economically significant lenses are approximately 250m E-W along strike, 80 m N-S across strike and have individual thicknesses up to 17 m. The average thickness is approximately 5 m based on selected Zn-rich sulphide intersections along the main trend of the Ridge Zone West (Table 5.1).



| Drill hole | Section m | Zone | Interval m | Au g/t | Ag g/t | Cu % | Pb % | Zn % | Ba % | Fe % |
|-----------------------------------|--------------|------|---------------|-----------|-----------|---------|---------|---------|---------|---------|
| LX12-2101 | -640E | RZW | 1.8 | 1.1 | 34 | 2.2 | 0.1 | 15.1 | 1.8 | 6.5 |
| LX10-2054 | -250E | RZW | 9.0 | 2.4 | 194 | 1.4 | 1.6 | 12.2 | 0.9 | 6.0 |
| LX14-0666 | -075E | Main | 0.7 | 0.6 | 11 | 0.6 | 0.1 | 4.8 | 0.0 | 6.8 |
| LX14-0664 | -075E | Main | 0.4 | 0.0 | 37 | 1.2 | 1.0 | 7.3 | 0.3 | 7.9 |
| LX14-0663 | -075E | Main | 3.8 | 6.6 | 103 | 1.2 | 1.4 | 10.2 | 0.5 | 9.7 |
| LX10-2041 | -075E | Main | 0.9 | 0.3 | 14 | 0.6 | 0.4 | 6.1 | 0.1 | 5.2 |
| LX10-2046 | 050E | Main | 5.5 | 0.8 | 44 | 1.1 | 0.9 | 7.6 | 0.3 | 8.7 |
| LX10-2045 | 050E | Main | 15.2 | 2.9 | 164 | 2.2 | 2.4 | 22.4 | 1.7 | 8.1 |
| LX10-2047 | 050E | Main | 14.5 | 1.7 | 64 | 0.7 | 0.8 | 6.1 | 0.9 | 5.3 |
| LX10-2048 | 050E | Main | 17.9 | 3.0 | 120 | 1.1 | 1.4 | 10.5 | 1.5 | 5.9 |
| LX14-0642 | 050E | Main | 7.3 | 6.2 | 129 | 1.6 | 1.4 | 12.6 | 0.8 | 9.5 |
| LX14-0630 | 150E | Main | 6.5 | 3.2 | 103 | 0.9 | 0.8 | 9.9 | 0.4 | 5.3 |
| LX14-0626 | 200E | Main | 3.9 | 3.2 | 163 | 1.1 | 1.1 | 9.6 | 0.5 | 7.7 |
| LX14-0633 | 250E | Main | 1.6 | 1.5 | 12 | 0.4 | 0.6 | 2.5 | 0.0 | 4.6 |
| LX10-2049 | 350E | Main | 1.2 | 0.5 | 9 | 0.6 | 0.4 | 3.9 | 0.1 | 4.7 |
| LX10-2050 | 350E | Main | 0.5 | 3.0 | 82 | 1.0 | 1.2 | 8.7 | 0.6 | 8.8 |
| LX14-0656 | 400E | RZW | 3.5 | 3.4 | 18 | 0.5 | 0.4 | 2.3 | 0.0 | 4.1 |
| LX14-0657 | 400E | RZW | 0.4 | 3.7 | 102 | 2.0 | 1.3 | 10.4 | 0.8 | 10.7 |
| Average drill hole intersection = | | | 5.3 | m | | | | | | |
| Approximate strike length = | | | 1,000 | m | | | | | | |

5.3.3 Ridge Zone West Geological Inventory and Mining Reserve Estimates

The current geological inventory and mining reserve is for Zn-rich mineralization located along a 100 m strike length centered about 0+00E. The area is outlined in Fig. 5.1. The geological inventory estimate is based on mineralization located within 30 m of a drill hole intersection. The current mining reserve estimate is based on mineralization located within 15 m of a drill hole intersection. An economic NSR cut-off value of \$45 CDN with mining factors applied. The current mining factors are 31% dilution and 43% extraction. The Ridge Zone West has a current geological inventory gross value of approximately \$36 M CDN and a current mining reserve gross value of approximately \$18 M CDN, based on long-term economic parameters established by Boliden-Westmin (Canada) Ltd during 2004. The estimates are listed in Table 5.2.

| Reserve Type | Tonnes t | NSR \$ (cdn) | Au g/t | Ag g/t | Cu % | Pb % | Zn % | Ba % | Fe % |
|----------------------|-------------|-----------------|-----------|-----------|---------|---------|---------|---------|---------|
| Geological Inventory | 416,000 | \$ 88 | 2.3 | 77 | 1.1 | 0.9 | 8.5 | 0.9 | 6.4 |
| Mining Reserve | 234,000 | \$ 78 | 2.0 | 65 | 0.9 | 0.8 | 7.6 | 0.8 | 5.1 |

Based on the limited area used to generate the preliminary geological inventory and mining reserve estimates, the upside potential for adding future mineral resources to the geological inventory and mining reserve is optimistic. The optimism is supported by two significant Zn-rich intersections on sections -250E and -640E along the same strike as the current Ridge Zone West (Table 5.1). These intersections indicate the potential for more Zn rich sulphide mineralization to occur for at least 565 m west of the current resource estimate.

5.4 Styles of mineralization and H-W Horizon volcanic facies

As discussed in chapter 3, the H-W Horizon has fine-grained volcanic facies distributed near its basal and upper contacts separated by a polymict pebble conglomerate. Sulphide mineralization of the Ridge Zone West is hosted by fine and coarse-grained volcanic rocks throughout the vertical extent of the H-W Horizon. Sulphide fragments and other polymict mass flow clasts are spatially associated with the Hangingwall Mafic Complex located south and higher up in the stratigraphic sequence.

5.4.1 Mineralization associated with fine-grained volcanic facies

Lower and Main lens mineralization associated with fine-grained volcanic facies rocks are characterized by sphalerite-pyrite+/-chalcopyrite+/-galena hosted by mudstone, argillaceous mudstone, and weakly silicified mudstone. Lower lens mineralization occurs as fine disseminations, bands, and semi-massive accumulations (Fig. 5.2). Banded mineralization near the base of the H-W Horizon has soft-sediment deformation textures similar to adjacent mudstone beds (Fig. 5.2d). Banded pyrite-sphalerite-galena mineralization associated with argillaceous mudstone has fining-up grain size gradations and flame structures (Fig. 5.2a). Semi-massive sulphide mineralization commonly displays contorted textures with ragged to diffuse contacts (Fig 5.2b, c). The sulphide grains range from very fine- to fine-grained.

Towards the top of the H-W Horizon, Upper lens mineralization is hosted by fine-grained rocks. The host rocks are characterized by silicified mudstone with banded and breccia facies. The most common style of Upper lens mineralization occurs as pyrite-chalcopyrite+/-sphalerite veining associated with brittle fractures. The brittle fractures are at random orientations (Fig. 5.3a, b). Mineralization also occurs as disseminations in sandstone-rich bands (Fig. 5.3a).

Upper lens mineralization associated with breccia facies silicified mudstone can have either sandstone or argillaceous mudstone matrices. Silicified mudstone breccia with an argillaceous mudstone matrix has sphalerite-pyrite+/-chalcopryite rich mineralization occurring as disseminations, veins, and semi-massive accumulations (Fig. 5.3c, d). Mineralized contacts with the argillaceous mudstone host rocks are diffuse and are commonly contorted. This style of mineralization may be either Upper lens or Main lens mineralization.

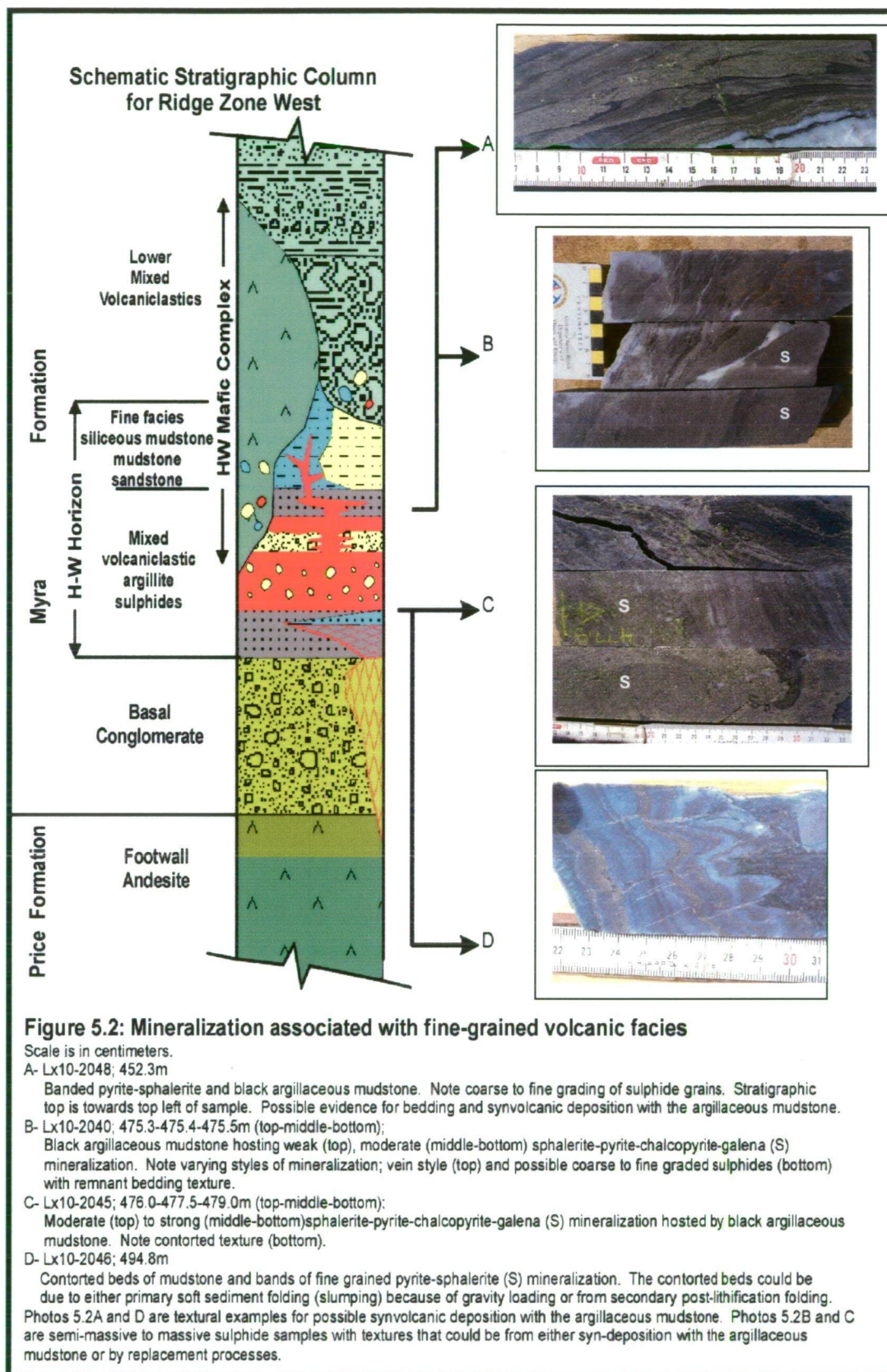
5.4.2 Mineralization associated with coarse-grained volcanic facies

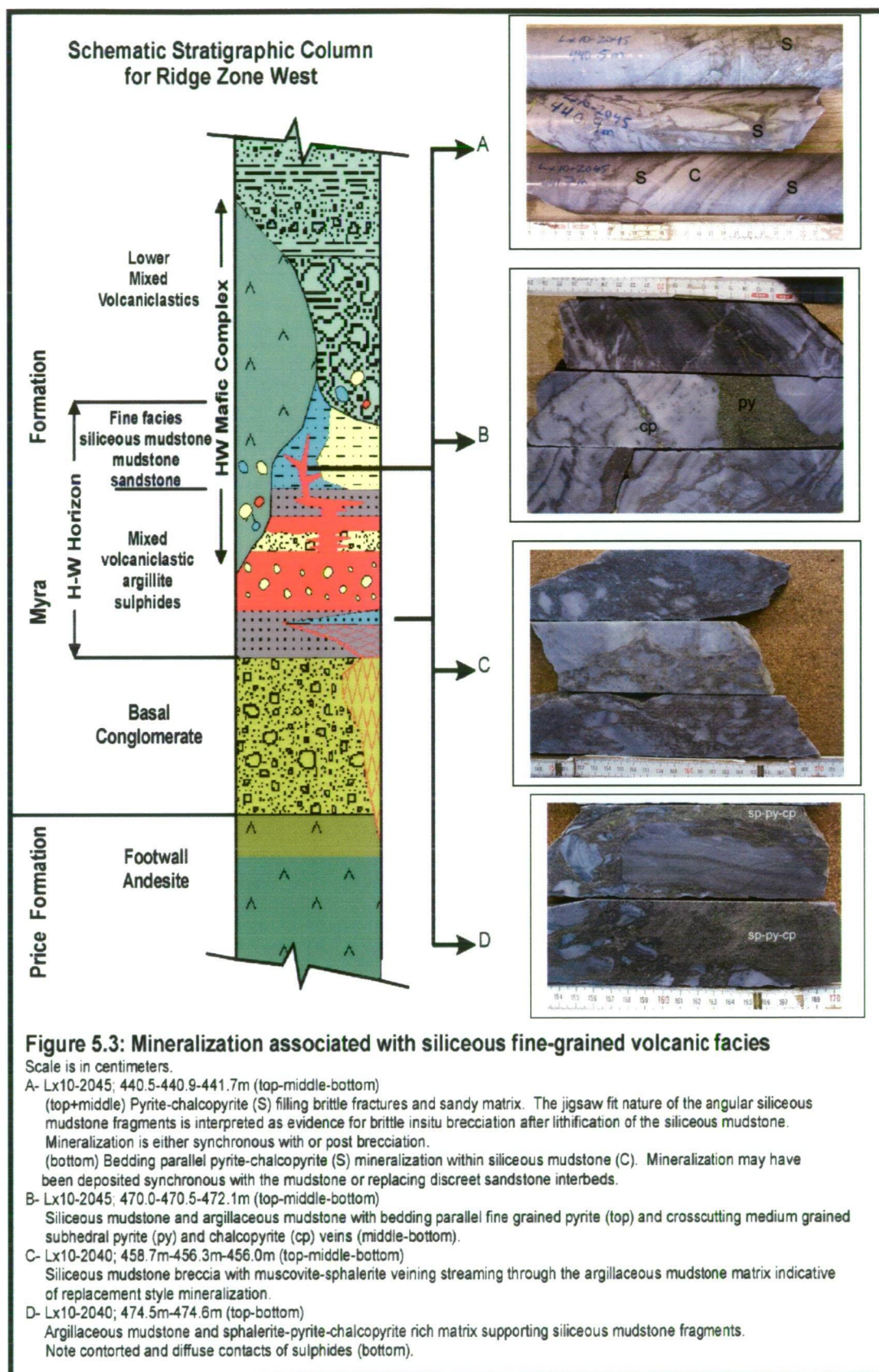
The majority of Main lens mineralization is associated with coarse-grained volcanic rocks and is supported by argillaceous mudstone or polymict sandstone matrices. Lithic clasts are typically well preserved but have been hydrothermally altered to sericite and quartz. Sphalerite-pyrite-chalcopryite+/-galena+/-barite+/-tennantite mineralization occurs as disseminations, veins, and semi-massive to massive accumulations (Figs. 5.4 and 5.5).

Vein style mineralization for the Main lens is associated with pebblestone. The pebblestone typically has a sandstone-granulestone matrix. Anastomosing veins of fine to medium grained sphalerite-pyrite-chalcopryite+/-galena appear to “flow” through the matrix material (Fig. 5.4). The vein style mineralization increases in intensity often taking on semi-massive to massive textures (Figs. 5.4 and 5.5). Barite-quartz-galena-tennantite-sphalerite rich veins have undulating, moderate to steep orientations (Fig. 5.5d). This appears to be a separate style of mineralization.

Sphalerite-rich clasts in coarse-grained, polymict, pebble conglomerate vary in colour from light to reddish brown. The clasts are pebble sized and have subangular to minor subrounded shapes (Fig. 5.4a). The subangular outlines of the sulphide clasts and the vicinity of similar mineralization indicate a proximal source for the clasts.

Other coarse-grained volcanic facies are dominated by mafic autoclastic rocks located at peripheral margins of the Hangingwall Mafic Complex. Autoclastic and associated peperite quench textures. Included with the polymict pebblestone are sphalerite-rich sulphide fragments (Fig. 5.6). Sulphide fragments have angular to subangular form. Contacts range from well defined to diffuse. Subangular sphalerite-rich sulphide fragments are observed in autoclastic mafic dominated rock with jigsaw-fit quench textures (Fig. 5.7). Fluidal and diffuse contacts are interpreted to be produced by localized remobilization of mineralization. The remobilization is attributed to reheating of the sulphides during emplacement of the Hangingwall Mafic Complex.





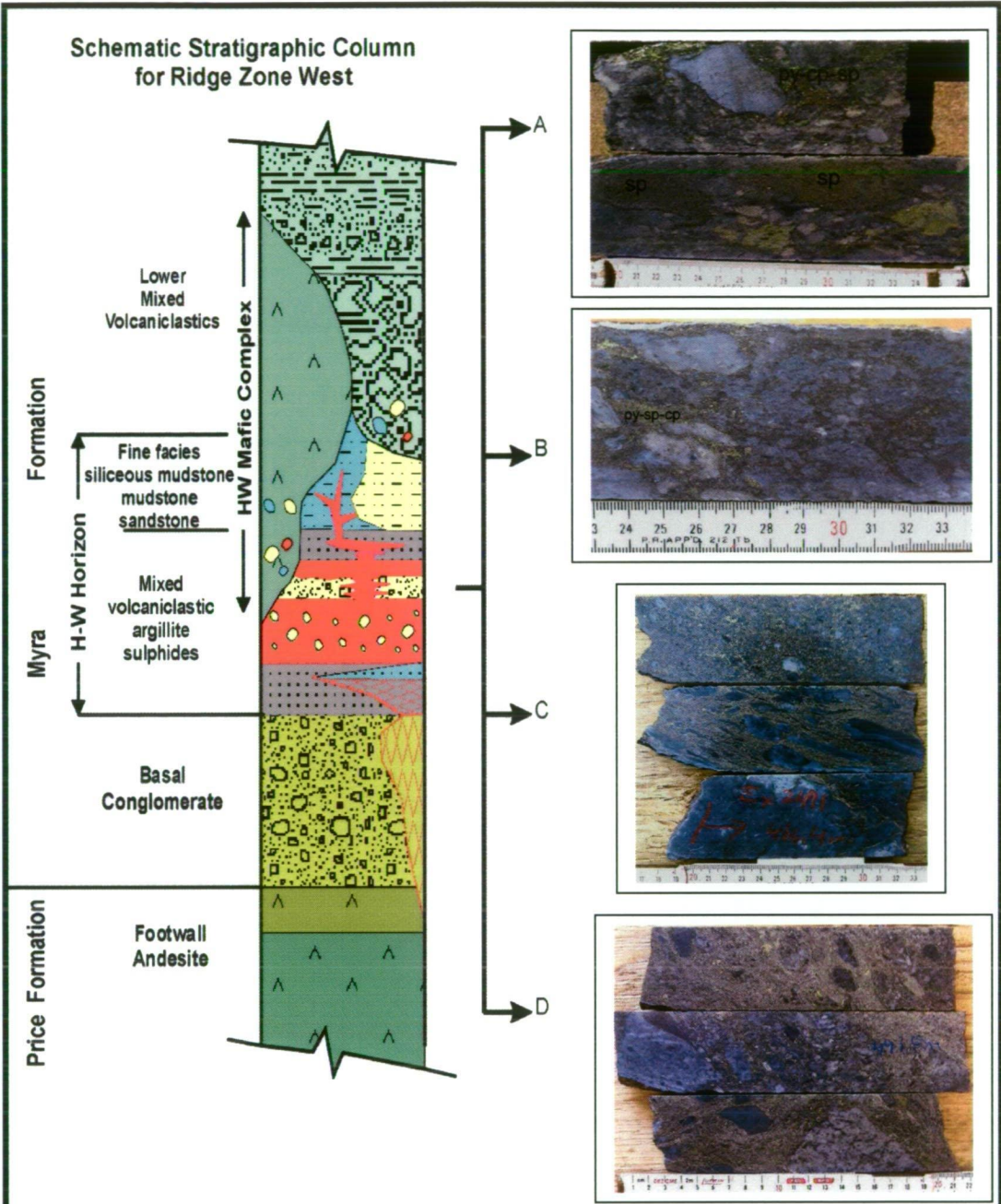


Figure 5.4: Mineralization associated with coarse-grained volcanic facies - 1

Scale is in centimeters.

The photographs illustrate progressive degrees of vein to massive style of mineralization in polymict pebblestone and sandstone. The textures are interpreted to represent subseafloor replacement style mineralization within coarse-grained volcanic facies rocks.

A- Lx10-2045; 486.8m-489.2m (top-bottom);

(top) Polymict pebble conglomerate with anastomosing pyrite-chalcopryite-sphalerite (py-cp-sp) veining.

(bottom) Possible sphalerite (sp) clasts (?) in polymict pebble conglomerate.

B- Lx10-2046; 488.3m

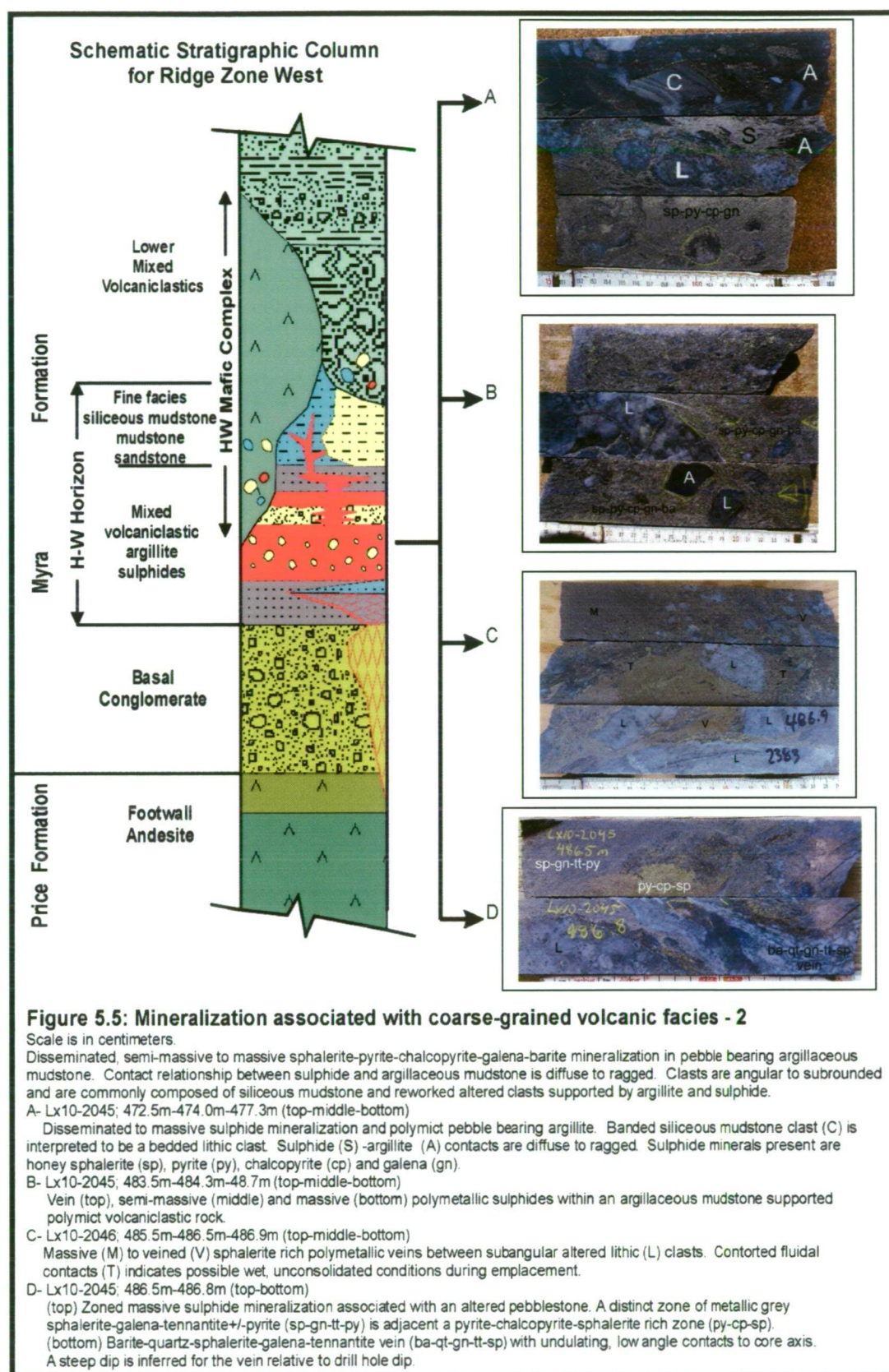
Anastomosing pyrite-sphalerite-chalcopryite (py-sp-cp) veining in pebble bearing sandstone.

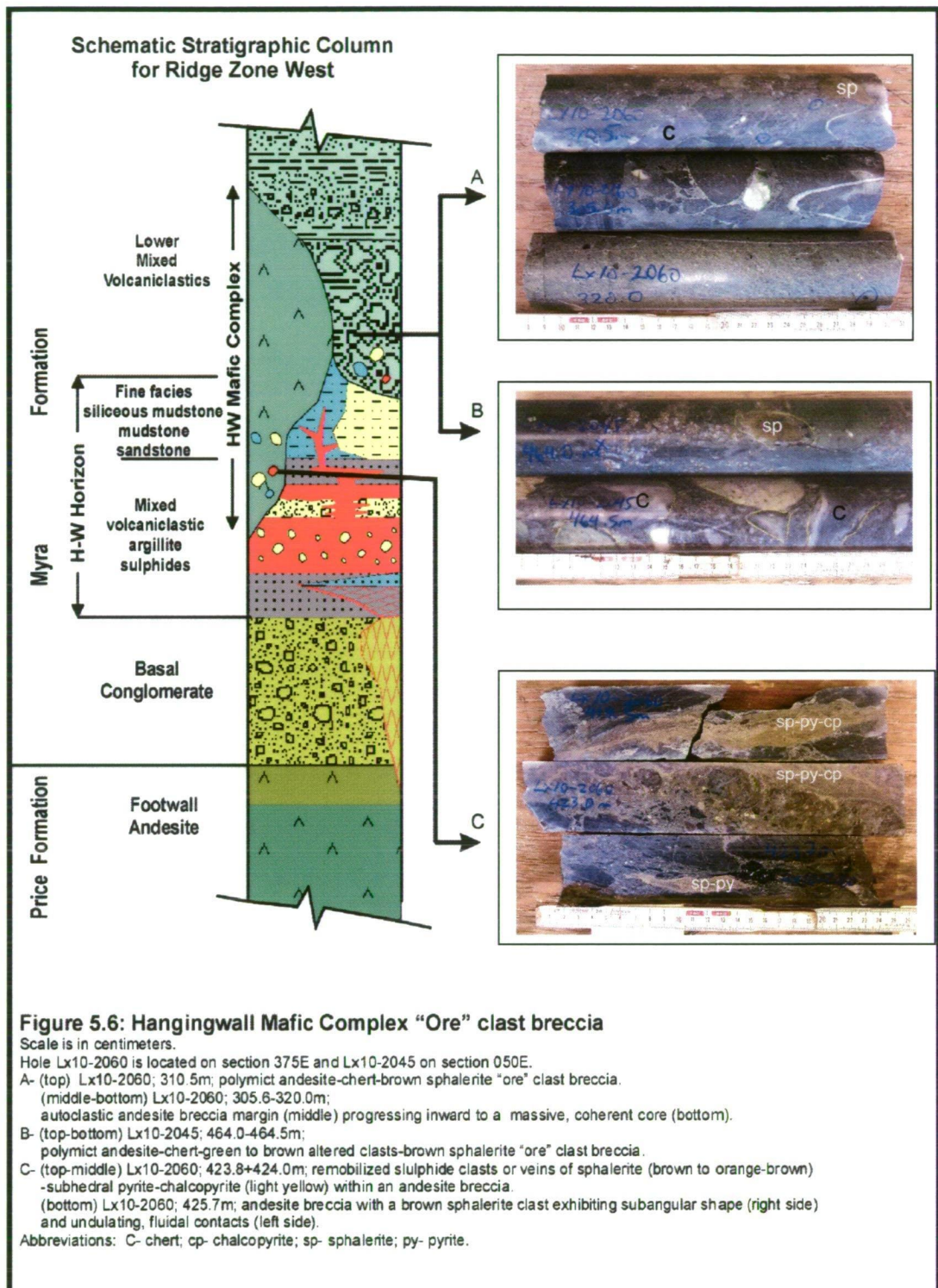
C- Lx10-2048; 465.5m-466.0m-466.4m (top-middle-bottom)

Semi-massive (top) and vein (middle-bottom) style sphalerite-pyrite-chalcopryite-galena mineralization in polymict pebble conglomerate.

D- Lx10-2048; 490.0-493.8m-495.0m (top-middle-bottom)

Massive (top-bottom) and vein (middle) style sphalerite-pyrite-chalcopryite-galena mineralization in polymict pebble conglomerate.





5.4.3 Discussion on styles of mineralization and volcanic facies

The styles of mineralization relative to volcanic facies and time of deposition can be separated into four phases.

Phase 1: Mineralization within the Lower and Main lenses is associated with fine-grained volcanic rocks and occur as fine disseminations and bands in bedded mudstone (Fig. 5.2a, d). These textures could have been produced by two different processes. The first option is deposition of mineralization on the ancient seafloor contemporaneous with mudstone deposition. A second possible process is selective sub-seafloor replacement of discrete individual mudstone beds with sulphide bands and disseminations. Based on the drill core textures observed in Fig. 5.2, the author favours a syndepositional interpretation as some sulphide and mudstone bands have grain-size gradation, flame structures and soft-sediment deformation textures typical of sedimentary processes. Soft-sediment deformation textures are formed by loading from overlying volcano-sedimentary deposits prior to lithification. A sub-seafloor replacement process would probably not preserve normal or reverse grain size gradation unless original individual grains were replaced by sulphide. Sub-seafloor replacement of discrete millimeter scale beds is not likely, as the mudstone beds do not have apparent grain size differences between individual beds lending to preferential lateral migration of hydrothermal fluids due to porosity. Therefore, banded mineralization with primary sedimentary textures is interpreted to have formed on the seafloor synchronous with the host mudstone.

Another style of mineralization associated with fine-grained volcanic rocks are semi-massive sulphides (Fig. 5.2b, c) that have contorted shapes and ragged to diffuse contacts relative to the enveloping argillaceous mudstone sediments. Subsequent deposition of angular silicified mudstone clasts and subangular polymict clasts on top of, and into an unconsolidated argillaceous mudstone may have deformed the unconsolidated mudstone substrate and hence contribute to the contorted textures observed. The ragged to diffuse sulphide contacts with argillaceous mudstone may have resulted from either synchronous deposition of the mineralization and mudstone on the seafloor or by sub-seafloor replacement processes. Therefore, based on the above discussion, disseminated, semi-massive and massive sulphide mineralization associated with argillaceous fine-grained volcanic facies rocks is interpreted to be transitional with deposition either on the seafloor or sub-seafloor prior to consolidation of the argillaceous mudstone.

Phase 2: Main lens mineralization associated with polymict coarse-grained volcanic facies rocks is dominantly vein style. Anastomosing veins of sphalerite-pyrite-chalcopyrite+/-galena appear to “flow” through the matrix and between clasts (Figs. 5.4 and 5.5). Some veins have curved and sharp contacts. Sphalerite-pyrite-chalcopyrite+/-galena rich veining increases in intensity to reach semi-massive or massive textures with preserved altered polymict clasts (Fig. 5.4 and 5.5). Barite-quartz-galena-tennantite-sphalerite rich veins with steep to moderate dip appear to have been emplaced synchronous with or post sphalerite-pyrite-chalcopyrite rich mineralization. The curved contacts appear fluidal and are interpreted as possible sulphide vein deposition (Fig. 5.5c) within an unconsolidated, hydrous environment prior to lithification. Based on the textures observed, permeable coarse-grained volcanic rocks are replaced by sphalerite-pyrite-chalcopyrite+/-galena and barite-quartz-galena-tennantite-sphalerite rich veins in a sub-seafloor environment. Depth appears to be within 15 m of the paleo-seafloor based on cross-section interpretations.

Sphalerite-pyrite rich clasts within the polymict coarse-grained volcanic facies deposits are dominantly subangular with minor subrounded outlines (Fig. 5.4). The sulphide clasts may have been subject to mechanical abrasion during transport. It is unclear whether the sulphide clasts observed are from proximal or distal sources. The inference of a proximal source is based on the subangular form and similar mineralogical assemblage to the surrounding mineralization.

Phase 3: Upper lens mineralization within fine-grained silicified mudstone is a combination of pyrite-chalcopyrite disseminations hosted by sandstone bands, mudstone-sandstone breccia, and pyrite-chalcopyrite veins associated with brittle fractures (Fig. 5.3). Pyrite-chalcopyrite rich mineralization associated with silicified mudstone-sandstone breccia could have been generated by synvolcanic deposition or sub-seafloor replacement along porous sandstone bands.

Phase 4: Upper lens mineralization pyrite-chalcopyrite+/-sphalerite veins are post-lithification of the silicified mudstone. Geological events that could have caused brittle fracturing and slumping of silicified mudstone are earthquakes, loading by subsequent volcano-sedimentary deposits, or intrusion of the Hangingwall Mafic Complex into partially lithified sediments. This style of mineralization could have been emplaced during a late mineralizing event or by secondary remobilization processes. Brecciation related to intrusion of the Hangingwall Mafic Complex is discounted as it appears unaltered and is interpreted to have been emplaced after cessation of the mineralizing event.

5.4.4 Summary on styles of mineralization and volcanic facies

Lower and Main lenses mineralization associated with fine-grained facies volcano-sedimentary rocks have banded, disseminated, and contorted textures in semi-massive to massive accumulations. Banded mineralization with grain size gradation, flame structures, and soft-sediment deformation textures are interpreted to have formed on the seafloor synchronous with the fine-grained facies mudstone.

Contorted textures in with argillaceous mudstone and semi-massive to massive mineralization are interpreted as soft-sediment deformation features generated prior to lithification. The mineralization could have been deposited synchronous with the host argillaceous mudstone or by shallow sub-seafloor replacement processes.

Main lens mineralization associated with fine and coarse-grained volcanic rocks have disseminated, vein, and semi-massive to massive textures. Sphalerite-pyrite-chalcopyrite+/-galena and barite-quartz-galena-tennantite-sphalerite rich veins range from weak anastomosing veins increasing in intensity to semi-massive or massive veins with remnant coarse-grained polymict volcanic facies rocks. The vein textures are interpreted as evidence that the mineralizing hydrothermal fluids passed through unconsolidated, coarse-grained volcanic rocks deposited by mass flow processes. This style of mineralization represents shallow sub-seafloor mineralization.

Upper lens mineralization within fine-grained silicified mudstone is a combination of pyrite-chalcopyrite disseminations hosted by sandstone bands, mudstone-sandstone breccia, and pyrite-chalcopyrite veins associated with brittle fractures. Pyrite-chalcopyrite rich sandstone bands and matrix within silicified mudstone and breccia could have been generated by synvolcanic deposition or sub-seafloor replacement related to porosity contrast.

Upper lens mineralization pyrite-chalcopyrite+/-sphalerite veins are post-lithification of the silicified mudstone. This style of mineralization could have been emplaced during a late mineralizing event or by secondary remobilization processes.

5.5 Ore microscopy and mineral chemistry

The ore and gangue minerals observed for the Ridge Zone West are typical for VHMS deposits. The main ore minerals in order of decreasing abundance are sphalerite, pyrite, chalcopyrite, galena and tetrahedrite-tennantite. Gangue minerals include quartz, muscovite, barite, chlorite, calcite, and rutile. The following section describes the ore mineral petrology based on microscopy and electron microprobe analyses. Average chemical composition and trace elements detected by electron microprobe analyses are listed and discussed following the microscope observations and discussion. The effect of metamorphism for a proposed paragenetic interpretation of the sulphide minerals is discussed.

5.5.1 Ore microscopy and analytical methods

The purpose of microscopy is for mineral identification, mineral textures, mineral chemistry and interpretation of a proposed mineral paragenetic sequence. Sixty-three polished thin sections were prepared from core samples representative of the Lower, Main, and Upper lenses. Techniques used were reflected-transmitted light microscopy and electron microprobe analyses. The author collected and rough cut all of the samples for final thin section preparation. Final preparation of the polished thin sections and off cuts was by Vancouver Petrographics Ltd., Langley, B.C., Canada.

Thin section microscopy and photography by the author was at the Centre for Ore Deposit Research, University of Tasmania. Diagnostic features used for assessment of ore minerals under reflected light are reflection behaviour (ie. colour, reflectivity, isotropism, internal reflections), fabric (twinning, zoning, deformations, exsolution, intergrowths), grain size, shape of grains or aggregates, relief, and hardness (Ramdohr, 1969; Kerr, 1977; Craig and Vaughn, 1994; Klein, 2002). Transparent gangue minerals are identified using colour (including pleochroism), form, cleavage, anisotropism (birefringence), extinction, and optical character (ie. uniaxial or biaxial). The samples assessed by microscopy and photography are listed in Appendix 2.

Microprobe analyses determined the compositions of the various ore minerals. The mineral formulas were derived from this information using the methods described by Klein (2002). Representative slides were chosen and probed using the Cameca microprobe SX-50 under the guidance of Dr. David Steele at the Central Science Laboratory, University of Tasmania. Analytical conditions, standards, and crystals are listed Appendix 3.

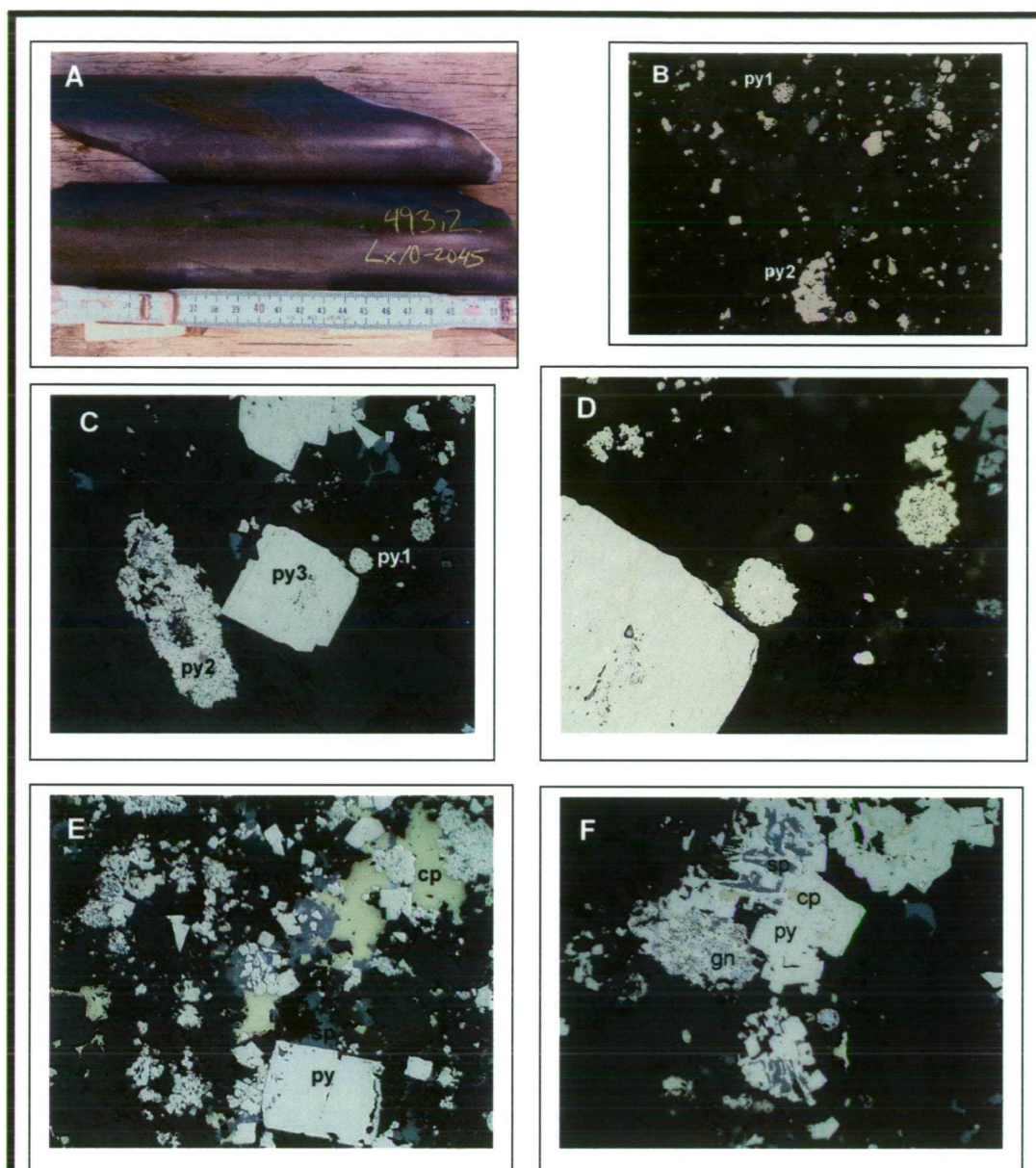


Figure 5.7: Pyrite facies - Lower lens mineralization in argillaceous mudstone

Styles of pyrite with increasing recrystallization. Pyrite-1 framboids (< 50 μm) to pyrite-2 spongey euhedra to pyrite-3 (> 50 μm) porphyroblasts (in order of increasing recrystallization).

A – Lx10-2045, 493.2m; Argillite drill core sample. Scale in centimeters.

B – Lx10-2045, 493.2m; disseminated pyrite-1 framboids (py1) and spongey pyrite-2 (py2). Reflected light. Width of view = 2100 μm .

C – Lx10-2045, 493.2m; disseminated pyrite-1 framboids (py1), spongey pyrite-2 (py2), and pyrite-3 porphyroblast (py3). Framboids are up to 25 μm . Reflected light. Width of view = 525 μm .

D – Lx10-2045, 493.2m; close up of pyrite-1 framboid from Fig. 5.7C. Reflected light. Width of view = 210 μm .

E – Lx10-2045; 293.2m; pyrite-2 recrystallizing to pyrite euhedra intergrown with recrystallized sphalerite, chalcopyrite and galena. Reflected light. Width of view = 1050 μm .

F – Lx10-2045, 493.2m; pyrite-1 framboids with sphalerite and galena at cores; pyrite intergrown with sphalerite, chalcopyrite and galena. Note careous textured pyrite intergrown with sphalerite (bottom middle). Reflected light. Width of view = 525 μm .

Abbreviations: chalcopyrite – cp; galena – gn; pyrite – py; sphalerite – sp

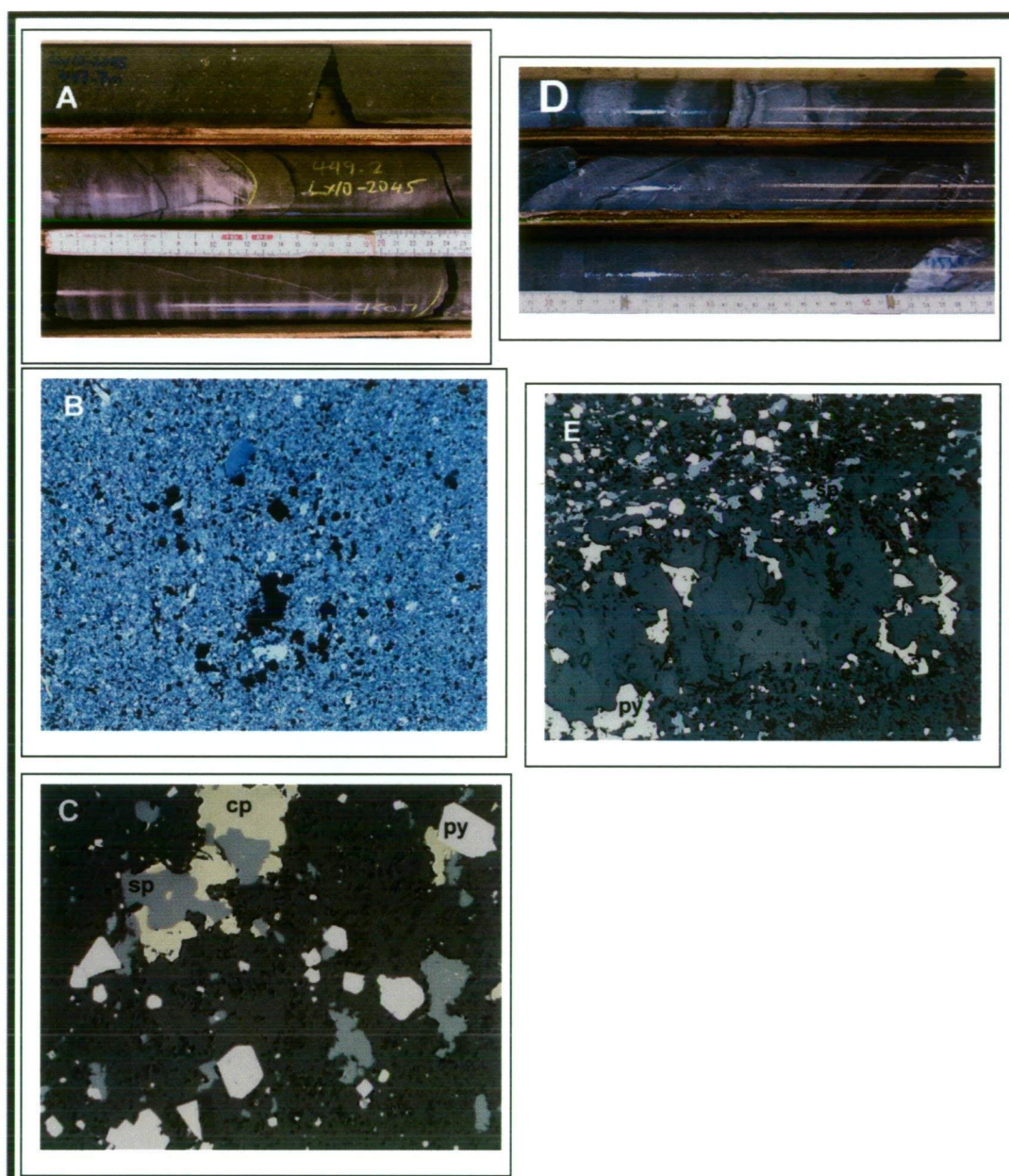


Figure 5.8: Upper lens mineralization in mudstone

Upper lens mineralization comprises disseminations and bands of pyrite and sphalerite.

A – Lx10-2045, 447.7-450.0m; grey to white mudstone in drill core. Scale in centimeters.

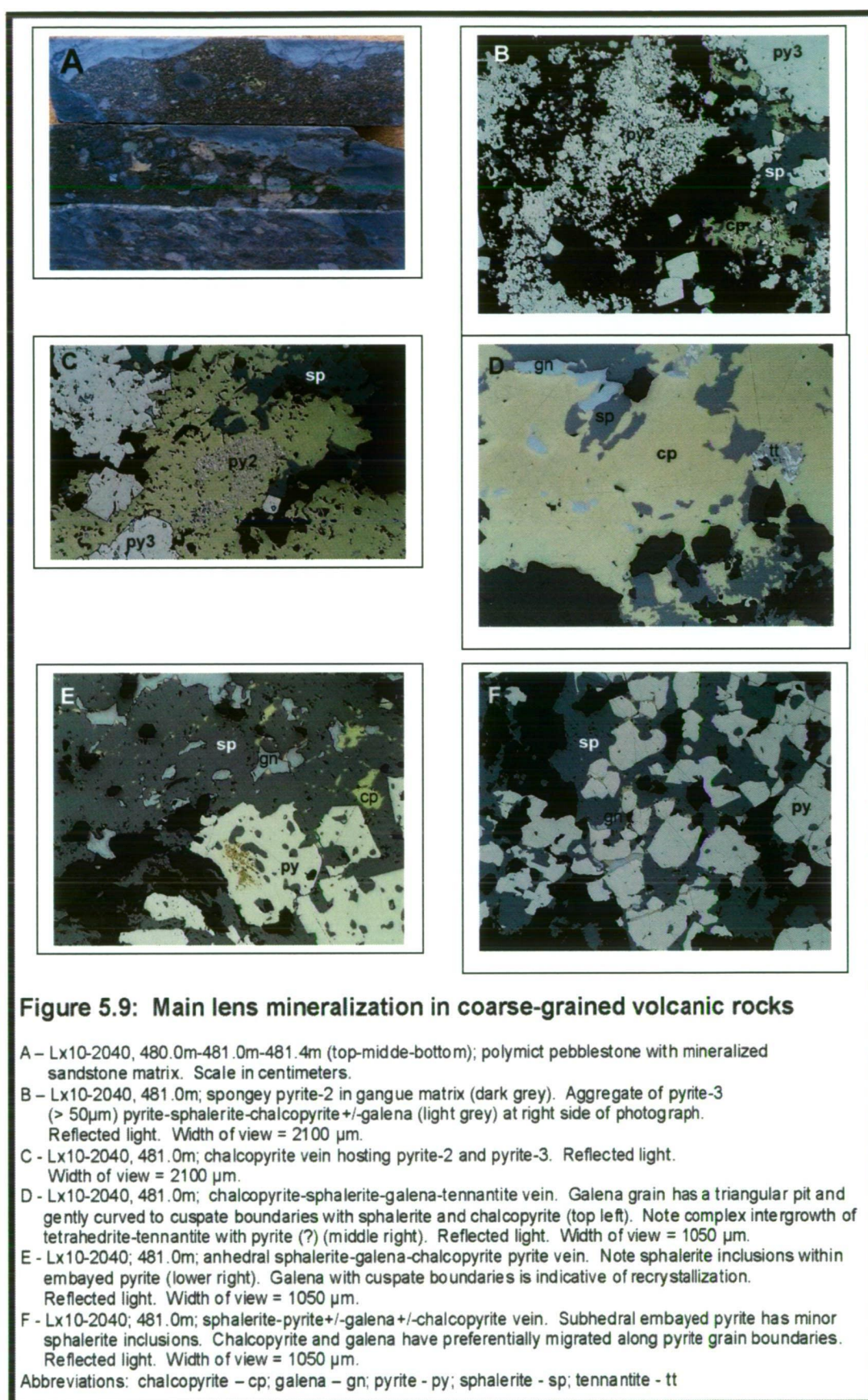
B – Lx10-2045, 450.0m; muscovite-rich matrix with disseminated opaque sulphides. Cross polars. Width of view = 2100 μ m.

C – Lx10-2045, 450.m; disseminated pyrite-1 (<50 μ m) and coarse-grained recrystallized pyrite, sphalerite and chalcopyrite. Pyrite has euhedral to subhedral form. Sphalerite and chalcopyrite are anhedral. One sphalerite grain has submicron yellow chalcopyrite blebs (middle right). Reflected light. Width of view = 525 μ m.

D – Lx10-2048, 450-453.0m; banded grey to white mudstone in drill core. Scale in centimeters.

E – Lx10-2048, 453.0m; banded pyrite-1 and coarser-grained recrystallized pyrite and sphalerite. Note weak alignment of sphalerite grains. Reflected light. Width of view = 1050 μ m.

Abbreviations: chalcopyrite – cp; galena – gn; pyrite – py; sphalerite – sp



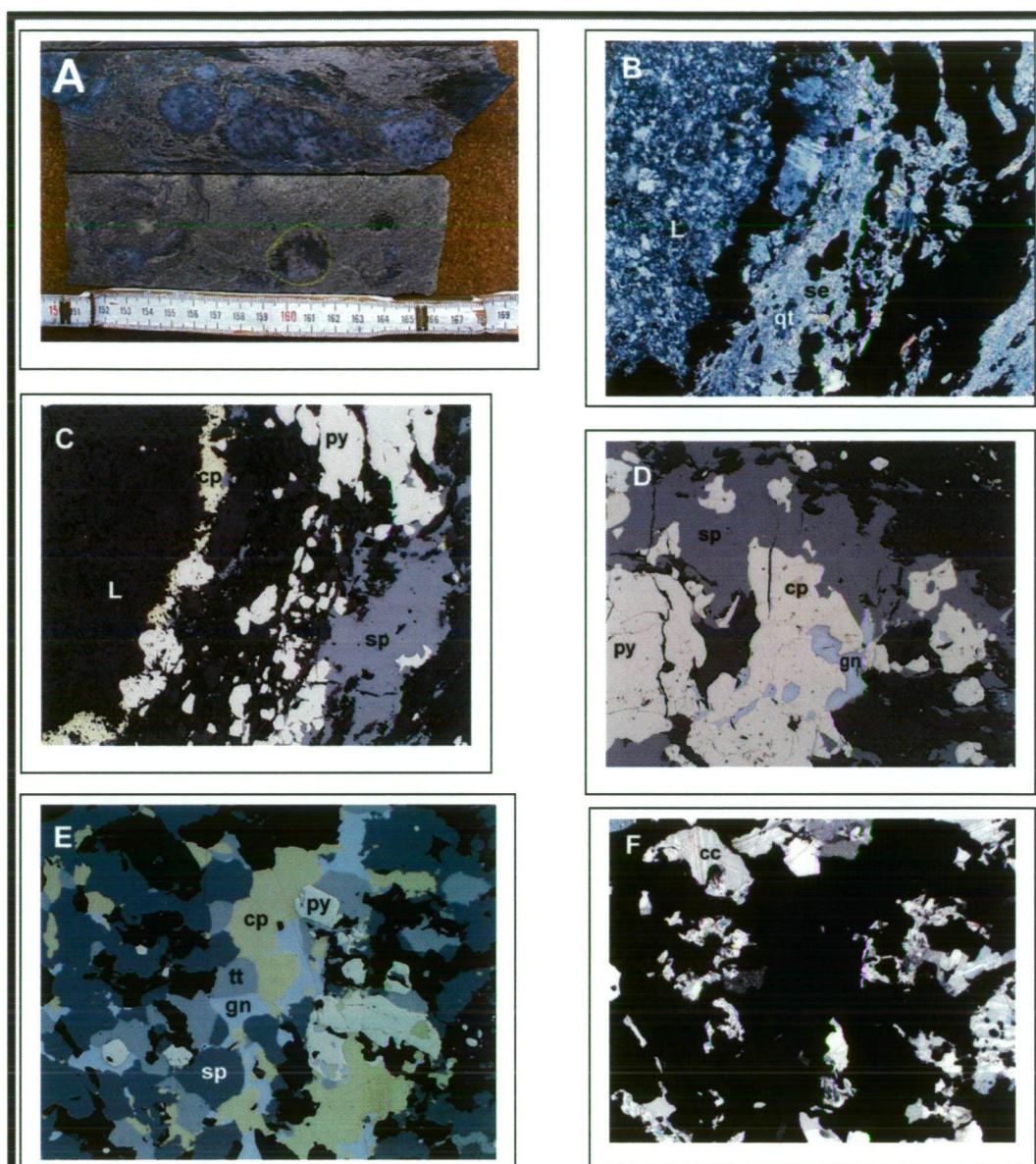


Figure 5.10: Main lens mineralization in coarse-grained volcanic rocks - 2

A – Lx10-2045, 474.0m-477.3m (top-bottom); argillite supported pebblestone with veined and semi-massive sphalerite-pyrite-galena-chalcopyrite. Scale in centimeters.

B – Lx10-2045, 474.0m; quartz altered lithic clast (L) on left side supported by a muscovite-quartz-feldspar+/- microcline argillaceous mudstone. Opaque minerals are sulphide veins as noted in photograph 5.10 C. Crossed polars. Width of view = 2100 μ m.

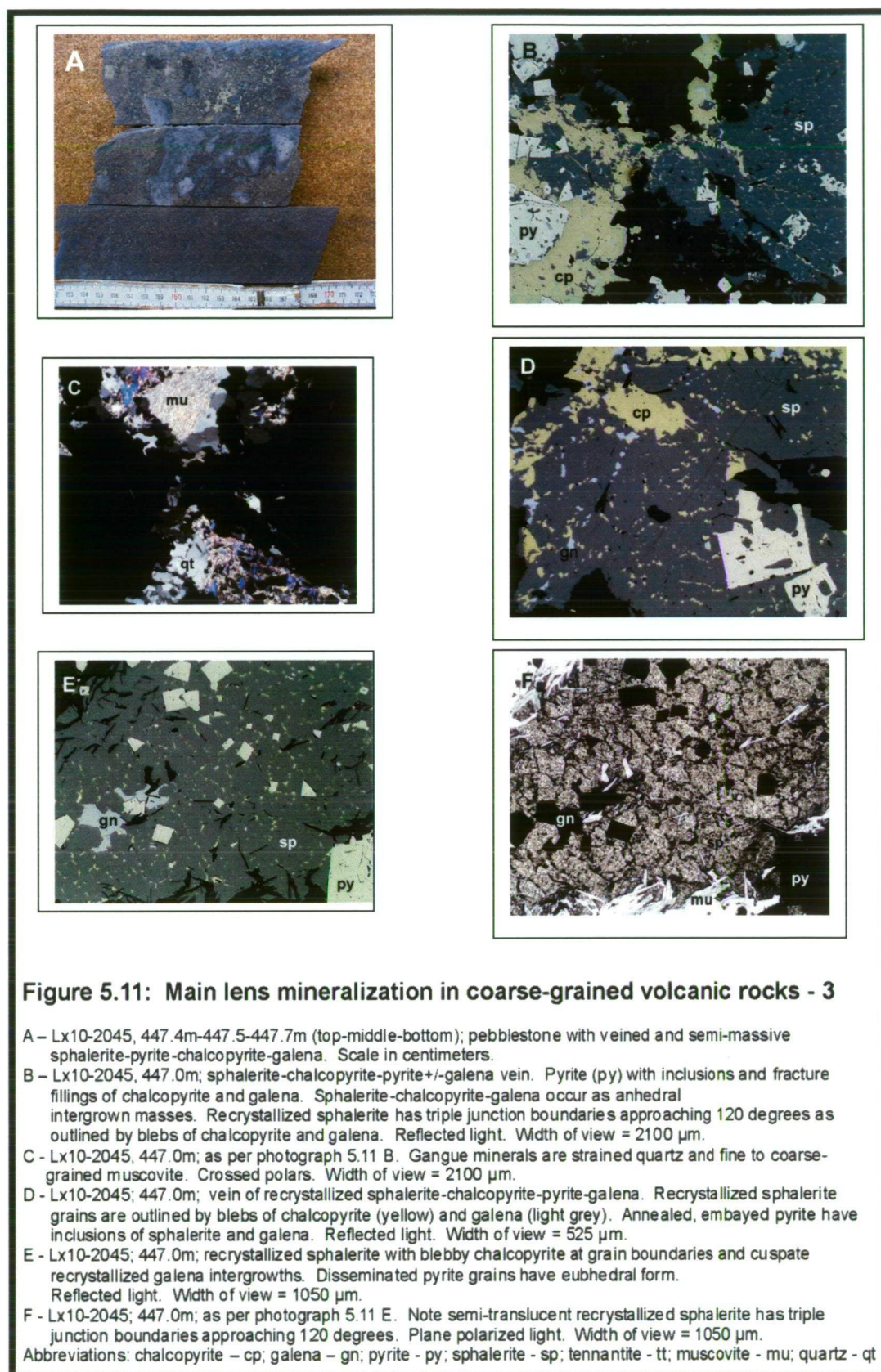
C – Lx10-2045, 474.0m; as per photograph 5.10 B. Sphalerite-pyrite-chalcopyrite veining around lithic clast (L). Note anhedral masses of sphalerite-pyrite and chalcopyrite in veining. Reflected light. Width of view = 2100 μ m.

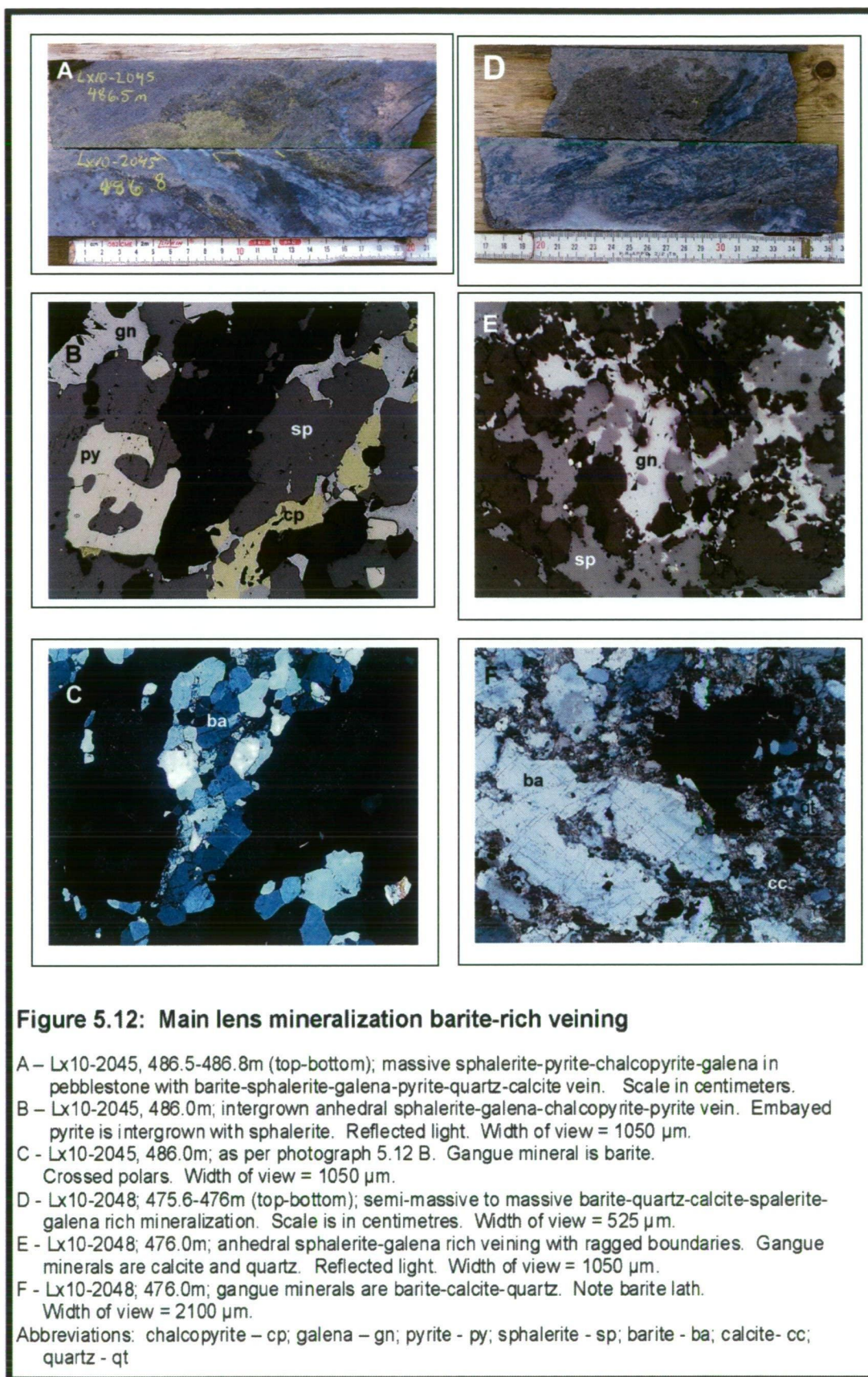
D – Lx10-2045; 474.0m; anhedral sphalerite-pyrite-galena-chalcopyrite vein. Inclusions of galena, chalcopyrite and sphalerite are hosted by embayed pyrite. Chalcopyrite bleb was verified by microprobe analyses. Reflected light. Width of view = 1050 μ m.

E – Lx10-2045; 481.0m; massive sphalerite-chalcopyrite-galena-tennantite-pyrite-calcite. Note granoblastic intergrowths of sphalerite, galena, and tennantite. Recrystallization textures include triple junction boundaries approaching 120 degrees and pyrite with rectilinear boundaries and overgrowths (middle right). Dark areas are calcite as shown in figure 5.10F. Reflected light. Width of view = 1050 μ m.

F – Lx10-2045; 481.0m; as per photograph 5.10 E. Note twinned calcite. Crossed polars. Width of view = 1050 μ m.

Abbreviations: chalcopyrite – cp; galena – gn; pyrite – py; sphalerite – sp; tennantite – tt; calcite – cc; se – sericite





5.5.2 Pyrite textures

There are three different types of pyrite that are characterized by size and mode of occurrence (Fig. 5.7). Pyrite-1 is characterized by fine-grained disseminated pyrite framboids and ring structures less than 50µm in diameter. Pyrite-2 is characterized by spongy pyrite composed of recrystallized pyrite framboids and fine-grained pyrite euhedra (Figs. 5.7 and 5.9). Pyrite-1 and pyrite-2 typically occur with fine-grained facies argillite and mudstone. Pyrite-3 grains occur as disseminated to banded, subhedral to euhedral cubes typically between 50 to 300 µm in fine-grained facies rocks. Coarse-grained pyrite idiomorphs and aggregates are noted to increase in size upwards to 1,000 µm and occur most commonly in coarse-grained volcanic rocks associated with the Main lens mineralization.

Pyrite-1 and pyrite-3 hosted by fine and coarse-grained facies volcanic rocks include embayed, and careous textured pyrite (Figs. 5.7f, 5.9e). Granoblastic polycrystalline aggregates of sphalerite, pyrite, galena and/or tetrahedrite-tennantite are common (Figs. 5.9 and 5.10). Granoblastic aggregates have coarse-grained, euhedral to subhedral pyrite with embayment textures. Chalcopyrite, sphalerite, and galena occur as inclusions in pyrite (Figs. 5.9 and 5.10). The chalcopyrite and galena inclusions are subrounded blebs and occur along grain boundaries.

Fine-grained pyrite framboids, ring structures and spongy pyrite are interpreted as primary textures formed during VHMS style mineralization (c.f. Eldridge et al., 1983). Coarse-grained granular pyrite could be formed by either metal zone refinement or annealing during metamorphism. The coarsening of grain sizes, embayment textures, and careous textures are indicative of recrystallization.

5.5.3 Pyrite chemistry

Microprobe analyses for five points on pyrite-1 and pyrite-2 are given in Table 5.3. Eighteen analyses of pyrite-3 grains are listed in Table 5.4. The average formula for all pyrite types analysed are similar at $\text{Fe}_{1.03}\text{S}_2$ for pyrite-1 and $\text{Fe}_{1.02}\text{S}_2$ for pyrite-2.

Copper, Zn, and As are typically below the detection level. The few analyses where these elements are detected is probably from chalcopyrite, sphalerite and tetrahedrite-tennantite inclusions in the pyrite. Nickel, Mn and Se are below detected limits for all the grains analysed. Minor Co was detected in two points analysed for pyrite-3. Generally, pyrite grains analysed for the Ridge Zone West have a simple chemical composition.

| Hole | Depth (m) | Point # | Wt%(S) | Wt%(Fe) | Wt%(Zn) | Wt%(As) | Total |
|--|-----------|---------|--------------|--------------|-------------|-------------|-----------------------------------|
| LX10-2040 | 481.2 | 1 | 51.92 | 46.92 | bd | bd | 98.84 |
| LX10-2048 | 452.8 | 2 | 51.94 | 46.48 | 0.19 | bd | 98.61 |
| LX10-2048 | 495.0 | 3 | 51.77 | 46.47 | bd | bd | 98.24 |
| LX10-2048 | 495.0 | 4 | 51.43 | 46.21 | 0.21 | 0.40 | 98.26 |
| LX10-2048 | 495.0 | 5 | 52.09 | 46.70 | bd | bd | 98.79 |
| Mean | | | 51.83 | 46.56 | 0.08 | 0.08 | 98.59 |
| Hole | Depth (m) | Point # | A%(S) | A%(Fe) | A%(Zn) | A%(As) | Total |
| LX10-2040 | 481.2 | 1 | 65.80 | 34.14 | 0.00 | 0.00 | 99.97 |
| LX10-2048 | 495.0 | 3 | 65.84 | 33.94 | 0.00 | 0.00 | 99.83 |
| LX10-2048 | 495.0 | 5 | 65.95 | 33.95 | 0.00 | 0.00 | 99.92 |
| Mean | | | 65.87 | 34.01 | 0.00 | 0.00 | 99.90 |
| Average Facies 1 pyrite formula (normalized to 1 sulphur atom) | | | | | | | Fe _{1.03} S ₂ |
| General pyrite formula (Deer et al., 1980) | | | | | | | FeS ₂ |
| Abbreviations: weight percent - Wt%; atomic percent - A%; bd - below detection | | | | | | | |
| Detection Limits: S=0.06 wt%; Fe=0.07wt%; Zn=0.10 wt%; As=0.05 wt% | | | | | | | |
| Mn=0.03 wt%; Cu=0.08 wt%; Ni=0.04 wt%; Co=0.01 wt%; Se=0.06 wt% | | | | | | | |
| Manganese, Cu, Ni, Co and Se analyses are below detection limits and are not listed. | | | | | | | |

| Table 5.4: Ridge Zone West Microprobe Analyses for Coarse Facies 3 Pyrite | | | | | | | | |
|--|-----------|---------|---------|---------|---------|---------|---------|-----------------------------------|
| HOLE | DEPTH (m) | Point # | Wt%(S) | Wt%(Fe) | Wt%(Co) | Wt%(Cu) | Wt%(Zn) | Total |
| LX10-2040 | 476.7 | 1 | 51.98 | 46.53 | bd | bd | bd | 98.51 |
| LX10-2040 | 476.7 | 2 | 51.99 | 46.19 | 0.22 | bd | bd | 98.40 |
| LX10-2040 | 481.2 | 3 | 52.07 | 46.96 | 0.02 | bd | bd | 99.03 |
| LX10-2040 | 481.2 | 4 | 51.82 | 46.79 | bd | bd | 0.16 | 98.78 |
| LX10-2045 | 447.4 | 5 | 52.18 | 46.06 | bd | bd | bd | 98.24 |
| LX10-2045 | 447.4 | 6 | 51.83 | 46.22 | bd | bd | bd | 98.04 |
| LX10-2045 | 474.0 | 7 | 52.55 | 46.63 | bd | bd | bd | 99.18 |
| LX10-2045 | 474.0 | 8 | 52.03 | 46.43 | bd | bd | bd | 98.46 |
| LX10-2045 | 474.0 | 9 | 52.71 | 46.73 | bd | bd | bd | 99.44 |
| LX10-2045 | 481.0 | 10 | 51.42 | 45.91 | bd | 1.06 | bd | 98.39 |
| LX10-2045 | 481.0 | 11 | 51.91 | 46.71 | bd | bd | bd | 98.62 |
| LX10-2045 | 486.7 | 12 | 52.47 | 47.33 | bd | bd | bd | 99.80 |
| LX10-2045 | 486.7 | 13 | 52.41 | 46.95 | bd | bd | bd | 99.36 |
| LX10-2048 | 453.5 | 14 | 51.83 | 45.76 | bd | bd | bd | 97.59 |
| LX10-2048 | 453.5 | 15 | 51.50 | 46.39 | bd | 0.11 | bd | 97.89 |
| LX10-2048 | 476.0 | 16 | 52.52 | 46.53 | bd | bd | bd | 99.06 |
| LX10-2048 | 495.0 | 17 | 51.93 | 46.61 | bd | bd | bd | 98.55 |
| LX10-2048 | 495.0 | 18 | 52.01 | 46.80 | bd | bd | bd | 98.82 |
| Mean | | | 52.06 | 46.53 | 0.01 | 0.06 | 0.01 | 98.69 |
| HOLE | DEPTH (m) | Point # | A%(S) | A%(Fe) | A%(Co) | A%(Cu) | A%(Zn) | Total |
| LX10-2040 | 476.7 | 1 | 66.00 | 33.92 | 0.00 | 0.00 | 0.00 | 99.93 |
| LX10-2045 | 447.4 | 5 | 66.23 | 33.57 | 0.00 | 0.00 | 0.00 | 99.81 |
| LX10-2045 | 447.4 | 6 | 66.05 | 33.82 | 0.00 | 0.00 | 0.00 | 99.89 |
| LX10-2045 | 474.0 | 7 | 66.22 | 33.74 | 0.00 | 0.00 | 0.00 | 99.97 |
| LX10-2045 | 474.0 | 8 | 66.11 | 33.87 | 0.00 | 0.00 | 0.00 | 99.99 |
| LX10-2045 | 474.0 | 9 | 66.24 | 33.72 | 0.00 | 0.00 | 0.00 | 99.97 |
| LX10-2045 | 481.0 | 11 | 65.88 | 34.04 | 0.00 | 0.00 | 0.00 | 99.93 |
| LX10-2045 | 486.7 | 12 | 65.85 | 34.10 | 0.00 | 0.00 | 0.00 | 99.95 |
| LX10-2045 | 486.7 | 13 | 65.99 | 33.94 | 0.00 | 0.00 | 0.00 | 99.94 |
| LX10-2048 | 453.5 | 14 | 66.32 | 33.62 | 0.00 | 0.00 | 0.00 | 99.96 |
| LX10-2048 | 476.0 | 16 | 66.26 | 33.70 | 0.00 | 0.00 | 0.00 | 99.97 |
| LX10-2048 | 495.0 | 17 | 65.96 | 34.00 | 0.00 | 0.00 | 0.00 | 99.97 |
| LX10-2048 | 495.0 | 18 | 65.92 | 34.06 | 0.00 | 0.00 | 0.00 | 99.99 |
| Mean | | | 66.08 | 33.85 | 0.00 | 0.00 | 0.00 | 99.94 |
| Average formula for facies 3 pyrite (normalized to 1 sulphur atom) | | | | | | | | Fe _{1.02} S ₂ |
| General formula for pyrite (Deer et al., 1980) | | | | | | | | FeS ₂ |
| Abbreviations: weight percent - wt%; atom percent - A%; bd - below detection | | | | | | | | |
| Detection Limits: S=0.06 wt%; Fe=0.07wt%; Zn=0.10 wt%; As=0.05 wt% | | | | | | | | |
| Mn=0.03 wt%; Cu=0.08 wt%; Ni=0.04 wt%; Co=0.01 wt%; Se=0.06 wt% | | | | | | | | |
| Manganese, Ni, As and Se analyses are below detection limits and are not listed. | | | | | | | | |

5.5.4 Sphalerite textures

Sphalerite and pyrite are the most common sulphide minerals present in the Ridge Zone West. Under reflected light sphalerite occurs as anhedral disseminations and polycrystalline aggregates with pyrite, chalcopyrite, galena, tetrahedrite-tennantite and barite. The reflected light colour is medium to dark grey. Relief is low relative to pyrite but similar to chalcopyrite. Plane polarized light characteristics for sphalerite include semi-translucent brown colour (Fig. 5.11).

Lower and Upper lens mineralization sphalerite grains are hosted by argillite and mudstone. Sphalerite grains in fine-grained facies rocks are disseminated and have anhedral forms (Figs. 5.7 and 5.8). Main lens mineralization sphalerite grains are coarser grained and occur as anhedral grains in veins and aggregates. Individual grains range in size up to 100 μm with massive polygonal aggregates greater than 1,000 μm (Figs. 5.9, 5.10, and 5.11). Coarse grains with hexagonal form have triple junctions approaching 120° indicative of annealing and recrystallization (Figs. 5.9) (Ramdohr, 1969; Stanton, 1972; Craig and Vaughn, 1994). Coarse-grained sphalerite aggregates appear as homogenized masses with the individual grain boundaries very difficult to distinguish.

Aggregates of sphalerite have granoblastic to homogenized anhedral form intergrown with pyrite, chalcopyrite, galena, and tetrahedrite-tennantite (Figs. 5.8c, 5.9, and 5.10e). The intergrowths do not show distinct age relationships.

Massive to semi-massive sphalerite aggregates with pyrite and chalcopyrite commonly have blebs of chalcopyrite occurring as anhedral, subrounded inclusions up to 1 μm . Anhedral chalcopyrite blebs within sphalerite masses commonly outline cleavage plains (Fig. 5.11). The blebs could be the result of exsolution, coprecipitation, recrystallization, or replacement (Eldridge et al., 1988). In massive sulphide deposits, this texture is typically referred to as chalcopyrite “disease” (Barton, 1978) and is discussed in further detail in section 5.8.

Sphalerite occurs as inclusions within pyrite-3 (Figs. 5.9e, 5.11d, and 5.12b). This texture is commonly formed when the pyrite is adjacent to or inside masses of sphalerite.

5.5.5 Sphalerite chemistry

The general formula for sphalerite is (Zn,Fe)S with Fe, Mn, Cd and Hg substituting for Zn in the structure (Deer, et al., 1980). Microprobe analyses of 21 points from selected sphalerite grains are listed in Table 5.5. From Table 5.5, the average formula for the relevant points normalized to 1 sulphur atom is $(\text{Zn}_{0.98}\text{Fe}_{0.02})\text{S}$.

From Table 5.5, Fe averages 1.06 wt %. Iron has been reported to comprise up to 26 wt % with increasing temperature (Deer et al., 1980). Based on this comparison, the sphalerite grains analysed for the Ridge Zone West have relatively low iron content.

Analyses for five sphalerite grains contain trace amounts of Cu. Copper in sphalerite is attributed to inclusions of chalcopyrite. Samples with Cu analyses above the detection limit have been omitted from the data used to derive the average stoichiometric formula for sphalerite in Table 5.5.

Cadmium averages 0.30 weight %. Trace contents of manganese were detected for five points analysed with an average of 0.03 wt %. Cadmium and Mn have been reported to comprise up to 4 to 5 wt % in natural sphalerites (Deer et al., 1980). The sphalerite grains analysed for the Ridge Zone West have relatively low Cd and Mn content. Selenium and Hg content was below detection limits for the grains analysed.

Table 5.5: Ridge Zone West Microprobe Analyses for Sphalerite

| HOLE | DEPTH (m) | Point # | Wt%(S) | Wt%(Mn) | Wt%(Fe) | Wt%(Cu) | Wt%(Zn) | Wt%(Cd) | Total |
|---|-----------|---------|--|---------|---------|---------|--|---------|-------|
| LX10-2040 | 476.7 | 1 | 32.71 | bd | 0.77 | bd | 64.83 | 0.33 | 98.64 |
| LX10-2040 | 476.7 | 2 | 32.32 | bd | 0.86 | 0.17 | 64.85 | 0.31 | 98.52 |
| LX10-2040 | 476.7 | 3 | 32.27 | bd | 1.07 | 0.25 | 64.97 | 0.33 | 98.89 |
| LX10-2040 | 481.2 | 4 | 32.36 | 0.10 | 2.24 | bd | 63.94 | 0.31 | 98.94 |
| LX10-2040 | 481.2 | 5 | 31.93 | bd | 3.39 | bd | 61.59 | 0.35 | 97.26 |
| LX10-2040 | 481.2 | 6 | 32.12 | bd | 1.52 | bd | 64.14 | 0.34 | 98.12 |
| LX10-2045 | 447.4 | 7 | 32.14 | bd | 1.76 | bd | 63.30 | 0.31 | 97.52 |
| LX10-2045 | 447.4 | 8 | 32.23 | 0.18 | 1.85 | bd | 63.61 | 0.28 | 98.16 |
| LX10-2045 | 474.0 | 9 | 32.38 | bd | 0.41 | bd | 65.16 | 0.32 | 98.27 |
| LX10-2045 | 474.0 | 10 | 32.35 | bd | 0.37 | bd | 65.05 | 0.30 | 98.07 |
| LX10-2045 | 474.0 | 11 | 32.51 | bd | 0.28 | bd | 65.54 | 0.33 | 98.66 |
| LX10-2045 | 474.0 | 12 | 32.53 | bd | 0.28 | bd | 65.91 | 0.31 | 99.02 |
| LX10-2045 | 481.0 | 13 | 31.98 | bd | 0.19 | 0.10 | 65.03 | 0.28 | 97.57 |
| LX10-2045 | 481.0 | 14 | 32.35 | 0.10 | 0.21 | bd | 66.03 | 0.29 | 98.98 |
| LX10-2045 | 481.0 | 15 | 31.97 | bd | 0.18 | bd | 65.21 | 0.29 | 97.64 |
| LX10-2045 | 486.7 | 16 | 32.66 | 0.18 | 0.60 | bd | 65.88 | 0.20 | 99.53 |
| LX10-2045 | 486.7 | 17 | 32.66 | 0.16 | 0.64 | bd | 64.56 | 0.20 | 98.22 |
| LX10-2048 | 453.5 | 18 | 32.02 | bd | 1.86 | 0.37 | 62.96 | 0.33 | 97.55 |
| LX10-2048 | 476.0 | 19 | 32.32 | bd | 0.19 | bd | 64.44 | 0.28 | 97.24 |
| LX10-2048 | 495.0 | 20 | 32.10 | bd | 1.40 | bd | 63.78 | 0.35 | 97.63 |
| LX10-2048 | 495.0 | 21 | 32.41 | bd | 2.16 | bd | 63.42 | 0.32 | 98.32 |
| Mean | | | 32.30 | 0.03 | 1.06 | 0.04 | 64.49 | 0.30 | 98.23 |
| HOLE | DEPTH (m) | Point # | A%(S) | A%(Mn) | A%(Fe) | A%(Cu) | A%(Zn) | A%(Cd) | Total |
| LX10-2040 | 476.7 | 1 | 50.28 | 0.00 | 0.68 | 0.00 | 48.88 | 0.15 | 99.98 |
| LX10-2040 | 481.2 | 4 | 49.66 | 0.09 | 1.97 | 0.00 | 48.13 | 0.13 | 99.98 |
| LX10-2040 | 481.2 | 5 | 49.72 | 0.00 | 3.03 | 0.00 | 47.05 | 0.16 | 99.96 |
| LX10-2040 | 481.2 | 6 | 49.72 | 0.00 | 1.35 | 0.00 | 48.71 | 0.15 | 99.94 |
| LX10-2045 | 447.4 | 7 | 49.99 | 0.00 | 1.57 | 0.00 | 48.28 | 0.14 | 99.98 |
| LX10-2045 | 447.4 | 8 | 49.81 | 0.16 | 1.65 | 0.00 | 48.22 | 0.12 | 99.96 |
| LX10-2045 | 474.0 | 9 | 50.06 | 0.00 | 0.36 | 0.00 | 49.41 | 0.14 | 99.97 |
| LX10-2045 | 474.0 | 10 | 50.09 | 0.00 | 0.33 | 0.00 | 49.40 | 0.13 | 99.96 |
| LX10-2045 | 474.0 | 11 | 50.05 | 0.00 | 0.25 | 0.00 | 49.50 | 0.15 | 99.94 |
| LX10-2045 | 474.0 | 12 | 49.95 | 0.00 | 0.25 | 0.00 | 49.65 | 0.13 | 99.98 |
| LX10-2045 | 481.0 | 14 | 49.77 | 0.09 | 0.18 | 0.00 | 49.81 | 0.13 | 99.98 |
| LX10-2045 | 481.0 | 15 | 49.78 | 0.00 | 0.16 | 0.00 | 49.81 | 0.13 | 99.89 |
| LX10-2045 | 486.7 | 16 | 49.87 | 0.16 | 0.52 | 0.00 | 49.34 | 0.09 | 99.98 |
| LX10-2045 | 486.7 | 17 | 50.35 | 0.14 | 0.57 | 0.00 | 48.83 | 0.09 | 99.97 |
| LX10-2048 | 476.0 | 19 | 50.39 | 0.00 | 0.17 | 0.00 | 49.27 | 0.12 | 99.95 |
| LX10-2048 | 495.0 | 20 | 49.92 | 0.00 | 1.25 | 0.00 | 48.65 | 0.15 | 99.98 |
| LX10-2048 | 495.0 | 21 | 49.95 | 0.00 | 1.91 | 0.00 | 47.94 | 0.14 | 99.95 |
| Mean | | | 49.96 | 0.04 | 0.95 | 0.00 | 48.88 | 0.13 | 99.96 |
| Average Sphalerite Formula (Normalized to 2 atoms) | | | | | | | (Zn _{0.98} ,Fe _{0.02})S | | |
| General Sphalerite Formula (Deer et al., 1980) | | | | | | | (Zn, Fe) S | | |
| Abbreviations: | | | weight percent - Wt%; atomic percent - A%; bd - below detection | | | | | | |
| Detection limits: | | | Zn = 0.13Wt%, S = 0.06Wt%, Fe = 0.03Wt%, Cd = 0.07 Wt%, Cu = 0.08Wt%, Mn=0.03Wt% | | | | | | |
| Selenium and Hg analyses are below detection limits and are not listed. | | | | | | | | | |

5.5.6 Chalcopyrite textures

Chalcopyrite occurs as anhedral disseminations and polycrystalline aggregates with pyrite, chalcopyrite, galena, tetrahedrite-tennantite and barite. Lower and Upper lens mineralization within fine-facies rocks has anhedral chalcopyrite up to 250 μm forming minor aggregates with sphalerite and pyrite (Fig. 5.8c). In Main lens mineralization, chalcopyrite occurs as veins, masses, and aggregates with granoblastic and homogenized sphalerite, pyrite, galena and/or tetrahedrite-tennantite (Figs. 5.9, 5.10e, and 5.11b, d).

Chalcopyrite is intergrown with granoblasts of sphalerite, pyrite, and galena. Grain size ranges between 100 to 250 μm . Anhedral homogenized masses and veins are up millimeter scale. Chalcopyrite also occurs along pyrite grain boundaries and as inclusions within pyrite (Figs. 5.7f, 5.10e, and 5.11b). Inclusions range from sub-micron up to 20 μm in size. Chalcopyrite occurs as subrounded inclusions within pyrite grains and along grain boundaries within pyrite masses. Chalcopyrite blebs in sphalerite rich aggregates occur along grain boundaries and cleavage planes (Fig. 5.11). This texture is referred to as chalcopyrite “disease” (Eldridge, 1988) and will be discussed in greater detail in section 5.8.

Twinning in chalcopyrite was not observed for the Ridge Zone West samples. This is likely due to recrystallization. Deformation is not apparent in chalcopyrite based on the lack of curved or spindle-shaped twin lamellae. This is likely due to the total annealing and recrystallization of chalcopyrite.

5.5.7 Chalcopyrite chemistry

Analyses of chalcopyrite from the Ridge Zone West are listed in Table 5.6. Chalcopyrite is relatively pure with an average formula of $\text{Cu}_{1.00}\text{Fe}_{1.01}\text{S}_2$. Zinc is the only significant impurity with seven grains having values above the detection limit. The Zn is likely due to minor inclusions within the grains analyzed. The purity of chalcopyrite reinforces the likelihood that the chalcopyrite has been recrystallized during metamorphism.

| Table 5.6: Ridge Zone West Microprobe Analyses for Chalcopyrite | | | | | | | |
|---|-----------|---------|--------|---------|---------|--|-------|
| HOLE | DEPTH (m) | Point # | Wt%(S) | Wt%(Fe) | Wt%(Cu) | Wt%(Zn) | Total |
| LX10-2040 | 476.7 | 1 | 34.31 | 29.59 | 34.10 | 0.14 | 98.14 |
| LX10-2040 | 481.2 | 2 | 34.13 | 29.94 | 34.54 | 0.34 | 98.94 |
| LX10-2040 | 481.2 | 3 | 34.29 | 30.20 | 33.95 | bd | 98.44 |
| LX10-2040 | 481.2 | 4 | 33.91 | 29.92 | 34.63 | bd | 98.46 |
| LX10-2045 | 447.4 | 5 | 33.92 | 28.93 | 33.08 | 0.88 | 96.81 |
| LX10-2045 | 474.0 | 6 | 34.24 | 29.67 | 33.80 | bd | 97.72 |
| LX10-2045 | 474.0 | 7 | 34.27 | 29.88 | 33.76 | bd | 97.90 |
| LX10-2045 | 474.0 | 8 | 34.65 | 30.16 | 34.00 | bd | 98.81 |
| LX10-2045 | 474.0 | 9 | 34.88 | 30.77 | 33.60 | bd | 99.25 |
| LX10-2045 | 474.0 | 10 | 34.29 | 30.39 | 34.38 | bd | 99.05 |
| LX10-2045 | 481.0 | 11 | 33.73 | 29.53 | 34.17 | 0.26 | 97.69 |
| LX10-2045 | 481.0 | 12 | 33.61 | 29.49 | 34.24 | 0.89 | 98.23 |
| LX10-2045 | 481.0 | 13 | 33.85 | 30.20 | 34.38 | bd | 98.43 |
| LX10-2045 | 486.7 | 14 | 34.25 | 29.70 | 33.61 | 0.16 | 97.71 |
| LX10-2045 | 486.7 | 15 | 34.39 | 29.83 | 33.80 | 0.11 | 98.13 |
| LX10-2048 | 452.8 | 16 | 33.74 | 29.23 | 33.48 | bd | 96.45 |
| LX10-2048 | 452.8 | 17 | 33.78 | 30.13 | 34.00 | bd | 97.91 |
| LX10-2048 | 495.0 | 18 | 33.69 | 30.35 | 33.82 | bd | 97.86 |
| Mean | | | 34.11 | 29.88 | 33.96 | 0.15 | 98.11 |
| HOLE | DEPTH (m) | Point # | A%(S) | A%(Fe) | A%(Cu) | A%(Zn) | Total |
| LX10-2040 | 481.2 | 3 | 49.86 | 25.21 | 24.91 | 0.00 | 99.98 |
| LX10-2040 | 481.2 | 4 | 49.46 | 25.05 | 25.48 | 0.00 | 99.99 |
| LX10-2045 | 474.0 | 6 | 50.09 | 24.92 | 24.95 | 0.00 | 99.97 |
| LX10-2045 | 474.0 | 7 | 50.03 | 25.05 | 24.87 | 0.00 | 99.96 |
| LX10-2045 | 474.0 | 8 | 50.11 | 25.04 | 24.81 | 0.00 | 99.96 |
| LX10-2045 | 474.0 | 9 | 50.17 | 25.41 | 24.38 | 0.00 | 99.96 |
| LX10-2045 | 474.0 | 10 | 49.60 | 25.24 | 25.09 | 0.00 | 99.93 |
| LX10-2045 | 481.0 | 13 | 49.38 | 25.29 | 25.30 | 0.00 | 99.96 |
| LX10-2048 | 452.8 | 16 | 50.01 | 24.88 | 25.04 | 0.00 | 99.93 |
| LX10-2048 | 452.8 | 17 | 49.46 | 25.33 | 25.12 | 0.00 | 99.92 |
| LX10-2048 | 495.0 | 18 | 49.40 | 25.55 | 25.02 | 0.00 | 99.97 |
| Mean | | | 49.78 | 25.18 | 25.00 | 0.00 | 99.96 |
| Average formula for chalcopyrite (normalized to 1 sulphur atom) | | | | | | Cu _{1.00} Fe _{1.01} S ₂ | |
| General formula for chalcopyrite (Deer et al., 1980) | | | | | | CuFeS ₂ | |
| Abbreviations: Weight percent - Wt%; Atomic percent - A%; bd - below detection | | | | | | | |
| Detection Limits: S = 0.06Wt%, Fe = 0.06Wt%, Cu = 0.08Wt%, Zn = 0.13Wt%, Ag = 0.08Wt% | | | | | | | |
| Mn = 0.03Wt%, Co = 0.01 Wt%, Ni = 0.04Wt%, As = 0.05Wt%, Se = 0.06Wt% | | | | | | | |
| Manganese, Co, Ni, As and Se analyses are below detection limits and not listed. | | | | | | | |

5.5.8 Galena textures

Galena under reflected light is a light metallic grey colour with occasional triangular pits. It is typically anhedral. Galena associated with Lower and Upper lens mineralization occurs in minor amounts as fine-grained disseminations up to 100 µm or as intergrowths with spongy pyrite-2 (Fig. 5.7f). Galena associated with Main lens mineralization occurs with polycrystalline aggregates of anhedral to granoblastic sphalerite, pyrite, tennantite, chalcopryite, and barite (Figs. 5.9, 5.10, and 5.11). Barite-rich veins are commonly associated with sphalerite-galena rich mineralization. Galena in Main lens mineralization ranges from 5 µm inclusions to recrystallized anhedral galena up to 300 µm. Triangular pits are not always present within individual grains.

Coarse polycrystalline aggregates of galena have subrounded intergrowths of minor sphalerite. Grain boundaries approach 120° triple junctions when intergrown with recrystallized sphalerite. Subrounded galena inclusions within pyrite range from 5 to 50 µm. Galena commonly occurs at pyrite grain boundaries. Tetrahedrite-tennantite-galena aggregates are common. Evidence for recrystallization include triangular pits (cleavage), grain boundaries approaching 120° triple junctions, and occurring at tetrahedrite-tennantite / annealed pyrite grain boundaries.

5.5.9 Galena chemistry

Microprobe analyses of 17 points in selected galena grains are listed in Table 5.7. The average formula for the grains analysed is $Pb_{1.07}S$ based on 7 grains with Fe contents below the detection limit. Iron is the most significant substitution or impurity with a mean of 0.48 wt %. Some of the grains contain high Fe ranging up to 6.83 wt % Fe suggesting pyrite inclusions. Selenium averages 0.06 wt % for the galena grains analysed. Se may occur through limited solid solution substituting for S (Stanton, 1972). Tellurium was not analysed. There is a complete range of solid solution between galena (PbS) and clausthalite (PbSe) (Deer et al., 1980). Based on the insignificant amount of Se present, the dominant mineral present is galena.

| Table 5.7: Ridge Zone West Microprobe Analyses for Galena | | | | | | | |
|--|------------------|----------------|---------------|----------------|----------------|---------------------------|--------------|
| HOLE | DEPTH (m) | Point # | Wt%(S) | Wt%(Fe) | Wt%(Se) | Wt%(Pb) | Total |
| LX10-2040 | 476.7 | 1 | 12.35 | 0.11 | bd | 85.85 | 98.31 |
| LX10-2040 | 476.7 | 2 | 12.40 | 0.19 | bd | 84.88 | 97.47 |
| LX10-2040 | 481.2 | 3 | 12.15 | 0.13 | bd | 85.35 | 97.63 |
| LX10-2040 | 481.2 | 4 | 13.58 | 3.38 | bd | 82.99 | 99.94 |
| LX10-2040 | 481.2 | 5 | 12.27 | 0.86 | 0.21 | 85.20 | 98.54 |
| LX10-2045 | 447.4 | 6 | 12.30 | 0.79 | bd | 84.42 | 97.51 |
| LX10-2045 | 447.4 | 7 | 12.30 | bd | bd | 86.07 | 98.37 |
| LX10-2045 | 474.0 | 8 | 12.67 | bd | bd | 85.20 | 97.87 |
| LX10-2045 | 474.0 | 9 | 12.33 | 0.17 | bd | 85.86 | 98.36 |
| LX10-2045 | 481.0 | 10 | 12.20 | 0.13 | bd | 84.86 | 97.19 |
| LX10-2045 | 481.0 | 11 | 12.24 | bd | bd | 85.31 | 97.56 |
| LX10-2045 | 481.0 | 12 | 12.46 | bd | bd | 85.51 | 97.97 |
| LX10-2045 | 486.7 | 13 | 12.55 | bd | bd | 86.46 | 99.01 |
| LX10-2045 | 486.7 | 14 | 12.36 | bd | bd | 86.31 | 98.67 |
| LX10-2048 | 476.0 | 15 | 12.58 | bd | bd | 86.69 | 99.26 |
| LX10-2048 | 495.0 | 16 | 11.98 | 0.71 | 0.38 | 85.23 | 98.30 |
| LX10-2048 | 495.0 | 17 | 12.24 | 1.71 | 0.44 | 84.20 | 98.59 |
| Mean | | | 12.41 | 0.48 | 0.06 | 85.32 | 98.27 |
| HOLE | DEPTH (m) | Point # | A%(S) | A%(Fe) | A%(Se) | A%(Pb) | Total |
| LX10-2045 | 447.4 | 7 | 47.88 | 0.00 | 0.00 | 51.87 | 99.75 |
| LX10-2045 | 474.0 | 8 | 48.93 | 0.00 | 0.00 | 50.92 | 99.85 |
| LX10-2045 | 481.0 | 11 | 48.06 | 0.00 | 0.00 | 51.83 | 99.89 |
| LX10-2045 | 481.0 | 12 | 48.48 | 0.00 | 0.00 | 51.48 | 99.96 |
| LX10-2045 | 486.7 | 13 | 48.35 | 0.00 | 0.00 | 51.55 | 99.89 |
| LX10-2045 | 486.7 | 14 | 48.02 | 0.00 | 0.00 | 51.90 | 99.92 |
| LX10-2048 | 476.0 | 15 | 48.38 | 0.00 | 0.00 | 51.60 | 99.98 |
| Mean | | | 48.30 | 0.00 | 0.00 | 51.59 | 99.89 |
| Average formula for galena (normalized to 1 sulphur atom) | | | | | | Pb_{1.07}S | |
| General formula for galena (Deer et al., 1980) | | | | | | PbS | |
| Abbreviations: Weight percent - Wt%; Atomic percent - A%; bd - below detection | | | | | | | |
| Detection Limits: Pb = 0.29Wt%, S = 0.11Wt%, Fe = 0.08Wt%, Se = 0.047Wt%, Ag = 0.082Wt% | | | | | | | |
| Silver analyses are below detection limit and are not listed | | | | | | | |

5.5.10 Tetrahedrite-tennantite textures

Tetrahedrite-tennantite has only been observed in Main lens mineralization hosted by the coarse-grained facies volcanic rocks. In hand sample, tetrahedrite-tennantite comprises only trace amounts of the sulphides present. It is very fine grained, anhedral, greenish-black in colour, and has a metallic luster.

Under reflected light, tetrahedrite-tennantite occurs as subrounded anhedral to granoblastic crystals within polycrystalline aggregates with sphalerite, galena, chalcopyrite, pyrite, and barite (Fig. 5.10e). The tetrahedrite-tennantite has a metallic, pale greenish-grey reflection. Relief is similar to galena and chalcopyrite. Anhedral to granoblastic tetrahedrite-tennantite grains range between 100 to 250 μm .

Mineral inclusions within tetrahedrite-tennantite are galena and chalcopyrite. Galena is the most common sulphide associated with tetrahedrite-tennantite. Galena and chalcopyrite occur as inclusions and along tetrahedrite-tennantite grain boundaries. This texture is consistent with metamorphic recrystallization.

5.5.11 Tetrahedrite-tennantite chemistry

Microprobe analyses of tetrahedrite-tennantite grains are shown in Table 5.8. From the five points analysed in tetrahedrite-tennantite grains, the average chemical composition is $(\text{Cu}_{9.9}\text{Ag}_{0.2})(\text{Zn}_{1.4}\text{Fe}_{0.6})(\text{Sb}_{0.7}\text{As}_{3.3})\text{S}_{13}$. Therefore, the mineral analysed is the arsenic rich end-member tennantite with an average arsenic content of 16.06 wt %. Other elements present are Fe, Ag, and Se. Se contains on average 0.14 wt % for the points analysed and substitutes for S. Silver accounts for 1.45 wt % of the tennantite grains analysed. Therefore, tennantite is a significant source of residency for silver relative to the sulphide-sulphosalt minerals analysed.

| Table 5.8: Ridge Zone West Microprobe Analyses for Tetrahedrite-Tennantite | | | | | | | | | | | |
|--|-----------|---------|--------|---------|---------|---------|---------|---------|---------|---------|--------|
| HOLE | DEPTH (m) | Point # | Wt%(S) | Wt%(Fe) | Wt%(Cu) | Wt%(Zn) | Wt%(As) | Wt%(Se) | Wt%(Ag) | Wt%(Sb) | Total |
| LX10-2045 | 474 | 1 | 27.86 | 2.56 | 41.74 | 6.23 | 17.52 | 0.14 | 1.80 | 3.24 | 100.90 |
| LX10-2045 | 481 | 2 | 27.03 | 2.17 | 41.30 | 6.16 | 19.10 | 0.16 | 1.10 | 1.09 | 98.10 |
| LX10-2045 | 481 | 3 | 27.46 | 2.12 | 42.20 | 6.30 | 18.93 | 0.15 | 0.83 | 1.31 | 99.30 |
| LX10-2045 | 486 | 4 | 26.36 | 2.82 | 39.03 | 4.99 | 10.49 | 0.10 | 2.72 | 13.59 | 100.11 |
| LX10-2048 | 476 | 5 | 26.98 | 1.92 | 40.26 | 6.74 | 14.25 | 0.14 | 0.99 | 8.13 | 99.42 |
| Mean | | | 27.14 | 2.32 | 40.91 | 6.09 | 16.06 | 0.14 | 1.46 | 5.47 | 99.57 |
| HOLE | DEPTH (m) | Point # | A%(S) | A%(Fe) | A%(Cu) | A%(Zn) | A%(As) | A%(Se) | A%(Ag) | A%(Sb) | Total |
| LX10-2045 | 474 | 1 | 44.70 | 2.36 | 33.79 | 4.90 | 12.03 | 0.09 | 0.77 | 1.37 | 100.00 |
| LX10-2045 | 481 | 2 | 44.31 | 2.04 | 34.17 | 4.96 | 13.40 | 0.11 | 0.54 | 0.47 | 100.00 |
| LX10-2045 | 481 | 3 | 44.42 | 1.97 | 34.45 | 5.00 | 13.10 | 0.10 | 0.40 | 0.56 | 100.00 |
| LX10-2045 | 486 | 4 | 44.64 | 2.74 | 33.36 | 4.15 | 7.61 | 0.07 | 1.37 | 6.06 | 100.00 |
| LX10-2048 | 476 | 5 | 44.74 | 1.83 | 33.70 | 5.49 | 10.12 | 0.10 | 0.49 | 3.55 | 100.00 |
| Mean | | | 44.56 | 2.19 | 33.89 | 4.90 | 11.25 | 0.09 | 0.71 | 2.40 | 100.00 |
| Average formula for tetrahedrite-tennantite (normalized to 13 sulphur atoms) $(\text{Cu}_{3.9}\text{Ag}_{0.2})(\text{Zn}_{1.4}\text{Fe}_{0.6})(\text{Sb}_{0.7}\text{As}_{0.3})\text{S}_{13}$ | | | | | | | | | | | |
| General formula for tetrahedrite-tennantite (Stanton, 1972) $(\text{Cu}_x\text{Ag})_{10}(\text{Zn}_y\text{Fe}_z)(\text{Sb}_a\text{As}_b)\text{S}_{13}$ | | | | | | | | | | | |
| Results for the five grains analysed show the average composition as the As-rich end member tennantite | | | | | | | | | | | |
| Abbreviations: weight percent - Wt%; atomic percent - A%; below detection - bd | | | | | | | | | | | |
| Detection Limits: S = 0.12Wt%, Fe = 0.03Wt%, Ni = 0.04Wt%, Cu = 0.10Wt%, Zn = 0.11Wt%, As = 0.20Wt%, Se = 0.06 Wt%, Ag = 0.05Wt%, Sb = 0.07Wt% | | | | | | | | | | | |

5.6 Gangue mineral microscopy and chemistry

Gangue minerals for the Ridge Zone West are quartz, barite, muscovite, and calcite based on hand samples and microscopy. Mineral chemistry is discussed only for barite and muscovite.

5.6.1 Quartz textures

Quartz occurs as fine-grained to coarse, inclusion-rich polycrystalline aggregates. Anhedral intergrowths of quartz with sulphide minerals are common. Quartz veins typically have anhedral grains. Relict, angular volcanic quartz crystals are often overgrown by quartz rims. Quartz grains are dominantly fine-grained up to 50 µm with coarse-grained recrystallized quartz up to 250 µm.

5.6.2 Barite textures

Barite typically occurs with sphalerite, galena, and quartz in aggregates and veins with minor pyrite, chalcopyrite and tennantite. Barite rich veins have significant associated calcite. Barite has orthorhombic diamond to rectangular, prismatic crystal form (Fig. 5.12). Coarse-grained barite laths have cleavage at approximately 90°. Barite grains vary from 50 to 100 µm with laths up to 1,100 µm.

5.6.3 Barite chemistry

Microprobe analyses for nine barite grains have an average chemical formula of $\text{Ba}_{1.03}\text{Sr}_{0.01}\text{S}_{0.99}\text{O}_4$ (Table 5.9). The average SrO is 0.36 wt %. This indicates the barite grains analysed represent are fairly pure barite.

| Table 5.9 Ridge Zone West Microprobe Analyses for Barite | | | | | | |
|--|-----------|---------|---------|---------|---|-----------|
| Hole | Depth (m) | Point # | SO3 Wt% | SrO Wt% | BaO Wt% | Total Wt% |
| LX10-2045 | 486 | 1 | 32.28 | 0.23 | 65.90 | 98.41 |
| LX10-2045 | 486 | 2 | 32.63 | 0.36 | 65.89 | 98.88 |
| LX10-2045 | 486 | 3 | 32.77 | 0.51 | 65.17 | 98.45 |
| LX10-2048 | 476 | 4 | 32.79 | 0.79 | 65.14 | 98.72 |
| LX10-2048 | 476 | 5 | 32.91 | 0.32 | 65.16 | 98.39 |
| LX10-2048 | 476 | 6 | 33.05 | 0.49 | 64.94 | 98.48 |
| LX10-2048 | 476 | 7 | 32.95 | 0.12 | 66.37 | 99.44 |
| LX10-2045 | 481 | 8 | 32.48 | 0.19 | 64.00 | 96.67 |
| LX10-2045 | 481 | 9 | 32.16 | 0.24 | 64.60 | 97.00 |
| Mean | | | 32.67 | 0.36 | 65.24 | 98.27 |
| Molecular Weight | | | 80.06 | 103.62 | 153.33 | |
| Molecular Proportions | | | 0.41 | 0.00 | 0.43 | |
| Cations | | | S | Sr | Ba | Total |
| Atomic Proportions Cations | | | 0.41 | 0.00 | 0.43 | 0.84 |
| Atomic Proportions Oxygen | | | 1.22 | 0.00 | 0.43 | 1.65 |
| Basis of 4 Oxygens | | | 0.99 | 0.01 | 1.03 | |
| Average formula on basis of 4 oxygens | | | | | (Ba _{1.03} ,Sr _{0.01})S _{0.99} O ₄ | |
| General formula for barite (Klein, 2002) | | | | | (Ba,Sr)SO ₄ | |
| Abbreviations: weight percent - wt% | | | | | | |

5.6.4 Muscovite textures

Muscovite occurs as veins and fine to coarse-grained blades and masses intergrown with quartz and sulphides. Fine-grained muscovite and quartz up to 50 µm are the main components for mudstone and argillaceous mudstone (Fig. 5.8b). Fine to coarse-grained muscovite laths up to 150 µm long are associated with quartz and sulphides in veins (Figs. 5.10b and 5.11c). Muscovite inclusions occur in recrystallized sphalerite (Fig. 5.11f).

5.6.5 Muscovite chemistry

Microprobe analyses for 8 muscovite grains associated with mineralization are shown in Table 5.10. The average formula for the muscovite grains analysed is $(K_{0.89}Na_{0.04}Ba_{0.06})(Al_{1.82}Mg_{0.18}Fe_{0.02})(Al_{0.87}Si_{3.13}O_{10})(OH)_2$. Minor substitutions are Na and Ba for K; Mg for Al. The most significant substitution is Ba where BaO has values ranging from 0.51 to 2.77 wt%.

| Table 5.10 Ridge Zone West Microprobe Analyses for Muscovite | | | | | | | | | | | |
|--|-----------|-------|-----------|------------|----------|--|-----------|----------|----------|-------------|------------|
| Hole | Depth (m) | Point | SiO2 wt % | Al2O3 wt % | FeO wt % | MgO wt % | Na2O wt % | K2O wt % | BaO wt % | H2O(c) wt % | Total wt % |
| Lx10-2045 | 450 | 1 | 46.65 | 34.27 | 0.49 | 1.49 | 0.30 | 10.79 | 0.51 | 4.43 | 98.93 |
| Lx10-2045 | 450 | 2 | 46.17 | 33.15 | 0.54 | 1.55 | 0.29 | 10.21 | 0.90 | 4.32 | 97.13 |
| Lx10-2048 | 479 | 3 | 46.25 | 33.86 | 0.30 | 1.75 | 0.28 | 10.15 | 2.45 | 4.42 | 99.46 |
| Lx10-2048 | 479 | 4 | 45.95 | 33.46 | 0.31 | 1.80 | 0.28 | 10.22 | 2.55 | 4.38 | 98.95 |
| Lx10-2048 | 479 | 5 | 47.04 | 33.85 | 0.18 | 2.00 | 0.26 | 10.12 | 2.77 | 4.46 | 100.68 |
| Lx10-2048 | 479 | 6 | 45.81 | 34.01 | 0.39 | 1.71 | 0.25 | 10.28 | 2.58 | 4.40 | 99.43 |
| Lx10-2048 | 479 | 7 | 45.79 | 33.86 | 0.27 | 1.77 | 0.32 | 10.12 | 2.43 | 4.38 | 98.94 |
| Lx10-2048 | 479 | 8 | 46.19 | 33.36 | 0.24 | 1.88 | 0.24 | 10.15 | 2.66 | 4.41 | 99.13 |
| Mean | | | 46.23 | 33.73 | 0.34 | 1.74 | 0.28 | 10.26 | 2.11 | 4.40 | 99.08 |
| Molecular Weight | | | 60.08 | 101.96 | 71.85 | 40.30 | 61.98 | 94.20 | 153.33 | 18.02 | |
| Molecular Proportion | | | 0.77 | 0.33 | 0.00 | 0.04 | 0.00 | 0.11 | 0.01 | 0.24 | |
| Cations | | | Si | Al | Fe2+ | Mg | Na | K | Ba | | Total |
| Cation atomic proportion | | | 0.77 | 0.66 | 0.00 | 0.04 | 0.01 | 0.22 | 0.01 | | |
| Oxygen atomic proportion | | | 1.54 | 0.99 | 0.00 | 0.04 | 0.00 | 0.11 | 0.01 | | 2.71 |
| On basis of 11 oxygens | | | 3.13 | 2.69 | 0.02 | 0.18 | 0.04 | 0.88 | 0.06 | | |
| Average formula for muscovite (basis of 11 oxygen atoms) | | | | | | (K _{0.88} Na _{0.04} Ba _{0.06})(Al _{1.82} Mg _{0.18} Fe _{0.02})(Al _{0.87} Si _{3.13} O ₁₀)(OH) ₂ | | | | | |
| General formula for muscovite (Klein, 2002) | | | | | | KAl ₂ (AlSi ₃ O ₁₀)(OH) ₂ | | | | | |
| Abbreviations: weight percent = wt % | | | | | | | | | | | |

5.6.6 Calcite textures

Calcite occurs as anhedral grains, masses and veins commonly associated with quartz. Twin lamellae are common. Grain sizes range from 50 to 250 μm (Figs. 5.10f and 5.12f). It is not common in most mineralized rocks. The most prominent occurrence of calcite is associated with barite-rich veins. This observation suggests that barite and calcite are stable together in the veins (Fig. 5.12f).

Previous workers have attributed the presence of calcite at Myra Falls to regional metamorphism. Calcite related to regional metamorphic effects occur as quartz-calcite veins and filling void spaces such as tension gashes and amygdules. The calcite observed in hand sample could be related to filling of void space. Hence the association of calcite to regional metamorphism in this case is possible. However, calcite is not restricted to late veins and some calcite may have been deposited during early alteration.

5.7 Textures in metamorphosed orebodies

The coarsening of pyrite from framboidal pyrite-1 to spongy pyrite-2 to euhedral pyrite-3 (Figs. 5.8 and 5.9) are examples of the recrystallization process. Progressive annealing textures include pyrite with embayment and careous textures progressing to completely incorporating inclusions of chalcopryrite, sphalerite, and galena. The framboidal and spongy pyrite textures are typically associated with argillaceous mudstone.

Sphalerite, galena, and chalcopryrite have been recrystallized. Recrystallization textures include coarsening of grains, grain boundaries approaching 120° triple junctions and the migration of other phases to grain boundaries. Pyrite has retained some primary features and recrystallization was incomplete due to its refractory nature.

As recrystallization increases, interactions of the crystal structures with adjacent grains leads to grain shapes and sizes yielding the minimum total interfacial free energy attainable under the conditions prevailing. Other interfaces achieve energy minima by the development of crystal faces on either of the two substances in contact (Stanton, 1976). This process can yield the 120° triple junctions between grains (Fig. 5.10e) progressing to hexagonal forms as observed for recrystallized sphalerite (Fig. 5.11).

Recrystallization is also responsible for the migration of chalcopryrite and galena to grain boundaries of pyrite and sphalerite (Fig. 5.9f). Sphalerite-chalcopryrite-galena aggregates occur as granoblastic intergrowths (Fig. 5.10e) and as extremely fine

chalcopyrite blebs intergrown with sphalerite, or chalcopyrite disease (Fig. 5.11). The presence of chalcopyrite, sphalerite, and galena rich veins and the association of galena blebs and annealed galena with 120° boundaries within the recrystallized sphalerite infer the migration of chalcopyrite and galena to the grain boundaries.

Ore mineral grain size generally increases in massive base metal ore bodies either with an increase in temperature during evolution of the massive sulphide lens and / or the increase in temperature and pressure due to metamorphism of the containing rocks (Stanton, 1976; Craig and Vaughn, 1994). Regional metamorphism at Myra Falls is lower greenschist as discussed in Chapter 2 (Juras, 1987). Effects of later superimposed burial metamorphism in the Price and Myra Formations are limited (Juras, 1987). Phyllosilicate phases are recrystallized to coarser grain sizes and there is some pressure shadow development (Juras, 1987). At greenschist facies metamorphic conditions, recrystallization is expected for most sulphide minerals. At lower prehnite-pumpellyite to greenschist facies metamorphism (250-400° C), chalcopyrite and galena are recrystallized, sphalerite acts in a ductile manner, and pyrite remains brittle (Kelly and Clark, 1975; Sinclair, 2000). Chalcopyrite recrystallization can occur at 200° C (Kelly and Clark, 1975). The question remains as to how much of the recrystallization observed for the Ridge Zone West was driven by metal zone refining in the sub-seafloor hydrothermal setting and how much was during regional metamorphism?

5.8 Chalcopyrite disease and metal zone refinement processes

Massive to semi-massive sphalerite aggregates with pyrite and chalcopyrite commonly have anhedral, subrounded inclusions of chalcopyrite up to 1 μm diameter (Fig. 5.11). Anhedral chalcopyrite blebs within sphalerite masses commonly outline cleavage planes. In massive sulphide deposits, this texture is referred to as chalcopyrite “disease” texture (Barton, 1978).

Chalcopyrite disease could be the result of co-precipitation, replacement, and recrystallization (Eldridge et al., 1988). The blebs are not due to exsolution as quantitative experimental evidence suggests that sphalerite could not have contained enough copper to have exsolved any significant amounts of chalcopyrite during cooling (Hutchinson, 1978).

In non-metamorphosed orebodies such as at Kuroko, chalcopyrite disease represents the earliest stages of replacement of sphalerite by chalcopyrite and the process may proceed to total replacement (Barton, 1978). The replacement model has since been refined to a form of solid-state diffusion texture (Barton and Bethke, 1987). The disease texture is found at the leading edge of a much larger replacement event and explains how in Kuroko-type orebodies yellow ore may stratigraphically underlie black ore and yet be younger than the black ore.

Recrystallization has migrated chalcopyrite and galena blebs to the rims of recrystallized sphalerite grains and hence overprints most primary textures relevant to forming a paragenetic model. Therefore, the chalcopyrite disease texture within sphalerite may have formed by either co-precipitation or by replacement methods similar to the Kuroko model (Barton, 1978).

5.9 Sulphide paragenesis

The following sulphide paragenesis is based on the style of mineralization in association with the host rock lithology and textures. The hydrothermal system may have been continuous through more than one of the phases described.

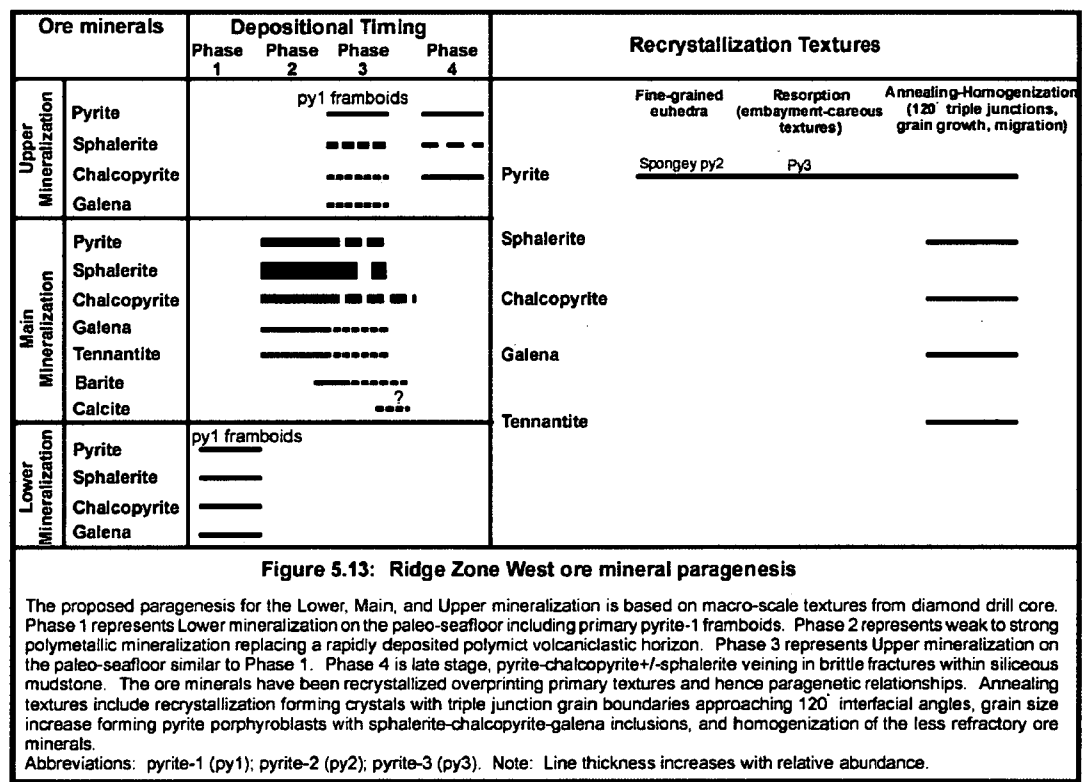
Phase 1: Lower lens mineralization in fine-grained facies volcanic rocks have pyrite framboids and coarser grained recrystallized pyrite that show occasional fining up textures within bands. Soft sediment deformation textures are also common. Discreet sphalerite bands within banded mudstone are also observed. Microscopic textures for the Lower and Upper lens mineralization have pyrite, sphalerite, chalcopryrite, and galena disseminations and bands that range between 50 and 250 μm . Based on the macro and micro-textures discussed, Lower lens mineralization pyrite-1 and coarser-grained recrystallized pyrite, sphalerite, chalcopryrite and galena associated with sedimentary macro-textures are interpreted to have co-precipitated on the paleo-seafloor synchronous with the fine-grained facies volcanic mudstones.

Phase 2: Main lens mineralization is interpreted to have formed by replacing a rapidly deposited coarse-grained facies volcanic horizon supported by argillaceous mudstone. Sphalerite-pyrite-chalcopryrite-galena disseminations represent either synchronous or replacement style mineralization. Weak to massive veins of sphalerite-pyrite-chalcopryrite-galena-tennantite+/-barite represents mineralization that has infiltrated the porous, coarse-grained facies volcanoclastic horizon and replaced void space or possibly matrix material. Chalcopryrite disease texture is either by co-precipitation or chalcopryrite replacement of sphalerite. Barite-quartz rich veins are either synchronous with or later than the sphalerite-pyrite-chalcopryrite-galena+/-barite mineralization based on drill core textures. Calcite-quartz veining or void space filling is attributed to either syn-barite rich veining or metamorphism.

Phase 3: Upper lens mineralization has two distinct styles of mineralization. Phase 3 is the first style and consists of pyrite framboids, banded mineralization with bedded mudstone, and pyrite grain-size gradation that are similar to Lower lens mineralization. Depositional environment is interpreted as synchronous with the fine-grained volcanic mudstone on the paleo-seafloor.

Phase 4: This is a second style of Upper lens mineralization. Phase 4 Upper lens mineralization is characterized by cross-cutting pyrite-chalcopyrite+/-sphalerite veins filling brittle fractures within brecciated, siliceous mudstone. Phase 4 mineralization is interpreted as a late stage event occurring post-lithification of siliceous mudstone and possibly synchronous with, or after brecciation.

Recrystallization: The only primary texture is interpreted to be relict pyrite-1 framboids in Lower and Upper lens mineralization hosted by fine-grained facies mudstone and argillaceous mudstone. Generally, the ore minerals have been recrystallized. Coarsening of grains, grain boundaries approaching 120° triple junctions, migration of other phases to grain boundaries, and embayment-careous textures in pyrite are common textures supporting the recrystallization process. Recrystallization is interpreted to have likely occurred concurrently in the sub-seafloor hydrothermal environment possibly during phases 2, 3, and 4. Some recrystallization may also be related to lower greenschist metamorphism making confident paragenetic interpretation difficult. Based on the above discussion a depositional and recrystallization paragenetic sequence for the different mineralized horizons and their associated minerals is proposed in Fig. 5.13.



5.10 Comparison to other mineralogical studies at Myra Falls

Other detailed mineralogical studies of ore minerals at Myra Falls include the Battle-Gap deposit (Sinclair, 2000; Robinson, 1994) and the H-W deposit (Chrysosoulis, 1989; Wilson, 1993). The Battle-Gap deposits have the greatest variety of ore mineral assemblages. Sinclair (2000) proposed a Cu-Pb-Zn-Fe rich mineral assemblage, a Cu-rich assemblage, and a late Ag-Au-rich assemblage. The Cu-Pb-Zn-Fe assemblage comprises sphalerite, pyrite, galena, tennantite, chalcopyrite, and colusite. The Cu-rich assemblage comprises bornite, renierite, and anilite. The late Ag-Au rich assemblage comprises stromeyerite and electrum. The minerals associated with the Ridge Zone West best match the Cu-Pb-Zn-Fe assemblage as defined by Sinclair (2000). Table 5.11 summarizes the various ore minerals and their element associations based on this study and other previous mineralogy studies at Myra Falls.

Primary framboidal pyrite within fine-grained sediments has also been documented (Robinson, 1994; Sinclair, 2000; Jones, 2001). The Battle deposit has had two independent interpretations for sulphide recrystallization. Robinson (1994) attributed recrystallization of pyrite, sphalerite, galena, and chalcopyrite to progressive zone replacement similar to metal zone refinement processes during mound growth as described by Eldridge et al., (1983). Sinclair (2000) attributed sphalerite, galena, and chalcopyrite recrystallization textures and spatial distribution to zone refinement processes followed by a second recrystallization process related to regional metamorphism. The increase in size and abundance of pyrite porphyroblasts toward the base of massive sulphide lenses suggest recrystallization during mound growth and / or metamorphism (Sinclair, 2000). Metamorphic pyrite textures include inclusion free grains and careous growth embayments indicative of metablastic growth (Sinclair, 2000). The Ridge Zone West has annealing and recrystallization ore mineral textures similar to those documented for the Battle-Gap deposits (Sinclair, 2000; Robinson, 1994).

Electron microprobe analyses for the Battle-Gap deposits by Sinclair (2000) reported the following substitutions. Pyrite has nickel values up to 1,100 ppm and arsenic values up to 6,700 ppm with the higher values from the Gap deposit. Sphalerite is typically the iron poor variety with iron values ranging between detection limits up to 1.4 wt %. Cadmium values in sphalerite range up to 5,000 ppm. Galena has selenium values up to 7,400 ppm. Chalcopyrite is relatively pure with impurities attributed to inclusions. Tetrahedrite-tennantite is the arsenic rich end-member tennantite and contains up to 7,300 ppm silver and up to 1,100 ppm selenium. The Cu-rich assemblage ore mineral colusite,

observed only in the Gap deposit has the formula $\text{Cu}_3(\text{AsGeV})\text{S}_4$ with major substitutions by barium and antimony. Bornite in the Gap deposit and Upper Zones of the Battle deposit has up to 7,500 ppm silver and up to 2,900 ppm barium. Renierite has copper, iron, germanium, zinc, arsenic, and minor substitutions of vanadium, antimony, and barium. The late Ag-Au rich assemblage mineral stromeyerite contains copper and silver. Electrum was observed in the Gap and Upper Zones spatially associated with stromeyerite filled fractures and bornite. Electrum grain size ranged between 10 to 70 μm .

Electron microprobe analyses for the H-W deposit, have silver associated with tennantite (0.1 to 1.2 wt %) and in galena (60 to 250 ppm) (Wilson, 1993). Cadmium is present in sphalerite (0.33 wt %) and tennantite (0.1 wt %). Chalcopyrite has minor amounts of selenium and indium. Tennantite contains up to 500 ppm tellurium. Pyrite and chalcopyrite have minor amounts of molybdenum and between 25 to 1,000 ppb gold. Pyrite has the higher values of gold. Though not reported by Wilson (1993) or Chryssoulis (1989), electrum and stromeyerite have been observed and identified from the Zn-Pb-Ba rich polymetallic south fringe of the H-W deposit by the author, other Myra Falls geologists, and Sinclair (pers. comm.).

The Ridge Zone West ore mineralogy is similar to the Cu-Pb-Zn-Fe mineral assemblage proposed by Sinclair (2000). Sphalerite is typically the iron-poor variety similar to the Battle-Gap (Sinclair, 2000; Robinson, 1994) and sphalerite found in the Zn-Pb-Cu-Fe-Ba rich polymetallic south fringe of the H-W deposit. Cadmium in sphalerite averages 0.3 wt % and is similar to results for the Battle-Gap and H-W deposits. Galena analyses for the Ridge Zone West have minor substitutions of Fe and Se. Chalcopyrite is relatively pure with impurities attributed to inclusions. Ridge Zone West tetrahedrite-tennantite is the arsenic-rich end member tennantite and is similar to analyses by Sinclair (2000) and Robinson (1994). Tennantite is the main residency for Ag in the minerals analysed for the Ridge Zone West and is similar with results from the Battle-Gap. Gold was not observed or analysed for by either microscopy or electron microprobe in this study. Barite has minor Sr substitution. Muscovite has minor Ba and Mg substitution for K and Al respectively. Barite and muscovite were not analysed by previous studies. Table 5.11 highlights the ore mineralogy at Myra Falls including results from this study.

Table 5.11: Ridge Zone West and Myra Falls Ore Body Mineralogy

| Assemblage | Type | Mineral | General Formula | Chemical Formula (this study) | Other elements | Inclusions - Impurities | Sources |
|-----------------|-----------------|----------------|---|--|------------------------|------------------------------|------------|
| Cu-Pb-Zn-Fe | Sulphides | Pyrite | FeS ₂ | Py-1, Py-2: Fe ₁₀₀ S ₂ ; Py-3: Fe ₁₀₀ S ₂ | Ni, As, Co** | Zn*, Cd, Cu, Pb, As*, Mn, Au | W; S; RZW |
| | | Sphalerite | ZnS | (Zn ₉₉ Fe _{0.01})S | Fe*, Cd*, Mn** | Cu* | S; RZW |
| | | Galena | PbS | Pb ₁₀₀ S | Se*, Te | Zn, Fe*, Cu | S; RZW |
| | | Chalcocopyrite | CuFeS ₂ | Cu ₁₀₀ Fe _{1.01} S ₂ | Se, In | Ba, Zn*, Au | W; S; RZW |
| | | Pyrrhotite | Fe ₁₄ S | | | | RW |
| | | Arsenopyrite | FeAsS | | | | RW |
| | Sulphosalts | Tennantite | (Cu ₁₀ Ag)Zn ₂ Fe(Sb, As ₃)S ₁₃ | (Cu _{9.9} Ag _{0.2})Zn _{1.4} Fe _{0.6} (Sb _{0.7} As _{3.3})S ₁₃ | Fe*, Se*, Cd | | RW; S; RZW |
| | Trace Minerals | Rutile | TiO ₂ | | | Si, Al, Fe | S |
| | | Colusite | Cu ₃ (As, Ge, V)S ₄ | | Ba, Sb | Ag, Mo, Zn, Fe | R; S |
| | Tellurides | Altaitite | PbTe | | | | S |
| | | Hessite | Ag ₂ Te ₃ | | | | S |
| | | Pilsenite | Bi ₂ Te ₃ | | | | S |
| Cu-Rich | Sulphides | Bornite | Cu ₅ FeS ₄ | | Ag, Ba | Zn, Cd | S |
| | | Covellite | CuS | | | | B |
| | | Renierite | Cu ₁₀ (Zn ₁₄ Cu)Ge ₂₄ As ₄ Fe ₄ S ₁₆ | | V, Sb, Ba | | R; S |
| | | Anilite | Cu ₂ (Ag)S | | Ag, Ba | | R; S |
| Late Ag-Au Rich | Sulphides | Stromeyerite | CuAgS | | Fe | | C, S |
| | Precious metals | Electrum | AuAg | | | | S |
| | | Native silver | Ag | | | | W |
| Gangue | | Barite | BaSO ₄ | (Ba ₁₀₀ Sr _{0.01})S _{0.99} O ₄ | Sr** | | S; RZW |
| | | Quartz | SiO ₂ | | | | S; RZW |
| | | Muscovite | KAl ₂ (AlSi ₃ O ₁₀)(OH) ₂ | (K _{0.99} Na _{0.01} Ba _{0.02})(Al _{1.98} Mg _{0.02} Fe _{0.02})(Al _{0.97} Si _{3.03} O ₁₀)(OH) ₂ | Na**, Ba**, Mg**, Fe** | | S; RZW |
| | | Chlorite | (Mg, Fe) ₃ (Si, Al) ₄ O ₁₀ (OH) ₂ (Mg, Fe) ₃ (OH) ₄ | | | | MFO |
| | | Epidote | Ca ₂ (Al, Fe) ₃ Si ₃ O ₁₂ (OH) | | | | MFO |
| | | Calcite | CaCO ₃ | | | | S; RZW |
| | | Gypsum | CaSO ₄ ·2H ₂ O | | | | B |
| | | Anhydrite | CaSO ₄ | | | | B |
| | | Jasper | SiO ₂ | | | Fe | MFO |
| | | Specularite | Fe ₂ O ₃ | | | | B |
| | | Smithsonite | ZnCO ₃ | | | | B |

Assemblages adapted from the Battle-Gap study by Sinclair (2000)

Abbreviations: an - anilite; bo - bornite; cp - chalcocopyrite; gn - galena; py - pyrite; sp - sphalerite; strom - stromeyerite; tt - tennantite**Data sources:** B- pers. comm. M. Becherer; C - Chrysoullis (1989); MFO - Myra Falls geology department; R - Robinson (1994); RW - Walker (1985); RZW - this study; S - Sinclair (2000); W - Wilson (1993)

* indicates elements consistent with Ridge Zone West electron microprobe analyses for this study.

** indicates a new element association not recognized or analysed for by previous studies.

5.11 Metallurgical aspects relative to ore mineralogy

Application of the mineral textures and chemical compositions observed and derived from this study are important in the milling and metallurgical extraction processes required to produce an economically viable concentrate. The purpose of this section is to highlight various milling and metallurgical aspects relative to the results of this study. A proper in-depth assessment of the milling and metallurgical characteristics for the Ridge Zone West is outside the scope of the study.

The primary milling circuit at Myra Falls currently involves crushing and grinding the ore to a size fraction whereby 75% of the material is less than 75 μm (ie. -200 mesh). A regrind circuit for the copper and zinc cleaning circuit grinds the ore to 80% passing 35 μm (G. Locke, pers. comm.). The majority of the ore minerals for the Ridge Zone West are between 50 to 300 μm . Coarse grained recrystallized ore minerals such as chalcopyrite and sphalerite are noted to occur as homogenized masses greater than 1,000 μm (ie. millimeter scale). From a size aspect, the current grinding method at Myra Falls should be adequate to liberate the coarse ore minerals. Ore grains less than 75 μm can affect recovery based on the liberation size limitation for the primary grinding circuit. The grains and blebs under 35 μm could be problematic for future metallurgy. This would involve inclusions of sphalerite, chalcopyrite, and galena reporting to the wrong concentrate effectively lowering the concentrate grade. Also, pyrite is depressed in the circuit and subsequently transported out to tails or underground as part of a pyritic backfill. Inclusions less than 35 μm would be lost, thus affecting the recovery.

Hardness of the ore relative to the Moh hardness scale is inferred to be between 3.6 and 6.0. The dominant minerals sphalerite and chalcopyrite have hardness factors ranging from 3.5 to 4. Pyrite with a hardness of 6 to 6.5 comprises between 10 to 30% of the ore minerals present. Galena has a hardness of 2.5. Tennantite has a hardness range between 3.5 and 4.5. The hardest mineral present is quartz with a hardness of 7. Based on the types of ore minerals present and their varying quantities, the ore is inferred to have a hardness range between that of sphalerite and pyrite, or 3.5 to 6.0.

Potential locking of the ore minerals is dependant on the ore mineral intergrowths. Recrystallized minerals that are plus 75 μm in size commonly have 120° interfacial grain boundaries. The boundaries have straight, cusped, and gently curved shaped boundaries with negligible interpenetration. This style of intergrowth is considered to have simple locking characteristics and hence easy liberation properties. Coarse grains imply

reasonable liberation of the sulphide minerals by normal grinding methods without interlocking issues (Ramdohr, 1969; Craig and Vaughn, 1994). Locking problems may arise from the relatively complex intergrowths of fine-grained blebs of chalcopyrite and galena associated with recrystallized sphalerite or from inclusions of chalcopyrite, sphalerite, and galena less than 35 μm within annealed pyrite-3.

After grinding the ore slurry is processed by copper and zinc flotation circuits. Coarse gold is gravimetrically separated by a Knelson concentrator prior to the copper and zinc flotation circuits. Fine gold and silver not liberated by the gravity circuit report to the copper concentrate. Zinc and lead report to the zinc concentrate.

Copper concentrate smelting penalties are applied when the $\text{Pb}+\text{Zn}>4\%$ or $\text{As}+\text{Sb}>0.1375\%$. Zinc concentrate smelting penalties are applied when $\text{Fe}>8\%$ and $\text{As}>0.075\%$. Based on the mining reserve grades prior to concentration, the Ridge Zone West has a combined $\text{Pb}+\text{Zn}=8.4\%$. Therefore, separation of the Pb and Zn from the copper concentrate is critical. Based on microprobe analyses for this study, the tetrahedrite-tennantite grains analysed are the As-rich end member tennantite. Tennantite is also the host mineral for Ag. Therefore, future work should incorporate As in the suite of elements analysed as well as the liberation of Ag from tennantite.

The lack of Ag in galena should be considered as it will have a negative economic impact on the viability for a future lead circuit installation. Finally, gold was not observed by the methods used and requires more work to resolve how it occurs.

5.12 Summary

Lower and Upper lens mineralization is associated with fine-grained volcanic mudstone. Pyrite, sphalerite, chalcopyrite, and galena are the common ore minerals. The mineralization is typically disseminated or banded. Siliceous mudstone has brittle fracture controlled pyrite-chalcopyrite mineralization. Primary framboidal pyrite is associated with Lower and Upper lens mineralization.

Main lens mineralization for the Ridge Zone West is hosted by coarse-grained, polymict, volcanoclastic rocks of the H-W Horizon. Mineralization occurs as disseminations, anastomosing veins, and semi-massive to massive veins. The ore minerals have annealing and recrystallization ore mineral textures attributed to metamorphism. Typical textures include straight or cusped, gently curved shaped boundaries with negligible interpenetration at triple junction interfacial boundaries approaching 120°, coarsening of annealed grains, embayed pyrite grains, and migration of galena and chalcopyrite to pyrite grain boundaries.

The Ridge Zone West ore mineralogy is similar to the Cu-Pb-Zn-Fe mineral assemblage proposed by Sinclair (2000). Sphalerite is typically the Fe-poor variety. Cadmium in sphalerite averages 0.3 wt %. Galena analyses for the Ridge Zone West have minor substitutions of Se for S. High Fe contents in galena are attributed to inclusions of pyrite. Chalcopyrite is relatively pure. Impurities in chalcopyrite are attributed to inclusions. Tetrahedrite-tennantite is the arsenic-rich end member tennantite and is the main residency for Ag in the minerals analysed. Gold was not observed or analysed for by either microscopy or electron microprobe in this study. Barite has minor Sr substitution. Muscovite has minor Ba and Mg substitution for K and Al respectively.

Based on microscopy, the majority of the ore minerals for the Ridge Zone West are between 50 to 300 µm. Coarse grained recrystallized ore minerals such as chalcopyrite and sphalerite are noted to occur as homogenized masses greater than 1,000 µm. From a size aspect, the current grinding method at Myra Falls should be adequate to liberate the coarse ore minerals. Ore grains less than 75 µm can affect recovery based on the liberation size limitation for the primary grinding circuit. The grains and blebs under 35 µm could be problematic for future metallurgy. This would involve inclusions of sphalerite, chalcopyrite, and galena reporting to the wrong concentrate effectively lowering the concentrate grade.

Metallurgical aspects concerning grinding and beneficiation are as follows. The style of intergrowth between the sulphide minerals is considered to have simple locking characteristics and hence easy liberation properties. Coarse grains > 75 µm imply reasonable liberation of the sulphide minerals by normal grinding methods without interlocking issues. Locking problems may arise from relatively complex intergrowths of fine-grained blebs of chalcopryrite and galena associated with recrystallized sphalerite or from inclusions of chalcopryrite, sphalerite, and galena within pyrite-3. Future metallurgical and geological work should incorporate As in the suite of elements analysed. The lack of Ag in galena should be considered as it will have a negative economic impact on the viability for a future lead circuit installation.

6.1 Introduction

The purpose of this chapter is to characterize the metal zoning for the Ridge Zone West deposit. The Ridge Zone West and other deposits in the Myra Falls property are classified using a metal content classification scheme derived by Large (1992). Distribution of the various base and precious metals identify spatial, numerical, and mineralogical relationships. The Cu ratio $[100 \cdot \text{Cu} / (\text{Cu} + \text{Zn})]$ is used to infer temperature regimes for the mineralizing fluids during deposit formation.

Property wide and deposit scale metal zoning studies have characterized the metal distribution for the Myra Falls property (Gemmell, 1998), the Battle-Gap deposit (Sinclair, 2000, Hayward, 2001), and the H-W deposit (Barrett and Sherlock, 1996; Hayward, 2001). Detailed metal zoning has not been previously documented for the Ridge Zone West and the remaining deposits at Myra Falls.

6.2 Methods

The metal zoning model represents the metal distribution for the Lower lens, Main lens, and Upper lens. These lenses are located south of 4200N along the entire strike length of the study area. Assessment of disseminated and vein style mineralization north of 4200N has been excluded due to the paucity of geologic and assay data.

A total of 644 rock samples from 66 diamond drill holes have been analyzed for the Ridge Zone West. Of the total sample set, 273 samples were collected and submitted for assay by the author and other Myra Falls geologists during a 2000-2001 diamond drill campaign and the remainder during a prior diamond drill campaign in 1987. The block model for the Lower, Main, and Upper lenses was generated using a subset of 232 of the 644 analyses. Sample analyses include Cu, Pb, Zn, Fe, and Ba by atomic absorption spectrophotometry and Au and Ag analyses by fire assay methods at the Myra Falls assay laboratory. A detailed description on the analytical procedures and detection limits utilized at the Myra Falls assay lab is included in Appendix 4.

The author constructed two and three-dimensional computer models of the mineralized lenses for this study by interpreting geology and assay sections using Compass / Minesite 3-D mining software. Mineralized lenses are extrapolated and interpolated 45m

along strike from the nearest diamond drill information which is consistent with the inferred resource category for mineral resource estimation at Myra Falls.

A block model based on the geologic model and assay data utilizes an inverse distance cubed algorithm. Individual blocks measure 5m E-W, 5m N-S, and 4m vertical. These parameters are consistent with other ore reserve and mineral resource estimation procedures at Myra Falls. Detailed parameters for generating the block model are described in Chapter 5, section 5.3.1 and in Appendix 4.

Distribution of the metals and pertinent ratios are plotted using the block model. The diagrams are used to compare and contrast the spatial distribution of the different metals. Element associations are inferred using the spatial distribution and features from Chapter 5. Assay data are plotted on scatter diagrams with linear regression trend lines to identify and quantify the element associations.

6.3 Ridge Zone West block model metal zoning

As established in Chapters 3 and 5 on the geology and mineralization, the Lower and Upper lenses are associated with argillaceous and siliceous mudstones. The mineralization has a variety of textures including disseminations, bands, and veins. The Main lens mineralization is the dominant type and is associated with argillaceous mudstones and polymictic coarse-grained volcanoclastic rocks. Textures are typified by varying degrees of weak to strong anastomosing veins permeating a volcanoclastic deposit. Relic altered clasts are common in semi-massive to massive sulphides.

The element zoning of the Ridge Zone West lenses has been assessed using assay data for correlation purposes and a block model for spatial distribution. Block model diagrams for the various elements and ratios incorporate plan, E-W longitudinal, and N-S cross-sections (Figs. 6.1 to 6.7). Plan view plots utilize Minesite 3-D generated “grade shells”. Grade shells are three-dimensional computer meshes based on the block model and for this study, value ranges for the different elements or metal ratios. Plan view images use grade shells because of their semi-transparent capabilities allowing the viewer to discern the various zones throughout the deposit. The E-W longitudinal and N-S cross sections are two-dimensional views of the block model zoning. Metal zoning is discussed for the different mineralized zones from stratigraphic footwall to hangingwall.

6.3.1 Block model base metal zoning

Compositional metal zoning for the elements Fe, Cu, Zn, and Pb is illustrated in Figs. 6.1, 6.2, 6.3, and 6.4 respectively. Sulphide mineralogy based on reflected light microscopy and microprobe analyses from Chapter 5 indicate Fe to be contained in pyrite-chalcopyrite and -tennantite, Cu to be contained in chalcopyrite and tennantite, Zn in sphalerite and tennantite, Pb in galena, and Ag in tennantite. Iron is widely dispersed throughout all the mineralized zones and has no apparent variation as represented by the lack of any distinct pattern in Fig. 6.1.

Lower lens: Copper, Zn, and Pb blocks show similar spatial distributions in the Lower lens (Figs. 6.2, 6.3, and 6.4). High concentrations of Cu, Zn, and Pb are centred on two zones near minus 250E and 250E within Lower lens mineralization. A strong Zn-Pb-Cu spatial correlation is inferred for the Lower lens mineralization based on the similar zoning patterns for these elements.

Main lens: Zinc, Pb and Cu have similar spatial distribution patterns for the Main lens (Figs. 6.2, 6.3, and 6.4). Above average grade Zn, Pb and Cu block model values between -

50E to 110E are bounded to the north by an ESE-WNW trending, steep dipping normal fault. A similar trending fault is located south of the Zn-Pb-Cu zone. The southern fault offsets the ore and is not as continuous along strike as the northern fault. Copper concentrations > 2.0 % Cu occur in blocks near the Main lens base and decreases with increasing lateral distance and vertically upward (Fig. 6.2). High Zn and Pb concentrations extend from the Main lens base upward to the Main lens upper contact on N-S section 25E. Zinc and Pb concentrations decrease laterally away from this zone as shown on the plan and 4150N longitudinal section (Figs. 6.3 and 6.4). Based on the block model diagrams, a positive Zn-Pb-Cu spatial association is inferred for the Main lens mineralization.

Upper lens: Mineralization has low Cu and Zn block grades (< 1 % Cu and < 4 % Zn) for an area between 50E to 105E. Sporadic blocks with grades between 0.5 and 1.0 % Pb also occur within this mineralized area. Based on the block model plots, a positive Zn-Cu+/-Pb spatial association is interpreted for the Upper lens mineralization.

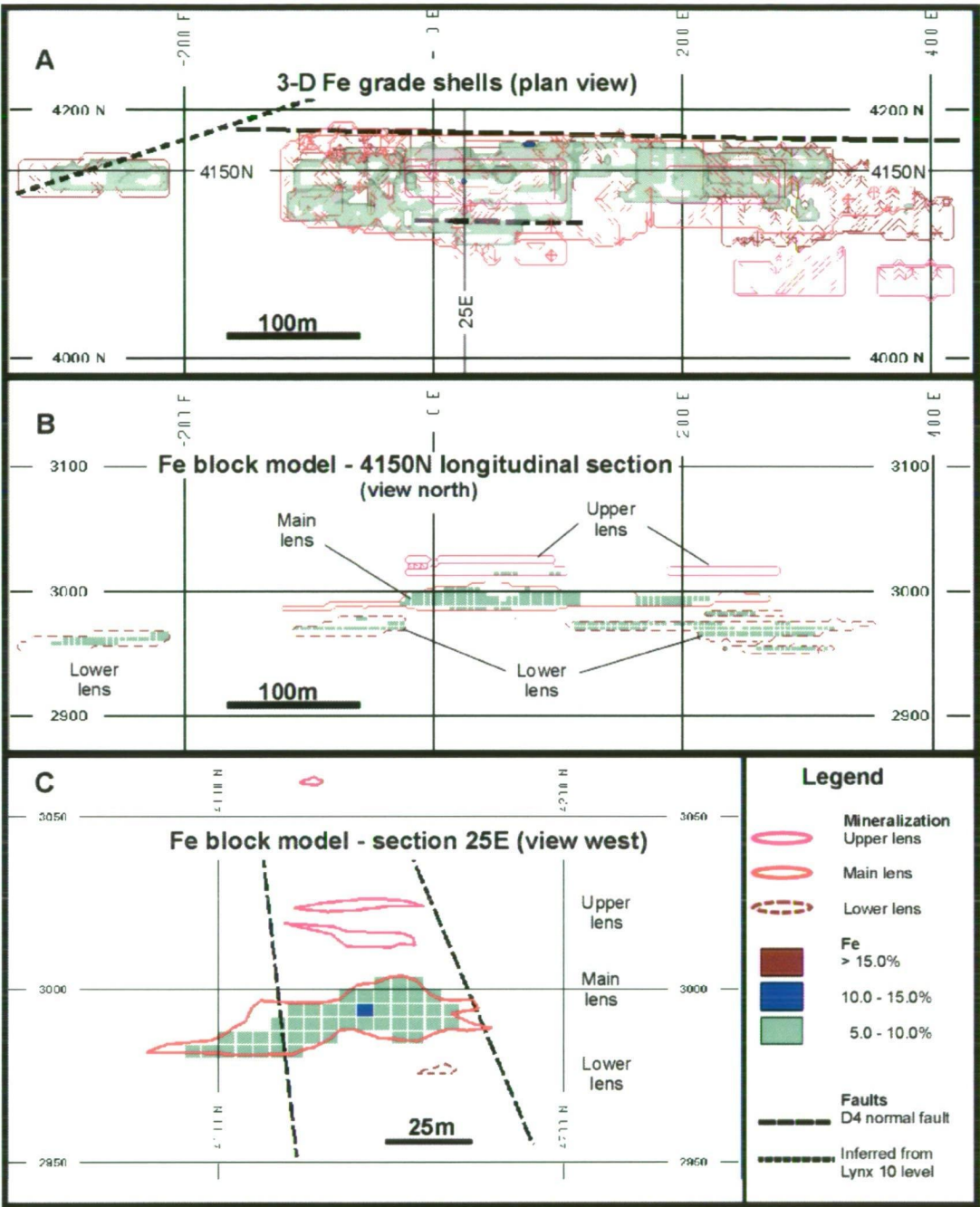


Figure 6.1: Ridge Zone West - Fe zoning

The Ridge Zone West has an average grade estimate of 6.7% Fe for the pre-mining mineral resource (Chong and Bakker, 2004). Iron content is considered low relative to other massive sulphide lenses at Myra Falls. The Fe content is relatively uniform and lacks recognizable zoning. (A) Grade shells are Minesite 3-D mining software generated three-dimensional objects based on the block model and grade parameters. The application of grade shells in plan view allow semi-transparent visualization of the three-dimensional blocks. (B-C) The block model is used for two-dimensional visualization on the longitudinal and north-south cross section. Individual blocks have dimensions measuring 5m east-west, 5m north-south, and 4m vertical. Blocks with < 5.0% Fe are omitted for clarity. Faults have been omitted from the longitudinal section (B) for clarity.

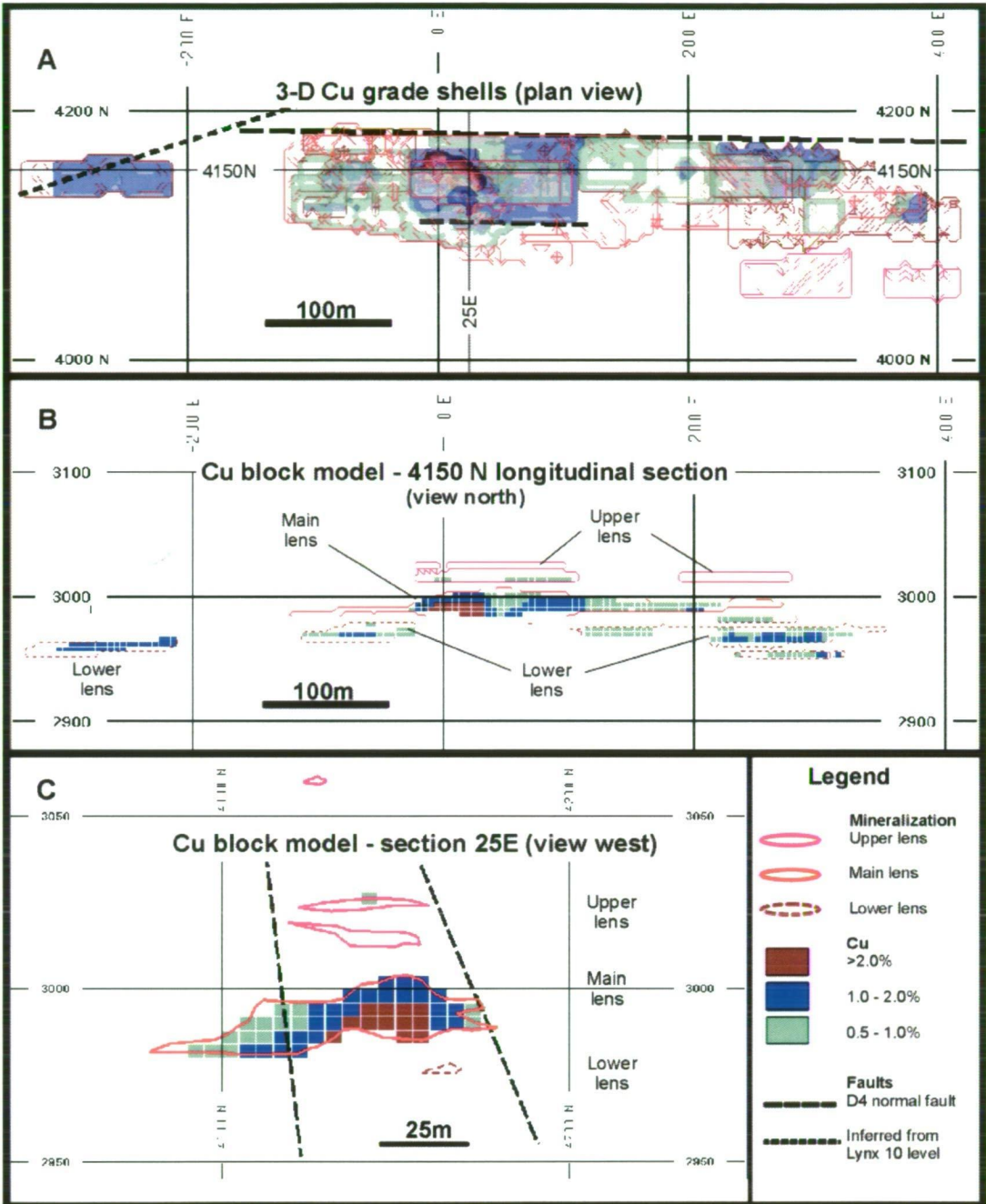


Figure 6.2: Ridge Zone West - Cu zoning

The Ridge Zone West has an average grade estimate of 0.9% Cu for the pre-mining mineral resource (Chong and Bakker, 2004) and is Cu-poor compared to deposits at Myra Falls. (A-B) Lower lens mineralization associated with fine-grained argillaceous mudstone have Cu-enrichment areas (> 1.0% Cu) proximal to -250E, -75E, and 250E. Main lens mineralization associated with coarse-grained volcaniclastic rocks have two possible Cu-enrichment areas between -50E to 40E and 50E to 110E. Upper lens mineralization is typically Cu-poor with block grades < 1.0%. (A and C) The best Cu mineralization is bounded by two ESE-WNW striking normal faults interpreted from diamond drill core. Copper grade decreases upward and laterally away from the base of the Main lens mineralization. Grade shell and block model parameters are discussed in the text and Figure 6.1. Blocks < 0.5% Cu are not displayed. Faults have been omitted from the longitudinal section for clarity.

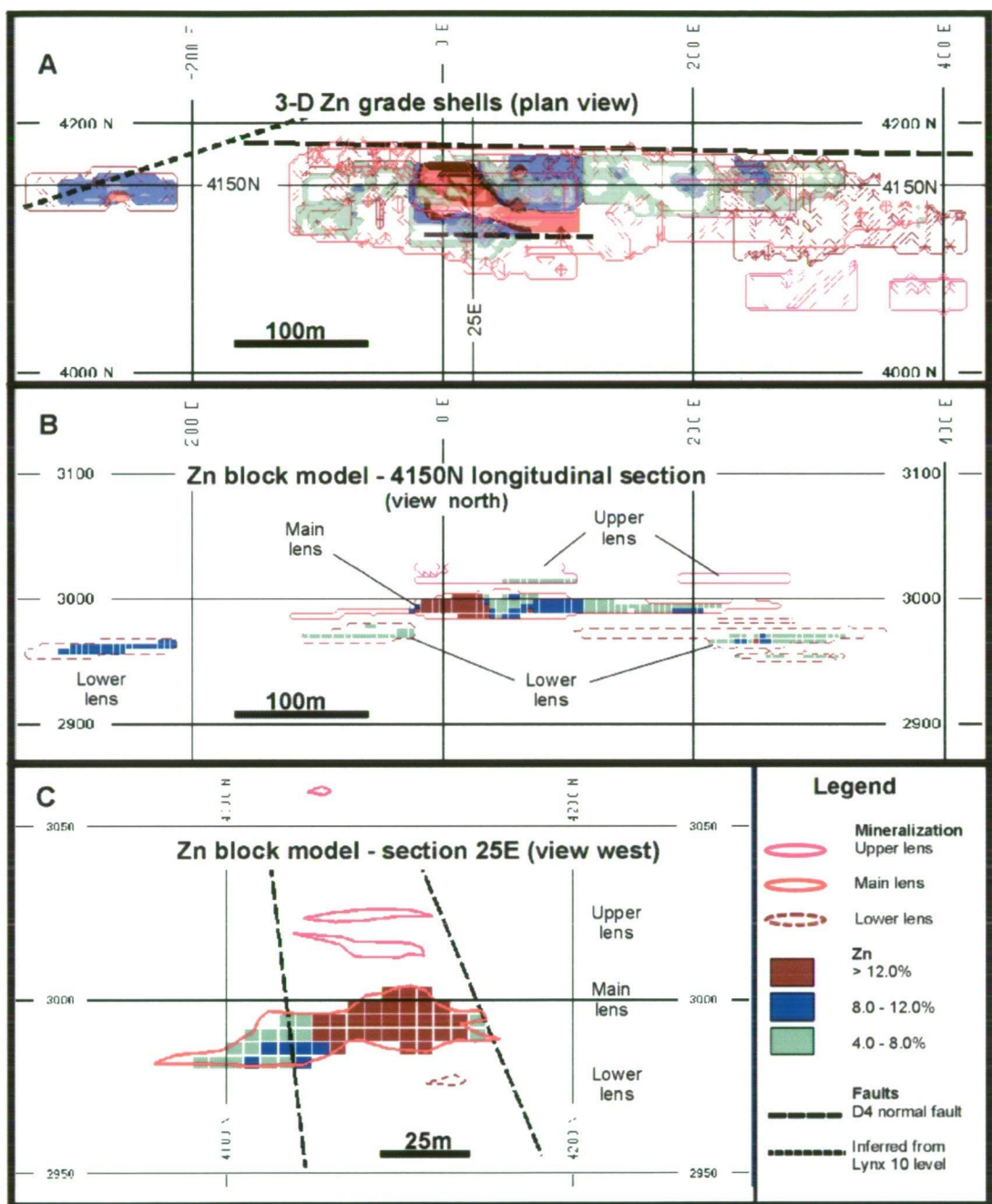


Figure 6.3: Ridge Zone West - Zn zoning

The Ridge Zone West has an average grade estimate of 6.8% Zn for the pre-mining mineral resource (Chong and Bakker, 2004). (A-B) Lower lens mineralization associated with fine-grained volcano-sedimentary rocks have two Zn-enrichment areas >8% proximal to -250E and 250E. Main lens mineralization associated with coarse-grained volcanoclastic rocks have two possible Zn-enrichment areas between -50E to 110E and proximal to 200E. Upper lens mineralization has weak mineralization proximal to 75E. (B-C) Zn values >12% extend from the base upward through to the top of the Main lens mineralization. Zinc grade decreases laterally away from the high grade zones. (A and C) The northern ESE-WNW striking fault bounds the mineralization. Grade shell and block model parameters are discussed in the text and Figure 6.1. Zinc blocks < 4.0% are not shown for clarity. Faults have been omitted from the longitudinal view for clarity.

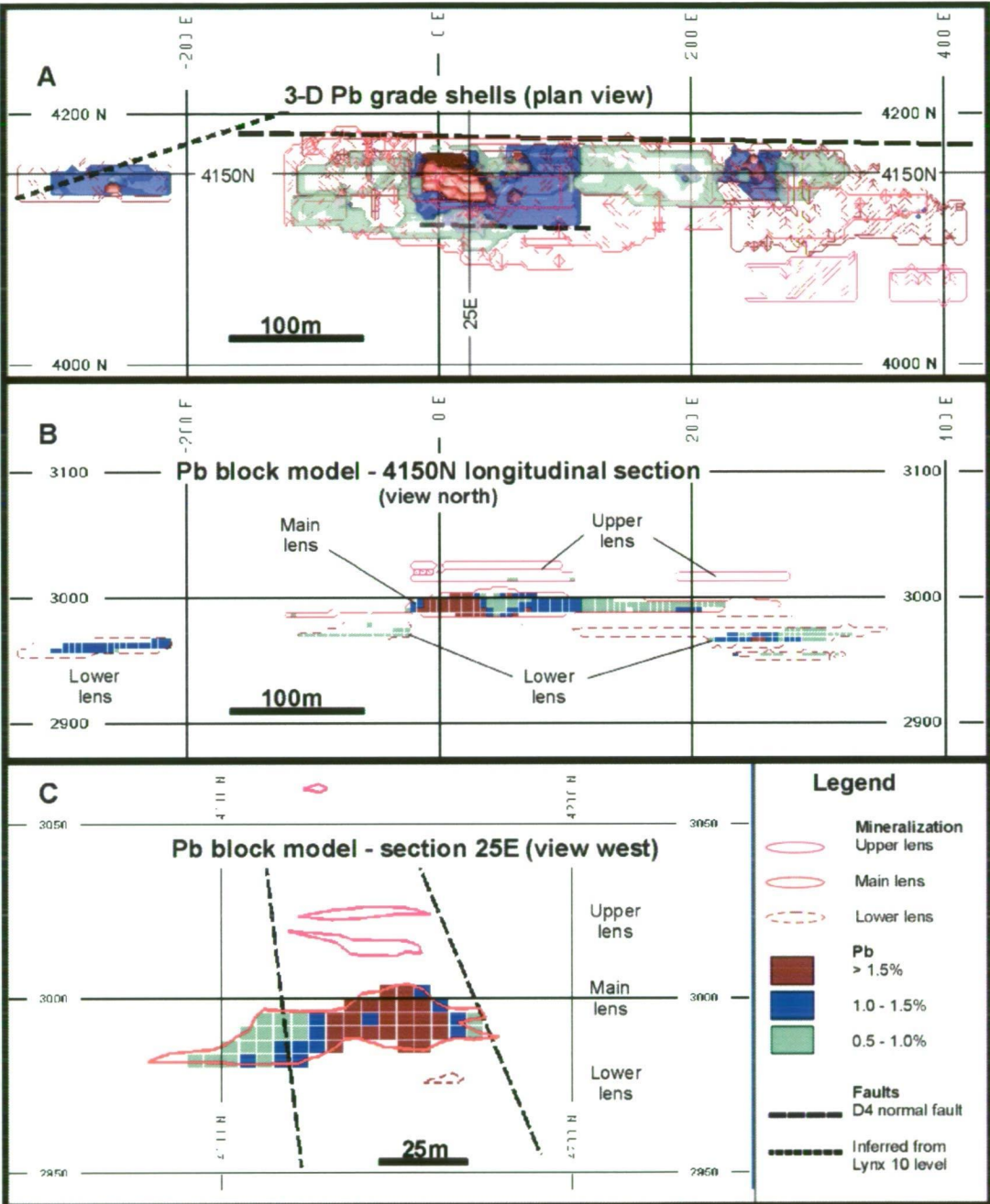


Figure 6.4: Ridge Zone West - Pb zoning

The Ridge Zone West has an average grade estimate of 0.8% Pb for the pre-mining mineral resource (Chong and Bakker, 2004). (A-B) Lower lens mineralization has Pb grades > 1.0% proximal to -250E and 250E. Main lens blocks with > 1.0% Pb are located between -20E to 110E. Upper lens mineralization is typically Pb-poor. (A and C) The northern ESE-WNW striking fault bounds the mineralization. (A-C) All three views illustrate the decrease in Pb grade with increasing distance from the areas > 1.5% Pb. The Pb zonation is similar to the Zn distribution (Fig. 6.3) for all mineralized horizons. Grade shell and block model parameters are discussed in the text. Blocks < 0.5% Pb are omitted for clarity. Faults have been omitted from the longitudinal view for clarity.

6.3.2 Block model precious metal and sulphate zoning

Precious metal and sulphate zoning is assessed for the elements Au, Ag, and Ba in Figs. 6.5, 6.6, and 6.7. Lower lens mineralization located between -300E to -210E has blocks with Ag > 125 g/t. Blocks for this area have relatively low Au and Ba values (1.0 to 2.0 g/t Au and 0.5 to 1.0 % Ba). Based on the block model, Ag is not necessarily associated with Au or Ba in this part of the Lower lens. However, Ag appears to be spatially associated with moderate Cu, Pb, and Zn concentrations in the Lower lens proximal to -250E.

Lower lens: Mineralization located between 220E to 310E near the northern ESE-WNW trending fault has blocks with elevated Au, Ag, and Ba grades (> 2.5 g/t Au, > 75 g/t Ag, and > 2.0% Ba) (Figs. 6.5, 6.6, and 6.7). Higher grade blocks with > 4.0 g/t Au, > 125 g/t Ag, and 1.0 to 2.0 % Ba are sporadically distributed near the base of the same Lower lens area. Based on the block model diagrams, Lower lens mineralization has a positive Zn-Pb-Cu-Au-Ag-Ba association proximal to 250E.

Main lens: Mineralization has elevated Au, Ag, and Ba in blocks between -110E to 220E (Figs. 6.5, 6.6, and 6.7). The elevated Au and Ag blocks appear to be more continuous along the Main lens mineralization trend than Cu, Pb, Zn and Ba. Gold grades above 4.0 g/t and Ag grades between 75 and 125 g/t occur near the southern ESE-WNW trending fault between -110E to -70E and 30E to 110E. These high-grade Au-Ag blocks appear to flank high-grade Zn-Pb-Cu-Au-Ag-Ba zones centred about 25E. This flanking zonation is best illustrated on the plan view and longitudinal sections 4150N and 4120N for Figs. 6.5 and 6.6. Based on the block model diagrams, Main lens mineralization has a positive spatial association for Au and Ag. Gold and Ag also have positive spatial associations with Cu-Pb-Zn-Ba, but are not mutually dependant.

Upper lens: Mineralization is essentially Ag and Ba-poor. Gold grades between 1.0 to 2.5 g/t Au occur within Upper lens mineralization between -10E to 110E above the Main lens mineralization (Figs. 6.5B and D).

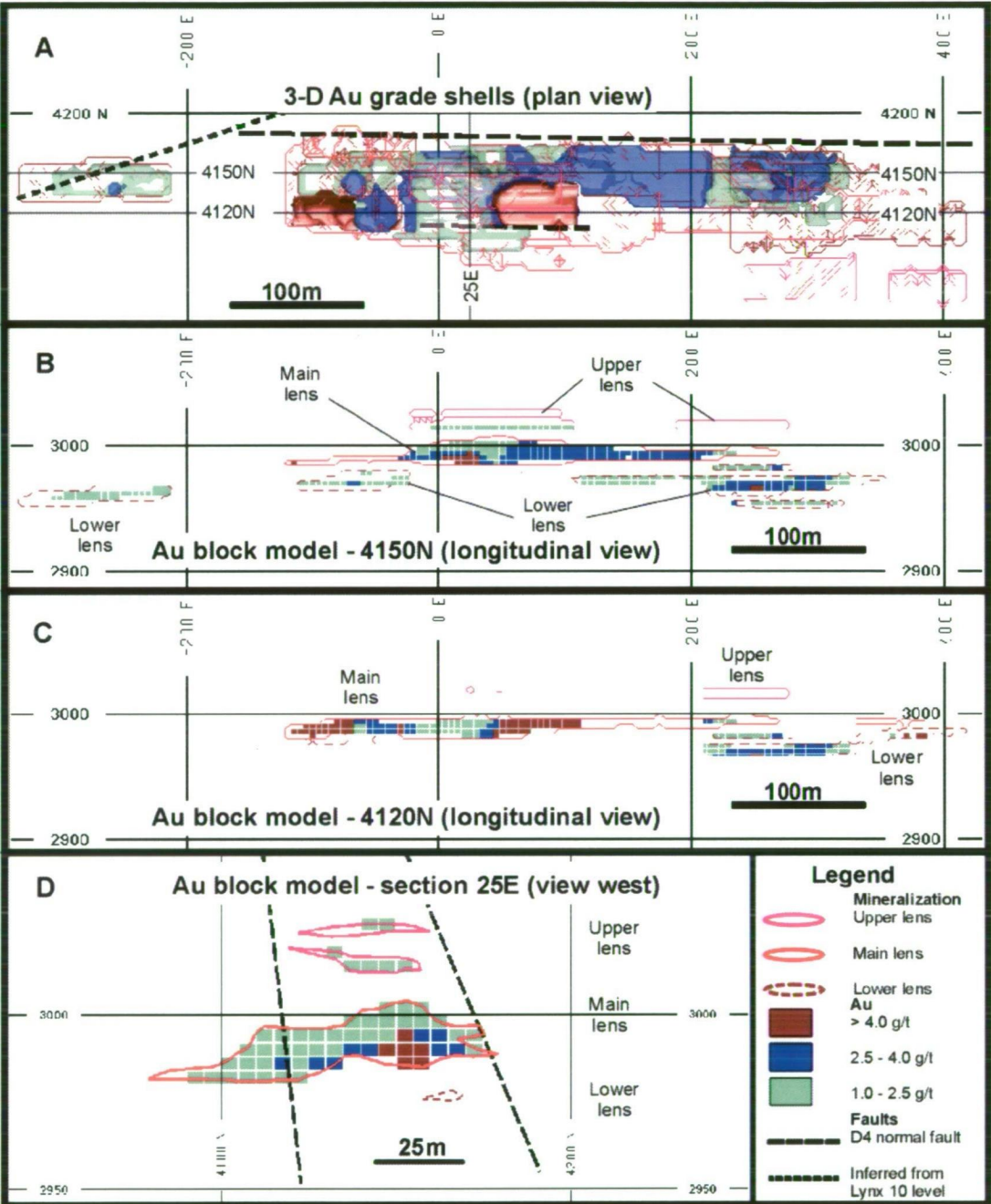


Figure 6.5: Ridge Zone West - Au zoning

The Ridge Zone West has an average grade estimate of 2.0 g/t Au for the pre-mining mineral resource (Chong and Bakker, 2004). Plan view (A) and longitudinal sections 4150N (B) and 4120N (C) show Lower lens mineralization with one area near 250E having Au content >2.5 g/t. Main lens mineralization has two Au-enriched areas. The first area is between -110E to -70E and the second area between 40E to 210E. Plan view (A) and longitudinal section 4120N (C) show high grade Au zones > 4.0 g/t are proximal to the southern ESE-WNW striking fault. These two zones appear to flank an area enriched in Cu, Zn, and Pb (Figs. 6.2, 6.3, 6.4) near 25E. The high grade Au zone between -110E to -70E does not have a spatial correlation with any of the other elements modeled. Longitudinal section 4150N (B) and section 25E (D) show a decrease in Au content upward and laterally away from the base of the Main lens mineralization. Upper lens mineralization with Au block grades between 1.0-2.5 g/t Au are located between -10E to 110E. Plan view (A) and section 25E (D) illustrate the bounding nature of the ESE to WNW striking normal faults.

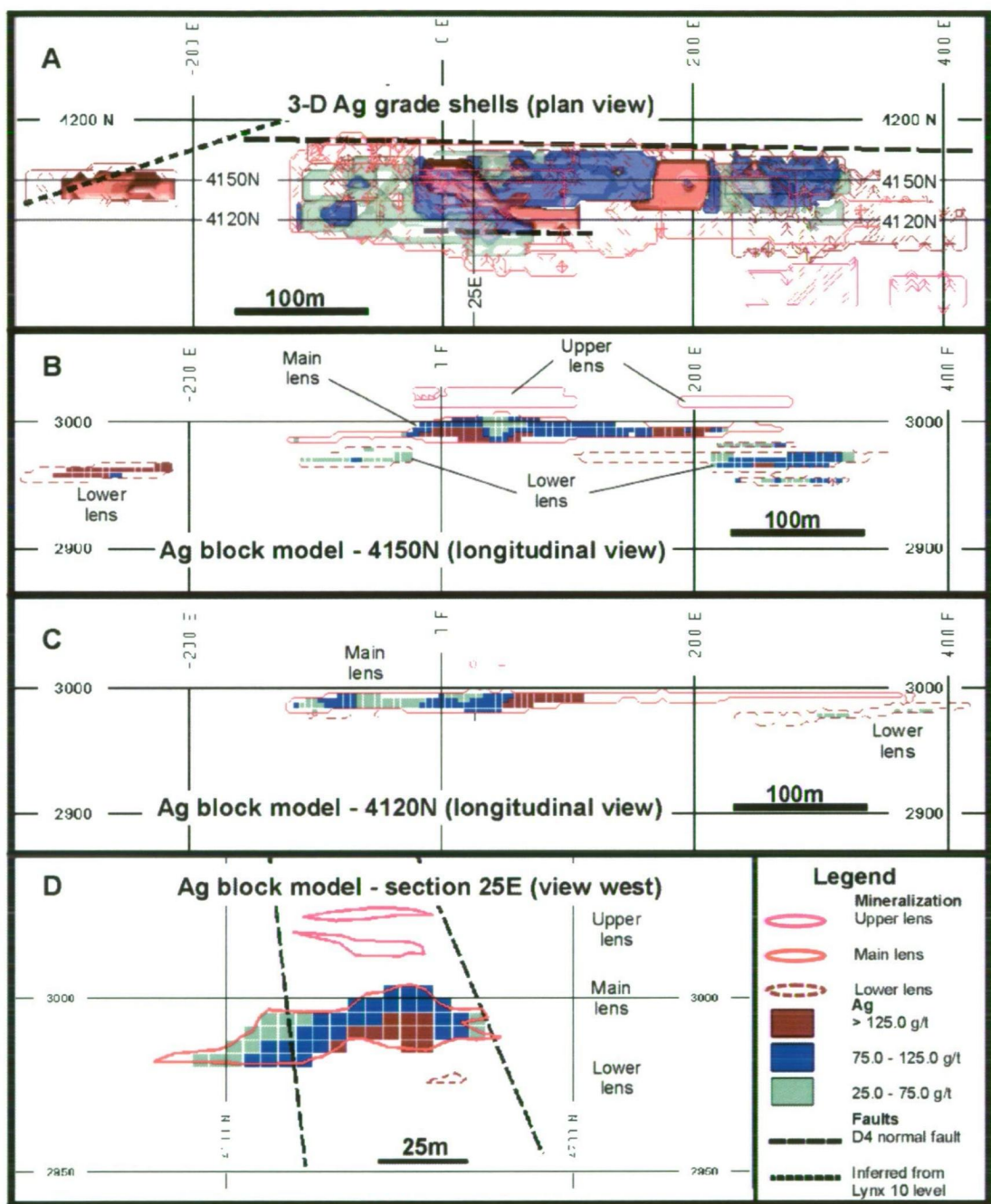


Figure 6.6: Ridge Zone West - Ag zoning

The Ridge Zone West has an average grade estimate of 71.8 g/t Ag for the pre-mining mineral resource (Chong and Bakker, 2004). (A-B) Lower lens mineralization has two areas with elevated Ag (> 75.0 g/t) proximal to -250E and 250E. The Lower mineralization zoning is similar to the distribution for Cu, Zn, and Pb (Figs. 6.2, 6.3, 6.4). (A, B, and C) Main lens mineralization has two general areas with elevated Ag content. The first area is between -100E to -70E on section 4120N (C). The second area is between -20E to 220E. The second area has three high grade zones (>125 g/t Ag) centred about 0E, 75E and 200E. (C) Silver zoning near the southern ESE-WNW striking fault flanks the Cu, Zn, Pb, and Au-rich zone centred about 0E. (A, B, and D) Elevated Ag grades are generally bounded by the two ESE-WNW striking faults. (D) Section 25E illustrates decreasing Ag content with increasing distance from the base of the Main lens mineralization. This zonation is similar to Cu, Zn, and Pb (Figs. 6.2, 6.3, 6.4). Upper lens mineralization has block grade contents < 25 g/t Ag and hence are not displayed.

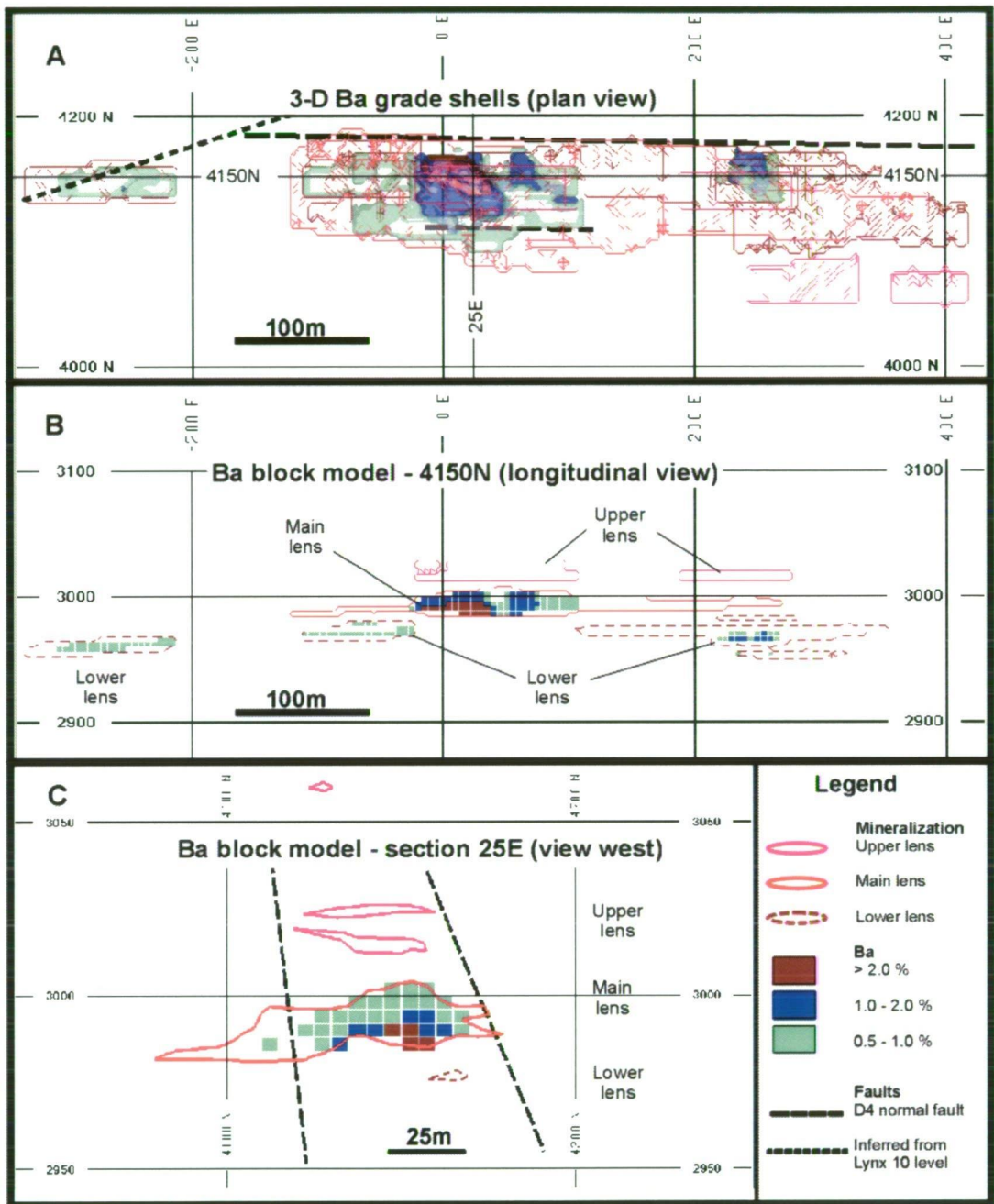


Figure 6.7: Ridge Zone West - Ba zoning

The Ridge Zone West has an average grade estimate of 0.8% Ba for the pre-mining mineral resource (Chong and Bakker, 2004). (A, B, and C) The blocks with above average grade Ba are part of the Main lens mineralization associated with coarse-grained volcanoclastic rocks. The highest grade Ba blocks (2.0 to 4.0% Ba) are between -20E to 40E and 50E to 70E bounded by the two WNW-ESE striking faults. (B and C) Barium content decreases upward and laterally away from the base of the Main mineralization. This zonation is similar to that observed for Main lens Au, Ag, Cu, and Pb. Lower lens mineralization associated with fine-grained volcano-sedimentary rocks are typically < 1.0% Ba except for an area centred about 250E. Grade shell and block model parameters are discussed in the text. Blocks < 0.5% Ba are omitted for clarity. Faults have been omitted from the longitudinal view for clarity.

6.4 Assay data metal associations

The purpose of this section is to graphically and statistically evaluate element associations amongst Zn, Pb, Cu, Fe, Au, Ag, and Ba. Assay data for the Lower lens, Main lens, and Upper lens mineralization are compared and contrasted in a series of bivariate scatter diagrams with linear regression trend lines (Figs. 6.8 to 6.13). The assay data are from 232 samples selected from the Myra Falls database constrained by geological boundaries for the Lower, Main, and Upper lenses. Appendix 4 describes the assay laboratory methods and quality control procedures at Myra Falls.

6.4.1 Assay data statistics

Frequency histograms, bivariate scatter diagrams, linear regression trend lines, and correlation statistics presented in this study were calculated and plotted using “Microsoft Excel”™ software. Statistics are used to measure the correlation between a dependant variable and an independent variable. The statistic used for this study is the coefficient of determination (r^2). The coefficient of determination measures the portion of the total variance in a dependant variable (e.g. Au) that is explained or accounted for by the introduction of an independent variable (e.g. Pb) (Sanders, et al., 1985). The r^2 coefficient is expressed as a percentage and cannot exceed 1.00 or 100%. As an example, if the linear regression trend line for Au versus Pb has an $r^2=0.60$, then 60% of the Au can be accounted for by the variation in Pb. Higher values of r^2 indicate a stronger correlation than lesser values. The coefficient of determination values are divided into the following qualitative groupings for discussion purposes: poor correlation (r^2 is > 0 and ≤ 0.50), weak correlation (r^2 is > 0.50 and ≤ 0.65), moderate correlation (r^2 is > 0.65 and ≤ 0.80), and strong correlation (r^2 is > 0.80 and ≤ 1.00). Bivariate scatter diagrams have data points, r^2 values, and linear regression trend lines plotted. Linear regression trend lines are plotted for elements with weak to strong correlations ($r^2 > 0.50$). Elements with poor correlations ($r^2 < 0.50$) have only their data points and r^2 values plotted. Linear regression trend lines illustrating poor correlations are omitted for clarity.

6.4.2 Zinc assays

The sample population of 232 analyses generally has an apparent bimodal distribution (Fig. 6.8A). Seventy-seven percent of the sample population is ≤ 10.0 % Zn. The average Zn value for the assay data is 7.9 %. The overall range is 0.1 to 44.0 % Zn. Sample lengths vary between 0.1 to 1.5 m. A second population of 16 analyses ranges between 28.0 – 32.0 % Zn and the samples occur in the Main and Lower lenses between -250E to 250E. Therefore, a spatial association cannot be inferred.

Based on scatter diagrams for Zn versus Ba, Pb, Cu, and Fe (Fig. 6.8B-E), the moderate and strong correlations for Zn are with Upper lens-Cu ($r^2=0.83$) and Upper lens-Fe ($r^2=0.88$) (Fig. 6.8D and E). Coefficient of determination values indicating weak correlations with Zn are Lower lens-Pb, Main lens-Pb, and Main lens-Cu (Fig. 6.8C and D).

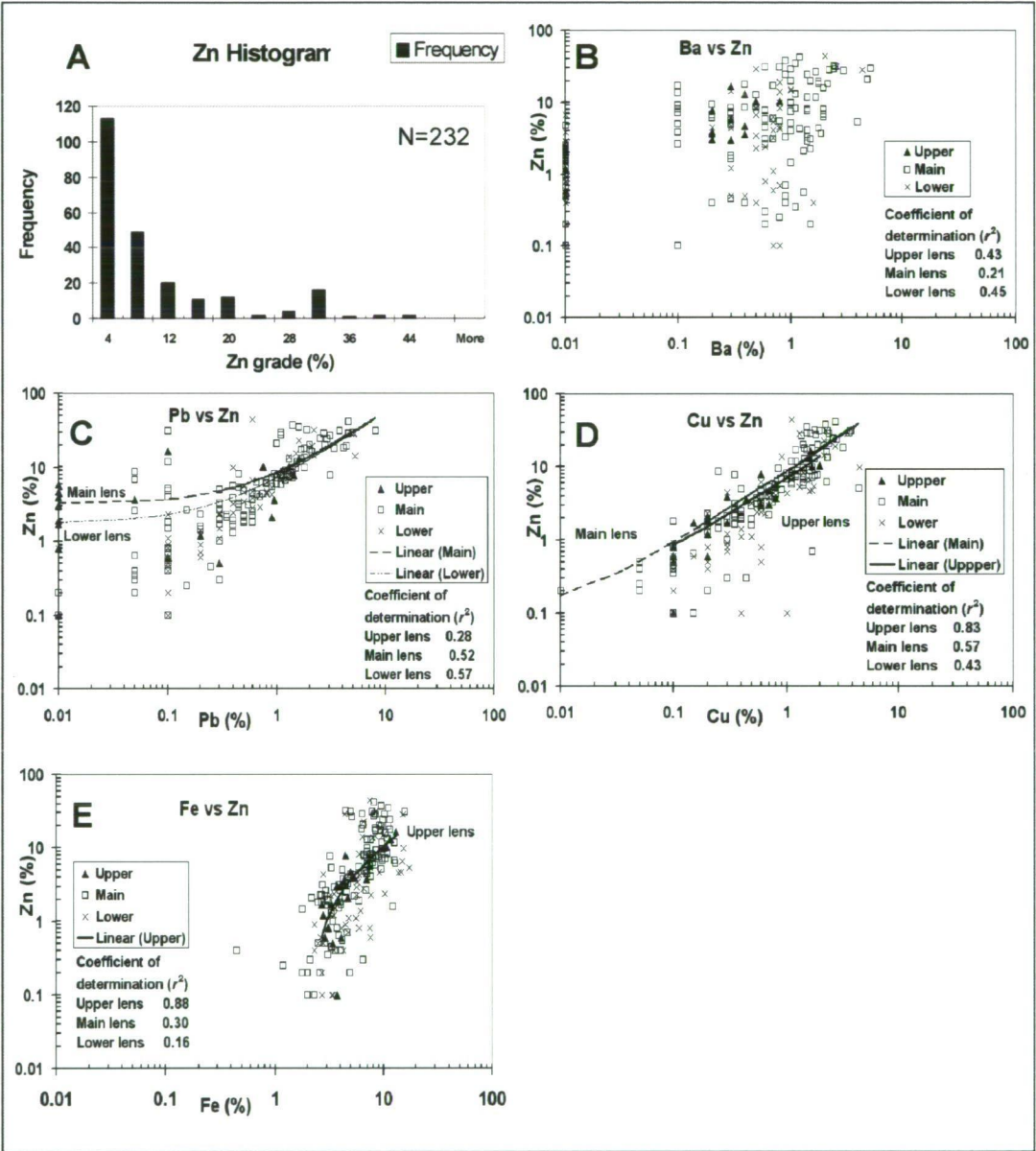
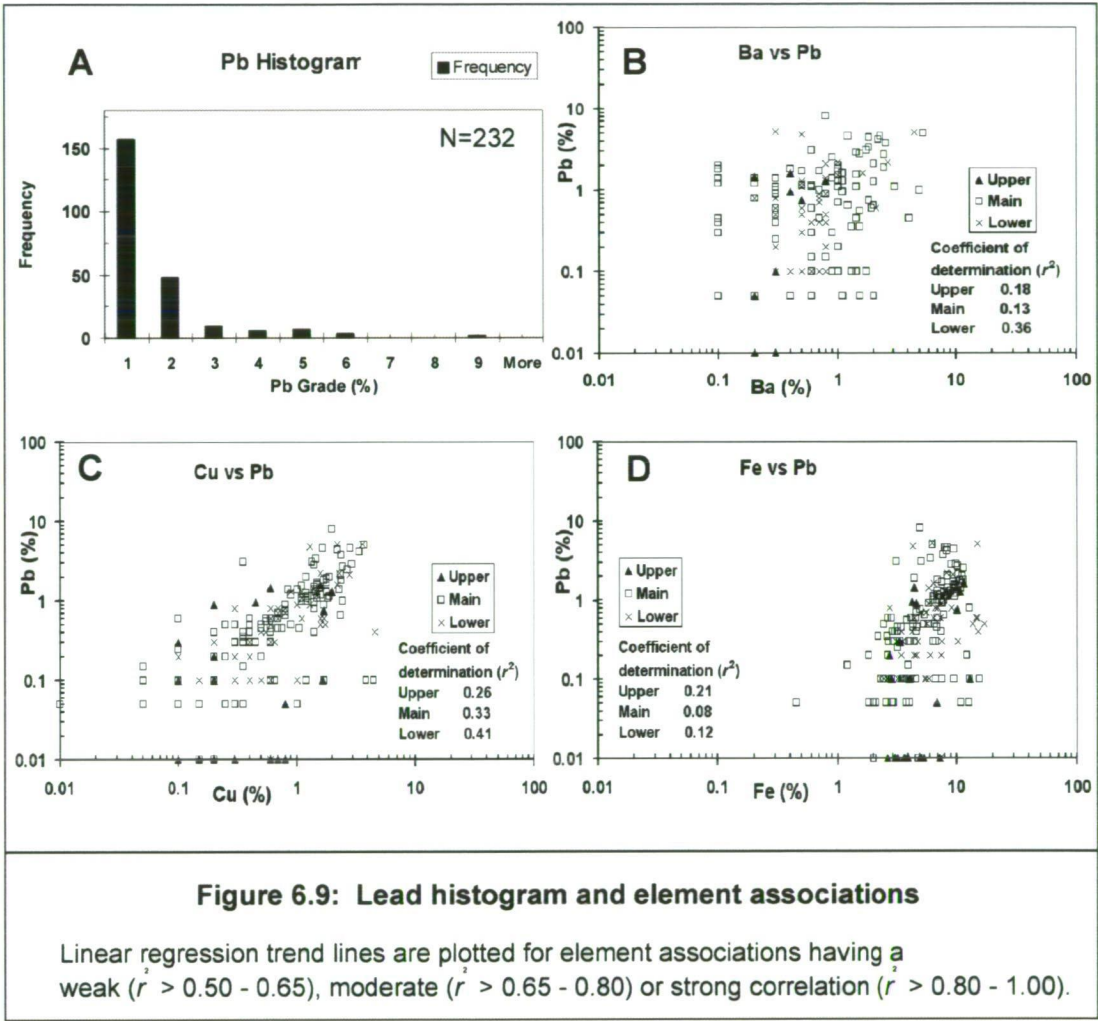


Figure 6.8: Zinc histogram and element associations

Linear regression trend lines are plotted for element associations having a weak ($r^2 > 0.50 - 0.65$), moderate ($r^2 > 0.65 - 0.80$) or strong correlation ($r^2 > 0.80 - 1.00$).

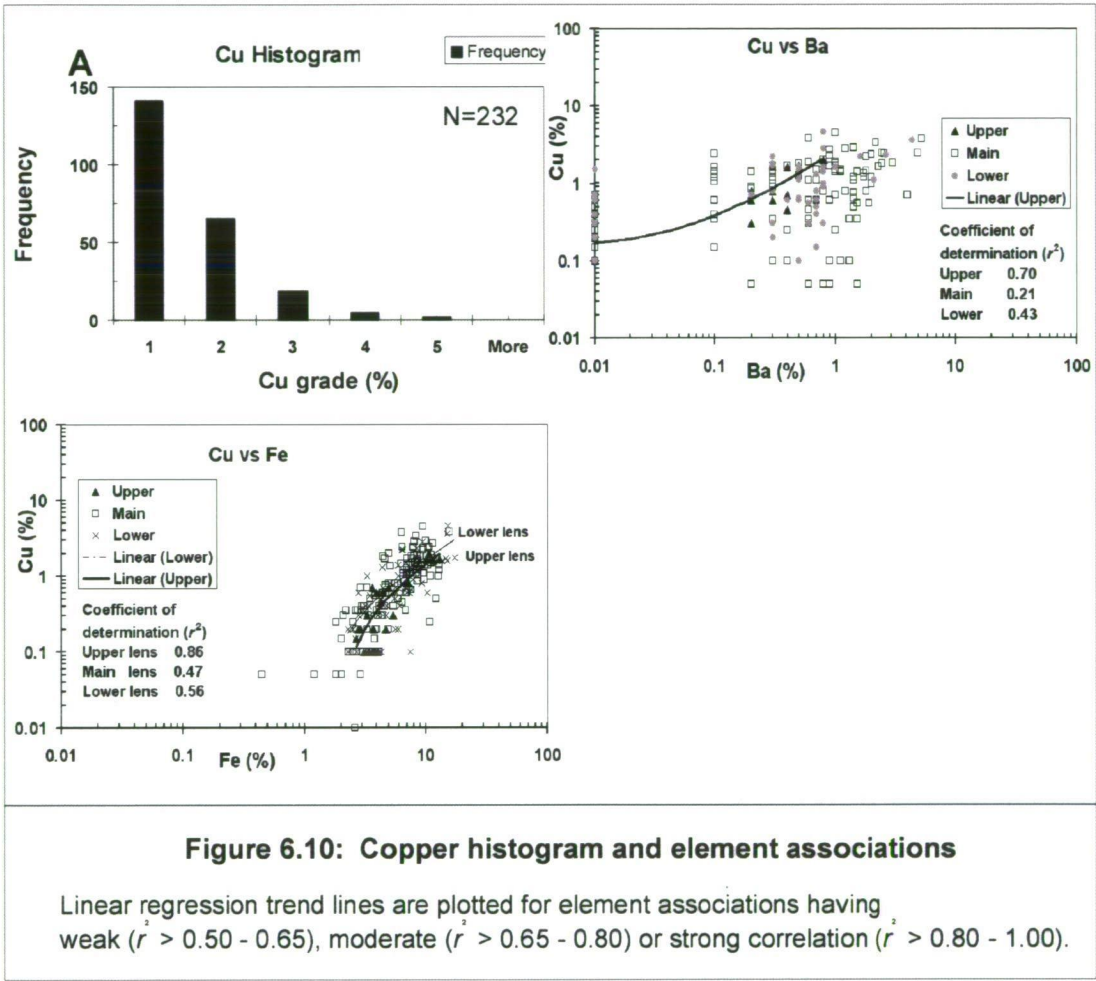
6.4.3 Lead assays

Eighty-eight percent of the sample population is ≤ 2.0 % Pb. The sample population has a positive skew (Fig. 6.9A). Concentrations of Pb range from 0.0 to 8.1 % and average 0.97 %. Aside from an association with Zn, poor correlations are noted for Pb with Ba, Cu, and Fe for which r^2 values are < 0.50 (Fig. 6.9B-D).



6.4.4 Copper assays

Eighty-eight percent of the sample population is $\leq 2.0\%$ Cu. The sample population has a positive skew. Concentrations of Cu range from 0.0 to 4.6 % and average 0.98 %. A strong correlation ($r^2=0.86$) is noted for Cu with Upper lens-Fe (Fig. 6.10C). Main lens-Zn, Upper lens-Zn (Fig. 6.8D), Lower lens-Fe (Fig. 6.10C), and Upper lens-Ba (Fig. 6.10B) have weak to moderate correlation with Cu.

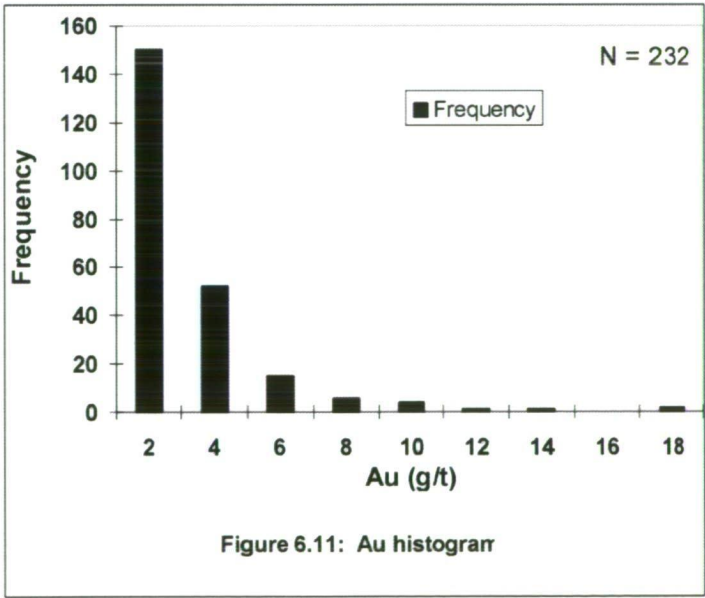


6.4.5 Gold assays

The gold histogram has an overall positive skew with 87% of the sample population ≤ 4.0 g/t Au (Fig. 6.11). Two general groupings are highlighted on bivariate scatter diagrams. Group 1 comprises Au values ≤ 4.0 g/t Au (Fig. 6.12). The Au values are variably distributed throughout the range for all the elements and generally do not correlate based on the trend lines. The only exception to this interpretation is for Upper lens-Ag and Group 1-Au for which $r^2 = 0.79$ (Fig. 6.12A).

Group 2-Au assays are > 4.0 g/t Au. Visual inspection of Group 2 data suggests general minimum values for each of the elements relative to elevated Au values. However, lower values below the inferred minimums exist. An inferred minimum line is plotted for relevant scatter diagrams (Fig. 6.12) showing elevated Au values with the following associations: Ag > 60 g/t, Pb $> 0.6\%$, Zn $> 2.0\%$, Fe $> 4.0\%$, and Cu $> 0.6\%$.

A subset of Lower lens-Ag and Main lens-Ag for Group 2-Au has an apparent continuation along the same trend as Upper lens-Ag for Group 1-Au (Fig. 6.12A). The trend suggests a possible correlation between Au and Ag for Lower lens, Main lens, and Upper lens mineralization. The apparent Au-Ag trend suggests a possible association of gold with Ag-bearing tennantite.



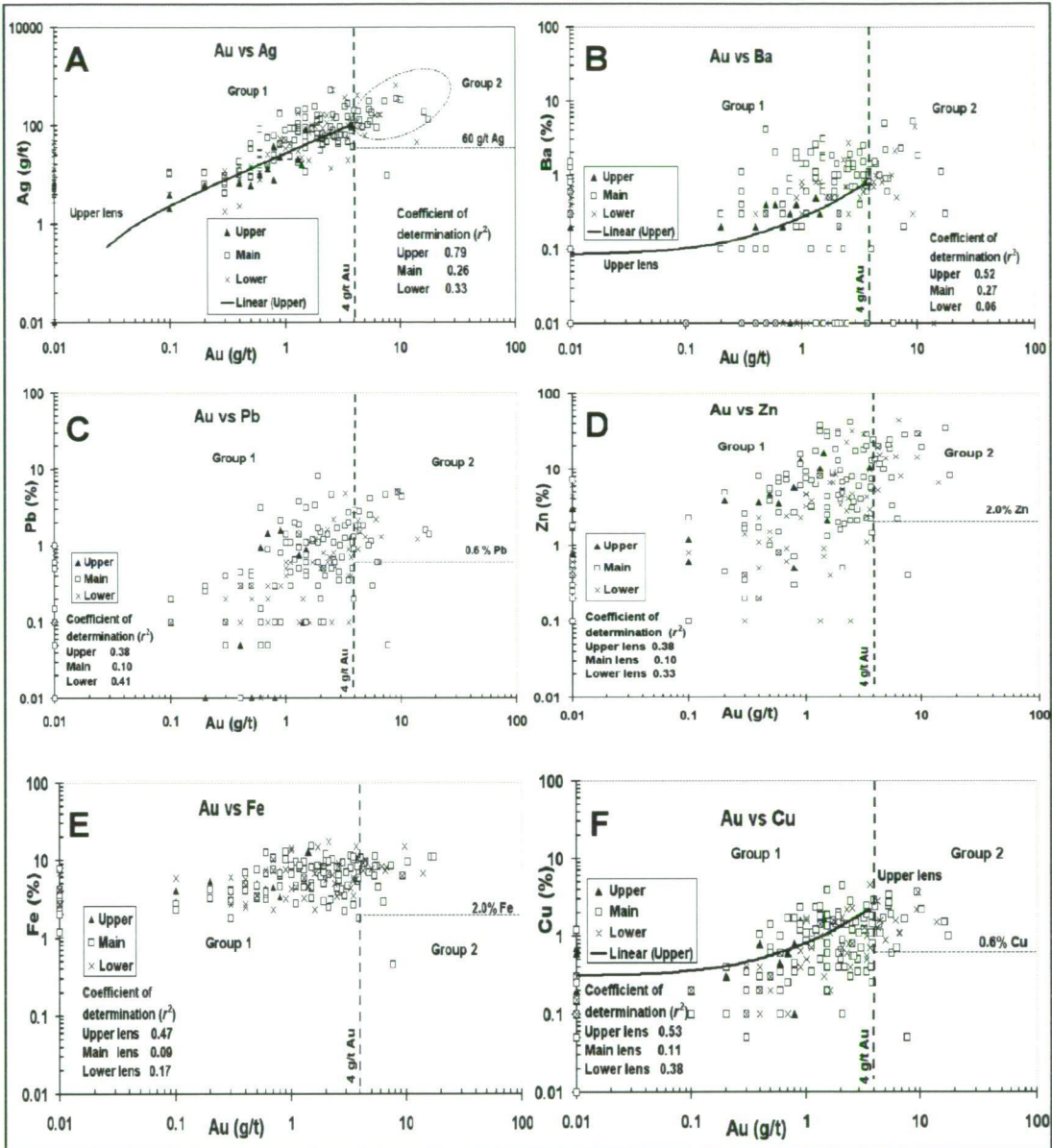


Figure 6.12: Gold associations

Two general groupings of Au are interpreted based on the Au histogram (Fig. 6.14). Group 1-Au (≤ 4 g/t Au) comprises 87% of the sample population. Group 2-Au (> 4 g/t Au) has the following general interpreted visual associations, even though lower values exist for all the elements: (A) Ag >60 g/t (B) Ba - no correlation, (C) Pb $>0.6\%$, (D) Zn $>2.0\%$, (E) Fe $>2.0\%$, and (F) Cu $>0.6\%$.

(A) Upper lens-Ag has a good trend line correlation ($r^2=0.79$) that appears to continue for a portion of the Main lens and Lower lens-Ag populations. There are weak correlations between Ag and Upper lens-Ba (B) and Upper lens-Cu (F). The remainder of the element associations have poor correlations ($r^2 = 0.0 - 50.0$). Linear regression trend lines are plotted for element associations having weak ($r^2 > 0.50 - 0.65$), moderate ($r^2 > 0.65 - 0.80$) or strong correlation ($r^2 > 0.80 - 1.00$).

6.4.6 Silver assays

The silver histogram has a positive skew with 84% of the sample population occurring at ≤ 150 g/t (Fig. 6.13A). Two groupings have been inferred based on the histogram and bivariate scatter plots. The groupings include Group 1-Ag (≤ 150 g/t Ag) and Group 2-Ag (> 150 g/t Ag). The best correlation is between Pb and Ag in Lower lens mineralization where $r^2=0.74$ (Fig. 6.13C).

Group 1-Ag is variably distributed throughout the entire range for Ba, Zn, Fe, and Ag. The exception to the variable distribution is a restricted grouping of assays typically < 2.0 % Pb. This observation supports a possible Lower lens-Pb association with Group 1-Ag.

Group 2-Ag comprises Ag assays > 150 g/t Ag. Inferred minima interpreted by the author for each of the elements imply the following associations with Ag > 150 g/t: Ba $> 0.3\%$, Pb $> 1.0\%$, Zn $> 8.0\%$, Fe $> 4.0\%$, and Cu $> 1.0\%$.

Group1-Ag and Group 2-Ag have weak correlations with Main lens-Pb ($r^2=0.54$), Main lens-Zn ($r^2=0.57$), and Lower lens-Zn ($r^2=0.58$). The Main lens Pb-Ag correlation suggests an association of Ag with galena, although 17 galena microprobe analyses had Ag concentrations all below the detection limit of 0.2 wt% (Table 5.7). However, 5 tennantite microprobe analyses had an average of 1.45 wt % Ag (Table 5.8) and there is petrographic evidence of a galena-tennantite assemblage (Fig. 510E).

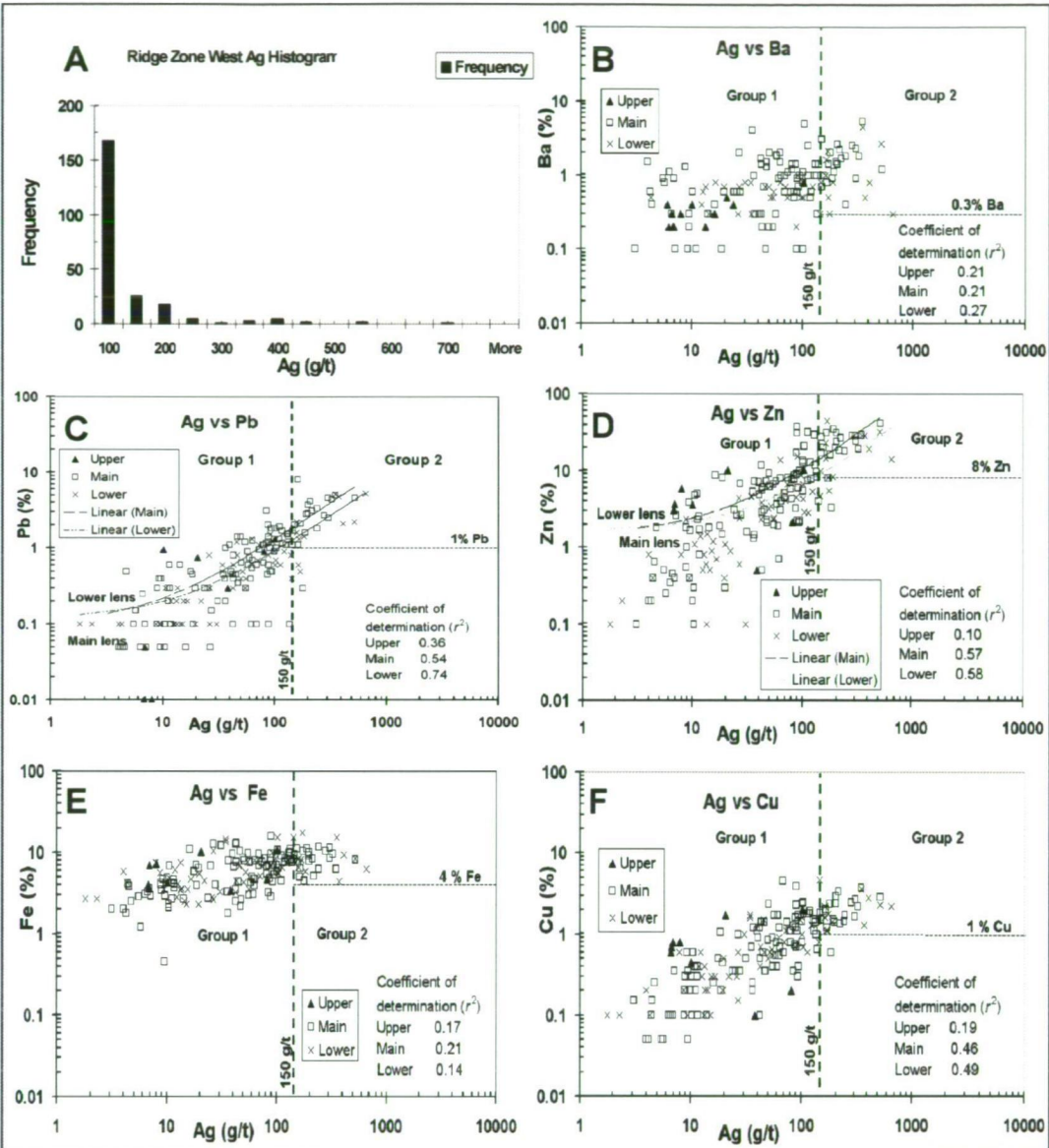


Figure 6.13: Silver histogram and associations

Two general groupings of Ag are interpreted based on the Ag histogram (A). Group 1 (≤ 150 g/t Ag) comprises 84% of the sample population. The range for Group 1-Ag is variably distributed for all the elements except Pb (C). Group 2 (> 150 g/t Ag) has the following general interpreted visual associations, even though lower values for Zn-Pb-Cu exist: (B) Ba $> 0.5\%$, (C) Pb $> 1.0\%$, (D) Zn $> 8.0\%$, (E) Fe $> 4.0\%$, and (F) Cu $> 1.0\%$. Lower-Pb (C) has the most significant linear regression correlation ($r = 0.74$). Lower-Zn, Main-Zn (D), and Main-Pb (C) have weak correlations. The remainder of the element associations have poor correlations ($r = 0.0 - 0.50$). Linear regression trend lines are plotted for element associations having weak ($r > 0.50 - 0.65$), moderate ($r > 0.65 - 0.80$) or strong correlation ($r > 0.80 - 1.00$).

6.5 Element association discussion

6.5.1 Assay data

This section discusses the element associations interpreted by inspection of linear regression trend lines with r^2 correlations > 0.50 and uses the textural, mineralogical, and chemical data from Chapter 5 to infer mineral assemblages for the Lower, Main, and Upper lenses.

The strongest element association is Zn-Pb+/-Ag for the Lower, Main, and Upper lenses as represented by the mineral assemblage sphalerite-galena+/-tennantite. Sphalerite-galena+/-tennantite occurs as anastomosing veins increasing in intensity to massive accumulations within Main lens mineralization and as bands within fine-grained facies rocks of the Lower and Upper lenses. Tennantite has not been observed in the banded style mineralization. The block model distributions for Zn and Pb (Figs. 6.3 and 6.4) show similar spatial distribution patterns within selected grade ranges. Silver in the Lower and Main lenses also has a similar block model distribution pattern as Zn and Pb. An exception to the association is the Ag-poor Upper lens where a Zn-Pb association has statistical, mineralogical, and spatial correlations.

As previously discussed in Section 6.5.6, silver occurs within two main groupings based on the histogram and scatter diagrams (Fig 6.13). Group 1-Ag is ≤ 150 g/t Ag and Group 2-Ag > 150 g/t Ag. The minimum values inferred by visual assessment of the scatter plots for Group 2-Ag are: Ba $> 0.3\%$, Pb $> 1.0\%$, Zn $> 8\%$, Fe $> 4.0\%$, and Cu $> 1.0\%$. The element minimum values associated with Group 2-Ag support the statistical Zn-Pb-Ag correlation.

The second strongest element association is Cu+/-Zn+/-Fe for the Lower, Main, and Upper lenses as represented by the mineral assemblage chalcopyrite+/-sphalerite+/-pyrite. This assemblage occurs as chalcopyrite-rich veins with pyrite+/-sphalerite, semi-massive to massive sphalerite with chalcopyrite veins or blebs, and disseminated pyrite+/-chalcopyrite+/-sphalerite. Block model distribution for Cu-Zn is very similar for all horizons (Figs. 6.2 and 6.3). Block model Fe distribution is relatively uniform for the grade ranges assessed and does not reflect the same spatial distribution as Cu and Zn.

The block model for Fe (Fig. 6.1) illustrates poor to non-existent zoning patterns for the grade ranges plotted. Iron is hosted by pyrite, chalcopyrite, sphalerite, and tennantite in the lenses studied. Iron is noted to statistically correlate only with Cu-Zn for Lower lens

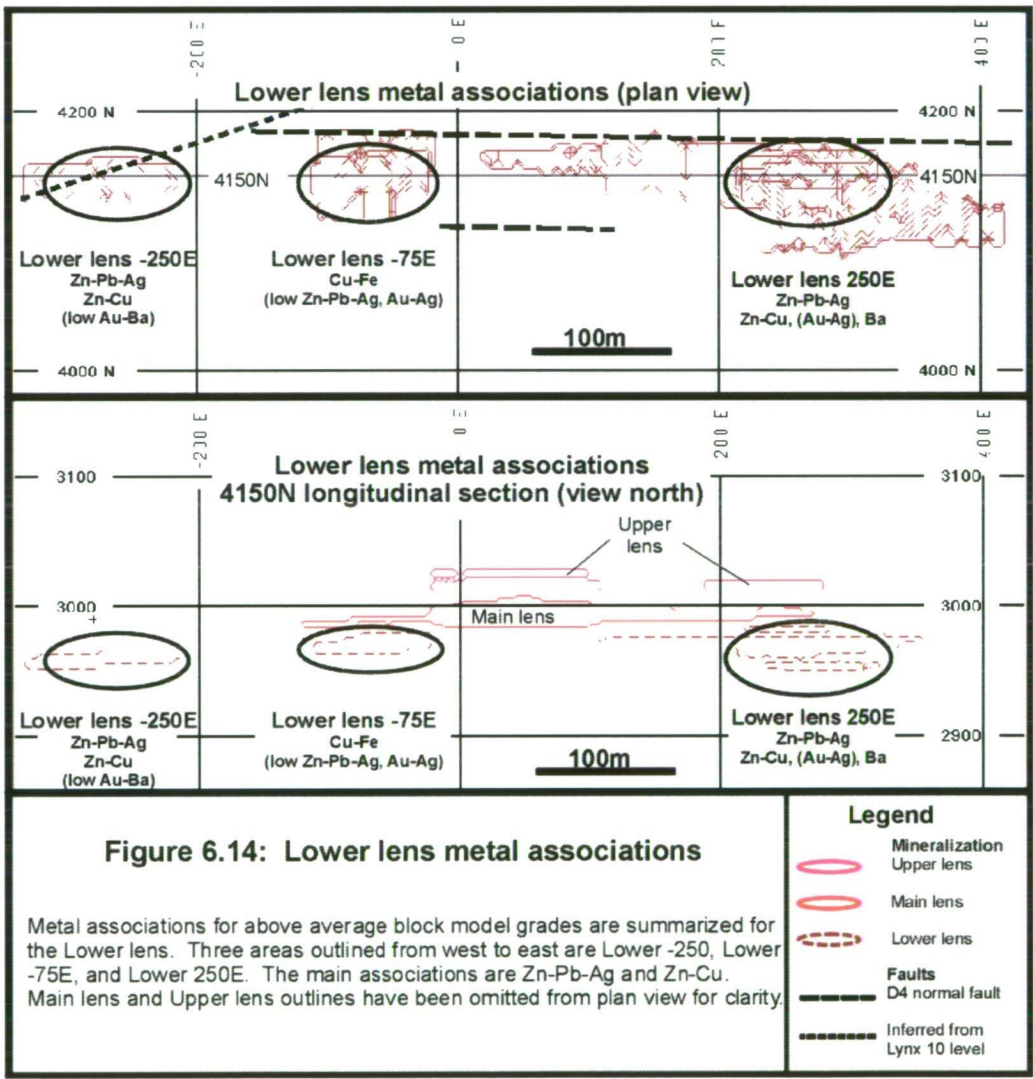
mineralization. Pyrite occurs as fine-grained disseminations, bands within fine-grained sediments, and veins associated with chalcopyrite+/-sphalerite+/-galena.

Two general groupings of Au are inferred based on the Au histogram and scatter diagrams (Figs. 6.11 and 6.12). The first grouping is ≤ 4.0 g/t Au (Group 1-Au). The Lower lens and Main lens do not have significant Group 1-Au associations with the other elements assessed. Upper lens mineralization has significant statistical correlations between Group 1-Au and Ba, Cu, and Ag. The mineralogical associations with Group 1-Au are interpreted to be barite (Au1-Ba), chalcopyrite (Au1-Cu), and tennantite (Au1-Ag). The block model grade ranges plotted are not adequate to resolve any spatial relationships.

Group 2-Au (> 4.0 g/t Au) has the following general associations based on visual distribution within scatter diagrams: Ag > 60 g/t, Pb $> 0.6\%$, Zn $> 2.0\%$, Fe $> 4.0\%$, and Cu $> 0.6\%$ (Fig. 6.12). All Group 2-Au values are from the Lower and Main lenses. Though not statistically consistent, a possible association between Group 2-Au and Group 2-Ag may exist for parts of the Lower and Main lenses (Fig. 6.12A). The block model spatial distribution for Au > 4.0 g/t and Ag > 125 g/t are very similar and support this inference (Figs. 6.5 and 6.6).

6.5.2 Spatial distribution

Lower lens mineralization associated with fine-grained argillaceous mudstone is found in three areas. These areas will be referred to as Lower lens -250E, Lower lens -75E, and Lower lens 250E. Spatial associations for these above average grade areas are illustrated in Fig. 6.14. Lower lens -250E has a positive Zn-Pb-Ag and Zn-Cu association. Lower lens -75E has a weak positive Cu-Fe association with below average grade Zn-Pb-Ag and Au-Ag. Lower lens 250E has a positive Zn-Pb-Ag, Zn-Cu, and Au-Ag+/-Ba spatial association.



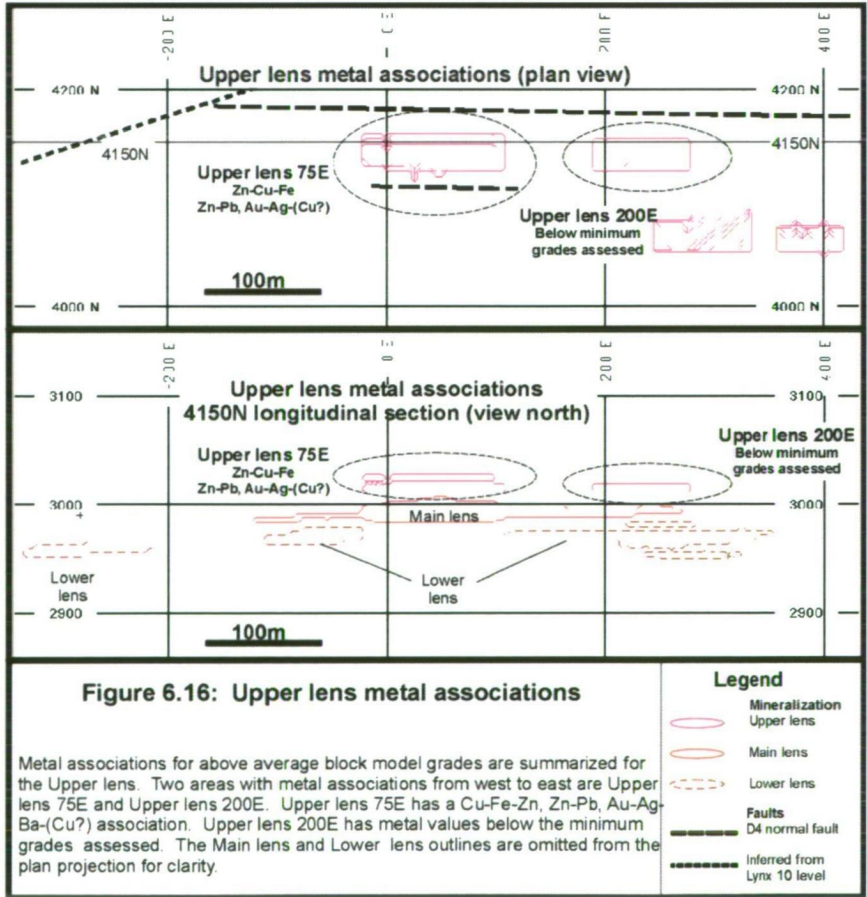
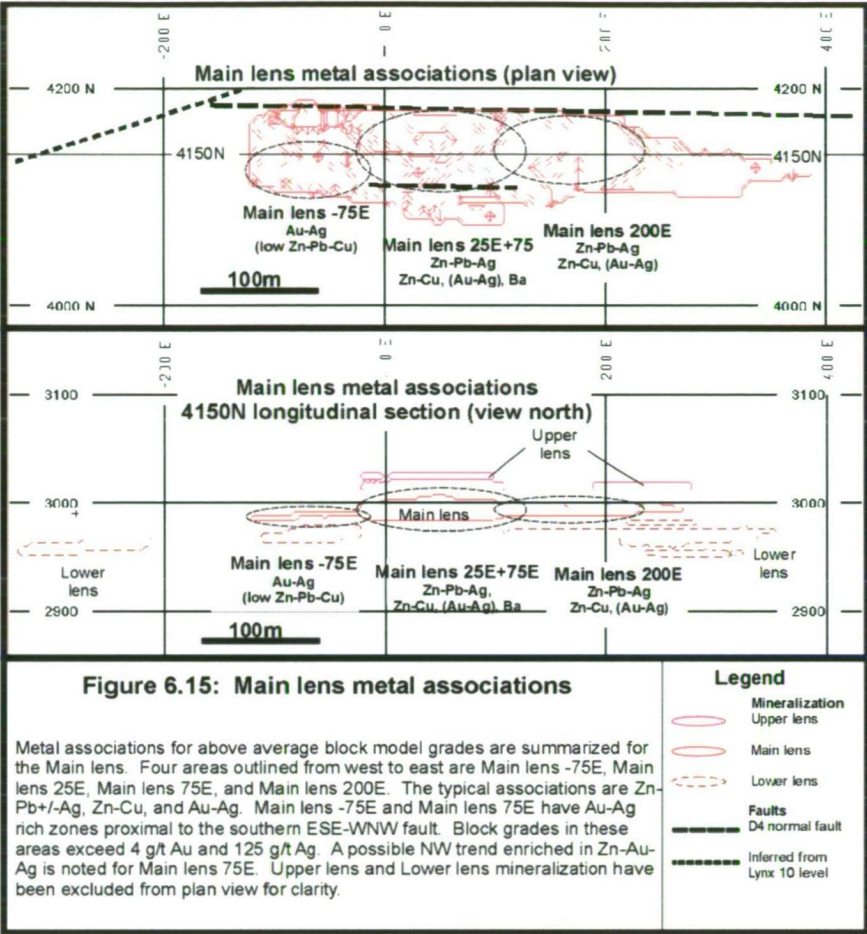
Main lens mineralization associated with a coarse-grained, volcanoclastic horizon and subordinate argillaceous mudstone occurs in three areas with varying metal relationships. The areas will be referred to as Main lens -75E, Main lens 25E+Main lens 75E, and Main lens 200E. Figure 6.15 summarizes the areas with above average grade metal associations. Main lens -75E is located proximal to the southern fault and has a positive Au-Ag enrichment with below average Zn-Pb+/-Cu values. Main lens -75E is Ba deficient.

Main lens 25E is an interesting area with a positive Zn-Pb-Ag, Zn-Cu, (Au-Ag), Ba spatial association. Grades decrease laterally away from a core zone enriched in the element associations Zn-Pb-Ag, Zn-Cu, Au-Ag, and Ba. The steep orientation of sphalerite-galena+/-chalcopyrite+/-tennantite+/-barite rich veins explains why above average Zn, Pb, Ag, Cu, and Ag blocks extend from the base upward to the hangingwall contact of the Main lens mineralization. Copper and Ag blocks show a slight decrease in grade with increasing vertical distance from the Main lens base but still have above average grades.

Main lens 75E has a similar positive Zn-Pb-Ag, Zn-Cu, Au-Ag, and Ba metal association as Main lens 25E. High-grade Au-Ag and Zn blocks occur proximal to the southern fault. Block grades appear to decrease with increasing distance eastward for Zn, Pb, Cu, and Ba. Gold and Ag have continuous above average block grades to Main lens 200E. This is possibly due to an area enriched in tennantite. The observation that Pb block grades do not follow the same trend as Ag supports the microprobe findings that tennantite is the main residency for Ag in the Ridge Zone West. Main lens 25E and Main lens 75E have the same metal associations and could possibly be combined as one area with a possible NW trend enriched with Zn, Au, and Ag.

Main lens 200E has a positive Au-Ag association with localized above average block grades for Zn, Pb, and Cu proximal to the base of the mineralization. Block grades for Zn, Pb, and Cu decrease with increasing vertical and lateral distance. Block grades for Au-Ag are generally elevated between Main lens 75E and Main lens 200E.

Upper lens mineralization associated with siliceous mudstone is defined by two areas. The two areas are referred to as Upper lens 75E and Upper lens 200E (Fig. 6.16). Upper lens 75E has as weak Zn-Cu-Au+/-Fe+/-Pb association. Upper lens 200E block grades are below the minimum grade criteria used for all the metal zone diagrams. Hence, Upper lens 200E is metal deficient based on the block grades assessed.



6.6 Gold association

The occurrence of Au in the Ridge Zone West has not been determined by either microscopy or microprobe work. Hence, further investigation is required to infer mineralogical assemblage associations for Au. Based on the assessment of the block model and assay data the following observations and inferences related to Au are noted:

- The gold histogram has a positive skew with 87% of the values ≤ 4.0 g/t Au.
- Au grades >0.9 g/t Au (deposit average) are spatially located in the areas Lower lens 250E and Main lens -75E through to Main lens 200E (Figs. 6.5, 6.14, and 6.15)
- Lower lens and Main lens element associations include Zn-Pb-Ag, Cu-Zn, and Group 2 Au-Ag. Barium enrichment is also noted.
- Main lens mineralization has three high-grade Au zones between -75E and 75E (Fig. 6.5). Two Au rich zones are proximal to the southern ESE-WNW fault flanking a high grade Zn-Pb-Ag, Zn-Cu, and Au-Ag \pm -Ba rich core. Main lens mineralization has continuous elevated Main lens Group-1 and Main lens Group-2 Au and Ag blocks between 75E and 200E. This contrasts with below average Zn, Pb, and Cu grades and an absence of Ba (Fig. 6.5).
- Upper lens mineralization has Au grades less than 4.0 g/t Au. The most significant statistical association is Upper lens Group-1 Au-Ag located above the high grade Main lens mineralization between -75E and 75E.

Gold in VHMS deposits typically occurs within two or three element associations. The associations are Cu-Au, pyritic Au, and Au-Zn-Pb-Ag (i.e. polymetallic) (Huston and Large, 1989; Poulsen and Hannington, 1995). The two associations pertinent for Myra Falls are Cu-Au and Au-Zn-Pb-Ag. The Cu-Au association is typified by Au concentration at the base of a massive sulphide mound or in the stringer zone (Huston and Large (1989). The Au-Zn-Pb-Ag association is concentrated at the top or along the margins of a massive sulphide lens or in the baritic cap (Huston and Large, 1989). The mineralogy of Au in VHMS deposits includes electrum, native gold, Au tellurides, auriferous pyrite, and auriferous arsenopyrite (Huston, 2000). Auriferous Au minerals for deposits with Au-Zn-Pb-Ag associations include electrum, pyrite, and arsenopyrite. As a deposit becomes more deformed electrum becomes increasingly present and Au is associated with either pyrite or a number of sulphides and barite (Huston et al., 1992; Larocque et al., 1993; Huston, 2000).

The H-W deposit is a strongly zoned Zn-Cu deposit with a pyrite-chalcopyrite rich core and a sphalerite-galena-barite-chalcopyrite rich south fringe (Walker, 1985; Pearson, 1993). Gold in the H-W deposit involves coarse and fine-grained electrum (Chrysoullis, 1989), pyrite, and chalcopyrite (Wilson, 1993). Barrett and Sherlock (1996) suggest gold occurs as submicroscopic inclusions at grain boundaries and as scattered grains of free gold or electrum. Chrysoullis (1989) noted a fine-grained electrum associated with pyrite and sphalerite and that tennantite had 6.3 ppm Au in solid solution. Hayward (2001) noted that 60% of the gold occurrences above 12 g/t Au are found within small polymetallic Upper Zone lenses located up to 15m above the H-W Main lens. An additional 14% of the known occurrences over 12 g/t Au in the H-W deposit are found within the polymetallic Zn-Pb-Cu-Ba rich south fringe area.

Hayward (2001) noted that 82% of the gold assays greater than 12 g/t Au for the Battle deposits are found within Zn-Pb-Ba rich Upper Zone lenses located up to 70 m above the Main lens. Though classified as a Zn-Cu deposit (Table 6.2), the Gap lens is a Zn-Pb-Cu-Ag-Ag-Ba rich pipe shaped lens at the same stratigraphic position as Upper Zone lenses above the Battle Main lens. The host for Au in the Gap lens is the assemblage electrum-stromeyerite (Sinclair, 2000).

Based on the above review, two Au associations occur at Myra Falls:

- (1) Cu-Au association for the pyrite-rich core of the H-W deposit; and
- (2) A more significant Au-Zn-Pb-Ag association in polymetallic mineralization that is common in the H-W deposit south fringe, Upper Zone mineralization in the H-W and Battle deposits, and the Gap lens.

The Au-Zn-Pb-Ag association is interpreted for the Ridge Zone West based on the element associations from assay data and the block model. Minerals suggested to contain Au for the Ridge Zone West mineralization includes electrum, pyrite, stromeyerite, and tennantite.

6.7 Metal ratios

Metal ratio variations reflect the type and distribution of the metallic mineral phases. The Cu ratio (CR) expressed as $100*[Cu / (Cu+Zn)]$ (Solomon, 1976) is a good indicator for temperature variations within a VHMS system. Knuckey et al. (1982) demonstrated a decrease in the CR with increasing distance from the main hydrothermal feeder system for a cluster of lenses of the Millenbach deposit, Noranda. Where lenses form at successive horizons vertically above each other, the higher copper content of the lower lenses is attributed, in part, to replacement and veining. Individual lenses have Cu-rich cores grading outward to Zn-rich margins. High relative CR values reflect higher relative temperatures for the mineralizing fluids and can be used to target vector hydrothermal feeder systems in conjunction with Fe-zoning and geological mapping.

Similarly, the Zn ratio (ZR) expressed as $100*[Zn / (Zn+Pb)]$ is an indicator of temperature variation in Zn-Pb enriched VHMS systems such as the Mount Read Volcanics in Tasmania (Huston and Large, 1987). Zinc ratios for solutions saturated in Zn and Pb at varying temperatures and salinities as calculated from thermodynamic data indicate a general inverse relationship between the ratio and temperature of the mineralizing fluids (Huston and Large, 1987). An exception to this relationship are solutions greater than or equal to 1 M and between the temperatures 200 °C and 250 °C, where a reversal occurs and the ZR increases with an increase in temperature (Table 6.1). Gemmell and Large (1992) used low ZR values coincident with high CR values and abundant pyrite within the footwall alteration zone to define high temperature feeder zones for the Hellyer deposit.

| Table 6.1: Zinc Ratios of saturated solutions at varying temperatures and salinities as calculated from thermodynamic data (from Huston and Large, 1987) | | | | | | |
|--|------------------------|-------|-------|-------|-------|-------|
| Temperature (°C) | Salinity (equiv. NaCl) | | | | | |
| | 0.25 m | 0.5 m | 1.0 m | 1.5 m | 2.0 m | 3.0 m |
| 25 | 99 | 99 | 98 | 98 | 98 | 98 |
| 50 | 97 | 97 | 97 | 97 | 97 | 98 |
| 100 | 93 | 91 | 91 | 92 | 93 | 94 |
| 150 | 86 | 83 | 83 | 85 | 87 | 90 |
| 200 | 73 | 66 | 62 | 65 | 68 | 73 |
| 250 | 61 | 58 | 68 | 77 | 83 | 89 |
| 300 | 34 | 24 | 15 | 11 | 9 | 6 |
| Numbers within the box correspond to the likely conditions of sphalerite and galena deposition in volcanic hosted massive sulphide deposits | | | | | | |

The Ridge Zone West CR and ZR are calculated based on block model grades and plotted using Minesite 3-D software. The purpose is to characterize the CR and ZR for the mineralization. Temperature regimes are discussed using the geology, CR, ZR, and the individual elements.

6.7.1 Ridge Zone West Cu ratios

Figure 6.17 illustrates the block model CR distribution for the Ridge Zone West. Generally, the Lower, Main, and Upper lenses all have CR values > 10 except for an area west of Main lens 75E (Fig. 6.17A and B). The area west of Main lens 75E has CR values < 10 and is coincident with the greatest sulphide thickness and zoning. The depressed CR blocks are bounded to the north and south by blocks with CR values between 10 and 20 proximal to the WNW-ESE trending faults (Fig. 6.17C). This trend suggests a hotter fluid temperature regime adjacent to the faults. This trend is only partly supported by the Cu zoning demonstrated in Figure 6.2 where Cu values > 2.0% are centred midway between the faults. The disparity between the CR and the Cu grades are attributed to Zn values > 12 % throughout the area between the north and south faults.

The CR values for Lower lens 250E range between 11 and 26. Two areas within Lower lens 250E mineralization have several contiguous blocks with CR values >20 (Fig. 6.17A and C). These two areas are centred about 175E and 250E. Upon further investigation, both areas of interest have low Cu block grades between 0.5 to 1.0% Cu, < 4.0% Zn, and < 7% Fe. Therefore, high CR values (CR > 20) for Lower lens 250E are not considered significant from a fluid temperature aspect.

Excluding apparent elevated CR values with insignificant Cu and Zn grades for Lower lens 250E, the CR has a narrow range between 10 and 20 for Lower lens, Main lens, and Upper lens mineralization. Higher CR values are also spatially associated with the north and south WNW-ESE trending faults.

6.7.2 Ridge Zone West Zn ratios

Figure 6.18 illustrates the block model ZR values and distribution. The areas with ZR values >90 are Lower lens -250E, Lower lens -75E, Main lens 25E, Main lens 75E, Upper lens 75E and Upper lens 200E (Fig. 6.18A and B). Areas with low ZR values (ZR < 90) are Main lens -75E to Main lens 25E proximal to the southern fault, Main lens 200E, and Lower lens 250E. Hotter fluid temperature proximal to the southern fault and in the eastern portion of the study area is inferred based on the thermodynamic data by Huston and Large (1987). The validity of this inference will be discussed further in the discussion portion of this chapter.

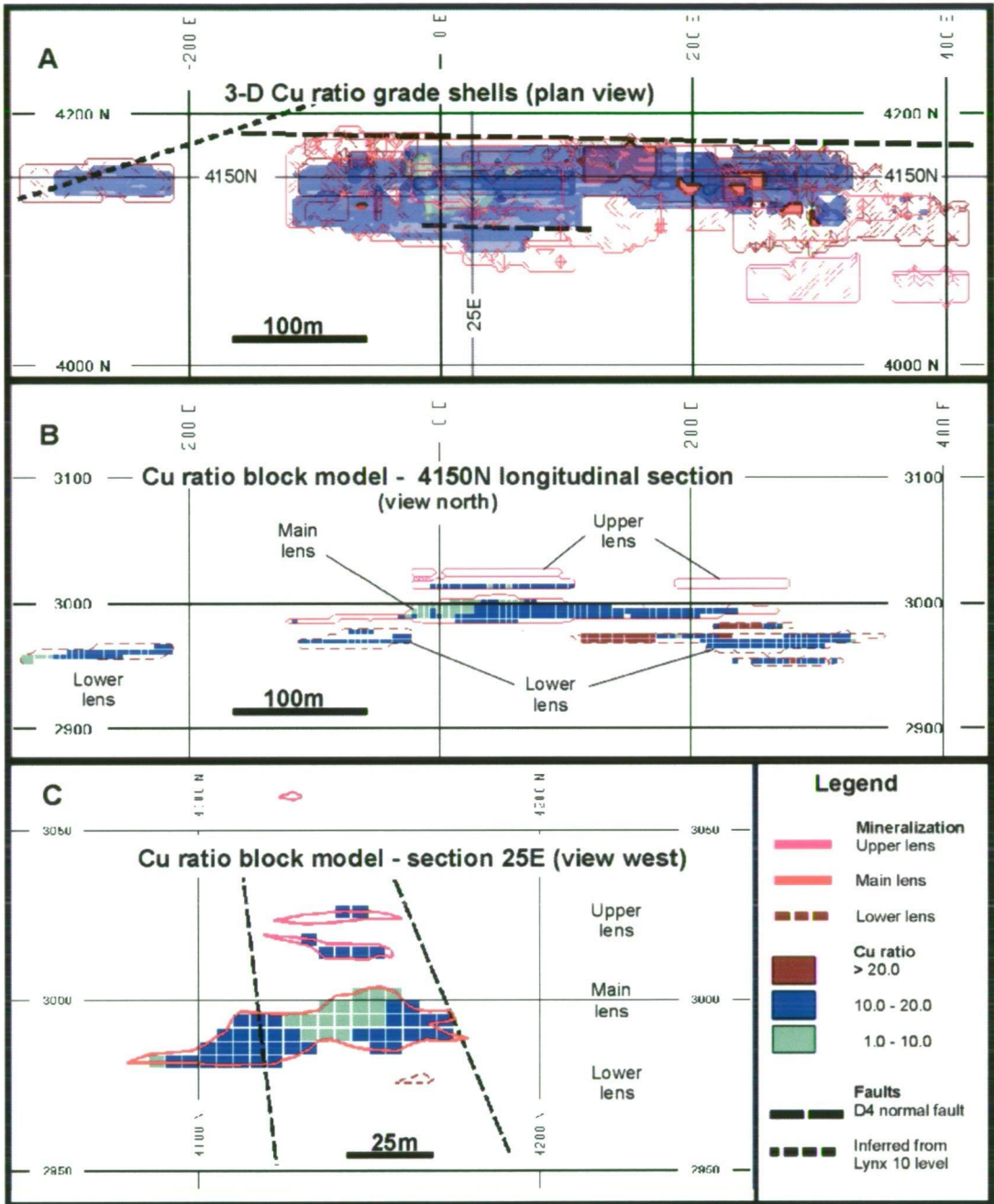


Figure 6.17: Ridge Zone West - Cu ratio zoning

The Cu ratio (CR) is based on the formula $100 \cdot \text{Cu} / (\text{Cu} + \text{Zn})$ (Solomon, 1976). The Ridge Zone West CR is 11 based on the pre-mining mineral resource estimate (Table 6.1). CR block model values are < 35 and hence Cu-poor. (A-B) Lower lens mineralization has sporadic elevated CR values (> 11) centred about 175E and 225E. (B) Main lens and Upper lens Cu ratios are between 10 to 20 or lower. (C) Section 25E has two areas with elevated CR values situated immediately south of the two faults with values ranging between 10 to 20. CR values > 20 are not synchronous with the elevated Cu values for section 25E (Figure 6.2C). Grade shell and block model parameters are discussed in the text. Copper ratios < 1 are omitted for clarity. Faults have been omitted from the longitudinal view for clarity.

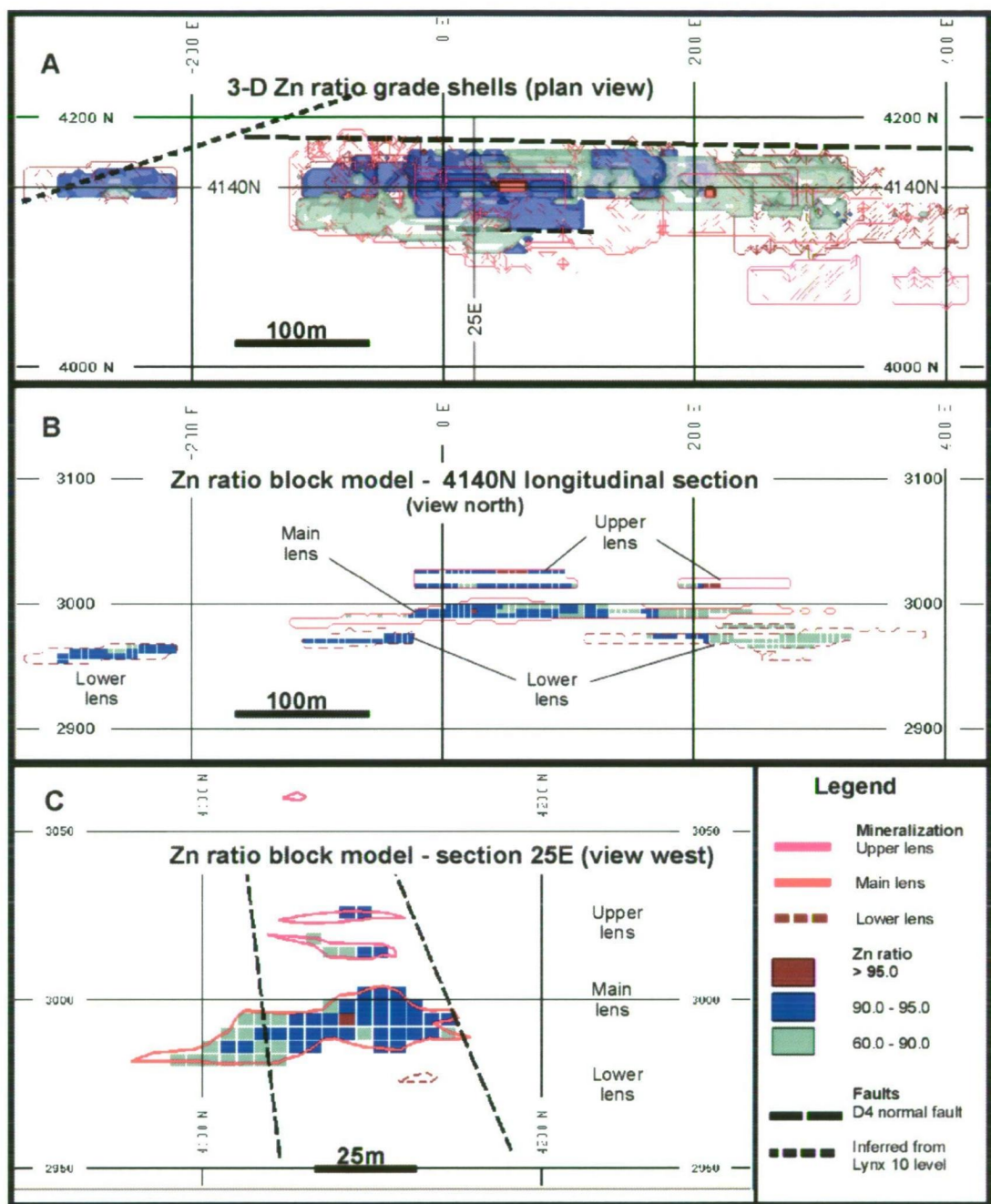


Figure 6.18: Ridge Zone West - Zn ratio zoning

The Zn ratio (ZR) is based on the formula $100 \cdot \text{Zn} / (\text{Zn} + \text{Pb})$ (Huston and Large, 1987). The Ridge Zone West average ZR is 90 based on the pre-mining mineral resource estimate (Chong and Bakker, 2004) and hence borderline between a Zn-Cu or a Zn-Pb-Cu deposit relative to the criteria outlined by Large (1992). (A-B) Lower lens mineralization has elevated ZR values centred about -250E, -75E, and 200E. Main lens mineralization has elevated ZR values (>90) between -25E to 180E. (B) Longitudinal section 4140N is used to illustrate elevated Upper mineralization ZR values (>90) between -25E to 100E and proximal to 210E. (C) Elevated ZR blocks occur between the ESE-WNW striking faults. Grade shell and block model parameters are discussed in the text. ZR blocks < 60 are omitted for clarity. Faults have been omitted from the longitudinal view for clarity.

6.7.3 Ridge Zone West metal ratio discussion

Overall, there appears to be no areas with focused high temperature regimes. Instead, broad areas with CR values < 20 and ZR values ranging between 60 and 90 suggest warmer temperature regimes are proximal to the southern+/- northern WNW-ESE faults, Main lens 200E, and Lower lens 250E.

Fluid temperatures are interpreted to be relatively consistent throughout the Ridge Zone West system with no significant up-flow or feeder zone based on relatively consistent CR values between 10 and 20 (Fig. 6.17). This is consistent with the weakly dispersed Fe block model distribution (Fig. 6.1). Copper enrichment (Fig. 6.2) at the base of the mineralization for Main lens 25E is partly inconsistent with variable CR values due to the high Zn content of the area. The elevated CR values are spatially associated with the northern and southern WNW-ESE trending faults instead of centred between the faults.

Main lens 200E and Lower lens 250E have overall higher CR and depressed ZR values suggesting a warmer temperature regime than mineralization westward. Interestingly, the thickness and grade of the mineralization of Main lens 200E and Lower lens 250E are considerably less than mineralization found westward. Therefore, temperature regime is not considered a significant pathfinder towards economically significant mineralization with greater thicknesses. Instead, Zn-rich mineralization within a permeable, coarse volcanoclastic horizon and the presence of possible fluid pathway controlling faults are considered to have greater significance towards forming economically significant mineralization for the Ridge Zone West lenses.

6.8 Property scale metal zoning

VHMS deposits have a number of proposed classification schemes based on metal content (Hutchinson, 1973; Solomon, 1976; Franklin et al., 1981; Large, 1992), tectonic setting (Sawkins, 1976; Hutchinson, 1980), and host-rock composition (Sangster and Scott, 1976; Barrie and Hannington, 1999). The classification used in this study is based on metal content as proposed by Large (1992) because it is simple to apply, not based on interpretation (e.g. tectonic environment), and not limited by lack of available data (e.g. geochemical data). Large (1992) quantifies the categories as follows:

- (1) Cu deposits: Cu Ratio (CR) > 60, Zinc Ratio (ZR) > 60
- (2) Zn-Cu deposits: CR < 60 and ZR > 90
- (3) Zn-Pb-Cu deposits: CR < 60 and ZR = 60 – 90

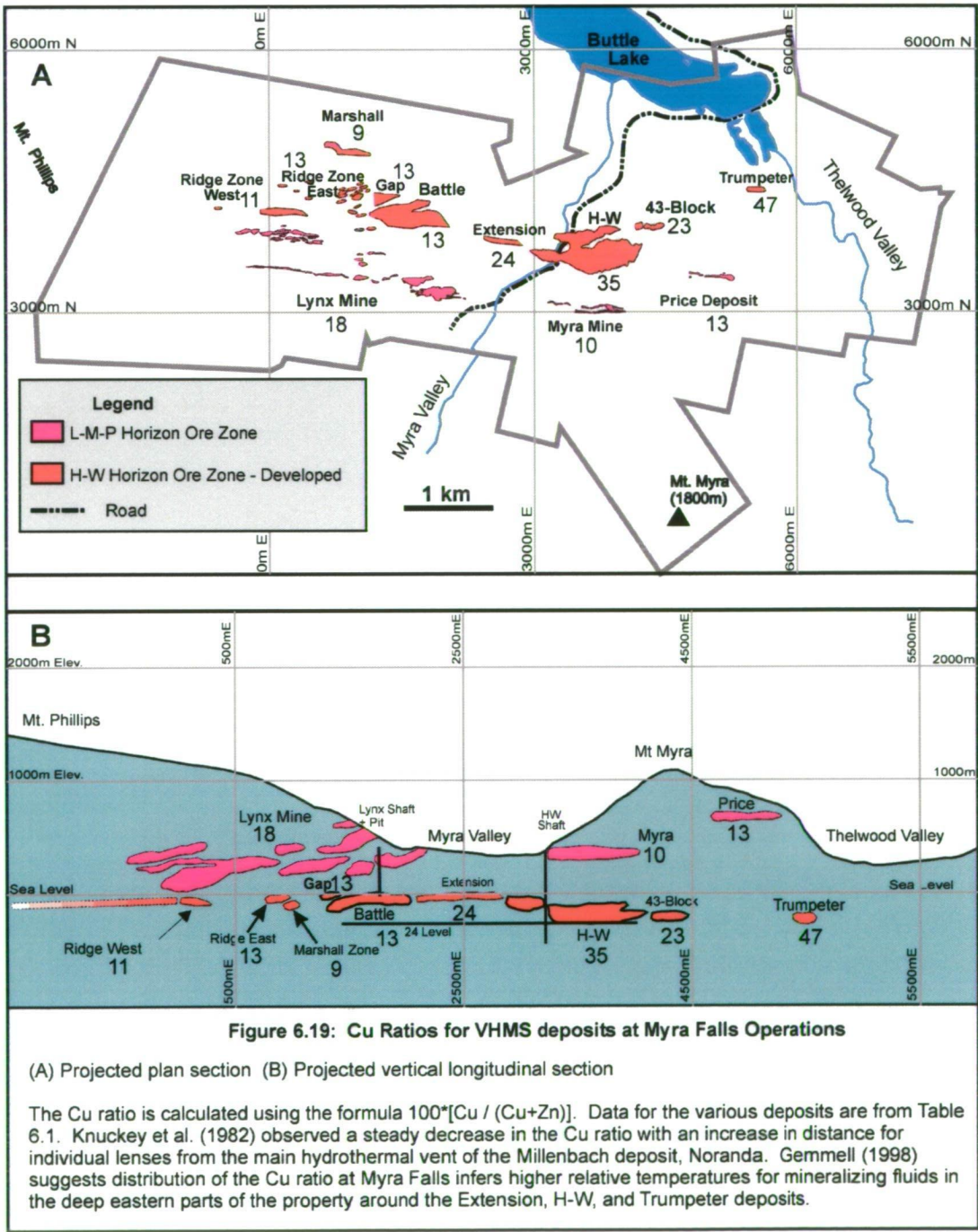
The VHMS deposits at Myra Falls are classified as either Zn-Cu or Zn-Pb-Cu deposits based on their CR and ZR (Gemmell, 1998; Chong, 2003). Based on pre-mining geological mineral resource estimates (all categories), the Ridge Zone West has a ZR of 90 and is between a Zn-Cu deposit and a Zn-Pb-Cu deposit (Table 6.2).

| Deposit | Tonnes | Average Deposit Size | Au g/t | Ag g/t | Cu % | Pb % | Zn % | Zn Ratio (1) | Cu Ratio (2) | Metal Content Classification ⁽³⁾ |
|-----------------------|-------------------|----------------------|------------|-----------|------------|------------|------------|--------------|--------------|---|
| lynx-mine | 5,809,000 | | 2.5 | 90 | 1.6 | 1.0 | 7.5 | 88 | 18 | Zn-Pb-Cu |
| myra | 1,037,000 | | 3.0 | 160 | 1.0 | 1.5 | 9.5 | 86 | 10 | Zn-Pb-Cu |
| price | 381,000 | | 2.1 | 73 | 1.4 | 1.3 | 9.2 | 88 | 13 | Zn-Pb-Cu |
| ridge-east | 326,000 | | 0.8 | 41 | 0.7 | 0.8 | 4.7 | 86 | 13 | Zn-Pb-Cu |
| ridge-west | 983,000 | | 2.0 | 72 | 0.9 | 0.8 | 6.8 | 90 | 11 | Zn-Pb-Cu |
| marshall | 1,210,000 | | 1.6 | 80 | 0.5 | 0.6 | 5.3 | 89 | 9 | Zn-Pb-Cu |
| Zn-Pb-Cu Total | 9,746,000 | 1,624,333 | 2.3 | 92 | 1.3 | 1.0 | 7.3 | 88 | 15 | Zn-Pb-Cu |
| hw-mine | 22,137,000 | | 2.2 | 27 | 2.0 | 0.3 | 3.7 | 93 | 35 | Zn-Cu |
| 43-block | 971,000 | | 2.6 | 53 | 1.7 | 0.5 | 5.8 | 92 | 23 | Zn-Cu |
| trumpeter | 211,000 | | 2.4 | 58 | 3.4 | 0.3 | 3.9 | 93 | 47 | Zn-Cu |
| extension | 1,156,000 | | 1.0 | 29 | 1.4 | 0.3 | 4.5 | 94 | 24 | Zn-Cu |
| battle | 5,965,000 | | 1.4 | 53 | 1.8 | 0.7 | 12.5 | 95 | 13 | Zn-Cu |
| gap | 778,000 | | 2.0 | 121 | 2.0 | 1.0 | 13.8 | 93 | 13 | Zn-Cu |
| Zn-Cu Total | 31,218,000 | 5,203,000 | 2.0 | 35 | 1.9 | 0.4 | 5.7 | 93 | 25 | Zn-Cu |

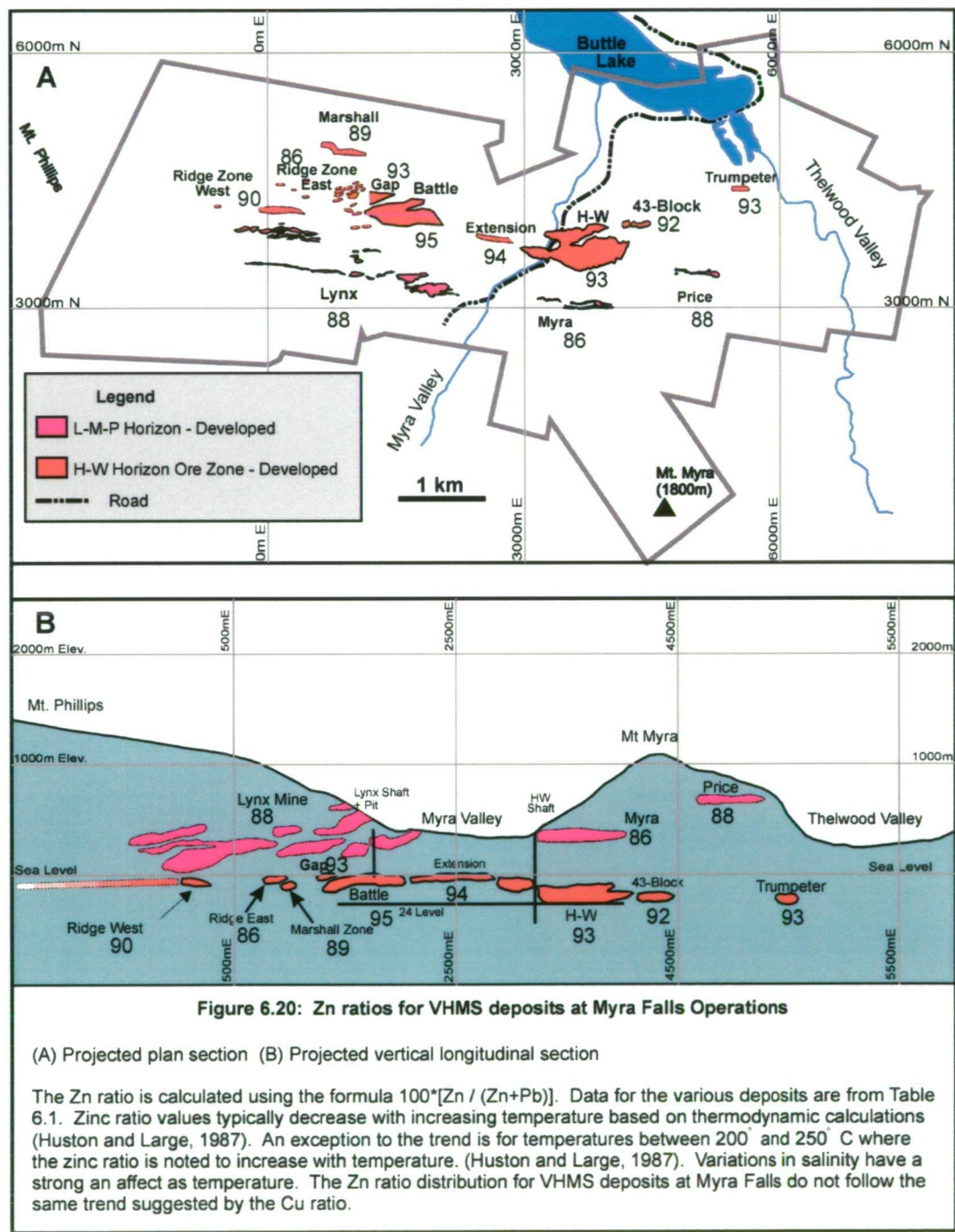
(1) Zn ratio = $100 * (Zn+Pb) / Zn$
 (2) Cu ratio = $100 * (Cu+Zn) / Cu$
 (3) Deposit metal classification after Solomon (1976) and Large (1992)

6.9 Comparison to other Myra Falls deposits

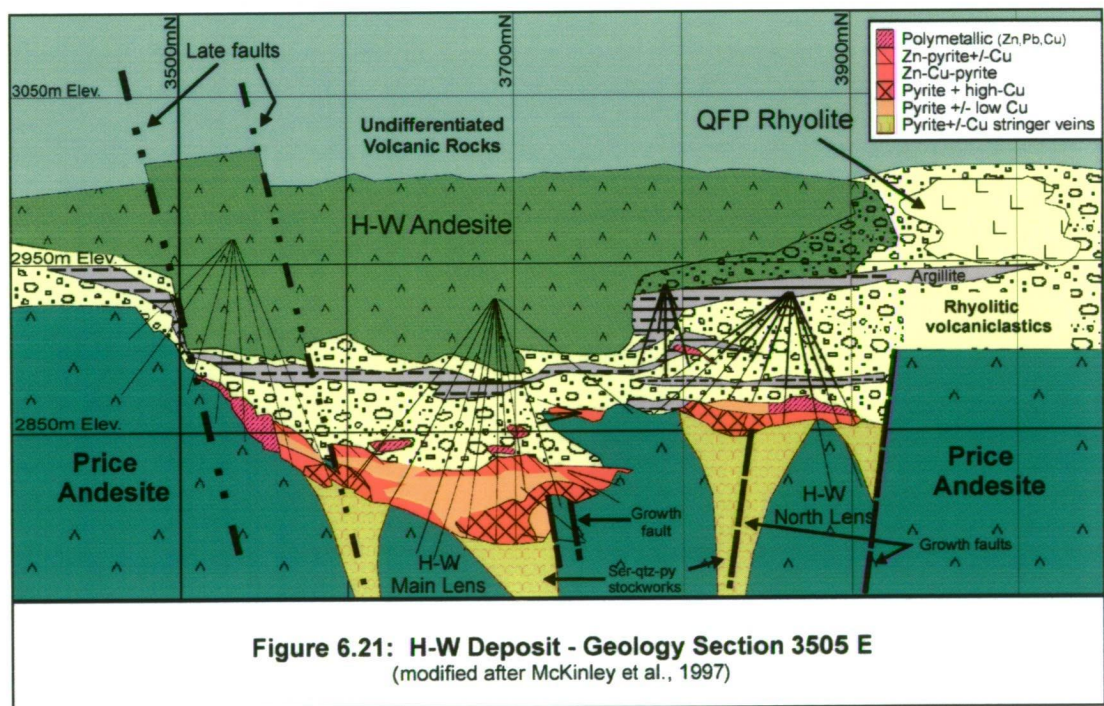
Property-scale metal zoning for the Myra Falls VHMS deposits has been assessed by Gemmell (1998). Copper ratio data suggests that the highest temperature parts of the Myra Falls mineralizing system are located in the Extension-HW-Trumpeter area based on CR values (Fig. 6.19). Gemmell (1998) inferred that fluid movement was from the deep eastern parts of the property to the shallow portions of the district in the west with a large lateral component. Based on pre-mining geological mineral resource estimates, the Ridge Zone West CR of 11 is considered low relative to deposits such as the Trumpeter (CR=47), H-W (CR=35), and Extension Zone (CR=24) (Table 6.2 and Fig. 6.19).



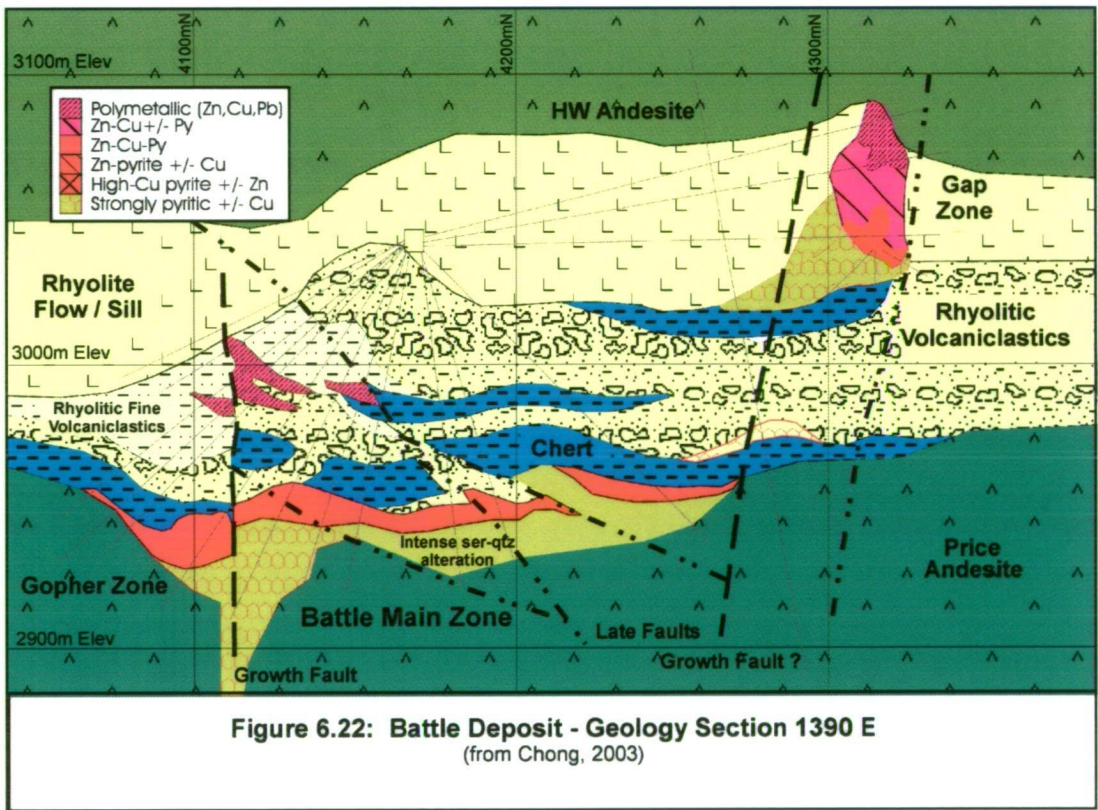
The ZR is > 90 for the Extension, H-W, and Trumpeter deposits and hence elevated relative to other deposits at Myra Falls (Fig. 6.20). The ZR trend expected by the thermodynamic calculations (Huston and Large, 1987) is not consistent with the CR trend. Therefore, more work is required to understand the ZR at Myra Falls. Possible explanations for the ZR values are mineralizing fluids under-saturated in Pb, fluid temperatures within a regime that has a positive relationship with the ZR, and salinity of the mineralizing fluids.



Barrett and Sherlock (1996) describe the metal zoning for the H-W deposit based on N-S sections 3460E and 3940E using surface exploration holes and underground definition holes. Copper grades > 2% are in the lower to middle levels of the thickest part of the orebody with Zn and Ag enrichment in the southern portion of the ore lens and the upper levels of the thick northern portion of the Main lens. Gold is evenly distributed throughout the bulk of the massive sulphide intervals with typical grades of 2 to 4 g/t. Section 3940E has zoning similar to 3460E for Cu, Zn, and Ag. Two Cu-high areas (>2 %) occur in the north and south of the Main lens. Significant Au values (>2 g/t) in section 3940E are generally found in the higher-Cu portions of the orebody. Copper-rich areas also have low Au values. The trends suggest one area of higher-temperature discharge, where the majority of the sulphide tonnage accumulated, followed by a capping phase of Zn-rich (lower temperature) sulphide deposition that extended to the south (Barrett and Sherlock, 1996). McKinley et al. (1997) assessed the mineralogical distribution for the H-W and found similar zoning for the H-W deposit on section 3505E (Fig. 6.21).



The Battle lenses demonstrated typical VHMS metal zoning from Fe and Fe-Cu-rich base through Cu-Zn-rich sulphides to Pb-Zn-Ba-rich tops (McKinley et al., 1997; Sinclair, 2000). An exception to the typical zoning is the Upper Zone lenses located up to 70 m above the Price Formation. The Upper Zone lenses are polymetallic lenses deposited on and within felsic volcanoclastic deposits that in-filled the Battle basin prior to cessation of the mineralizing system (Sinclair, 2000). Metal zoning for the Upper Zones do not have the footwall to hangingwall zonation as for the underlying lenses. Instead, Zn-Pb-Cu-Ba-Au-Ag-As-Hg and Cd are evenly distributed through out the lenses, are underlain by Fe, and have a halo of Ag and As extending into the hangingwall (Sinclair, 2000).



Sinclair (2000) also noted the following observations for the Gap deposit. The Gap deposit has high Au-Ag-Ba-As-Pb values similar to the Upper Zone lenses, but also has a strong mineralogical and metal zonation. The base of the Gap deposit is Fe-rich due to pyrite and grades up through Cu-Fe-rich sulphides to Zn-Cd and Pb-Ba-As-(Hg) enrichment at the top of the lens. The Gap zonation is overprinted by a Cu-Ag-Bi-Mo rich spine that runs up the centre of the lens and corresponds with a bornite-chalcocite assemblage. Gold and Ag values are elevated through out the Gap deposit and correspond to a late electrum-stromeyerite assemblage. The Gap deposit is in a similar stratigraphic position above the Battle Main lenses as the Upper Zone lenses.

Sinclair (2000) used the CR in conjunction with geological mapping, structure, and Fe-enrichment to identify feeder systems for the Battle and Gap deposits. The ZR values ranged between 68 and 97 with the highest values in the Battle and Gopher lenses corresponding with high CR and Fe-enrichment. The Upper Zone lenses have low ZR values with the majority of values between 68 and 92. The ZR values for the Gap deposit decrease in value with increasing distance from the base of the deposit towards the top of the deposit. The observations of ZR trends for the Battle, Gap, and Upper Zone mineralization are inconsistent with the general thermodynamic temperature trends proposed by Huston and Large (1987). Gemmell (1998) reported similar inconsistent trends on a deposit scale. Therefore, more work is required before using the ZR as an exploration tool to infer temperature regimes on a deposit or an individual lens scale at Myra Falls.

The Ridge Zone West has a similar geological setting to the Upper Zones of the Battle deposit area. The Basal Conglomerate is immediate footwall instead of the Price Formation andesite. This interpretation is supported by a lack of typical Cu-Fe metal zoning characteristic of the H-W, Battle, and Gap lenses. Instead, the metal zoning for the Ridge Zone West is similar to the Upper Zones of the Battle deposit area as described by Sinclair (2000). The Ridge Zone West metal zoning is characterized by diffuse, unfocussed Fe-zoning, and the following weak to moderate element associations for Lower lens and Main lens mineralization: Zn-Pb-Ag, Au-Ag+/-Ba, and Zn-Cu. Another piece of evidence supporting the similarity of the Ridge Zone West with the Upper Zones of the Battle deposit area is the CR. The relatively weak CR range and distribution support the lack of an identifiable, significant up-flow zone or higher temperature regime relative to values characterizing the H-W, Trumpeter, and Extension zones. The existence, or non-existence, of a significant hydrothermal feeder up-flow zone is not clear as more detailed information is required.

6.10 Summary and conclusions

The Ridge Zone West is characterized by weak to moderate element associations of Zn-Pb-Ag, Au-Ag+/-Ba, and Zn-Cu. Group 2-Au (> 4 g/t) occurs with the following associations: Ag > 60 g/t, Pb > 0.6%, Zn > 2.0%, Fe > 4.0%, and Cu > 0.6%. Group 2-Ag (>150 g/t) occurs with Ba > 0.3%, Pb > 1.0%, Zn > 8.0%, Fe > 4.0%, and Cu > 1.0%.

The main Au association inferred for the Ridge Zone West is Au-Zn-Pb-Ag. This association is based on the element associations from assay data and the block model. Minerals suggested to have possible associations with Au for the Ridge Zone West include electrum, pyrite, stromeyerite, and tennantite. Further work is required to verify the mineralogical inference based strictly on the literature and previous Au studies at Myra Falls.

The Ridge Zone West lenses are bounded to the north by a reactivated, steep dipping, WNW-ESE trending normal fault. A similar trending fault located to the south is not a bounding fault in the strictest sense. Both the north and south faults have inferences of higher temperature regimes based on the CR. Above average grade Au-Ag+/-Ba blocks are also located proximal to the southern fault inferring a possible structural influence on the mineralization.

A focused up-flow zone of hydrothermal discharge has not been identified as metal zoning patterns for Fe and the Cu ratio are broadly dispersed and unfocussed. Relative warmer temperature regimes are in the vicinity of Lower lens 250E and Main lens 200E based on CR values. Low relative ZR values support the CR trend, but reliability of the ZR for inferring temperature regimes is questionable at Myra Falls.

The Ridge Zone West is similar in geological setting and metal zoning as the Upper Zones of the Battle deposit area. Temperature regime is not considered a significant pathfinder towards economically significant mineralization with greater thicknesses. Instead, sub-seafloor mineralization within a permeable, coarse volcanoclastic horizon and the presence of possible fluid pathway controlling faults are considered to have greater significance towards forming economically significant mineralization for the Ridge Zone West.

Chapter 7 Genesis of the Ridge Zone West VHMS deposit

7.1 Introduction

The chapter begins with characteristics of synvolcanic faults and sub-seafloor replacement compared to observations for the Ridge Zone West. This comparison establishes guidelines for observations and inferences of this study. A genetic model is then presented for the polymetallic Ridge Zone West VHMS deposit. The genetic model is compared and contrasted with models for other deposits at Myra Falls, the Cordilleran Tulsequah Chief VHMS deposit, and the modern analogue Vai Lili hydrothermal vent field, Valu Fa Ridge, of the Lau Basin. The Basal Conglomerate is compared with the footwall rocks of the Cambrian Que River VHMS deposit to highlight its exploration potential for Au-rich stockwork mineralization. In conclusion, the styles of VHMS deposits for the H-W Horizon at Myra Falls are summarized using the genetic model derived by this study and findings by previous workers.

7.2 Structure and synvolcanic faults

Gibson et al. (1999) highlighted five criteria for distinguishing synvolcanic structures:

1. The presence of dykes or apophyses of synvolcanic intrusions;
2. An intensification of discordant hydrothermal alteration and / or abrupt change in alteration type with respect to the volcanic stratigraphy;
3. An abrupt change in unit(s) thickness;
4. Offset of a unit with subsequent units not offset; and
5. Localized deposits of monolithic to heterolithic coarse breccia.

Jones (2001) identified several large-scale synvolcanic faults at the Myra Falls property (Fig. 4.4) based on the following criteria:

1. Rapid changes in paleo-seafloor elevation represented by a reconstruction of the upper contact of the footwall Price Formation andesite;
2. Elevation changes in the younger Thelwood Formation basal contact;
3. Stratigraphic thickness changes in the Myra Formation and H-W Horizon; and
4. Marked facies variation for fine-grained facies rocks and porphyry bodies.

ESE-WNW normal faults in the study area are suggested to have a spatial relationship with mineralization based on the following observations:

- The discordant geometry of the footwall alteration near the faults,

- The spatial distribution of weak disseminated to vein style sulphide mineralization in the footwall Basal Conglomerate and Price Formation andesite near the faults, and
- The inference of warmer temperature regimes based on Cu ratios near the faults.

The observations described above are not considered sufficient evidence to classify the ESE-WNW faults as synvolcanic faults. The only observation from this study that coincides with the above criteria is the limited N-S extent of the argillaceous mudstone inferring a marked facies variation. It is not clear if the Basal Conglomerate qualifies as a localized breccia as its total extent is not known. The lack of evidence can be attributed to insufficient information based on limited diamond drill holes in the area of the faults. Petrography and quantitative mass balance calculation of the alteration is required to fully characterize the intensity, distribution, and type of alteration relative to distance from the faults.

7.3 Sub-seafloor replacement

Doyle and Allen (2003) have outlined five criteria for identifying replacement style mineralization. The criteria are:

1. Mineralized intervals are enclosed within rapidly emplaced volcanic or sedimentary deposits;
2. Relics of the host rocks occur within the mineral deposit;
3. Replacement fronts occur between the mineral deposits and the host rocks;
4. The mineral deposit is discordant to bedding; and
5. Strong hydrothermal alteration continues into the hanging wall without an abrupt break in intensity.

Doyle and Allen (2003) consider criteria 1 to 3 as diagnostic of replacement. Criteria 4 and 5 may suggest replacement but are not alone diagnostic. Criteria 2 can not be applied to clastic ore.

Rapidly deposited fine and coarse-grained volcanoclastic rocks are the host lithofacies for the Main lens mineralization. Semi-massive to massive sulphides contain relic altered clasts. The progression from disseminations to massive textures is interpreted to represent a mineralizing replacement front between the deposit and the host rocks. The deposit as a whole is a series of stacked lenses with some steep dipping veins connecting the various lenses. The steep dip of the Ba-rich and Zn-Pb-Cu rich veins is discordant to bedding.

Siliceous mudstone is located below, above, and lateral to the Main lens mineralization. As discussed in Chapter 3 on alteration, hand sample textures suggest silicification of mudstone and argillaceous mudstone (Fig 5.3b; Lx10-2045, 470m).

Siliceous mudstone is inferred to have formed by silica alteration of mudstone based on quantitative evidence for the Battle deposit chert located 1 km east of the study area (Jones, 2001). Therefore, hydrothermal alteration is suggested to continue into the hangingwall without an abrupt break in intensity.

Based on the above observations and suggestions, sub-seafloor replacement is an acceptable genetic interpretation for the Main lens. The Main lens mineralization meets diagnostic criteria 1 to 4 required for sub-seafloor replacement deposits. Criteria 5 related to hydrothermal alteration needs validation by quantitative characterization using geochemistry and mass balance techniques.

7.4 Ridge Zone West Genetic Model

The geological setting has been separated into three stages composed of the following geological units:

- Stage 1(pre-mineralization): the Price Formation andesite and the Basal Conglomerate,
- Stage 2 (syn-mineralization): the mineralization hosting H-W Horizon, and
- Stage 3 (post-mineralization): the Hangingwall Mafic Complex (HWMC) and Lower Mixed Volcaniclastic unit (LMV).

Stage 2 mineralization is described in the context of a four phase paragenetic sequence as developed in Chapter 5 on mineralization. The paragenetic sequence is:

Stage 2 – phase 1: Lower lens mineralization (disseminated and banded textures)

Stage 2 – phase 2: Main lens mineralization (veins and massive textures)

Stage 2 – phase 3: Upper lens mineralization (disseminated and banded textures)

Stage 2 – phase 4: Upper lens mineralization (vein textures)

7.4.1 Stage 1 (pre-mineralization basin development)

Stage 1 represents the geological setting prior to onset of the mineralizing hydrothermal system. Early rifting formed a series of basins most notably in the Battle and H-W deposit areas (Juras, 1987; Jones, 2001). The Price Formation represents the oldest rocks at Myra Falls and is composed of subaqueous andesitic flows, breccias, and volcanic sediments. The Basal Conglomerate conformably overlies the Price Formation. The Basal Conglomerate is a polymictic cobble conglomerate that is interpreted to have been rapidly deposited. A westerly provenance is inferred based on a decrease in thickness from west to east on section 4150N and its absence east of the study area.

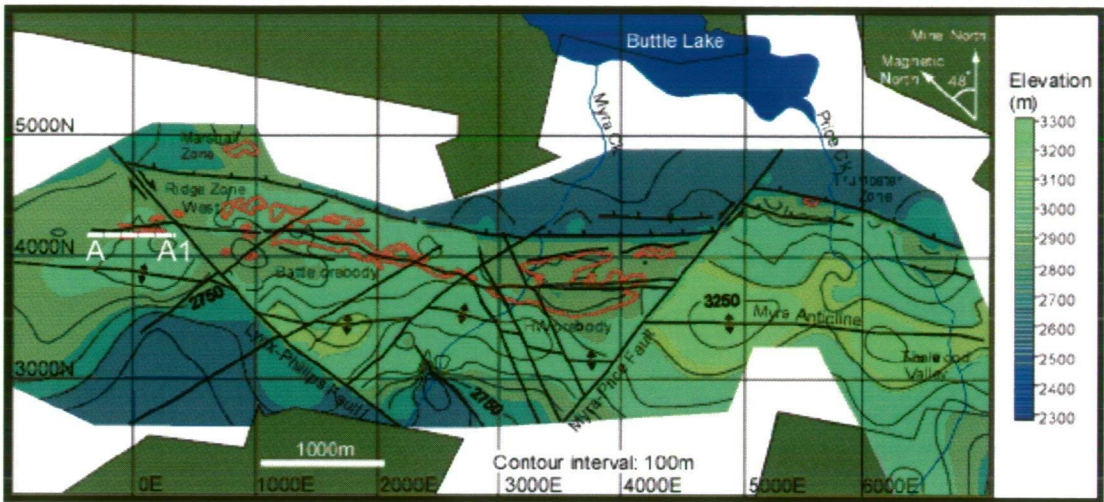


Figure 7.1 a: Ridge Zone West Stage 1: Pre-mineralization – Plan Map
(from Jones, 2001; reprinted with permission)

The plan map illustrates the present day surface contours of the Price Formation andesite (or paleo-seafloor) and shows the effects of deformation. The large topographic high in the centre of the diagram is largely a result of D2 folding forming the Myra Anticline (Jones, 2001), and the large topographic low to the north is due to large down throw on the North Fault. Section 4150 N is highlighted by section A-A1 and will be used to illustrate the genetic model proposed for the Ridge Zone West in Figures 7.1b, 7.2, and 7.3.

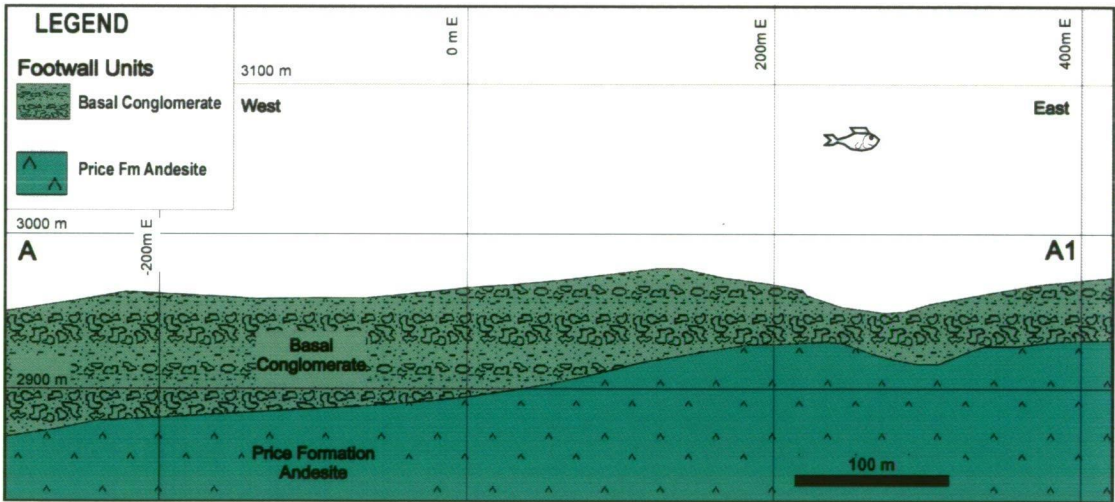


Figure 7.1 b: Ridge Zone West Stage 1: Pre-mineralization
(Longitudinal section 4150m N; view north)

The Basal Conglomerate is a cobble conglomerate that was deposited by high-energy mass flow processes originating from a westerly provenance. In the study area, the upper contact of the Basal Conglomerate is footwall to the Ridge Zone West and the H-W Horizon.

7.4.2 Stage 2 (syn-mineralization)

The late Devonian H-W Horizon (Parrish and McNicoll, 1992; Barrett and Sherlock, 1996) is a sequence of predominantly felsic, coarse to fine-grained volcano-sedimentary rocks that host the Ridge Zone West mineralization. A subordinate paleo-depression is interpreted to have a linear, E-W striking geometry up to approximately 80 m wide based on the spatial distribution of argillaceous mudstone. The interpretation is supported by the Basal Conglomerate having its greatest apparent thickness below the argillaceous mudstone.

A below wave-base, restricted basin setting is inferred from fine-grained mudstones. An unstable, volcanically active environment is inferred based on the occurrence of volcanoclastic deposits containing sulphide clasts intercalated with mudstone, which in places have been silicified and brecciated prior to lithification.

The footwall Price Formation and Basal Conglomerate are altered to the mineral assemblage sericite-quartz+/-chlorite. The alteration is weak and most evident in the upper 30 m in the Price Formation whereas in the Basal Conglomerate, the alteration is pervasive, non-destructive, and of moderate intensity. The alteration assemblage extends to greater depths near ESE-WNW striking normal faults which also appear to be spatially associated with up to 3% pyrite-chalcopyrite+/-sphalerite veins and disseminations.

The H-W Horizon has been altered to a sericite-quartz+/-chlorite mineral assemblage similar to the footwall rocks. It is weak to moderately developed within volcanoclastic rocks. A more intense silicification facies of the sericite-quartz alteration assemblage has apparently altered argillaceous mudstone to a siliceous mudstone below, lateral to, and above the massive sulphide lenses.

The mineralization assessed comprises sulphide lenses, veins and disseminations over a volume measuring approximately 1,000 m E-W, 80 m N-S, and a stratigraphic thickness of up to 70 m. The only primary textures observed are disseminated framboidal pyrite hosted by argillaceous mudstone. Pyrite, sphalerite, chalcopyrite, galena, and tennantite grains have been recrystallized in the sub-seafloor hydrothermal environment and probably by subsequent regional metamorphism. A four phase paragenetic sequence describes the styles of mineralization with respect to time of deposition.

Phase 1 mineralization: Lower lens mineralization is associated with fine-grained facies volcano-sedimentary rocks. It is characterized by disseminated and banded textures exhibiting grain-size gradation, soft-sediment deformation textures, and framboidal pyrite (Figs. 5.2 and 5.7). These textural observations lead to the interpretation of seafloor deposition synchronous with fine-grained facies rocks (Fig. 7.2a).

Phase 2 mineralization:

Main lens mineralization is associated with fine and coarse-grained facies volcanic rocks. Disseminated to massive sulphide textures in fine-grained rocks have contorted shapes and ragged to diffuse contacts with the surrounding argillaceous mudstone. These contact characteristics may have resulted from either synchronous deposition of mineralization and mudstone on the seafloor or by sub-seafloor replacement (Fig. 5.2).

Sphalerite-pyrite-chalcopyrite-galena veins associated with coarse-grained volcanoclastic rocks are inferred as a mineralizing replacement front based on the occurrence of sparse anastomosing veins grading into zones of semi-massive or massive veins with relic clasts (Figs 5.4 and 5.5). Barite-quartz-galena-tennantite-sphalerite rich veins have steep to moderate dip (Fig. 5.5). Emplacement of the barite-rich veins is interpreted as either synchronous with or after sphalerite-pyrite-chalcopyrite-galena rich mineralization. The top contact of Main lens mineralization appears to be within 15 m of banded mudstone interpreted to have formed on the seafloor and is therefore considered a shallow sub-seafloor environment (Fig. 7.2b).

Sphalerite-pyrite rich clasts found in coarse-grained volcanic facies deposits are dominantly subangular with minor subrounded shapes. The inference of a proximal source is based on the subangular form and similar mineralogical assemblage to the surrounding mineralization.

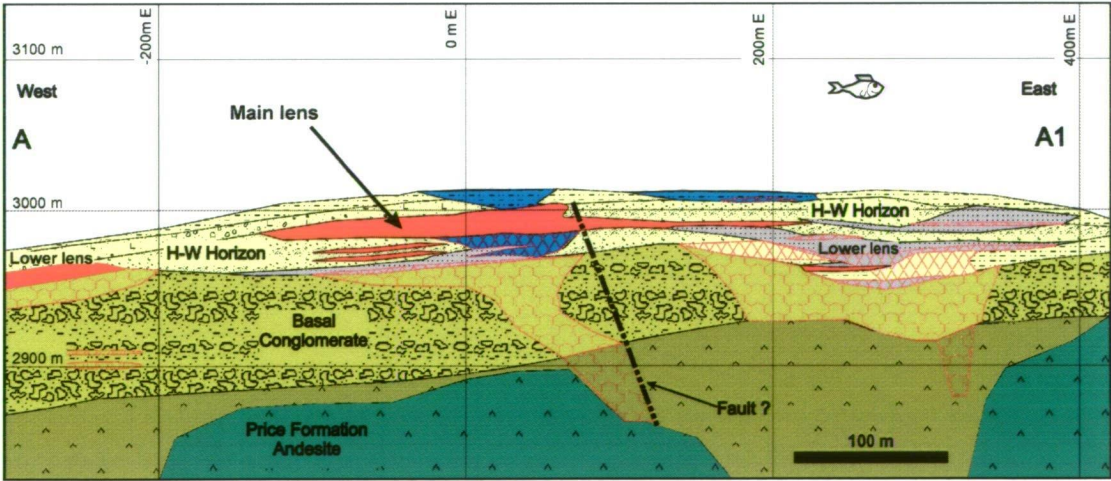
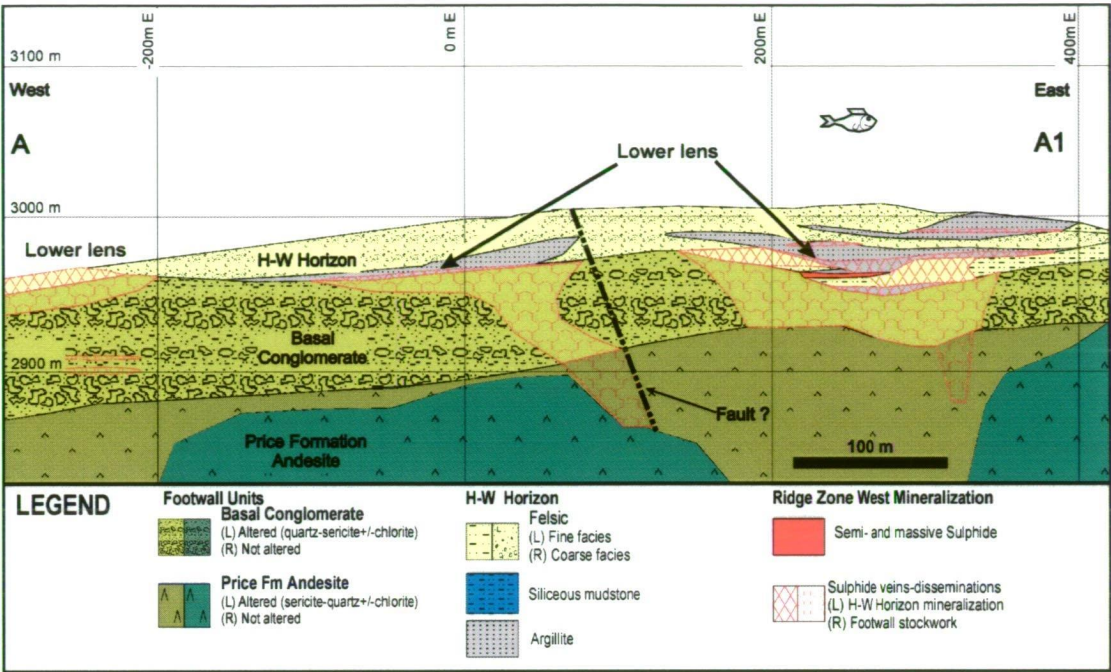
Metal associations include Zn-Pb-Ag, Au-Ag+/-Ba, and Zn-Cu. The main Au association is Au-Zn-Pb-Ag based on statistical inference. Both the northern and southern WNW-ESE faults have inferences of higher temperature regimes based on the Cu ratio (CR). Metal zoning has not identified a significant hydrothermal up-flow zone based on the current information. Instead a weak, unfocussed system is interpreted to characterize the metal distribution for the Ridge Zone West based on CR values (Fig. 6.17).

Phase 3 mineralization: Deposition of argillaceous mudstone and sandstone demonstrates a continuing influx of fine-grained volcano-sedimentary deposits. Upper lens mineralization associated with argillaceous mudstone have disseminated and banded textures. Banded mineralization is interpreted to have formed on the seafloor and displays grain-size gradation, flame structures, and soft-sediment deformation textures. This style of mineralization is a minor component of the overall mineralizing system leading to the inference of intermittent exhalation onto the seafloor in competition with the influx of fine-grained deposits (Fig. 7.2c).

Phase 4 mineralization: Upper lens pyrite-chalcopyrite+/-sphalerite disseminations and veins are hosted by variably silicified mudstone-sandstone bands and breccia. Pyrite-chalcopyrite rich mineralization associated with silicified mudstone-sandstone bands could have been generated by synvolcanic deposition, sub-seafloor replacement along porous sandstone bands, or metamorphic remobilization (Fig. 7.2c).

The pyrite-chalcopyrite+/-sphalerite veins are brittle fracture fillings in silicified mudstone. Geological events that could have caused brittle fracturing and in-situ brecciation are slope instability or slumping, earthquakes triggered by active volcanic processes, or loading by overlying strata. Silicification is suggested to be early based on the occurrence of siliceous mudstone breccia with angular shapes supported by argillaceous mudstone. Sulphide grain recrystallization in the sub-seafloor environment probably occurred during phases 2, 3, and / or 4.

The interpretation of silicification of mudstone and argillaceous mudstone is based on qualitative hand sample observations and inference from quantitative evidence from the Battle deposit hangingwall silicified mudstones (Jones, 2001). Quantitative assessment via petrography and geochemistry is required to verify this interpretation.



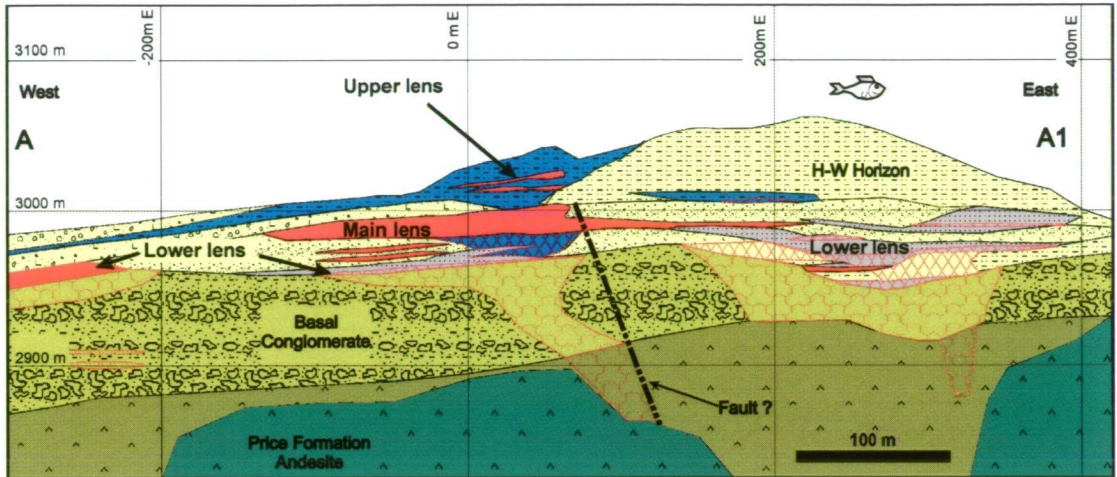


Figure 7.2c: Ridge Zone West Stage 2 – Phase 3 and 4 Upper lens mineralization
(Longitudinal section 4150 N - view north)

H-W Horizon fine-grained facies rocks continue to be deposited into the paleo-depression. Upper lens mineralization occurs as pyrite-chalcopyrite+/-sphalerite bands and veins associated with siliceous mudstone breccia. See Figure 7.2a for the legend.

7.4.3 Stage 3 (post-mineralization)

The H-W Horizon is partially overlain and intruded by the Hangingwall Mafic Complex (HWMC). The HWMC is characterized by the following facies: a massive coherent core surrounded by an autoclastic carapace that grade laterally into polymict, sulphide clast bearing autoclastic breccia and peperite. Peperite textures at the margins of the HWMC demonstrate intrusion and/or deposition as a flow or sill into wet unconsolidated sediments. Hyaloclastite textures and peperite are evidence for a subaqueous setting.

The Lower Mixed Volcaniclastic unit (LMV) overlies or is laterally equivalent to the HWMC. It is dominated by repeated fining upward sequences of pebblestone to sandstone from high and low-density turbidity currents. Minor massive coherent to brecciated andesite flows and / or sills are intercalated with the sediments. Turbidity current deposits are evidence for a subaqueous setting. The unaltered nature of the HWMC and the LMV, and the presence of peperite with sulphide clasts can be used to infer that they were emplaced after the Ridge Zone West hydrothermal mineralizing system had ceased (Fig. 7.3).

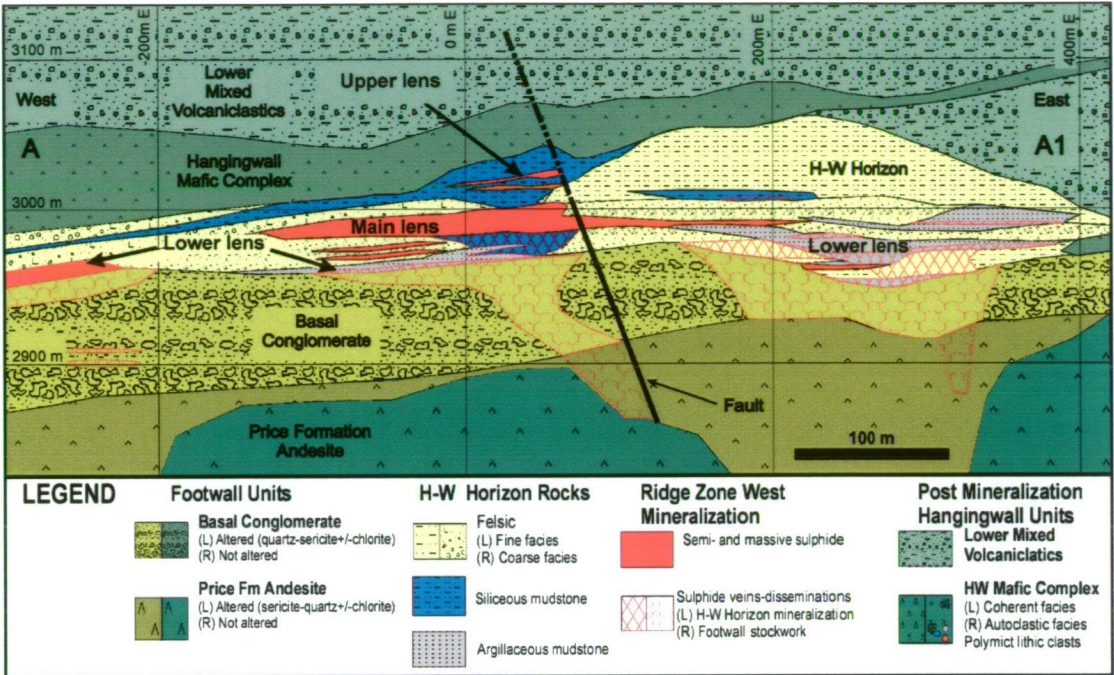


Figure 7.3: Ridge Zone West Genetic Model - Stage 3 - post mineralization
(Longitudinal section 4150 N - view north)

The Hangingwall Mafic Complex (H-WMC) is a flow-sill that thins to the north from cross-section interpretations. The Lower Mixed Volcaniclastic unit is composed of dominantly andesitic, turbidite deposits with graded beds and volcaniclastic breccias.

7.5 Comparison to other VHMS deposits

7.5.1 Comparison to other Myra Falls deposits

Geological Setting: The Ridge Zone West geological setting is unique in some aspects relative to VHMS deposits at Myra Falls while similar in other aspects. The main difference is the occurrence of the Basal Conglomerate. It forms the immediate footwall for the H-W Horizon and is not observed in the Battle and H-W deposit areas. The fragmental nature of the Basal Conglomerate is interpreted to be a significant contributing factor related to the diffuse, pervasive nature of the footwall alteration and possibly the relatively uniform Cu ratio and Zn ratio distribution.

The presence of argillaceous mudstone suggests a restricted basin similar to the Battle and H-W basins (Juras, 1987; Robinson, 1994; Barrett and Sherlock, 1996; Sinclair, 2000; Jones, 2001; this study). The suggested narrow, linear paleo-depression interpreted for the Ridge Zone West is similar to paleo-depression for the Gopher lens located at the southern edge of the Battle deposit. This paleo-depression is approximately 690 m long, 7 to 43 m wide, and up to 35m vertical based on core logging and geological drift mapping by the author during 1996 to 1998.

Mineralization: The Battle and H-W deposits were formed at or near the upper contact of the Price formation andesite. Barrett and Sherlock (1996) and Jones (2001) suggest the H-W deposit was formed as an asymmetric, strongly zoned, pyritic massive sulphide mound deposited on the paleo-seafloor and partially replacing coarse-grained rhyolitic deposits.

Robinson (1994) and Sinclair (2000) interpreted the Battle deposit as a sheet or lens shaped deposit that formed on the paleo-seafloor. Deposit growth was in the shallow sub-seafloor due to metal zone refinement processes (Eldridge et al., 1983; Large, 1992) based on sulphide mineral textures and metal distribution. The metal zoning is characterized by an upward and lateral decrease in Cu and Fe content and an increase in Zn-Pb-Ba-Ag content away from the vent sites (Robinson, 1994; Sinclair, 2000). Jones (2001) interpreted the Battle deposit to have formed primarily by diffuse, lateral fluid flow through a coarse-grained layer of rhyolitic detritus with minor venting onto the seafloor. The lateral flow of hydrothermal fluids during ore formation resulted in only weak footwall alteration away from the main vent zone interpreted to occur at the northern boundary of the Battle Main lens.

Upper Zone lenses above the Battle deposit are suggested to have formed as sub-seafloor replacement deposits within wet, unconsolidated volcanoclastic rocks of the H-W Horizon beneath an altered quartz-feldspar porphyritic flow-dome complex (Robinson, 1994; Sinclair, 2000). Lead-As-Ag-Ba rich mineralization precipitated due to mixing with seawater (Sinclair, 2000). Barite is interpreted to be more abundant due to the increase in oxidation state created by the mixing with seawater (Sinclair, 2000). The metal zoning within the Upper Zones above the Battle Main lens is characterized by Cu depletion, Pb-As-Ag-Au-Ba enrichment, and relatively uniform Zn ratio and Cu ratios.

The Ridge Zone West mineralization is unique relative to other VHMS deposits at Myra Falls based on textures that display progressive replacement of a coarse-grained volcanoclastic horizon by polymetallic, Zn-rich mineralization. However, the styles of mineralization in the Ridge Zone West are not unique at Myra Falls. Sub-seafloor replacement is suggested for the Battle and parts of the H-W deposit (Jones, 2001). Zn-Pb-Ag-Cu-As-Ba rich mineralization of the Ridge Zone West is similar to Upper Zone mineralization of the Battle and H-W deposits as well as the polymetallic south fringe of the H-W Main lens. The relatively uniform Zn ratio and Cu ratio distributions in the Ridge Zone West are similar to those of the Battle deposit Upper Zones (Sinclair, 2000). And lastly, the unfocussed nature of the footwall alteration and disseminated stockwork mineralization is similar to the stockwork mineralization in Upper Zones above the Battle Main lens.

7.5.2 Canadian Cordillera comparison – Tulsequah Chief

The geological information and interpretations of the Tulsequah Chief deposit are from Sebert and Barrett (1996) unless noted otherwise. The Carboniferous Tulsequah Chief polymetallic massive sulphide deposit occurs in the felsic portion of a bimodal volcanic sequence that is in the western part of the Stikine terrane, northwestern British Columbia. Ore reserves were estimated at 8.8 Mt of 1.3 % Cu, 1.2 % Pb, 6.4 % Zn, 2.4 g/t Au, and 99 g/t Ag (The Northern Miner, March 1996). Basaltic to basaltic andesite flows and breccias form the footwall of the deposit and are strongly altered to sericite and crosscut by quartz-pyrite stringers to > 100m below the lenses.

The mineralization occurs in a series of stacked sulfide-rich lenses hosted by sericite-quartz altered felsic volcanoclastic rocks and local flows situated in the lower part of the volcanic pile. The mineralized interval is overlain by relatively unaltered massive rhyolite flows and breccias. The ore lenses consist of varying proportions of disseminated to banded sulfides, which include pyrite, sphalerite, galena, and chalcopyrite are interstratified and mixed with altered volcanic debris, which also contains sulfide and barite fragments. High precious metal concentrations occur in veinlets of chalcopyrite, tetrahedrite, sphalerite, and galena.

Two post-ore faults may have followed pre-existing seafloor faults that focused hydrothermal fluids responsible for the sericite alteration and intense quartz-sulfide stringer mineralization in the footwall of the deposit. The elongate morphology of the main ore lens and the presence of sulphide-clast bearing mass flows cover a portion of the ore lenses implying that sulfide deposition took place in an elongate, localized paleo-depression or graben during the accumulation of felsic volcanoclastic debris. Sulphide clasts and volcanic debris in the sulphide lenses suggest reworking by mass flows and slumping into the paleo-depression was an important depositional process. The preservation of finely banded layers of sphalerite and rare graded beds of pyrite laminations suggest that exhalation on the seafloor occurred locally. In addition, some of the sulfide-rich intervals within felsic volcanoclastic intervals may have replaced highly permeable felsic debris close to the seafloor. Copper and precious metal rich veinlets crosscut the ore sheets and represent an ongoing later phase of hydrothermal activity.

The Tulsequah Chief deposit is similar to the Ridge Zone West deposit with respect to metal content, geological environment, and mineralizing process. The similarities include:

- A mafic footwall basement,
- The environment of deposition is an elongate, localized paleo-depression,
- Coarse-grained debris flow deposits,
- Sulphide clasts entrained with the debris flow deposits,
- Mineralization occurs near the bottom of the volcanic pile,
- Stacked sulphide lenses interstratified and mixed with altered volcanic debris,
- Seafloor deposition of exhalative sulphides,
- Sub-seafloor replacement within highly permeable felsic debris close to the seafloor, and
- It is a polymetallic Zn-Pb-Cu-Au-Ag rich VHMS deposit.

Based on the above description and comparison, the Tulsequah Chief is a Cordilleran VHMS deposit with numerous geological features very similar to the Ridge Zone West deposit.

7.5.3 Modern analogue – Lau basin (Vai Lili)

Barrett and Sherlock (1996) suggest the mafic rocks in the vicinity of the H-W deposit at Myra Falls are “transitional” from tholeiitic to “mildly calc-alkaline” based on whole rock and rare earth element chemistry with specific reference to island arc or early back-arc volcanism. The Lau Basin is located in the south-west Pacific near the island of Fiji (22°20'S, 176°40'W) and represents a modern back-arc basin measuring 2 to 5 km wide and approximately 150 km long (Fouquet et al., 1993). Three major hydrothermal fields on the Valu Fa Ridge (Hine Hina, Vai Lili, and White Church) have been identified including nine occurrences that are enriched in Ba, Zn, As, Pb, Ag, Au and Hg relative to midocean ridges (Fouquet, et al., 1993). Vai Lili is located at approximately 1,720 to 1,740m depth below sea-level and measures 100m by 400m. Volcanic mounds are up to 60 m high. Black smokers are 2 to 5 m high at a 15m high fault scarp and discharge fluids up to 342° C. White smokers are up to 15 m high and are located at the base and top of a fault. Hydrothermal fluids at Vai Lili are interpreted to migrate up normal faults through lavas and volcanoclastic rocks to the seafloor (Fouquet, et al., 1993). Sulphides are precipitated within volcanoclastic rocks and as chimneys on the seafloor (Fouquet et al., 1993; Gemmell, 1995).

Some characteristics of the fluids include no evidence for a magmatic fluid contribution, low pH (2), and low concentration of H₂S attributed to subsea-floor sulphide

formation (Fouquet, et al., 1993). For one white smoker at the Vai Lili vent field, gold was rapidly precipitated at about 230°C with gold contents averaging 30 ppm Au in a central sphalerite-rich zone, but decreased sharply to less than 0.02 ppm Au in a gold-depleted, barite-rich margin based on fluid inclusions in sphalerite and barite (Herzig et al., 1993). Freezing measurements indicate fluid salinities close to that of ambient seawater (5 wt% NaCl equiv). Gold is suggested to precipitate from aqueous sulfur complexes $[\text{Au}(\text{HS})^2]$ as a result of the combined effects of conductive cooling, mixing with seawater, and oxidation of H_2S (Herzig et al., 1993).

The modern analogue Vai Lili hydrothermal field has the following similarities to the Ridge Zone West:

- An inferred back arc setting;
- Aerial extent;
- Seafloor deposition analogous to the Lower lens and parts of the Upper lens;
- Sub-seafloor replacement of volcanoclastic rocks analogous to the Main lens, and
- It is enriched in Zn-Pb-Au-As and -Ba.

7.5.4 Cambrian comparison - Que River: Gold enriched footwall stringer mineralization compared to the Ridge Zone West Basal Conglomerate

The Que River deposit is a small 3.3 M tonne, high grade polymetallic VHMS deposit hosted by Cambrian volcanic rocks and volcanoclastic sediments of the Mount Read Volcanics, Tasmania. Massive ore at Que River is interpreted to immediately overlie strongly silicified, sericitized, and pyritic andesite volcanoclastic rocks (Large et al., 1988). The orebody is surrounded by an extensive zone of low-grade stringer vein and disseminated mineralization. The stringer zone formed during hydrothermal alteration of the stratigraphic footwall. The hydrothermal alteration mineral assemblage is sericite-silica-pyrite+/-base metal sulphides+/-potash feldspar. The entire stringer zone is crudely zoned with a Cu-bearing core (Large et al., 1988) beneath the central part of the massive orebody surrounded by a Pb-Zn bearing stringer mineralization that merges with a distal Pb-Zn-Ag-Au-As-Sb-Ba stringer mineralization in the gold-enriched zone (McGoldrick and Large, 1992).

McGoldrick and Large (1992) characterize the gold mineralization as follows:

- Part of the stringer zone has elevated Au (up to about 5 ppm), Sb (up to 1,000 ppm) and Ba (up to 2,000 ppm) values.
- Much of the gold-enriched stringer zone occurs in a coarse polymictic volcanoclastic rock containing distinctive millimeter-size patches of cream-white alteration containing intergrowths of white mica and base metal sulphide.
- The gold-enriched zone is also characterized by the presence of solid inclusion-rich potash feldspar not observed elsewhere in the stringer zone.

McGoldrick and Large (1992) interpret the gold-enriched stringer zone to be the more distal part of the footwall alteration zone developed during formation of the main Que River massive sulphide orebody. The best development of this distal gold-bearing stringer mineralization occurred in permeable coarse-grained volcanoclastic rocks. The Au was transported as a bisulphide complex and precipitated in the outer portions of the stringer system where fluids were oxidized and cooled during mixing with seawater (McGoldrick and Large, 1992).

Similarities between Que River and the footwall Basal Conglomerate include:

- A polymictic volcanoclastic footwall sequence;
- The hydrothermal alteration mineral assemblage is sericite-silica-pyrite+/-base metal sulphides.

The intensity of alteration is a notable difference between the Que River footwall sequence and the Basal Conglomerate. At Que River, the footwall hydrothermal alteration is described as strong and has a mineral assemblage including potash feldspar. Hydrothermal alteration in the Basal Conglomerate is not considered strong as textures are preserved. Potash feldspar has not been observed in the Basal Conglomerate. Also of note is that metal zonation of footwall stockwork mineralization for the Ridge Zone West and other deposits at Myra Falls have not been previously assessed. Therefore, an opportunity exists for another style of mineralization in the footwall Basal Conglomerate that may be of economic significance.

7.6 Summary of VHMS deposits for the H-W Horizon at Myra Falls

Many other deposits have been classified as sub-seafloor replacement style deposits. Doyle and Allen (2003) recognized 12 styles of VHMS mineralization, including sub-seafloor replacement, in a variety of volcanic settings based on VHMS deposits in Canada, Australia, Sweden, Japan, Spain, and Portugal. The styles and settings are based on variation in ore deposit geometry textures, distribution of alteration assemblage, and the facies associations of the host succession. A continuum between the different styles and settings highlighted is acknowledged to exist.

Using the main settings and styles of VHMS mineralization described by Doyle and Allen (2003), the Ridge Zone West Lower lens and parts of the Upper lens are interpreted as seafloor deposits. The Ridge Zone West Main lens is interpreted as a sub-seafloor replacement deposit in lithic volcanoclastic rocks. Other examples of sub-seafloor replacement VHMS deposits in lithic volcanoclastic rocks cited by Doyle and Allen (2003) that are apparently comparable to the Ridge Zone West Main lens include Petiknäs North (Allen et al., 1996), Matsuki (Kuroda, 1983), and parts of Rosebery (Allen, 1994a). These deposits are only mentioned as additional examples of sub-seafloor replacement deposits but will not be elaborated. The Ridge Zone West and other deposits for the H-W Horizon at Myra Falls have been listed using the main settings and styles of VHMS mineralization outlined by Doyle and Allen (2003) in Table 7.1. Based on Table 7.1, the H-W Horizon at Myra Falls has several different settings and styles of VHMS mineralization of which the Ridge Zone West is a subset.

| Table 7.1: Styles of VHMS deposits compared to H-W Horizon deposits at Myra Falls (Setting and style classifications modified after Doyle and Allen, 2003) | | | |
|--|--|--|-------------------------------|
| Setting | Style | Myra Falls | Source |
| Seafloor | Mound | H-W Main lens; H-W North lens | RW, SJ1, CP, B-S |
| | Clastic apron-Depression fill | 43-Block | consensus (MFO geology dept) |
| | Sheet | RZW-Upper + Lower lenses (?) Battle; parts of H-W Main lens | AC MR, BJS |
| Seafloor (modified after burial) | Burial by lavas | OCBX (RZW, Battle, H-W, 43-Block?) | RW, SJ2, CP, B-S, MR, BJS, AC |
| | Burial by clastic deposits | 43-Block? | |
| Sub-seafloor Replacement | Replacement in pumiceous deposits | | |
| | Lithic volcanoclastic rocks (3 different scenarios) | RZW; Battle; UZ (Battle; H-W) 43-Block(?) | SJ2, BJS, AC |
| | Volcanoclastic rocks (below lavas or intrusions) | UZ (Battle; H-W) OCBX (RZW, Battle, H-W) | MR, BJS, B-S, AC |
| | Replacement in lavas and intrusions | Gap | BJS |
| | Replacement within limestone | | |
| ABBREVIATIONS: OCBX - ore clast breccia; RZW - Ridge Zone West; UZ - Upper Zone; AC - this study; BJS - Sinclair (2000) B-S - Barrett and Sherlock (1996); CP - Pearson (1997); MR - Robinson (1994); RW Walker (1985); SJ1 - Juras (1987); SJ2 - Jones (2001) | | | |

8.1 Introduction

This chapter summarizes the key findings of the study. Recommendations are proposed for future work related to ore reserves and exploration peripheral to the study area. Future mining, milling, and metallurgical issues of the Ridge Zone West are also discussed.

8.2 Summary

8.2.1 Geological Setting

The following summary on the geological setting is from Chapter 3 on geology of the Ridge Zone West and Chapter 7 on the genesis.

- Mine sequence geology in the study area from oldest to youngest is the Price Formation and the Myra Formation. The Ridge Zone West is hosted by the late Devonian H-W Horizon of the Myra Formation. The main stratigraphic units from footwall to hangingwall include:
 - Price Formation andesite,
 - Basal Conglomerate,
 - Massive sulphide hosting H-W Horizon volcano-sedimentary rocks,
 - Hangingwall Mafic Complex (HWMC), and
 - Lower Mixed Volcaniclastic unit.
- The deposit formed in a narrow, linear subordinate paleo-depression in a subaqueous below wave-base setting.
- The Basal Conglomerate is the immediate footwall to the H-W Horizon and the Ridge Zone West lenses. The Basal Conglomerate does not occur in the Battle and H-W deposit areas.

8.2.2 Hydrothermal Alteration

A brief discussion on the alteration mineralogy and distribution is included in Chapter 3. The key points from this study are:

- The Price Formation, the Basal Conglomerate, and the H-W Horizon have been variably altered to sericite-quartz+/-chlorite.
- The footwall alteration is semi-conformable to the Basal Conglomerate and extends down to approximately 30 m below the upper contact of the Price Formation. It is texturally non-destructive.

- Alteration extends to greater depths near ESE-WNW striking normal faults which also appear to be spatially associated with pyrite-chalcopyrite+/-sphalerite veins and disseminations.
- There is extensive silicification of the mudstone based on the following observations:
 - The siliceous sediments occur at the same stratigraphic position as argillaceous mudstones.
 - The siliceous sediments occur at varying elevations within the stratigraphic sequence proximal and coincident with sulphide mineralization.
 - Gradational silica alteration fronts occur between siliceous mudstone (chert) and argillite.
 - Silicification of the Battle chert approximately 1 km east of the study area was demonstrated by Jones (2001).

8.2.3 Structural geology

The geological structures for the Ridge Zone West are discussed in Chapter 4. The possibility of synvolcanic faults is briefly discussed in Chapter 7. The main findings are:

- The structures are post-mineralization.
- Three phases of deformation are interpreted and explained in the context of the Myra Falls structural model developed by Berry (2000) and Jones (2001):
 - D1: a weak WNW-ESE (mine grid) striking foliation related to a ductile Paleozoic folding event.
 - D3: Mesozoic D3a strike-slip faults and infrequent D3b shallow dipping thrust faults.
 - D4: Mesozoic normal faults with localized reactivation of strike-slip structures probably related to D3.
- No apparent folding is observed for the Ridge Zone West area.
- Strike-slip and dip-slip faults are common for the Ridge Zone West area. The most significant faults are a series of ESE-WNW trending, steep dipping normal faults located north of the Ridge Zone West mineralization.
- The ESE-WNW striking fault systems are suggested to have a possible genetic relationship with the mineralizing system based on the following:
 - spatial association with the Zn-rich mineralization,
 - footwall alteration having an apparent discordant geometry near the faults, and
 - Cu ratio metal zoning patterns near the faults suggest warmer temperature regimes.But, these observations are not sufficient to classify the faults as synvolcanic based on criteria outlined by Gibson (1999) and Jones (2001).

8.2.4 Mineralization

The ore body mineralization is discussed in Chapter 5. Key points of interest are:

- The mineralization comprises stacked sulphide lenses, veins and disseminations over an area measuring approximately 1,000 m E-W, 450 m N-S, and a stratigraphic thickness of up to 70 m. The study is focused on mineralization with a limited 80 m N-S extent due to availability of drill core.
- Three styles of polymetallic Zn-rich mineralization occur at varying stratigraphic elevations. The three styles are:
 - Banded polymetallic sphalerite-pyrite+/-chalcopyrite+/-galena mineralization associated with argillaceous mudstone and siliceous mudstone,
 - Disseminations and weak to massive veins of sphalerite-pyrite-galena-chalcopyrite+/-barite hosted by fine and coarse-grained facies volcanoclastic rocks,
 - Pyrite-chalcopyrite rich disseminations and veins associated with siliceous mudstone breccia.
- The only primary texture preserved is framboidal pyrite found in argillaceous mudstone.
- Sulphide mineral paragenesis is not resolved due to recrystallization overprinting most primary textures.
- The average chemical formulas for sulphide and ore related gangue minerals based on microprobe analyses are listed in Table 8.1.
- Tennantite is the main residency for silver in the sulphide grains assessed (Table 8.1).
- Gold was not observed in thin section.

| Table 8.1: Summary of averaged microprobe analyses for Ridge Zone West ore minerals | | | | |
|---|---|--------------|---|-------------|
| Mineral | Chemical Formula | Total points | Substitutions | Inclusions |
| Pyrite | Py-1 and Py-2: $\text{Fe}_{1.03}\text{S}_2$ Py-3: $\text{Fe}_{1.02}\text{S}_2$ | 23 | | |
| Sphalerite | $(\text{Zn}_{0.98}\text{Fe}_{0.02})\text{S}$ | 21 | 0.3 wt% Cd 0.14 wt% Mn | 0.22 wt% Cu |
| Chalcopyrite | $\text{Cu}_{1.00}\text{Fe}_{1.01}\text{S}_2$ | 18 | | 0.39 wt% Zn |
| Galena | $\text{Pb}_{1.06}\text{S}$ | 17 | 0.34 wt% Se | 0.82 wt% Fe |
| Tetrahedrite-tennantite | $(\text{Cu}_{0.9}\text{Ag}_{0.2})(\text{Zn}_{1.4}\text{Fe}_{0.6})(\text{Sb}_{0.7}\text{As}_{3.3})\text{S}_{13}$ | 5 | 1.45 wt% Ag 0.14 wt% Se | |
| Barite | $\text{Ba}_{1.03}\text{Sr}_{0.01}\text{S}_{0.99}\text{O}_4$ | 9 | 0.13 wt% SrO | |
| Muscovite | $(\text{K}_{0.89}\text{Na}_{0.04}\text{Ba}_{0.06})(\text{Al}_{1.82}\text{Mg}_{0.18}\text{Fe}_{0.02})(\text{Al}_{0.87}\text{Si}_{3.13}\text{O}_{10})(\text{OH})_2$ | 8 | 2.11 wt% Ba 1.74 wt% Mg 0.28 wt% Na | |

8.2.5 Metal Zoning

The metal zoning for the Ridge Zone West is discussed in Chapter 6.

- Metal associations based on statistical analyses of assay data include Zn-Pb-Ag, Au-Ag+/-Ba, and Zn-Cu.
- The main Au association is Au-Zn-Pb-Ag.
- Group 2-Au (> 4 g/t) occurs with the following associations: Ag > 60 g/t, Pb > 0.6%, Zn > 2.0%, Fe > 4.0%, and Cu > 0.6%.
- Group 2-Ag (>150 g/t) occurs with Ba > 0.3%, Pb > 1.0%, Zn > 8.0%, Fe > 4.0%, and Cu > 1.0%.
- WNW-ESE faults near or within the Main lens have a spatial correlation with higher temperature alteration zones based on the Cu ratio (CR).
- The Ridge Zone West has relatively consistent CR and Zinc ratio (ZR) values
- A focused up-flow zone of hydrothermal discharge has not been identified as metal zoning patterns for Fe and the Cu ratio are broadly dispersed and unfocussed.
- Higher relative temperature regimes in the eastern part of the study area are based on CR values.

8.2.6 Main lens evidence for sub-seafloor replacement

Observations suggesting sub-seafloor replacement for the Ridge Zone West Main lens have been discussed in Chapter 3 and Chapter 5. The criteria and evidence for identifying the Ridge Zone West Main lens as a sub-seafloor replacement deposit is discussed in Chapter 7 on deposit genesis. Sub-seafloor replacement is identified as an acceptable genetic interpretation for the Main lens as it meets most of the criteria outlined by Doyle and Allen (2003). The main observations identifying sub-seafloor replacement are:

- Rapidly deposited fine and coarse-grained volcanoclastic rocks are the host lithofacies for the Main lens mineralization.
- Semi-massive to massive sulphides contain relic altered clasts.
- The progression from disseminations to massive textures is interpreted to represent a mineralizing replacement front between the deposit and the host rocks.
- Stacked lenses are connected by steep dipping veins discordant to bedding.
- Siliceous mudstone is located below, above, and lateral to the Main lens mineralization and is suggested to be related to hydrothermal silica alteration based on hand sample textures and quantitative evidence for the Battle deposit chert (Jones, 2001). These observations lead to the interpretation that hydrothermal alteration is continuous from the footwall into the hangingwall without an abrupt break in intensity.

8.2.7 Ridge Zone West Genetic Model

The Ridge Zone West genetic model is discussed in Chapter 7. The geological setting has been separated into three stages based on timing relative to the polymetallic Zn-rich mineralization of the Ridge Zone West. The stages are:

- 1. Pre-mineralization
- 2. Syn-mineralization, and
- 3. Post-mineralization

Setting and style of deposition is described in the context of a four phase paragenetic sequence. The genetic model is summarized in Table 8.2.

| Table 8.2: Summary of the Ridge Zone West Genetic Model | | | | |
|--|---|-------|---|--|
| Stage | Geologic Units | Phase | Setting | Sulphide Textures |
| 1 | Footwall Units | | Andesitic basin development | Disseminations and stockwork veins |
| | Price Formation | | | |
| | Basal Conglomerate | | Onset of basin infill with mass flow deposit(s) | Disseminations and stockwork veins |
| 2 | Ore Horizon | | | |
| | H-W Horizon | | Felsic volcano-sedimentary deposition | |
| | RZW - Lower lens (F) | 1 | Seafloor | Disseminations, bands |
| | RZW - Main lens (F and C) | 2 | Sub-seafloor | Veins to massive sulphide |
| | RZW - Upper lens (F pre-lithification) | 3 | Seafloor | Disseminations, bands, graded sulphide grains, SSD |
| | RZW - Upper lens (F post-lithification) | 4 | Replacement / remobilization | Veins and bands |
| 3 | Hangingwall Units | | | |
| | Hangingwall Mafic Complex | | Intrusion and or extrusion | Entrained sulphide clasts |
| | Lower Mixed Volcaniclastic unit | | Volcano-sedimentary deposition | |
| Abbreviations: RZW- Ridge Zone West; F- Fine-grained facies rocks; C- Coarse-grained facies volcanic rocks SSD- soft sediment deformation | | | | |

8.3 Recommendations

8.3.1 Exploration Applications

The following are some ideas for future exploration at Myra Falls based on findings of this study.

Geological setting:

- The geological setting of the Ridge Zone West illustrates how narrow, elongate paleo-depressions are capable of hosting significant, polymetallic, Zn-rich mineralization.
- The identification of sub-seafloor replacement deposits hosted by fine and coarse-grained volcanoclastic horizons within the H-W Horizon highlights the relevance of volcanic facies mapping and sound geological interpretations to future exploration.

Alteration:

- Weak to moderate texturally non-destructive sericite-quartz \pm -chlorite alteration within fragmental rocks are proximal indicators of Zn-rich polymetallic mineralization having economically viable grades and a geometry amenable to mining.
- Siliceous mudstone, or chert, can be located in the stratigraphic footwall or hangingwall to significant mineralization.
- Metal zonation and alteration mapping of volcanoclastic footwall rocks with low-grade stockwork stringer mineralization is recommended as it may provide a vector towards Au-rich mineralization as discussed in Chapter 7 in a comparison with the Que River volcanoclastic footwall rocks.

Mineralization and trace element geochemistry:

- Fine-grained disseminations and veins of pyrite-sphalerite-chalcopyrite \pm -galena in argillaceous or siliceous mudstone suggests that mapping of the disseminations and veins and / or trace element geochemistry using the elements Zn-Pb-Cu-Fe-Cd are valid exploration tools for identifying proximal settings to mineralization. This inference supports the findings of Jones (2001).
- Microprobe analyses of muscovite from the Main lens host rocks have up to 2.11 wt % Ba substituting for potassium in the crystal structure (Tables 5.9 and 8.1). Microprobe analyses on tetrahedrite-tennantite grains determined the predominant mineral is the As-rich end member tennantite (Tables 5.8 and 8.1). Therefore, future geochemical analyses incorporating barium and arsenic are also potentially useful indicators for identifying settings proximal to mineralization.

Metal zoning:

- The Ridge Zone West is characterized by weak to moderate elemental associations of Zn-Pb-Ag, Au-Ag+/-Ba, and Zn-Cu.
- The Fe, Cu ratio, and Zn ratio for the Ridge Zone West have relatively narrow ranges of values and unfocussed distribution. Based on thermodynamic calculations by Huston and Large (1987), decreasing Zn ratio values are generally associated with an increase in temperature for hydrothermal fluids saturated in Zn and Pb. The Myra Falls deposits do not follow this general trend of decreasing Zn ratio values with increasing temperatures for the hydrothermal fluids. The Cu ratio values appear to be consistent with the convention of increasing Cu ratio values with increasing temperatures for the hydrothermal fluids as established by Knuckey et al. (1982). The application of metal ratios at Myra Falls is still in the initial stages and requires more effort towards understanding its significance.

8.3.2 Ore Reserves

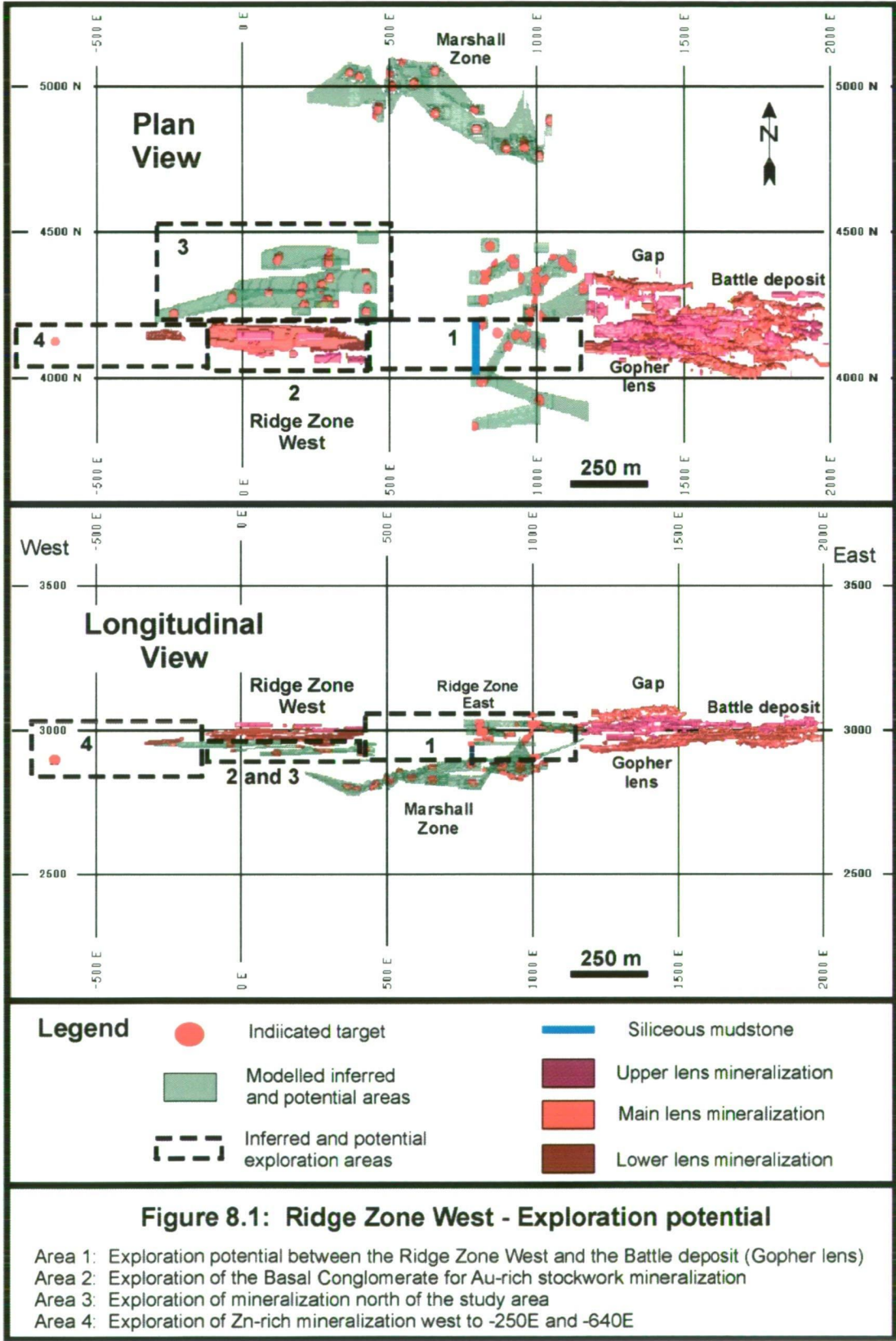
Sub-seafloor replacement style mineralization hosted by fine and coarse-grained volcanoclastic rocks is the most economically significant polymetallic Zn-rich mineralization for the Ridge Zone West. This style of mineralization is described in Stage 2-phase 3 of the genetic model. A Compass-Minesite geological model has been completed as part of this study for ore reserve estimation and mine development purposes. Future definition scale diamond drilling is required to upgrade mineral resources and enhance mining reserves.

Indicated category (30 m spaced drill information):

The mineral resources in this category represent the main focus of this study. Current diamond drill information is on N-S sections spaced up to approximately 100 m apart. Drill hole intersections in the Ridge Zone West Main lens on sections -50E and 50E are spaced up to 30 m apart. Definition scale diamond drilling is recommended on a 15 m grid pattern in accordance with current ore reserve standards at Myra Falls. This program will serve to improve the current interpretation of the geological model and upgrade current indicated resources to the measured category.

Inferred and Potential targets (30 to 45 m and > 45 m spaced drill information respectively): These targets are not reported in the January 2004 geological inventory or the mining reserve for Myra Falls (Chong and Bakker, 2004). The inferred and potential mineralized areas are based on geological extrapolation and represent areas that require further investigation for their economic potential.

Four areas peripheral to the main focus of this study deserve attention based on significant Zn-rich intersections and alteration. These areas are located east, below, north, and west of the main Ridge Zone West mineralization (Fig. 8.1).



Zn-rich intersections and a siliceous mudstone intersection in the vicinity of the study area are listed in Table 8.3.

| Table 8.3: Selected Ridge Zone West Exploration Targets (Area 3 - North intersections are based on > 10.0% Zn or > 3.0 m intersection) | | | | | | | | | |
|---|----------------------------|-----------------------------|-------------------------|-------------------------|-----------------------|-----------------------|-----------------------|-----------------------|-----------------------|
| Area Drill hole | Section m | Interval m | Au g/t | Ag g/t | Cu % | Pb % | Zn % | Ba % | Fe % |
| Area 1-East | | | Siliceous mudstone | | | | | | |
| Lx15-0429 | 785E | 47.9 | | | | | | | |
| Lx15-0349 | 860E | 16.7 | 1.4 | 24 | 0.5 | 0.1 | 5.4 | 0.1 | 2.3 |
| Area 2-North | | | | | | | | | |
| Lx10-1042 | -40E | 3.0 | 0.0 | 22 | 0.5 | 1.2 | 5.4 | 0.3 | 6.3 |
| Lx14-0649 | 120E | 1.1 | 3.0 | 327 | 0.8 | 4.4 | 19.4 | 6.5 | 3.9 |
| Lx14-0649 | 120E | 7.6 | 1.4 | 188 | 0.9 | 0.8 | 12.8 | 1.3 | 4.6 |
| Lx14-0629 | 280E | 0.9 | 2.6 | 92 | 1.6 | 0.9 | 22.1 | 0.2 | 11.1 |
| Lx14-0688 | 295E | 4.5 | 1.1 | 51 | 1.5 | 0.3 | 3.8 | 6.3 | 11.8 |
| Lx14-0658 | 420E | 0.5 | 0.1 | 31 | 1.3 | 2.2 | 32.0 | 0.1 | 10.9 |
| Lx14-0659 | 420E | 4.4 | 0.3 | 11 | 1.2 | 0.1 | 2.8 | 0.0 | 19.6 |
| Lx14-0662 | 435E | 1.1 | 5.4 | 276 | 2.2 | 2.8 | 31.9 | 9.5 | 2.7 |
| Area 4-West | | | | | | | | | |
| Lx12-2101 | -640E | 1.8 | 1.1 | 34 | 2.2 | 0.1 | 15.1 | 1.8 | 6.5 |
| Lx10-2054 | -250E | 9.0 | 2.4 | 194 | 1.4 | 1.6 | 12.2 | 0.9 | 6.0 |

Details on the four areas are as follows:

Area 1: East of the study area, a 47 m intersection of massive siliceous mudstone occurs on section 785E in drill hole Lx15-0429 representing possible hydrothermal alteration of fine-grained sediments and/or a possible paleo-depression (Fig. 8.1). Along the same trend on section 860E, hole Lx15-0349 on section 860E has a 16.7 m intersection of Zn-rich polymetallic mineralization (Table 8.3). This potential trend is approximately on strike with the Gopher lens of the Battle deposit (Fig. 8.1). The Gopher lens is interpreted to occur within a narrow elongate paleo-depression at the southern edge of the Battle Main lens basin based on drift mapping and core logging by the author during 1996 to 1998.

Area 2: As discussed in Chapter 7 and section 8.3.1 of this chapter, the Basal Conglomerate has some similarities to footwall volcanoclastic rocks of the Que River VHMS deposit, Tasmania. At Que River, Au-rich stockwork mineralization, containing up to 5.0 g/t Au, is located at the peripheral edge of a crudely zoned, footwall stockwork system that trends from a Cu-bearing core beneath the central massive orebody surrounded by Pb-Zn bearing stringer mineralization that merges with a distal Pb-Zn-Ag-Au-As-Sb-Ba enriched stringer veins (McGoldrick and Large, 1992)

Area 3: North of the study area, 12 intersections have Zn contents > 5.0% over a range of thicknesses up to a maximum of 7.6 m. Diamond drill information is widely spaced on 50 m to 100 m centres on a given section.

Area 4: Significant intersections occur on sections -250E and -640E west of the study area and are listed in Table 8.3. Hole Lx10-2054 on section -250E has a 9.0 m Zn-rich polymetallic massive sulphide intersection with similar geological host rocks described by this study.

8.3.3 Mining Applications

Geological information for this section is based on geology and alteration from Chapter 3 and structure from chapter 4. A preliminary engineering feasibility study (King, 2002) and a rock mechanic assessment (Dubois, 2004) have been completed by the Myra Falls Operations engineering department. The feasibility study is based on indicated reserves related to polymetallic Zn-rich Main lens along a strike length of approximately 100 m between -50E and 50E. The mineralization averages approximately 5m in thickness and ranges up to at least 17 m in height on section 50E. The rock mechanic assessment is based on information from this study.

The host rocks are considered to have similar characteristics to other rock units in the Battle and H-W mining areas. Graphic representation of the host rocks and their distribution are included in Chapter 3. The comparisons of the main host rock units with others mining areas at Myra Falls are listed in Table 8.4. The Ridge Zone West host rocks have been weak to moderately altered to the mineral assemblage sericite-quartz+/-chlorite. The weak sericite alteration is one possible explanation for the weakly developed S1 foliation of the area. The alteration and intensity of the S1 foliation are relatively weak compared to the texturally destructive, strong sericite-quartz+/-chlorite alteration envelopes associated with the Battle and H-W deposits. Rock quality testing is recommended on archived core.

| Table 8.4: Ridge Zone West rock quality comparison | | | |
|---|--|---|---|
| Rock Unit | Ridge Zone West | Battle | H-W |
| Hangingwall Rocks Hangingwall andesite flow-sill Siliceous mudstone Argillaceous mudstone | Unaltered Siliceous mudstone Argillaceous mudstone | Unaltered Chert Argillite | Unaltered Chert Argillite |
| Ore | Polymetallic Zn-Pb rich Main lens | Upper Zones, Zn-Pb rich Main lens | Polymetallic south fringe |
| Footwall Rocks Footwall Fragmental Price Formation andesite | Basal Conglomerate Weak ser-qtz-chl alteration | No comparison Strong ser-qtz-chl alteration | No comparison Strong ser-qtz-chl alteration |
| Structures Faulting S1 foliation (H-W Horizon) | Brittle-ductile; minor gouge Weak | Brittle-ductile; up to strong gouge Strong to moderate | Brittle-ductile; up to strong gouge Strong to moderate |
| Abbreviations: ser- sericite; qtz- quartz; chl- chlorite | | | |

The Ridge Zone West is located approximately 1,300 m below the surface of Mount Phillips. The H-W deposit is located approximately 475 to 1,000 m below the Myra valley floor and its mountain-side. The Battle deposit is located approximately 1,100 m below Mount Phillips. The increase in total rock mass overlying the Ridge Zone West will have an adverse affect on the behaviour of the host rocks and ore zone as mining proceeds.

8.3.4 Metallurgical Applications

Ore body mineralization, microscopic textures, and microprobe analyses are discussed in Chapters 5 and 6. Metallurgical aspects concerning grinding and beneficiation are discussed in Chapter 6. The main points of interest from microscopy are as follows:

- The sulphide, sulphosalt, and sulphate minerals of the Ridge Zone West have been recrystallized.
- The style of intergrowth between the sulphide minerals is considered to have simple locking characteristics and hence easy liberation properties.
- Coarse grains > 75 μm imply reasonable liberation of the sulphide minerals by normal grinding methods without interlocking issues.
- Locking problems may arise from relatively complex intergrowths of fine-grained blebs of chalcopyrite and galena associated with recrystallized sphalerite or from inclusions of chalcopyrite, sphalerite, and galena within pyrite-3.

The average chemical formulas for the ore minerals are listed in Table 8.1. Based on results from microprobe analyses by this study, the following considerations are noted:

- Future metallurgical and geological work should incorporate As in the suite of elements analysed as the sulphosalt tetrahedrite-tennantite is the As-rich end member tennantite.
- The main residency for Ag in the grains assessed is tennantite.
- The lack of Ag in galena should be considered as it will have a negative economic impact on the viability for a future lead circuit installation.

8.4 Concluding Remarks

The Ridge Zone West is a Zn-Pb-Cu-Au-Ag-Ba rich VHMS deposit comprising stacked lenses of disseminated to massive mineralization associated with fine and coarse-grained volcano-sedimentary rocks. Seafloor and sub-seafloor settings are interpreted for the mineralization. Main lens mineralization is the most economically significant mineralization observed and was formed by the infiltration and replacement of dominantly permeable, coarse volcanoclastic deposits in the shallow sub-seafloor environment. Exploration potential exists eastward to the Gopher lens of the Battle deposit, within the Basal Conglomerate below the Ridge Zone West, north of the study area, westward for at least 200m to -250E on the mine grid, and potentially up to approximately 590 m westward to -640E.

References

- Allen, R.L., 1993. Volcanic facies analysis of massive sulphide deposits in British Columbia: Preliminary results from field work August-September 1993. MDRU Library, University of British Columbia, Volcanogenic massive sulphide project annual technical report, Year 1.
- Bakker, F., 2002. January 2002 geological resources and mining reserves for Myra Falls Operations. Boliden-Westmin Limited internal company report. 127 p.
- Barton, P.B., Jr., 1978. Some ore textures involving sphalerite from the Furutobe mine, Akita Prefecture, Japan: *Mining Geology*, vol. 28, pp. 293-300.
- Barton, P.B., Jr. and Bethke, P.M., 1987. Chalcopyrite disease in sphalerite: pathology and epidemiology. *American Mineralogist*, vol. 72, pp. 451-467.
- Barrett, T.J., and Sherlock, R.L., 1996. Volcanic stratigraphy, lithogeochemistry, and seafloor setting of the H-W massive sulphide deposit, Myra Falls, Vancouver Island, British Columbia; *Exploration and Mining Geology*; vol. 5, no. 4, pp. 421-458.
- Barrett, T.J., MacLean, W.H., 2000. Chemostatigraphy, petrography and alteration of the Marshall Zone, Myra Falls, Vancouver Island, B.C. Unpublished Boliden-Westmin Ltd. internal company report. 126 p.
- Barrie, C.T. and Hannington, M.D., 1999. Classification of VMS deposits based on host-rock composition. *In* Volcanic-associated massive sulphide deposits: Processes and examples in modern and ancient settings, edited by Barrie, C.T. and Hannington, M.D., *Reviews in Economic Geology*, vol. 8, pp. 2-11.
- Becherer, M., 1992. Grade control and mining methods in the Lynx mine, Myra Falls Operations, Westmin Resources Limited. Westmin Resources Limited internal company report. 3 p.
- Berry, R., 2000. Structural geology of the Myra Falls Operation. Centre for ore deposit research, University of Tasmania. Internal company report. 16 p.
- Boldy, J., 1977. (Un)certain exploration facts and figures. *CIMM Bulletin*, May 1977, pp. 86-95.
- Brandon, M.T., Orchard, M.J., Parrish, R.R., Sutherland Brown, A., Yorath, C.J., 1986. Fossil ages and isotopic dates from the Paleozoic Sicker Group and associated intrusive rocks, Vancouver Island, British Columbia. *Current Research, Part A, Geological Survey of Canada, Paper 86-1A*, pp. 683-696.
- Carvalho, I.G., 1979. Geology of the Western Mines District, Vancouver Island, British Columbia; unpublished PhD thesis, University of Western Ontario.
- Chong, A., 2003. Part B - Overview of selected topics on the massive sulphide deposits at Myra Falls, *in* Massive sulphide deposits at Myra Falls Operations, Vancouver Island, British Columbia, Joint G.A.C.-M.A.C.-S.E.G. field trip, May 2003, unpublished internal company report, pp. 15-44.
- Chong, A.G., and Bakker, F.J., 2004. Geological resources and mining reserves for Myra Falls Operations. Unpublished Boliden-Westmin (Canada) Limited company report, 230 p.
- Craig, J.R., 1983. Metamorphic features in Appalachian massive sulphides. *Mining Magazine*, vol. 47, pp. 515-525.
- Craig, J.R., and Vaughn, D.J., 1994. Ore microscopy and ore petrography. John Wiley and Sons. New York. 434 p.
- Chrysoullis, S.L., 1989. Determination of invisible gold in flotation products and four our types from the HW mine, British Columbia, Westmin Resources Ltd., internal company report.
- Deer, W.A., Howie, R.A., and Zussman, J., 1980, An introduction to the rock-forming minerals, 2nd edition. Prentice Hall, Essex. 695 p.

- Doyle, M.G. and Allen, R.L., 2003. Sub-seafloor replacement in volcanic-hosted massive sulfide deposits. *Ore Geology Reviews*, vol. 23, pp. 183-222.
- Dubois, C., 2004. A preliminary rock mechanics assessment on: the in-situ stress regime for the Ridge Zone West deposit, Myra Falls Operations. Internal NVI Mining Limited company report, 7 p.
- England, T.D.J., and Calon, T.J., 1991. The Cowichan fold and thrust system, Vancouver Island, southwestern British Columbia. *Geological Society of America Bulletin*, v. 103, pp. 336-362.
- Eldridge, C.S., Barton, P.B., Jr., and Ohmoto, H., 1983. Mineral textures and their bearing on formation of the Kuroko orebodies. *Economic Geology, Monograph 5*, pp. 241-281.
- Eldridge, C.S., Bourcier, W.L., Ohmoto, H., and Barnes, H.L., 1988. Hydrothermal inoculation and incubation of the chalcopyrite disease in sphalerite. *Economic Geology*, vol. 83, pp. 978-989.
- Epstein, A.G., Epstein, J.B., and Harris, L.D., 1977. Conodont Color Alteration – an index to organic metamorphism. U.S. Geological Survey, Professional Paper 995, 27 p.
- Evans, E.V., 1976. Generalized geological map of the Canadian Cordillera, British Columbia Department of Mines and Petroleum Resources. In C.I.M.M. special volume 15, Porphyry Deposits of the Canadian Cordillera, 1:2,500,000 scale map.
- Fouquet, Y., Stackelberg, U.V., Charlou, J.L., Erzinger, J., Herzig, P.M., Muhe, R., and Wiedicke, M., 1993. Metallogenesis in back-arc environments: the Lau Basin example. *Economic Geology*, vol. 88, pp. 2154-2181.
- Franklin, J.M., Sangster, D.M., and Lydon, J.W., 1981. Volcanic-associated massive sulphide deposits: *Economic Geology*, 75th anniversary volume, pp. 485-627.
- Franklin, J.M. and Thorpe, R.I., 1982. Comparative metallogeny of the Superior, Slave, and Churchill Provinces. In *Precambrian Sulphide Deposits, H.S. Robinson Memorial Volume*. Edited by Hutchinson R.W., Spence, C.D., and Franklin, J.M., The Geological Association of Canada, Special Paper 25, pp. 3-90.
- Fyles, J.T., 1955. Geology of the Cowichan Lake area, Vancouver Island, British Columbia, British Columbia Department of Mines, Bulletin 37, 72 p.
- Gabrielse, H., 1991. Structural styles, Chapter 17. In *Geology of the Cordilleran Orogen in Canada*, edited by Gabrielse, H., and Yorath, C.J., Geological Survey of Canada, Geology of Canada, no. 4, pp. 571-675.
- Gabrielse, H., Monger, J.W.H., Wheeler, J.O., and Yorath, C.J., 1991. Morphogeological belts, tectonic assemblages, and terranes, Chapter 2, Part A. In *Geology of the Cordilleran Orogen in Canada*, edited by Gabrielse and C.J. Yorath, Geological Survey of Canada, Geology of Canada, no. 4, pp. 15-28.
- Gabrielse, H., and Yorath, C.J., 1991. Tectonic synthesis, Chapter 18. In *Geology of the Cordilleran Orogen in Canada*, edited by Gabrielse, H., and Yorath, C.J., Geological Survey of Canada, Geology of Canada, no. 4, pp. 677-705.
- Gemmell, J.B., 1995. Comparison of volcanic-hosted massive sulphide deposits in modern and ancient back-arc basins: examples from the southwest Pacific and Australia. In *PACRIM '95*, pp. 227-232.
- Gemmell, J.B., 1998. District scale metal zoning, Myra Falls VHMS Deposits, B.C., Canada. Internal Boliden-Westmin Limited company report. 31 p.
- Gibson, H.L. and Kerr, D.J., 1992. Giant volcanic-associated massive sulphide deposits: with emphasis on Archean examples. In *Whiting, B.H. Mason, R. and Hodgson, C.J. (editors) Giant Ore Deposits*; Queen's University, pp 492-522.

References

- Gibson, H., Morton, R.L., and Hudak, G.J., 1999. Submarine volcanic processes, deposits, and environments favourable for the location of volcanic-associated massive sulfide deposits. *In* Volcanic-associated massive sulfide deposits: processes and examples in modern and ancient settings, edited by Barrie, C.T. and Hannington, M.D., Reviews in Economic Geology, vol. 8, pp. 101-127.
- Greenwood, H.J., Woodsworth, G.J., Read, P.B., Ghent, E.D., Evenchick, C.A., 1991. Metamorphism Chapter 16. *In* Geology of the Cordilleran Orogen in Canada, edited by H. Gabrielse and C.J. Yorath, Geological Survey of Canada no. 4, pp. 533-570.
- Gunning, H.C., 1931. Buttle Lake map-area, Vancouver Island, B.C. *In* Canada Department of Mines Geological Survey, Summary Report, 1930, Part A. pp. 56-78.
- Hannington, M.D., Poulsen, K.H., Thompson, J.F.H., and Sillitoe, R.H., 1999. Volcanogenic gold in the massive sulfide environment. *In* Volcanic-associated massive sulfide deposits: processes and examples in modern and ancient settings, edited by Barrie, C.T. and Hannington, M.D., Reviews in Economic Geology, vol. 8, pp. 325-351.
- Hayward, L., 2001. Gold associations and recovery at Myra Falls Operations, Vancouver Island, British Columbia, Canada. Unpublished M.Sc. thesis, Leicester University, 149 p.
- Herzig, P.M., Hannington, M.D., Fouquet, Y., Stackelberg, U.V., and Petersen, S., 1993. Gold-rich polymetallic sulfides from the Lau back arc and implications for the geochemistry of gold in sea-floor hydrothermal systems of the southwest Pacific. *Economic Geology*, vol. 88, pp. 2182-2209.
- Holcombe, R., 2004. Georient, version 9 software.
- Hoy, T., 1991. Volcanogenic massive sulphide deposits in British Columbia. *In* Ore deposits, tectonics and metallogeny in the Canadian Cordillera. Ministry of energy, mines and petroleum resources, Geological Survey Branch Paper 1991-4, pp. 89-124.
- Huston, D.L., and Large, R.R., 1987. Genetic and exploration significance of the Zinc ratio ($100 \text{ Zn}/(\text{Zn} + \text{Pb})$) in massive sulfide systems. *Economic Geology*, vol. 82, pp. 1521-1539.
- Huston, D.L., and Large, R.R., 1989. A chemical model for the concentration of gold in volcanogenic massive sulphide deposits. *Ore Geology Reviews*, vol. 4, pp. 171-200.
- Huston, D.L., Bottrill, R.S., Creelman, R.A., Khin Zaw, Ramsden, T.R., Rand, S.W., Gemmell, J.B., Jablonski, W., Sie, S.H., and Large, R.R., 1992. Geologic and geochemical controls on the mineralogy and grain size of gold-bearing phases, eastern Australian volcanic-hosted massive sulfide deposits. *Economic Geology*, vol. 8, pp. 542-563.
- Huston, D. L., 2000. Gold in volcanic hosted massive sulfide deposits: distribution, genesis, and exploration. *In* Gold in 2000. Edited by Hagemann, S.G. and Brown, P.E., Reviews in Economic Geology, vol. 13, pp. 401-426.
- Hutchinson, R.W., 1973. Volcanogenic sulphide deposits and their metallogenic significance. *Economic Geology*, vol. 68, pp. 1223-1246.
- Hutchinson, M.N., 1978. Refinement and application of the sphalerite geobarometer. Ph.D. thesis, University of Toronto, Toronto, Ontario.
- Irving, E., Wynne P.J., Thorkelson, D.J., and Schiarizza, P., 1996. Large (1000 to 4000 km) northward movements of tectonic domains in the northern Cordillera, 83 to 45 Ma. *Journal of Geophysical Research*, vol. 101, no. B8, pp. 17901-17916.
- Jeffrey, W.G., 1970. Buttle Lake: B.C. Ministry of Energy, Mines and Petroleum Resources, Miscellaneous Open File Report, map with notes.
- Jones, D.L., Silberling, N.J., and Hillhouse, J., 1977. Wrangellia – A displaced terrane in northwest North America. *Canadian Journal of Earth Sciences*, vol. 14, pp. 2565 – 2577.

References

- Jones, S., 2001. Geology and alteration of the hangingwall "Cap" rocks of the Myra Falls VHMS district, British Columbia, Canada. Unpublished PhD study, University of Tasmania, Australia. 497p.
- Juras, S.J., 1987. Geology of the polymetallic volcanogenic Buttle Lake Camp, with emphasis on the Price hillside, Central Vancouver Island, British Columbia, Canada. Unpublished Ph.D. thesis, University of British Columbia, 279 p.
- Kelley, W.C. and Clark, B.R., 1975. Sulphide deformation studies III. Experimental deformation of chalcopyrite at 2000 bars and 500 degrees Celsius. *Economic Geology*, vol. 70, pp. 431-453.
- Klein, C., 2002. The manual of mineral science, (after James D. Dana), 22nd edition. John Wiley and Sons. 641 p.
- Knuckey, M.J., Comba, C.D.A., and Riverin, G., 1982. Structure, metal zoning and alteration at the Millenbach deposit, Noranda, Quebec. *In* Precambrian sulfide deposits, edited by Hutchinson, R.W., Spence, C.D., and Franklin, J.M., Geological Association of Canada, pp. 255-295.
- Large, R.R., 1992. Australian volcanic-hosted massive sulphide deposits: features, styles, and genetic models. *Economic Geology*, vol. 87, pp. 471-510.
- Large, R.R., McGoldrick, P.J., Berry, R.F., 1988. A tightly folded, gold-rich massive sulfide deposit: Que River mine, Tasmania. *Economic Geology*, vol. 83, pp. 681-693.
- Lowe, D.R., 1982. Sediment gravity flows: II. Depositional models with special reference to the deposits of high density turbidity currents. *Journal of Sedimentology and Petrology*, vol. 52, pp. 279-297.
- Massey, N.W.D., 1994. Geology and mineral resources of the Duncan sheet, Vancouver Island 92B13. Province of British Columbia, Ministry of Energy, Mines and Petroleum Resources, Mineral Resources Division, Geological Survey Branch, Paper 1992-4. 57 p.
- McGoldrick, P.J., and Large, R.R., 1992. Geologic and geochemical controls on gold-rich stringer mineralization in the Que River deposit, Tasmania. *Economic Geology*, vol. 87, pp. 667-685.
- McKinley, S.D.M., Juras, S.J., and Pearson, C.A., 1997. Paleotopography and ore zonation of the Battle Zn-Cu-Au-Ag VMS deposit, Vancouver Island, British Columbia. *In* 50th anniversary GAC/MAC annual meeting, Ottawa.
- McPhie, J., Doyle, M., and Allen, R., 1993. Volcanic textures: a guide to the interpretation of textures in volcanic rocks. CODES, University of Tasmania, Tasmanian Government Printing Office, Hobart, Australia. 197p.
- Monger, J.W.H., Clowes, R.M., and Riddihough, R.P., 1985. Continent-ocean transect B-2: Juan de Fuca plate Alberta Plains; explanatory pamphlet: Boulder, Colorado, Geological Society of America, 21p.
- Monger, J.W.H. and Price, R.H., 1979. Geodynamic evolution of the Canadian Cordillera. Progress and problems. *Canadian Journal of Earth Sciences*, vol. 16, pp. 770-791.
- Monger, J.W.H. and Price, R.A., 1996. Comment on "Paleomagnetism of the Upper Cretaceous strata of Mount Tatlow: Evidence for 3000 km of northward displacement of the eastern Coast Belt, British Columbia" by P.J. Wynne et al., and on "Paleomagnetism of the Spences Bridge Group and northward displacement of the Intermontane Belt, British Columbia: A second look" by E. Irving et al. *Journal of Geophysical Research*, vol. 101, pp. 13793-13799.
- Monger, J.W.H., Price, R.A., and Tempelman-Kluit, D.J., 1982. Tectonic accretion and the origin of the two major metamorphic and plutonic belts in the Canadian Cordillera. *Geology*, vol. 10, pp. 70-75.
- Muller, J.E., 1977. Geology of Vancouver Island. Geological Survey of Canada Open File Report 463, Marginal Notes.

References

- Muller, J.E., 1980. The Paleozoic Sicker Group of Vancouver Island, British Columbia. Geological Survey of Canada, Paper 79-30. 22p.
- Nixon, G.T., Hammack, J.L., Koyanagi, V.M., Payie, G.J., Panteleyev, A., Massey, N.W.D., Hamilton, J.V., Haggart, J.W., 1994. Preliminary geology of the Quatsino – Port McNeill map areas, Northern Vancouver Island (92L/12,11). In Geological Fieldwork 1993. Edited by Grant, B. and Newell, J.M. British Columbia Ministry of Energy, Mines and Petroleum Resources, Paper 1994-1, Pp. 63-86.
- Northcote, K.E. and Muller, J.E., 1972. Volcanism, plutonism, and mineralization: Vancouver Island. In The Canadian Mining and Metallurgical CIM Bulletin, October 1972, pp. 49-57.
- Parrish, R.R. and McNicoll, V.J., 1992. U-Pb age determinations from the southern Vancouver Island area, British Columbia. In Radiogenic Age and Isotopic Studies: Report 5. Geological Survey of Canada Paper 91-2, pp. 79-86.
- Pearson, C.A., 1993. Mining zinc-rich massive sulfide deposits on Vancouver Island, British Columbia. In International Symposium – World Zinc '93. Hobart, Australia. Pp. 75-83.
- Pearson, C.A., 1997. Minesite Exploration – The lifeblood of Myra Falls, Operations. In CIM Conference v. 97 Vancouver, British Columbia, Canada.
- Pearson, C.A., Juras, S.J., and McKinley, S.D., 1997. Paleotopography and ore zonation of the H-W and Battle Zn-Cu-Au-Ag VMS deposits, Myra Falls Camp, Vancouver Island, British Columbia, Canada. In SEG Field Conference. 1997. Neves Corvo-Lisbon, Portugal.
- Ramdohr, P., 1969. The ore minerals and their intergrowths. Pergamon Press, New York, 1019 p.
- Ramsay, J.G., 1967. Fold and fracturing of rocks. McGraw-Hill Book Company, New York, 568 p.
- Reid, R.R., 1993. Westmin Structure 18 and 20 level Data. Westmin Resources Ltd. internal company report. 48p.
- Robinson, M., 1994. Geology, mineralisation and alteration of the Battle Zone, Buttle Lake Camp, Central Vancouver Island Southwestern British Columbia. M.A.Sc. thesis, University of British Columbia, 268p.
- Sanders, D.H., Eng, R.J., Murph, A.F., 1985. Statistics: A fresh approach, 3rd edition. McGraw-Hill, New York, 524 p.
- Sangster, D.F., 1980. Quantitative characteristics of volcanogenic massive sulphide deposits. CIMM Bulletin, February 1980, pp. 74-81.
- Sangster, D.F. and Scott, S.D., 1976. Precambrian strata-bound massive Cu-Zn-Pb sulphide ores of North America. In Handbook of strata-bound and stratiform deposits, edited by Wolf, K.H., Elsevier, Amsterdam, pp. 129-222.
- Sawkins, F.J., 1976. Massive sulphide deposits in relation to geotectonics. Geological Association of Canada Special Paper 14, pp. 221-240.
- Scott, R., and Berry, R., 2003. A guide to obtaining structural data from oriented and unoriented core. Centre for ore deposit and exploration studies, University of Tasmania handout. 13 p.
- Sebert, C., and Barrett, T.J., 1996. Tulsequah Chief massive sulfide deposit, northwestern British Columbia. Exploration and Mining Geology, vol. 5, no. 4, pp. 281-308.
- Secombe, P.K., Godwin, C.I., Krouse, H.R. and Juras, S.J., 1990. Sulphur and lead isotopic studies of the Buttle Lake massive sulphide deposits, Vancouver Island, B.C., Canada: Sources of ore constituents in a submarine exhalative environment. In Pacific Rim 90 Congress. Gold Coast, Queensland, Australia: The Australian Institute of Mining and Metallurgy. Pp. 419-425.
- Seraphim, R.H., 1980. Western Mines – Myra, Lynx and Price deposits. In CIM Bulletin, December. Pp. 71-85.

References

- Sinclair, B.J., 2000. Geology and genesis of the Battle Zone VHMS deposits, Myra Falls District, British Columbia, Canada. Unpublished Ph.D. thesis, University of Tasmania, CODES-SRC, 313p.
- Solomon, M., 1976. "Volcanic" massive sulphide deposits and their host rocks – a review and an explanation, *In* handbook of strata-bound and stratiform ore deposits, II, Regional studies and specific deposits. Edited by Wolf, K.A., Amsterdam, Elsevier, pp. 21-50.
- Stanton, R.L., 1972. Ore Petrology. McGraw-Hill, New York. 713 p.
- Walker, R.R., 1985. Westmin Resources' massive sulphide deposits, Vancouver Island; Geological Society of America, Cordilleran Section Meeting, May 1985, Vancouver, B.C., Field Trip Guidebook, pp. 1-13.
- Wilson, G., 1993. Mineralogy of sulphide ores from the H-W Kuroko deposit, British Columbia, Part II, multi-element analysis of the ore minerals. Westmin Resources Ltd., internal company report, 42 p.
- Wynne, P.J., Irving, E., Maxson, J.A., and Kleinspehn, K.L., 1995. Paleomagnetism of the Upper Cretaceous strata of Mount Tatlow: Evidence for 3000 km of northward displacement of the eastern Coast Belt, British Columbia. *Journal of Geophysical Research*, vol. 100, pp. 6073-6091.
- Yorath, C.J. and Nasmith, H.W., 1995. The geology of Southern Vancouver Island – a field guide. Orca Book Publishers.
- Yorath, C.J., Sutherland Brown, A., and Massey, N.W.D., 1999. Lithoprobe, southern Vancouver Island, British Columbia. *Geology. Geological Survey of Canada Bulletin 498*, 145 p.

APPENDICES

APPENDIX 1: Drill log catalogue and selected logs

This appendix lists the drill holes used in the study for geological interpretation by the author. The list includes 97 drill holes from the 2000-2001 drill campaign and historical drill holes. Approximately 4,000 m of core was graphic logged in detail from 11 drill holes by the author.

Appendix A1-1: Drill hole catalogue

Appendix A1-2: Sample graphic drill log (LX10-2048)

A1-1: Drill hole catalogue

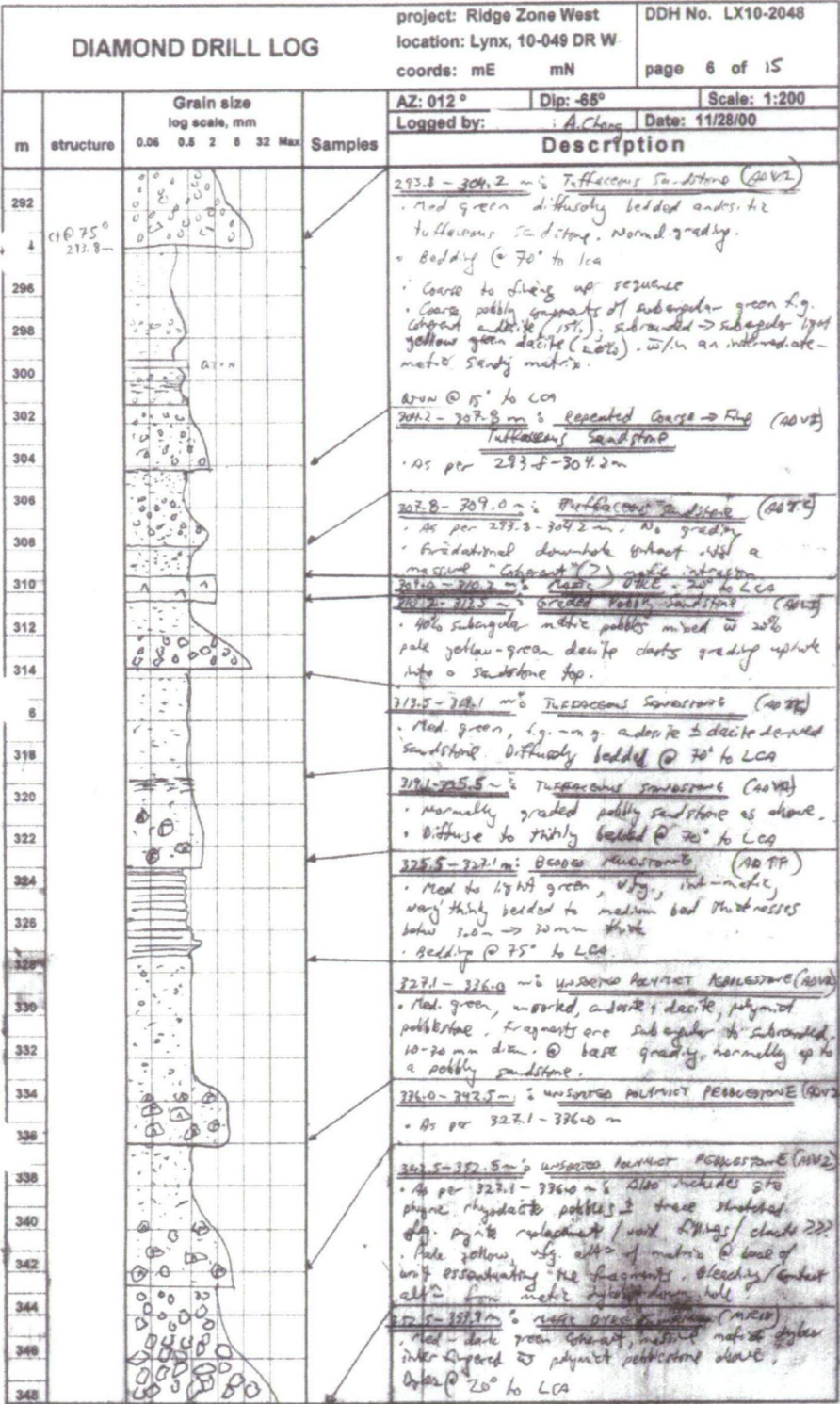
| Table A1-1.1: Drill hole catalogue and collar information | | | | | | | | | |
|--|----------------|-----------------|------------------|----------------------|------------------|---------------|------------|--------------|--------|
| All holes are used for the geological interpretation and block model created by the author for this study. | | | | | | | | | |
| Abbreviations: AC = Albert Chong (author); AH = Alison Hartley; CS = Chris Sebert | | | | | | | | | |
| DC = Dean Crick; TR = Tyler Ruks; SJ = Stephen Juras; SM = Sean McKinley | | | | | | | | | |
| Historical- diamond drill data acquired prior to recent 2000-2001 campaign | | | | | | | | | |
| Data in metric mine grid coordinates. Mine grid is rotated 48 degrees east of true north. | | | | | | | | | |
| Drill hole | Easting (m) | Northing (m) | Elevation (m) | Azimuth (degrees) | Dip (degrees) | Length (m) | Logger | A.Chong logs | |
| | | | | | | | | From | To |
| LX10-1265 | 149.0 | 4034.6 | 3434.2 | 355.0 | -89.0 | 568.1 | Historical | | |
| LX10-2007 | 305.0 | 4441.0 | 3434.5 | 20.0 | -52.0 | 961.6 | Historical | | |
| LX10-2008 | 305.0 | 4441.0 | 3434.5 | 24.0 | -51.0 | 1014.7 | Historical | | |
| LX10-2009 | 305.0 | 4441.0 | 3434.5 | 20.0 | -52.0 | 1009.2 | Historical | | |
| LX10-2010 | 362.5 | 4482.6 | 3430.0 | 40.0 | -53.0 | 910.3 | Historical | | |
| LX10-2011 | 362.5 | 4482.6 | 3430.0 | 39.0 | -50.0 | 972.3 | Historical | | |
| LX10-2012 | 362.5 | 4482.6 | 3430.0 | 45.0 | -45.0 | 987.6 | Historical | | |
| LX10-2030 | 301.5 | 4441.0 | 3435.8 | 280.0 | -74.0 | 668.1 | SM | | |
| LX10-2031 | 301.5 | 4441.0 | 3435.8 | 330.0 | -87.5 | 643.1 | CS | | |
| LX10-2032 | 302.8 | 4442.5 | 3435.8 | 347.5 | -49.3 | 959.5 | AH | | |
| LX10-2033 | 303.5 | 4442.5 | 3435.8 | 343.0 | -57.5 | 816.9 | AH | | |
| LX10-2034 | 303.5 | 4442.5 | 3435.8 | 343.0 | -66.0 | 762.6 | AH | | |
| LX10-2035 | 304.2 | 4437.0 | 3435.8 | 172.0 | -69.0 | 686.7 | AH | | |
| LX10-2036 | 304.2 | 4437.0 | 3435.8 | 170.5 | -59.8 | 630.3 | AH | | |
| LX10-2037 | 304.2 | 4437.0 | 3435.8 | 172.0 | -79.5 | 743.1 | TR | | |
| LX10-2038 | 304.2 | 4437.0 | 3435.8 | 175.0 | -57.3 | 206.7 | TR | | |
| LX10-2039 | 304.2 | 4437.0 | 3435.8 | 170.0 | -52.0 | 682.1 | AH | | |
| LX10-2040 | -91.3 | 3953.0 | 3435.0 | 0.0 | -68.5 | 612.7 | AC; AH | 369.30 | 612.60 |
| LX10-2041 | -91.3 | 3953.2 | 3435.0 | 1.5 | -62.8 | 612.7 | AC | 0.00 | 612.60 |
| LX10-2042 | -91.3 | 3953.4 | 3435.0 | 1.3 | -55.0 | 646.1 | AC | 0.00 | 646.10 |
| LX10-2043 | -91.3 | 3953.8 | 3435.0 | 0.0 | -50.0 | 750.8 | AH; TR | | |
| LX10-2044 | -1.8 | 3953.0 | 3434.5 | 0.0 | -75.0 | 606.5 | AH | | |
| LX10-2045 | -1.8 | 3958.0 | 3434.5 | 0.7 | -68.2 | 640.1 | AC; AH | 464.20 | 494.00 |
| LX10-2046 | -1.8 | 3958.3 | 3434.5 | 357.2 | -64.7 | 637.2 | AC; AH | 370.50 | 637.20 |
| LX10-2047 | -1.8 | 3957.8 | 3434.5 | 0.5 | -71.0 | 620.9 | AH | | |
| LX10-2048 | -1.8 | 3958.2 | 3434.5 | 11.0 | -65.0 | 658.4 | AC; DC | 211.00 | 658.40 |
| LX10-2049 | 393.8 | 3925.0 | 3435.2 | 345.0 | -65.0 | 661.4 | AC; AH | 120.50 | 661.40 |
| LX10-2050 | 307.5 | 4438.0 | 3432.0 | 95.0 | -55.0 | 844.3 | AH | | |
| LX10-2051 | 307.5 | 4438.3 | 3432.0 | 65.5 | -55.0 | 772.5 | AH | | |
| LX10-2052 | 307.5 | 4438.0 | 3435.8 | 85.0 | -55.1 | 844.3 | AH | | |
| LX10-2052B | 307.5 | 4438.0 | 3432.0 | 85.0 | -55.0 | 644.3 | AH | | |
| LX10-2053B | 307.5 | 4438.0 | 3432.0 | 85.0 | -49.0 | 703.5 | AH | | |
| LX10-2054 | -275.3 | 3956.4 | 3435.9 | 0.0 | -69.0 | 624.8 | AH | | |
| LX10-2055 | -275.3 | 3956.4 | 3435.9 | 0.0 | -65.0 | 621.8 | AH | | |
| LX10-2057 | -275.3 | 3956.4 | 3435.9 | 0.0 | -73.0 | 619.7 | AH | | |
| LX10-2058 | -275.3 | 3956.4 | 3435.9 | 12.0 | -67.0 | 588.3 | AH | | |
| LX10-2060 | 393.9 | 3925.1 | 3435.2 | 345.0 | -69.0 | 597.4 | AC | 0.00 | 597.40 |
| LX10-2061 | 393.9 | 3925.1 | 3436.0 | 345.0 | -67.0 | 145.0 | AH | | |
| LX10-2062 | 393.9 | 3925.1 | 3435.2 | 345.0 | -88.0 | 597.4 | SM | | |
| LX10-2063 | 395.5 | 3925.1 | 3435.2 | 180.0 | -68.0 | 128.0 | AH | | |
| LX10-2064 | 395.5 | 3925.1 | 3435.2 | 180.0 | -60.0 | 460.2 | AH | | |
| LX12-2100 | -640.1 | 4087.4 | 3344.9 | 180.0 | -77.0 | 524.9 | Historical | | |
| LX12-2101 | -640.1 | 4087.4 | 3344.9 | 0.0 | -85.0 | 556.9 | Historical | | |
| LX12-2102 | -640.1 | 4087.4 | 3344.9 | 0.0 | -77.0 | 560.8 | Historical | | |
| LX12-2103 | -640.1 | 4087.4 | 3344.9 | 0.0 | -69.0 | 557.5 | Historical | | |
| LX12-2104 | -640.1 | 4087.4 | 3344.9 | 0.0 | -55.0 | 630.3 | Historical | | |
| LX12-2105 | -640.1 | 4087.4 | 3344.9 | 180.0 | -35.0 | 976.0 | Historical | | |
| LX12-2106 | -640.1 | 4087.4 | 3344.9 | 180.0 | -85.0 | 503.5 | Historical | | |
| LX12-2107 | -640.1 | 4087.4 | 3344.9 | 180.0 | -70.0 | 289.3 | Historical | | |
| LX12-2108 | -640.1 | 4087.4 | 3344.9 | 180.0 | -20.0 | 305.7 | Historical | | |
| LX12-2109 | -640.1 | 4087.4 | 3344.9 | 202.0 | -33.0 | 1009.0 | Historical | | |

| Table A1-1.2: Drill hole catalogue and collar information | | | | | | | | |
|--|----------------|-----------------|------------------|----------------------|------------------|---------------|------------|-------------------------|
| All holes are used for the geological interpretation and block model created by the author for this study. | | | | | | | | |
| Abbreviations: AC = Albert Chong (author); AH = Alison Hartley; CS = Chris Seibert | | | | | | | | |
| DC = Dean Crick; TR = Tyler Ruks; SJ = Stephen Juras; SM = Sean McKinley | | | | | | | | |
| Historical- diamond drill data acquired prior to recent 2000-2001 campaign | | | | | | | | |
| Data in metric mine grid coordinates. Mine grid is rotated 48 degrees east of true north. | | | | | | | | |
| Drill hole | Easting (m) | Northing (m) | Elevation (m) | Azimuth (degrees) | Dip (degrees) | Length (m) | Logger | A.Chong logs From To |
| LX14-0622 | 181.4 | 4083.0 | 3249.8 | 187.0 | -73.3 | 344.7 | Historical | |
| LX14-0623 | 181.4 | 4082.0 | 3249.8 | 189.0 | -53.0 | 414.8 | Historical | |
| LX14-0624 | 181.4 | 4078.9 | 3250.0 | 181.0 | -33.0 | 488.6 | Historical | |
| LX14-0625 | 181.4 | 4080.5 | 3249.9 | 182.0 | -58.0 | 306.9 | Historical | |
| LX14-0626 | 181.4 | 4084.3 | 3249.8 | 3.0 | -76.4 | 429.2 | AC; SJ | 149.30 429.20 |
| LX14-0627 | 181.4 | 4084.3 | 3249.8 | 5.0 | -60.4 | 460.7 | AC; SJ | 268.20 331.90 |
| LX14-0628 | 181.4 | 4084.3 | 3249.8 | 0.0 | -55.0 | 529.7 | AC; SJ | 242.60 529.70 |
| LX14-0629 | 181.4 | 4084.3 | 3249.8 | 29.0 | -53.5 | 413.6 | Historical | |
| LX14-0630 | 181.4 | 4084.3 | 3249.8 | 319.0 | -69.4 | 398.4 | Historical | |
| LX14-0631 | 181.4 | 4084.3 | 3249.8 | 340.0 | -60.8 | 431.0 | Historical | |
| LX14-0633 | 182.9 | 4084.3 | 3249.8 | 43.0 | -72.0 | 398.4 | Historical | |
| LX14-0642 | 61.0 | 4145.3 | 3250.7 | 180.0 | -89.0 | 336.8 | Historical | |
| LX14-0643 | 61.0 | 4145.3 | 3250.7 | 180.0 | -77.0 | 370.9 | Historical | |
| LX14-0644 | 61.0 | 4145.3 | 3250.7 | 180.0 | -69.0 | 363.6 | Historical | |
| LX14-0645 | 61.0 | 4145.3 | 3250.7 | 180.0 | -56.0 | 371.9 | Historical | |
| LX14-0646 | 61.0 | 4145.3 | 3250.7 | 13.0 | -84.0 | 378.9 | Historical | |
| LX14-0647 | 61.0 | 4145.3 | 3250.7 | 5.0 | -74.5 | 386.5 | Historical | |
| LX14-0648 | 61.0 | 4145.3 | 3250.7 | 2.0 | -63.0 | 520.0 | Historical | |
| LX14-0649 | 61.0 | 4145.3 | 3250.7 | 0.0 | -52.0 | 569.7 | Historical | |
| LX14-0650 | 61.0 | 4145.3 | 3250.7 | 0.0 | -42.0 | 628.8 | Historical | |
| LX14-0651 | 61.0 | 4145.3 | 3250.7 | 0.0 | -43.0 | 572.4 | Historical | |
| LX14-0655 | 419.1 | 4224.5 | 3251.0 | 185.0 | -74.0 | 397.5 | Historical | |
| LX14-0656 | 419.1 | 4224.5 | 3251.0 | 185.0 | -67.0 | 389.2 | Historical | |
| LX14-0657 | 419.1 | 4224.5 | 3251.0 | 184.0 | -58.0 | 319.1 | Historical | |
| LX14-0658 | 419.1 | 4224.5 | 3251.0 | 0.0 | -88.0 | 392.3 | Historical | |
| LX14-0659 | 419.1 | 4224.5 | 3251.0 | 0.0 | -75.0 | 381.0 | Historical | |
| LX14-0660 | 419.1 | 4232.1 | 3251.0 | 3.0 | -67.0 | 427.6 | Historical | |
| LX14-0661 | 419.1 | 4232.1 | 3251.0 | 0.0 | -60.0 | 404.5 | Historical | |
| LX14-0662 | 419.1 | 4232.1 | 3251.0 | 0.0 | -50.0 | 493.8 | Historical | |
| LX14-0663 | -61.0 | 4244.3 | 3247.6 | 180.0 | -66.0 | 366.4 | Historical | |
| LX14-0664 | -61.0 | 4244.3 | 3247.6 | 187.0 | -72.0 | 397.8 | Historical | |
| LX14-0665 | -61.0 | 4244.3 | 3247.6 | 184.0 | -62.0 | 422.1 | Historical | |
| LX14-0666 | -61.0 | 4244.3 | 3247.6 | 185.0 | -76.0 | 417.0 | Historical | |
| LX14-0684 | 278.9 | 4147.1 | 3250.4 | 0.0 | -90.0 | 383.1 | Historical | |
| LX14-0685 | 278.9 | 4147.1 | 3250.4 | 0.0 | -79.0 | 374.0 | Historical | |
| LX14-0686 | 278.9 | 4147.1 | 3250.4 | 352.0 | -70.5 | 407.8 | Historical | |
| LX14-0687 | 278.9 | 4147.1 | 3250.4 | 348.0 | -60.0 | 438.0 | Historical | |
| LX14-0688 | 278.9 | 4147.1 | 3250.4 | 353.0 | -52.0 | 503.5 | Historical | |
| LX14-0689 | 278.9 | 4147.1 | 3250.4 | 180.0 | -81.0 | 366.1 | Historical | |
| LX14-0690 | 278.9 | 4147.1 | 3250.4 | 175.0 | -71.0 | 364.2 | Historical | |
| LX14-0691 | 278.9 | 4147.1 | 3250.4 | 175.0 | -60.0 | 342.3 | Historical | |
| LX14-0692 | 278.9 | 4147.1 | 3250.4 | 351.0 | -42.5 | 613.9 | Historical | |
| LX14-0699 | 278.9 | 4147.1 | 3250.4 | 352.0 | -30.0 | 154.5 | Historical | |
| LX10-2059 | -275.3 | 3956.4 | 3435.9 | 10.0 | -62.0 | 467.1 | Historical | |
| LX10-2056B | -275.3 | 3956.4 | 3435.9 | 0.0 | -60.0 | 637.0 | Historical | |
| W-0073 | 278.7 | 3975.4 | 4263.2 | 0.0 | -90.0 | 1098.5 | Historical | |

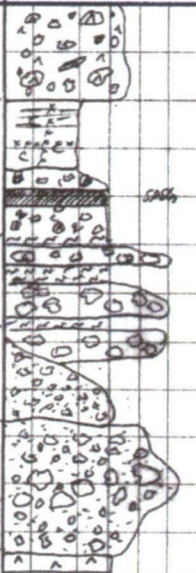
A1-2: Example of a detailed graphic log; LX10-2048

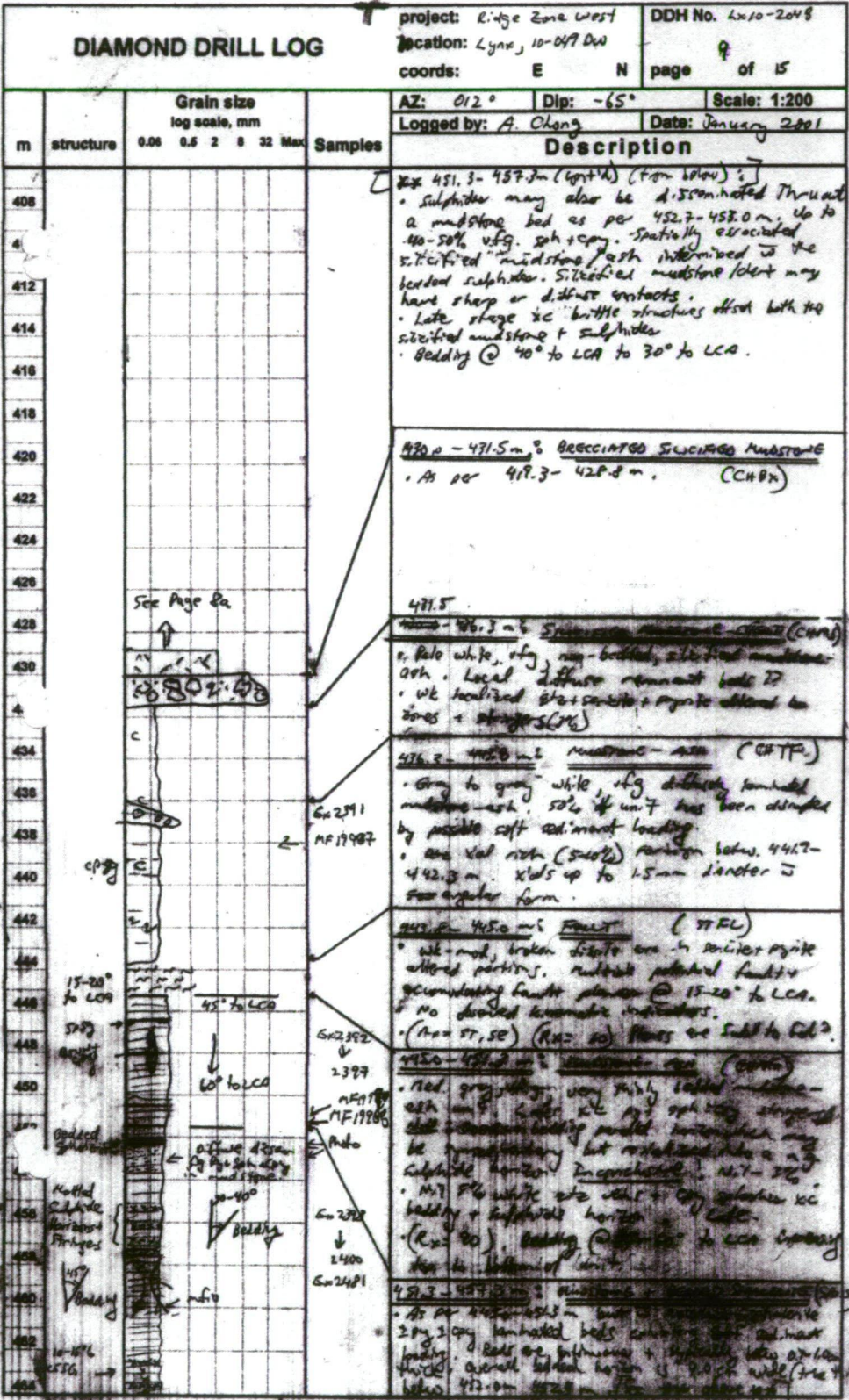
Section 050E: Lynx 10-049DW;

Collar at -1.8m E / 3958.2 m N / 3434.5 m elevation

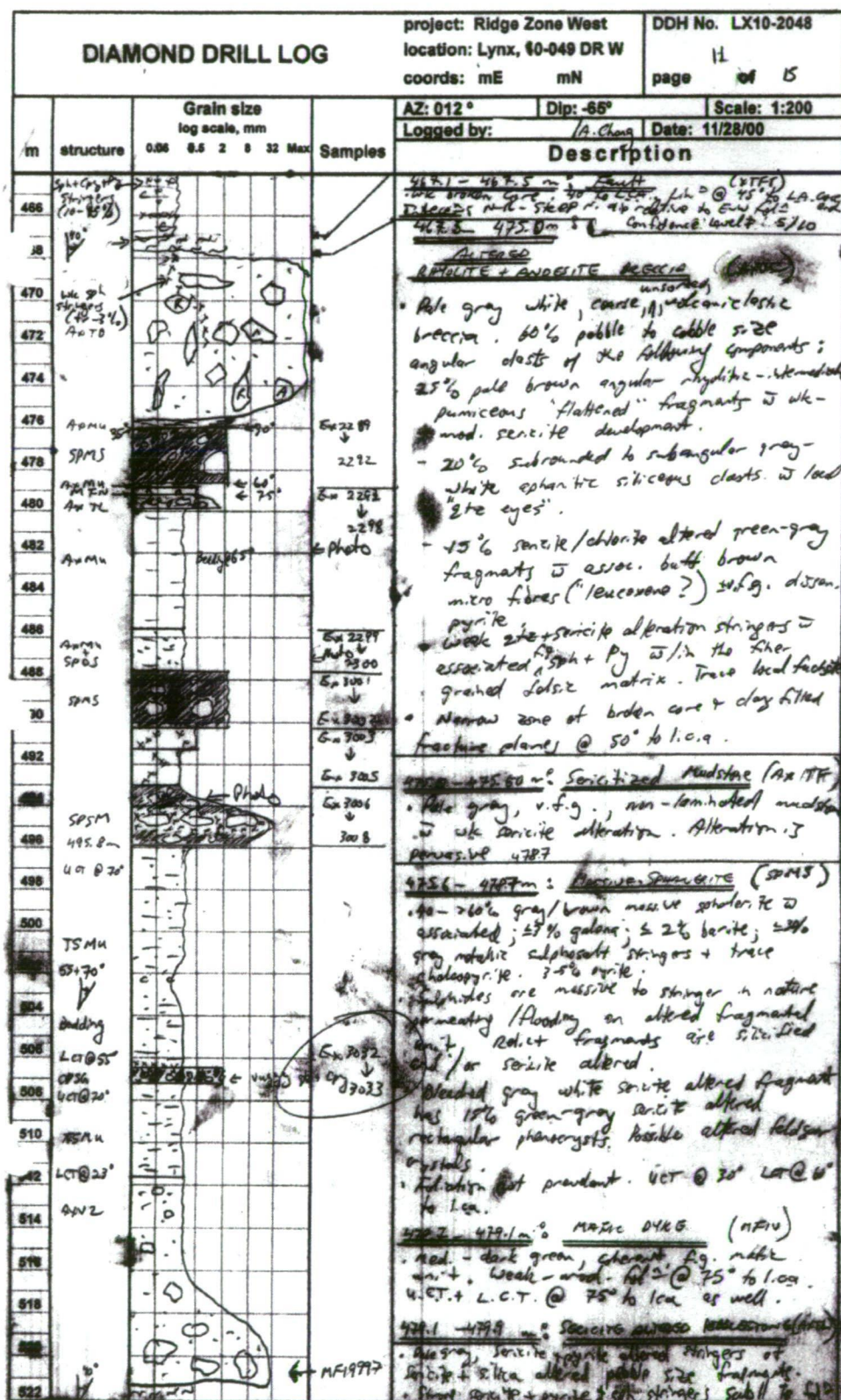


| DIAMOND DRILL LOG | | | | project: Ridge Zone West | DDH No. LX10-2048 | |
|-------------------|-----------|--|---------|--|-------------------|--------------|
| | | | | location: Lynx, 10-049 DR W. | | |
| | | | | coords: mE mN | page 7 of 15 | |
| m | structure | Grain size log scale, mm 0.06 0.5 2 8 32 Max | Samples | AZ: 012° | Dip: -65° | Scale: 1:200 |
| | | | | Logged by: A. Chong | Date: 11/28/00 | |
| Description | | | | | | |
| 350 | | | | 352.9 - 357.4 m: <u>MASSIVE ANDESITE (ADMS)</u> | | |
| 2 | | | | • Med-dark green, v. g - f g, massive, altered andesite. | | |
| | | | | • 15% stz + carbonate veins of late brittle shattering | | |
| 354 | | | | 357.4 - 358.5 m: <u>FAULT</u> (XFT) | | |
| 356 | | | | • 30° to LCA, clay filled planes. | | |
| 358 | | | | • Assoc. stz + carb. veining. Mod. slick. fault. | | |
| 360 | | | | • Relative EW strike with duk fts in edges | | |
| | | | | • Oblique dip slip fault | | |
| 362 | | | | • <u>Interd</u> : EW trending flat-mod dipping fault | | |
| | | | | as opposed to EW trending steep wrench | | |
| 364 | | | | Confidence Level = 5/10 R = 7/10 | | |
| 366 | | | | 358.5 - 381.8 m: <u>MASSIVE ANDESITE (ADMS)</u> | | |
| 368 | | | | • Red green, g - mg amphibole stz (10-20%) | | |
| | | | | massive coherent andesite | | |
| 370 | | | | • wk-mod epidote altz; patchy + pseudo fragmental texture to unit | | |
| 372 | | | | • (R = 80). | | |
| | | | | • 381.8 - 381.8 m: becoming progressively finer grained and bleached to a light green-grey colour. | | |
| 4 | | | | 381.8 - 382.0 m: <u>FAULT</u> (XFT) | | |
| 376 | | | | • Strong stz + carb. veining in mod. filled fracture plane @ 20° to LCA | | |
| | | | | • Inferred EW strike relative to a wt fault | | |
| 378 | | | | with adjacent massive andesite | | |
| 380 | | | | • <u>Interd</u> : Possible steep N. dipping EW strike fault. no LCA stz. Wrench ?? | | |
| | | | | CL = 5/10. | | |
| 382 | | | | 382.0 - 389.6 m: <u>ANDESITE FLOW / Rhyolite (ADFL)</u> | | |
| 384 | | | | • Red to light green massive andesite w | | |
| | | | | 5-10% to 10 mm amphibole phenocrysts. | | |
| 386 | | | | • 10% local micro breccia w glassy ft fragments | | |
| 388 | | | | 389.6 - 389.1 m: <u>Moderate stz + carbonate + 5% Pyrite stringers</u> | | |
| 390 | | | | 390.4 m: 5cm wide fg spy + spy stringer | | |
| | | | | within a 20cm wide breccia zone. | | |
| 392 | | | | 389.6 - 389.0 m: <u>FAULT</u> (XFT) | | |
| 394 | | | | • 30° to LCA. Reactivated | | |
| | | | | • Multiple locations trending EW wrench | | |
| 396 | | | | oblique dip slip @ ~ 20° to LCA of fault plane. | | |
| 398 | | | | • wk broken core + wk stz + carb. veining. | | |
| | | | | • (R = 50) <u>Interd</u> : Reactivated steep-mod dipping EW fault. | | |
| 400 | | | | 389.0 - 389.0 m: <u>ANDESITE FLOW BRECCIA (ADFB)</u> | | |
| 402 | | | | • Red-dark green, epidote altered, massive | | |
| | | | | brecciated coherent andesite | | |
| 404 | | | | • wk-mod. brecciation, which may be misinterpreted in part by pseudo fragmental textures via epidote alteration. | | |
| 406 | | | | • wk GCO, altz; mod. epidote patchy altz. | | |

| DIAMOND DRILL LOG | | | | | project: Ridge Zone West | DDH No. LX10-2048 | | | |
|-------------------|--|-----------------------------|-----|---|-----------------------------|-------------------|--|----------------|--------------|
| | | | | | location: Lynx, 10-049 DR W | 8 | | | |
| | | | | | coords: mE mN | page of 15 | | | |
| m | structure | Grain size log scale, mm | | | | | AZ: 012° | Dip: -65° | Scale: 1:200 |
| | | 0.06 | 0.5 | 2 | 8 | 32 Max | Logged by: A. Chong | Date: 11/28/00 | |
| | | | | | | | Description | | |
| 408 |  | | | | | | 405.4 - 410.0 m's <u>PAYMINT BRECCIA (PTBX)</u> • Polymet, unsorted, angular - subrounded fragmented in 30-40% fragments. 10-40mm along long axis. • Components of 0.6% leucocrystic massive, fig. coherent siderite; 15% subrounded s.l. clasts mudstone/chert fragments. • 10% fig. - ng pyrite pellets + disintegrated druses. One possible occurrence of pyrite "fagat" - rare waxy pyrite replacement of a prior clast of void. Interpretation: PAYMINT breccia along margin of massive to anhedral siderite flow. Fragments of a clast from flow as well as siliceous mudstone. Substrated from scouring. • LCT @ 40° to LCA. | | |
| 412 | | | | | | | 410.0 - 415.0 m's <u>MUDSTONE/CHERT (CHX)</u> • Med grey - white med g, siliceous mudstone. • Thinly bedded @ 45° to LCA. Local mud. Ph. + tectonic breccia zones created associated in pyrite-silica stockwork stringers (fig. ng pyrite). Stockwork stringers observed to be broadly parallel gr. as well as x-cutting bedding. | | |
| 414 | | | | | | | 415.0 - 417.0 m's <u>PAYMINT BRECCIA (PTBX)</u> • unsorted, polymet breccia in place. The fragments of siliceous mudstone (subrounded - angular), angular siderite, 10 mm etc. sh.?? | | |
| 416 | | | | | | | 417.0 - 418.5 m's <u>SPARKING SPONGE (SPSG)</u> • massive, orange-brown med. spherulitic 1 in. py. stringers in assoc. w/ sh + carbonate alteration (?). Trends sub parallel to LCP. Undulating while contact @ 65° to LCA. | | |
| 418 | | | | | | | 418.5 - 419.3 m's <u>FAULT (XFT)</u> • 40° to LCA • 30-60 cm fault breccia + gouge zones below. 30-60 cm wide. (K=50) • N-E lineations @ 30° to LCA of fault plane on one end. E-W trending relative to assumed faulted zone and. E-W trending relative to assumed faulted zone and. E-W trending relative to assumed faulted zone and. • Within a unit of subrounded white to grey white siliceous alt'd possible size fragments • Sh. fig. pyrite | | |
| 420 | | | | | | | 419.3 - 422.8 m's <u>PROCESSED SILICIFIED MUDSTONE (CHX)</u> • Pale white, sil. brecciated unit in spots, angular to subangular possible size fragments of laminated to non-laminated s.l. mudstone. The ph. very to rounded to angular form in fragments + matrix. Trace; up to 25-30 mm diameter. • Reddish pyrite + fig. - ng. subtotal pyrite altered - mineralized matrix. Wk. mud interst. | | |
| 422 | | | | | | | 422.8 - 427.0 m's <u>MAGNETIC DIKE (MDN)</u> • Medium green sil. mag. massive mag. dike. Sharp contacts @ 55° to LCA | | |
| 424 | | | | | | | | | |
| 426 | | | | | | | | | |
| 428 | | | | | | | | | |
| 430 | | | | | | | | | |
| 434 | | | | | | | | | |
| 436 | | | | | | | | | |
| 438 | | | | | | | | | |
| 440 | | | | | | | | | |
| 442 | | | | | | | | | |
| 444 | | | | | | | | | |
| 446 | | | | | | | | | |
| 448 | | | | | | | | | |
| 450 | | | | | | | | | |
| 452 | | | | | | | | | |
| 454 | | | | | | | | | |
| 456 | | | | | | | | | |
| 458 | | | | | | | | | |
| 460 | | | | | | | | | |
| 462 | | | | | | | | | |
| 464 | | | | | | | | | |

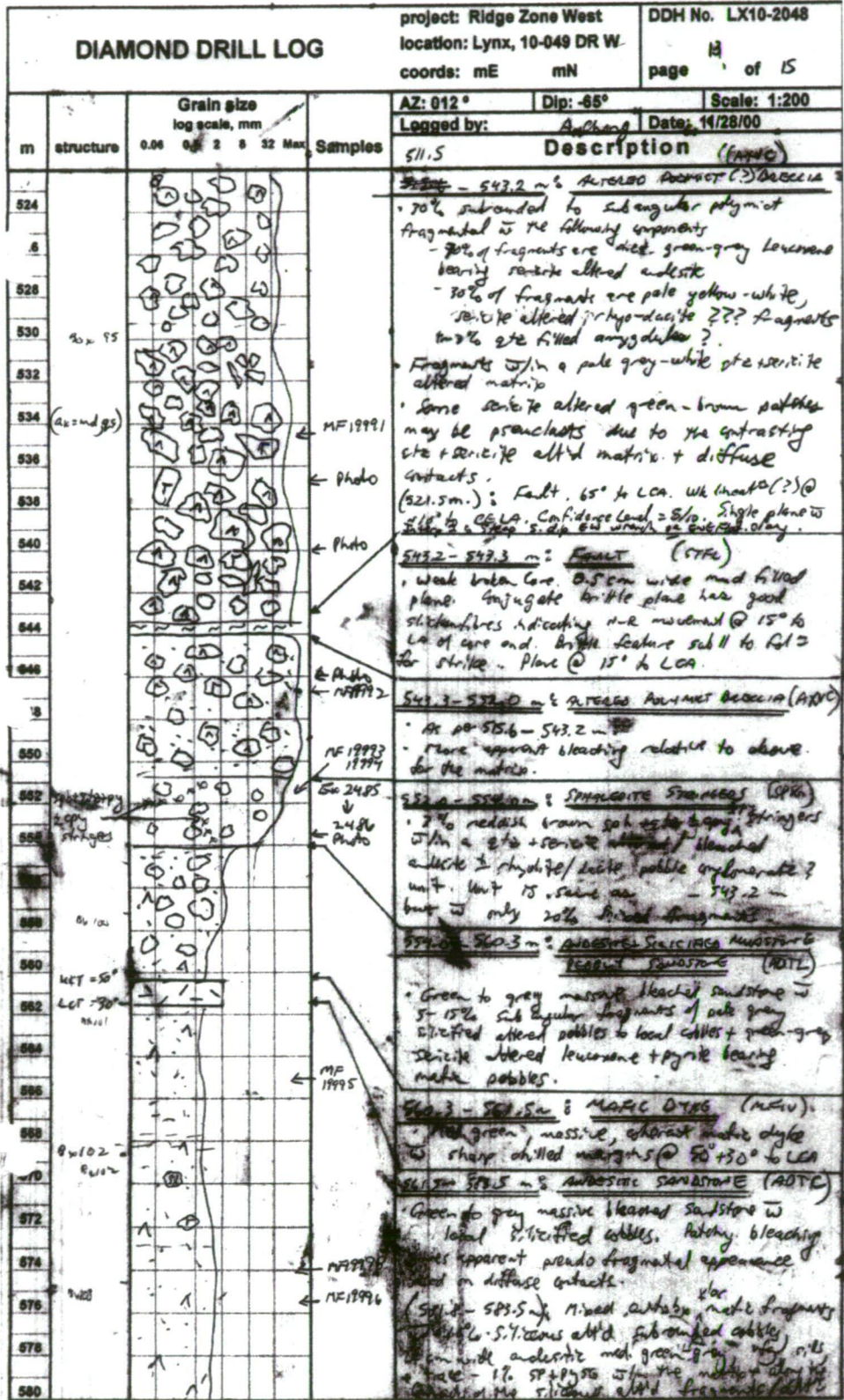


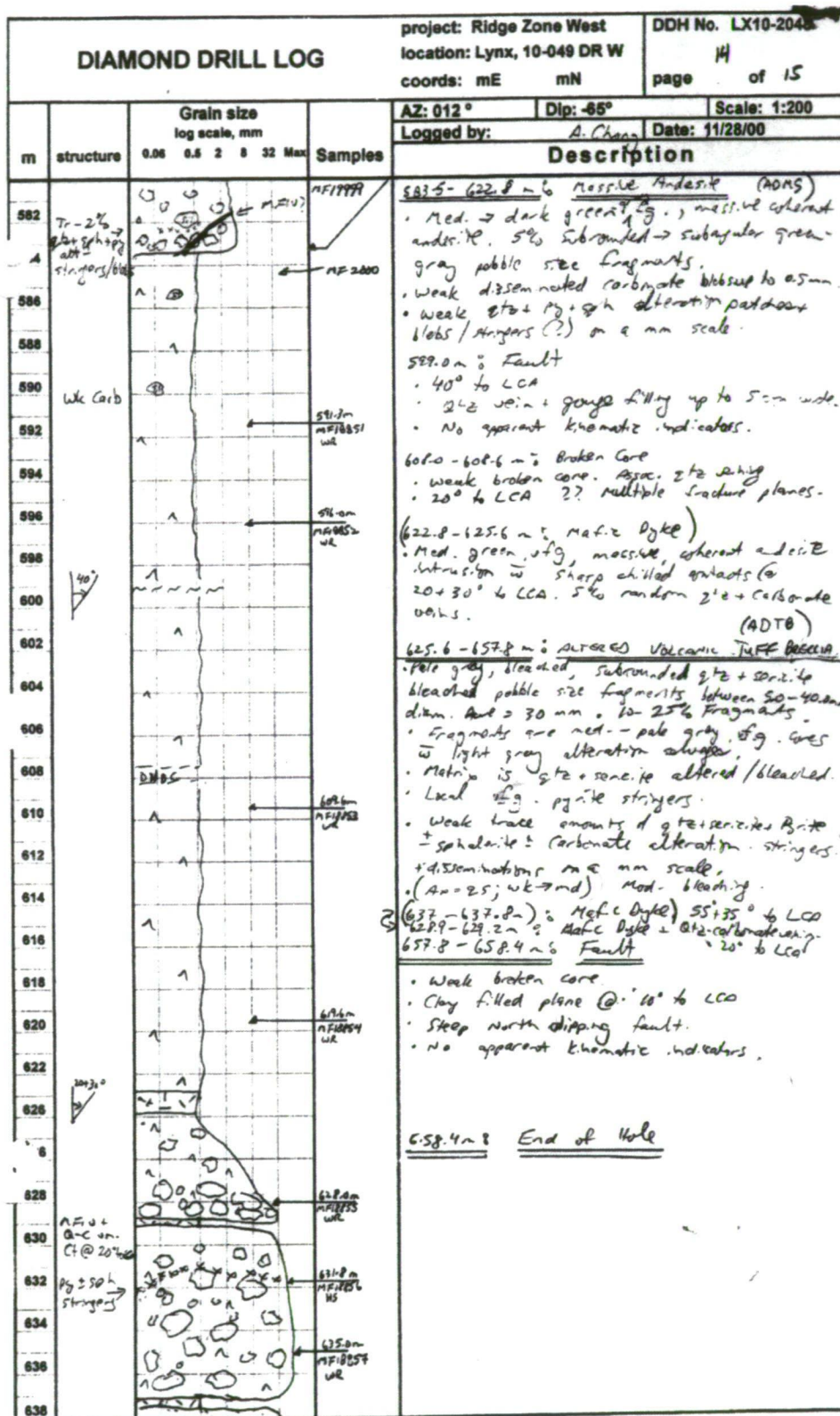
| DIAMOND DRILL LOG | | | | | project: Ridge Zone West | | DDH No. LX10-2048 | | |
|-------------------|-----------|-----------------------------|-----|---|---------------------------|-------------|---|--|--|
| | | | | | location: Lynx, 10-049 DW | | 10 | | |
| | | | | | coords: E N | | page 1 of 15 | | |
| | | | | | AZ: 012° | | Dip: -65° | | |
| | | | | | Logged by: A. Chong | | Scale: 1:200 | | |
| | | | | | | | Date: January 2001 | | |
| m | structure | Grain size log scale, mm | | | | Description | | | |
| | | 0.06 | 0.5 | 2 | 8 | 32 Max | | | |
| Samples | | | | | | | | | |
| 408 | | | | | | | 451.3 - 457.3 m: 5P01 (continued) | | |
| 410 | | | | | | | (452.7 - 452.8 m): Gray brown mudstone betw. 40-50% diam. vlg. sph + opy. Spatially associated w/ interbedded sulphides + silicified mudstone/chert. Silicified mudstone/chert may have sharp & diffuse contacts. | | |
| 412 | | | | | | | Late stage brittle xc structures offset both the silicified mudstone + overlying bedded sulphides between 452.0 - 452.5 m. | | |
| 414 | | | | | | | Bedding @ 30 + 40° to LCA. | | |
| 416 | | | | | | | Interpretation: | | |
| 418 | | | | | | | A fine mudstone - chert unit is deposition of synchronous sphalerite rich bedded sulphide on or very near the seafloor. Mottled + lenticular textures to both mudstone + sulphide indicate soft sediment loading. | | |
| 420 | | | | | | | | | |
| 422 | | | | | | | | | |
| 424 | | | | | | | | | |
| 426 | | | | | | | | | |
| 428 | | | | | | | | | |
| 430 | | | | | | | 457.3 - 457.5 m: <u>Greenish brown (mudstone)</u> (22) (DWC) | | |
| 432 | | | | | | | Moderate brown core to mud-filled planes @ 20° to LCA. No apparent laminar no. values. Planes @ mid to full. | | |
| 434 | | | | | | | 457.5 - 457.6 m: <u>Greenish brown (mudstone)</u> (22) (DWC) | | |
| 436 | | | | | | | Pale white to gray mudstone, strongly silicified, laminated to very thin bedded mudstone. | | |
| 438 | | | | | | | 10% vlg. sph + opy. silicified parallel + bedding xc structures. | | |
| 440 | | | | | | | Bedding @ 45° to LCA. | | |
| 442 | | | | | | | (457.7 - 458.6 m): <u>Mudstone</u> (22) (DWC) | | |
| 444 | | | | | | | Blended pale brown - green brown, dyed to enigmatis 40-2.5 mm diameter dark green chlorite (?) clots + 30-50 mm angular silicified mudstone - chert fragments; Encased from adjacent chert host. | | |
| 446 | | | | | | | Fine grained chert margins sub to contacts. | | |
| 448 | | | | | | | Contacts meander subparallel to mod. angles to LCA. | | |
| 450 | | | | | | | | | |
| 452 | | | | | | | | | |
| 454 | | | | | | | | | |
| 456 | | | | | | | | | |
| 458 | | | | | | | | | |
| 460 | | | | | | | | | |
| 462 | | | | | | | | | |
| 464 | | | | | | | | | |

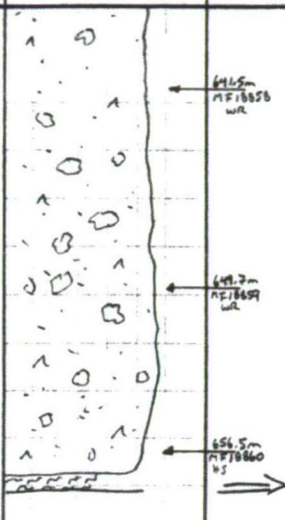


| DIAMOND DRILL LOG | | | | | project: Ridge Zone West | | DDH No. LX10-2048 | |
|-------------------|--------------------------|-----------------------------|-----|---|-----------------------------|-------------|---|---|
| | | | | | location: Lynx, 10-099 D.W. | | 12 | |
| | | | | | coords: E N | | page of 15 | |
| | | | | | AZ: 012 | | Dip: -6.5° | |
| | | | | | Logged by: A. Chong | | Scale: 1:200 | |
| | | | | | | | Date: 01/10/2001 | |
| m | structure | Grain size Log scale, mm | | | | Description | | |
| | | 0.06 | 0.5 | 2 | 8 | 32 | Max | Samples |
| 466 | See Strip Log on Page 11 | | | | | | | 466-481.9 m: <u>MUDSTONE (CHMS)</u> |
| 470 | | | | | | | | • Pale gray-brown, v.f.g., massive mudstone. |
| 472 | | | | | | | | • 3-5% silt filled gashes + mottled cavities |
| 474 | | | | | | | | to milky white silt w assoc. py + sph ± annularite- tetradite. Sph. occur as either granular |
| 476 | | | | | | | | across long axis of vein or as a laminated |
| 478 | | | | | | | | mass lining. |
| 480 | | | | | | | | • UCT @ 70' to LCA. LCT @ 40' to LCA |
| 482 | | | | | | | | 481.9-485.2 m: <u>CHERTY MUDSTONE (CHMS)</u> |
| 484 | | | | | | | | • Pale gray green v.f.g. massive to thinly bedded |
| 486 | | | | | | | | siltified mudstone. Siltification is variable to pale |
| 488 | | | | | | | | • UCT @ 40' to LCA. LCT @ 55' to LCA |
| 490 | | | | | | | | • Trace local 0.5 mm wide translucent silt |
| 492 | | | | | | | | veins x/c mudstone as stringers ± |
| 494 | | | | | | | | • Stringers x/c mudstone + stringers ± |
| 496 | | | | | | | | represented by 0.5 mm wide silt + py + sph |
| 498 | | | | | | | sub. H to bedding. | |
| 500 | | | | | | | 485.2-490.2 m: <u>MASSIVE SEMI-CRYSTALLINE (SAMS)</u> | |
| 502 | | | | | | | • Black to brown semi-massive to massive silt | |
| 504 | | | | | | | stringers + veins to trace to 15% mg. sub. H to | |
| 506 | | | | | | | pyrite + cpy stringers increasing downhole. | |
| 508 | | | | | | | • Trace 20% gray altered remnants of host rock | |
| 510 | | | | | | | occurring as a subrounded pebbly fragmental | |
| 512 | | | | | | | texture within the sulphide. Fragmental | |
| 514 | | | | | | | texture increases downhole. | |
| 516 | | | | | | | • Top of unit is a gray massive sandstone | |
| 518 | | | | | | | which grades from weakly disseminated | |
| 520 | | | | | | | to massively mineralized down unit. | |
| 522 | | | | | | | • Interpretation: locally normally graded | |
| | | | | | | | pebbly sandstone which has a partially | |
| | | | | | | | replaced by sph + py ± cpy veins, pervasive | |
| | | | | | | | flooding, + dissemination. | |
| | | | | | | | • Cpy stringers @ 45' to LCA (CHSS) | |
| | | | | | | | 490.2-495.8 m: <u>SEMIMASSIVE + CHALCOPRITE SANDSTONE</u> | |
| | | | | | | | • 5-25% sph + py ± cpy veins + stringers cross-cutting | |
| | | | | | | | a pale gray host. | |
| | | | | | | | • Host is an altered unit which appears | |
| | | | | | | | to be massive coherent to brittle structure | |
| | | | | | | | texture + assoc. sph + py ± cpy ± silica sub. H to | |
| | | | | | | | stringer. H. H. along to 50 cm wide zone | |
| | | | | | | | of siltified unsorted subangular, volcanoclastic | |
| | | | | | | | pebbles 5-11.5 m | |
| | | | | | | | 495.8-500.3 m: <u>MUDSTONE (CHMS)</u> | |
| | | | | | | | • Pale gray, f.g. - v.f.g., massive mudstone w | |
| | | | | | | | local very thin bedded sections. | |
| | | | | | | | • Beds @ 65-75' to LCA | |
| | | | | | | | • Patches of siltified mudstone (host) intertonguing | |
| | | | | | | | dominantly moderately siltified mudstone-like | |
| | | | | | | | sandstone. | |
| | | | | | | | • Trace mg. sub. H to pyrite ± sph ± brown semite | |
| | | | | | | | stockwork mineralization silt. to bedding as | |
| | | | | | | | well as locally x/c bedding | |
| | | | | | | | (500.3-504.3 m: <u>5 MINOR CPG stringers</u>) | |
| | | | | | | | assoc. to vuggy silt + cpy veins. | |

See Strip Log on Page 11





| DIAMOND DRILL LOG | | | | project: Ridge Zone West location: Lynx, 10-049 DR W coords: mE mN | | DDH No. LX10-2043 15 page of 15 | |
|-------------------|-----------|--|---------|--|--|---------------------------------------|--|
| m | structure | Grain size log scale, mm 0.06 0.5 2 8 32 Max | Samples | AZ: 012° Dip: -65° Scale: 1:200 | | Logged by: A. Chong Date: 11/28/00 | |
| | | | | Description | | | |
| 640 | |  | | • See Descriptions on page 11. | | | |
| 642 | | | | | | | |
| 644 | | | | | | | |
| 646 | | | | | | | |
| 648 | | | | | | | |
| 650 | | | | | | | |
| 652 | | | | | | | |
| 654 | | | | | 657.8-658.4m: Fault (XFT) • see description on page 11. | | |
| 656 | | | | | | | |
| 658 | | | | | <u>658.4m: End of Hole</u> | | |
| 660 | | | | | | | |
| 662 | | | | | | | |
| 664 | | | | | | | |
| 666 | | | | | | | |
| 668 | | | | | | | |
| 670 | | | | | | | |
| 672 | | | | | | | |
| 674 | | | | | | | |
| 676 | | | | | | | |
| 678 | | | | | | | |
| 680 | | | | | | | |
| 682 | | | | | | | |
| 684 | | | | | | | |
| 686 | | | | | | | |
| 688 | | | | | | | |
| 690 | | | | | | | |
| 692 | | | | | | | |
| 694 | | | | | | | |
| 696 | | | | | | | |

APPENDIX 2: Legend and Sample Catalogue

Appendix A2-1: Legend

Appendix A2-2: Sample catalogue

Appendix A2-1: Legend

| Table A2-1: Lithology Legend | |
|------------------------------|--|
| CODE | NAME |
| A3BX | andesite-dacite-rhyolite-argillite-cherty breccia |
| A4BX | andesite-dacite-rhyolite-argillite-chert-sulphide breccia |
| ACVC | andesite-dacite volcanoclastic |
| ADBX | andesite breccia |
| ADCT | andesite coarse tuff |
| ADFL | andesite flow |
| ADMS | andesite massive |
| ADTC | andesite coarse tuff |
| ADTF | andesite fine tuff |
| ADTL | andesite tuffaceous pebblestone |
| ADVC | andesite volcanoclastic |
| AHTL | andesite rhyolite pebblestone |
| ARMS | massive argillite |
| AXBX | altered breccia |
| AXFL | altered flow |
| AXMS | altered massive |
| AXTF | altered tuffaceous sandstone |
| AXVC | altered volcanoclastic (pebble or coarser) |
| BAVN | barite vein |
| CHBX | siliceous mudstone breccia |
| CHMS | siliceous mudstone massive |
| CHMU | siliceous mudstone |
| CHTF | siliceous tuffaceous mudstone-sandstone |
| CPDS | chalcopryite disseminated |
| CPSG | chalcopryite stringers-veins |
| CSSG | chalcopryite-sphalerite stringers-veins |
| DAVC | dacite-andesite volcanoclastic |
| IMV1 | intermediate volcanoclastic |
| MDST | mudstone undefined |
| MFBX | mafic breccia |
| MFIV | mafic intrusion |
| MFMS | mafic massive |
| OCBX/OCB | ore clast breccia |
| PYDS | pyrite disseminated |
| PYSG | pyrite stringers-veins |
| PYSM | pyrite semi-massive |
| PYMS | pyrite massive |
| QTVN | quartz vein |
| RABX | rhyolite andesite breccia |
| RDBX | rhyolite dacite breccia |
| RDVC | rhyolite dacite volcanoclastic |
| RGTL | rhyolite argillite tuffaceous pebblestone |
| RHBX | rhyolite breccia |
| RHVC | rhyolite volcanoclastic |
| SDST | sandstone |
| SPDS | sphalerite disseminated (+/-polymetallic) |
| SPMS | sphalerite massive (polymetallic) |
| SPSG | sphalerite stringers-veins (+/-polymetallic) |
| SPSM | sphalerite semi-massive (polymetallic) |
| SRSC | sericite schist |
| SSDS | sulphide disseminated (pyrite-chalcopryite+/-sphalerite+/-galena+/-tennantite) |
| SSSG | sulphide stringers-veins (pyrite-chalcopryite+/-sphalerite+/-galena+/-tennantite) |
| TSV2 | tuffaceous sandstone-upper stratigraphy |
| Abbreviations: | ax/alt-d-altered; tr-trace; wk-weak; md/mod-moderate; st/str-strong ad-andesite; rh/rhy-rhyolite; rd/rhyodac-rhyodacite; co3-carbonate; qcv's - quartz carbonate veins; qf-quartz-feldspar; qs-quartz-sericite ba-barite; cc-calcite; cp-chalcopryite; gn-galena; py-pyrite; sp-sphalerite; tt-tetrahedrite-tennantite amph-amphibole; chl-chlorite; epi-epidote; leucx-leucoxene; qt/qtz-quartz; se/ser-sericite fw-footwall; hw-hangingwall; volc-volcanic bx-breccia; frag/fragl-fragmental; lam-laminated; polymt-polymict; silicd- silicified; vn-vein; xal-crystal gn-green; gry-grey; ylw-yellow |

| DDH | Sample | Depth (m) | Code | Comments | HS | PTS | EMP |
|-----------------------|---------|-----------|---|-------------------------------|----|-----|-----|
| LX10-2040 | MF19901 | 383.0 | ADMS | qtz+co3vn | Y | Y | |
| LX10-2040 | MF19902 | 407.0 | ADMS | qtz+co3vn | Y | Y | |
| LX10-2040 | MF19903 | 447.0 | ADMS | qtz+co3vn | Y | | |
| LX10-2040 | MF19914 | 455.7 | RHBX | py+sph+tt/sg | Y | Y | |
| LX10-2040 | MF18939 | 461.5 | QTVN | Qz+gn vuggy epi vein? | Y | Y | |
| LX10-2040 | MF19915 | 474.2 | CHBX | SPSG(RZW) | Y | Y | |
| LX10-2040 | MF18940 | 475.3 | MDST | Gry; matrix betw cssg+chtl | Y | Y | |
| LX10-2040 | MF19916 | 476.5 | SPMS | SSDS | Y | | Y |
| LX10-2040 | MF19917 | 476.7 | SPMS | CPSG | Y | Y | |
| LX10-2040 | MF18941 | 478.0 | MDST | Gry; mottled mdst | Y | Y | |
| LX10-2040 | MF19918 | 481.2 | RHVC | PYSG+CPSG; red spsg | Y | Y | Y |
| LX10-2040 | MF19919 | 481.5 | RHVC | gr. Mica/ssds; pumice? | Y | Y | |
| LX10-2040 | MF19920 | 486.8 | RHVC | polymt bx; | Y | Y | |
| LX10-2040 | MF19921 | 506.8 | ARMS | Black mdst;Bedded PY | Y | Y | |
| LX10-2040 | MF19922 | 508.6 | ARMS | Black mdst | Y | Y | |
| LX10-2040 | MF18942 | 513.0 | SDST | Top of mass flow | Y | | |
| LX10-2040 | MF19904 | 527.5 | RHVC | | Y | Y | |
| LX10-2040 | MF19905 | 533.5 | SDST | | Y | | |
| LX10-2040 | MF19906 | 542.1 | SDST | RHVC | Y | | |
| LX10-2040 | MF19907 | 547.6 | RHBX | | Y | Y | |
| LX10-2040 | MF19908 | 572.5 | ADTF | RHVC | Y | Y | |
| LX10-2040 | MF19909 | 574.8 | ADVC | RHVC | Y | Y | |
| LX10-2040 | MF19910 | 577.7 | ADVC | | Y | | |
| LX10-2040 | MF19911 | 579.5 | ADVC | altd?; DAVC; amygdules | Y | Y | |
| LX10-2040 | MF19912 | 593.0 | ADMS/TF | altd?; DAVC; amygdules | Y | Y | |
| LX10-2040 | MF19913 | 609.5 | ADVC | altd?; DAVC; amygdules | Y | | |
| LX10-2041 | MF19875 | 320.6 | ADTF | diffusely bedded | Y | | |
| LX10-2041 | MF19876 | 338.1 | TSV2 | tuffaceous lapillist | Y | Y | |
| LX10-2041 | MF19877 | 360.5 | A3BX | clast free matrix | Y | | |
| LX10-2041 | MF19878 | 377.5 | A3BX | | Y | Y | |
| LX10-2041 | MF19923 | 419.5 | ADCT | | Y | | |
| LX10-2041 | MF19924 | 433.0 | ADBX | FP; SILL? Pseudobx? | Y | Y | |
| LX10-2041 | MF19925 | 436.0 | ADFL | FP; SILL? Pseudobx? | Y | | |
| LX10-2041 | MF19926 | 460.0 | ADBX | | Y | | |
| LX10-2041 | MF19927 | 473.0 | ADTC | monomictic | Y | Y | |
| LX10-2041 | MF19928 | 480.0 | CHBX | white silicic mdst; 5% pysg | Y | Y | |
| LX10-2041 | MF19929 | 485.0 | RHVC | polymict; frag types | Y | Y | |
| LX10-2041 | MF19930 | 541.5 | RHVC | polymict; frag types | Y | Y | |
| LX10-2041 | MF19931 | 543.0 | A3BX | No clasts; rhy? | Y | | |
| LX10-2041 | MF19932 | 548.5 | A3BX | siliceous siltst clasts | Y | | |
| LX10-2041 | MF19933 | 572.0 | IMV1 | volc sdst; qt grains | Y | Y | |
| LX10-2041 | MF19934 | 585.5 | IMV1 | volc sdst | Y | Y | |
| LX10-2042 | MF19935 | 477.5 | ADBX | RDVC | Y | | |
| LX10-2042 | MF19936 | 495.0 | RDVC | AD matrix; pseudofrag? | Y | | |
| LX10-2042 | MF19937 | 499.0 | RDVC | PEBBLE; AD matrix | Y | Y | |
| LX10-2042 | MF19938 | 515.5 | ADBX | Flow top bx; siliceous clasts | Y | Y | |
| LX10-2042 | MF19939 | 524.0 | ADMS | Tr. QV's | Y | | |
| LX10-2042 | MF19940 | 529.0 | ADMS | | Y | | |
| LX10-2042 | MF19941 | 597.1 | TSV2 | Pebblest; ser+qtz+co3 | Y | Y | |
| LX10-2042 | MF19942 | 632.0 | AXFL | CO3 altn | Y | Y | |
| LX10-2042 | MF19943 | 642.0 | AXFL | CO3+ser altn | Y | | |
| Abbreviations: | | | Code - see Table A2-1 Legend; Comments - see Table A2-1 Legend; HS - hand sample; PTS - polished thin section; EMP - electron microprobe | | | | |

Table A2-2.2: Ridge Zone West Sample Catalogue

| DDH | Sample | Depth (m) | Code | Comments | HS | PTS | EMP |
|-----------------------|---------|---|------|--|----|-----|-----|
| LX10-2043 | MF19957 | 286.5 | ADMS | 0+25E | Y | | |
| LX10-2045 | MF19971 | 556.0 | ADTF | 2% qcvn's | Y | | |
| LX10-2045 | MF19972 | 560.1 | ADBx | | Y | | |
| LX10-2045 | MF19973 | 613.0 | ADBx | | Y | | |
| LX10-2045 | MF19974 | 569.9 | ADBx | | Y | | |
| LX10-2045 | MF19944 | 435.7 | ADMS | Tr QCV; 1% c.g. pyds | Y | | |
| LX10-2045 | MF19945 | 439.0 | CHMS | Sandy matrix to chms sampled | Y | Y | |
| LX10-2045 | MF19946 | 447.4 | CPSG | Polymict pebblest host; altd and+scoria components | Y | Y | Y |
| LX10-2045 | MF19947 | 450.0 | MDST | mdst; ax=wk;se; tr vfg dissem py | Y | Y | Y |
| LX10-2045 | MF19948 | 464.0 | MFBx | Peperitic cts; hyalocl; sandy matr; | Y | Y | |
| LX10-2045 | MF19949 | 469.0 | CHBx | QE's??? Or altn | Y | Y | |
| LX10-2045 | MF18928 | 472.6 | SPSG | Replacing argillite; subl to lca; ragged cts | Y | Y | |
| LX10-2045 | MF18929 | 473.5 | SPSM | Replacing argillite; subl to lca; ragged cts | Y | Y | |
| LX10-2045 | MF18930 | 474.0 | CSSG | Replacing polymict pebblest in argillite | Y | Y | Y |
| LX10-2045 | MF18932 | 478.5 | CSSG | 20% scsg throug argillite+altd scoria fragmental | Y | Y | |
| LX10-2045 | MF18933 | 481.0 | SPMS | SPMS w 5% Gn+9%Cpy; 2.5g/t Au, 527g/t Ag; 1% Ba | Y | Y | Y |
| LX10-2045 | MF18934 | 483.0 | CHTF | vfg pyds+/-Ba?; 0.7%Cu, 0.5%Pb; 5% Zn, 4% Ba | Y | Y | |
| LX10-2045 | MF18935 | 485.0 | SPSM | xc by cp+sp+gnsg in polymict host | Y | Y | |
| LX10-2045 | MF18936 | 486.7 | BAVN | Hydrothermal vein; silica-Cc-Ba-Gn-Ser zoning | Y | Y | Y |
| LX10-2045 | MF18937 | 493.0 | MDST | Diffuse mottled beds; fw to zone | Y | Y | |
| LX10-2046 | MF19961 | 402.6 | ADMS | fsp phyrlic | Y | | |
| LX10-2046 | MF19962 | 420.6 | ADMS | | Y | | |
| LX10-2046 | MF19963 | 432.8 | ADMS | under flowtop | Y | | |
| LX10-2046 | MF19964 | 453.3 | CHMU | wk sssg; ax=md;si | Y | | |
| LX10-2046 | MF19965 | 456.7 | CHBx | strong sssg | Y | | |
| LX10-2046 | MF19966 | 457.0 | CHBx | mod sssg | | | |
| LX10-2046 | MF19967 | 468.5 | CHMU | Laminated; green-white; ax=md;qs; 5%pysg+silica | Y | | |
| LX10-2046 | MF19968 | 469.5 | CHBx | sssg | Y | | |
| LX10-2046 | MF19969 | 479.5 | RHVC | sssg | Y | | |
| LX10-2046 | MF19970 | 483.2 | CHMU | lam mudst; white; ax=st;si | Y | | |
| LX10-2046 | MF18938 | 492.0 | MDST | Grey; massive; ax=md;se; 1% pysg | Y | | |
| LX10-2046 | MF19975 | 501.3 | AXVC | polymt bx; qt xal | Y | | |
| LX10-2046 | MF19976 | 508.0 | AXVC | qs altd polymt bx | Y | | |
| LX10-2046 | MF19977 | 512.8 | AXVC | altd cobble bx; sssg | Y | | |
| LX10-2046 | MF19978 | 521.3 | AXVC | altd qt phyrlic bx; spds | Y | Y | |
| LX10-2046 | MF19979 | 524.2 | ADTL | ad pebbly sdst | Y | | |
| LX10-2046 | MF19980 | 527.5 | AXVC | polymt bx; qt xal | Y | | |
| LX10-2046 | MF19981 | 530.9 | AXVC | altd pebblest | Y | | |
| LX10-2046 | MF19982 | 535.3 | IMV1 | altd sdst; qtz xal bearing | Y | | |
| LX10-2046 | MF19983 | 552.9 | AXVC | bleached fragl | Y | | |
| LX10-2046 | MF19984 | 561.0 | AXTF | co3 altd sdst | Y | | |
| LX10-2046 | MF19985 | 571.5 | IMV1 | pebbly-sdst | Y | | |
| LX10-2046 | MF18890 | 583.0 | ADMS | md caco3 | Y | | |
| LX10-2046 | MF18891 | 595.5 | ADMS | md caco3 | Y | | |
| LX10-2046 | MF18892 | 607.0 | ADMS | 15% dissem. leucx | Y | | |
| LX10-2046 | MF18893 | 613.0 | ADMS | | Y | | |
| LX10-2046 | MF18894 | 623.0 | ADTC | 10-15% leucx; dac+/-"rhy" pebbles | Y | | |
| Abbreviations: | | Code - see Table A2-1 Legend; Comments - see Table A2-1 Legend; HS - hand sample; PTS - polished thin section; EMP - electron microprobe | | | | | |

| DDH | Sample | Depth (m) | Code | Comments | HS | PTS | EMP |
|-----------------------|---------|---|------|------------------------------------|----|-----|-----|
| LX10-2048 | MF19986 | 428.8 | CHBX | 3-5% pysg | Y | Y | |
| LX10-2048 | MF19987 | 439.8 | CHBX | cssg | Y | Y | |
| LX10-2048 | MF19988 | 451.5 | MDST | mdst loading | | | |
| LX10-2048 | MF19989 | 452.3 | SPMS | bedded ms+chert ct | Y | Y | |
| LX10-2048 | MF19990 | 452.8 | MDST | csds in mdst | Y | Y | Y |
| LX10-2048 | MF18871 | 463.2 | SPMS | mudst replacemt | Y | Y | |
| LX10-2048 | MF18872 | 466.5 | SPSG | 3%scgsg; mudst replacemt; tr. Pyds | Y | Y | |
| LX10-2048 | MF18876 | 474.0 | AXVC | polymt bx betw minlzn | Y | Y | |
| LX10-2048 | MF18873 | 476.0 | SPSM | axvc replacemt | Y | Y | Y |
| LX10-2048 | MF18874 | 479.5 | AXVC | qs altn | Y | Y | Y |
| LX10-2048 | MF18875 | 480.5 | MDST | qt+py+/-cpy epi(?) vein | Y | Y | |
| LX10-2048 | MF18880 | 495.0 | MDST | 15-20% cssg | Y | Y | Y |
| LX10-2048 | MF19997 | 520.8 | AXVC | polymt bx | Y | Y | |
| LX10-2048 | MF19991 | 534.5 | AXVC | polymt bx | Y | Y | |
| LX10-2048 | MF19992 | 546.5 | AXVC | bleached polymt bx | Y | Y | |
| LX10-2048 | MF19993 | 551.0 | AXVC | cssg in bleached polymt bx | Y | | |
| LX10-2048 | MF19994 | 553.5 | AXVC | cssg in bleached polymt bx | Y | Y | |
| LX10-2048 | MF18877 | 554.5 | AXVC | ser alt fragl | Y | | |
| LX10-2048 | MF19995 | 565.5 | ADTF | Bleached sdst; siliceous pebbles | Y | Y | |
| LX10-2048 | MF19996 | 575.5 | ADTF | FW / qt xals??? | Y | | |
| LX10-2048 | MF19998 | 574.0 | ADMS | | Y | | |
| LX10-2048 | MF19999 | 581.9 | AXVC | siliceous clast in adtf; sssg | Y | | |
| LX10-2048 | MF20000 | 584.5 | ADMS | | Y | | |
| LX10-2048 | MF18851 | 591.3 | ADMS | not altd; wk qcv; 2% pyds | Y | | |
| LX10-2048 | MF18852 | 596.0 | ADMS | wk qcv | Y | | |
| LX10-2048 | MF18853 | 609.6 | ADMS | 2% f.g. pyds | Y | Y | |
| LX10-2048 | MF18854 | 619.6 | ADMS | fresh | Y | | |
| LX10-2048 | MF18855 | 628.0 | AXVC | matrix only; wk ser | Y | | |
| LX10-2048 | MF18856 | 631.8 | AXVC | wk-md ser+py+/-sph; wk co3 | Y | Y | |
| LX10-2048 | MF18857 | 635.0 | AXVC | matrix only; wk ser+py+co3 | Y | | |
| LX10-2048 | MF18858 | 641.5 | AXVC | matrix only; wk ser | Y | | |
| LX10-2048 | MF18859 | 649.7 | AXVC | wk ser; tr. pyds+/-cpds | Y | | |
| LX10-2048 | MF18860 | 656.5 | AXVC | ssds | Y | Y | |
| LX10-2049 | MF18881 | 286.0 | ADTF | 3% qcv | Y | | |
| LX10-2049 | MF18882 | 298.7 | ADTF | | Y | | |
| LX10-2049 | MF18883 | 340.0 | OCB | polymt OCB with mdst ct | Y | | |
| LX10-2049 | MF18884 | 344.2 | OCB | qf xal tuff mx in polymt OCB | Y | | |
| LX10-2049 | MF18885 | 359.7 | ADMS | | Y | | |
| LX10-2049 | MF18886 | 370.5 | ADMS | | Y | | |
| LX10-2049 | MF18887 | 351.4 | A4BX | q xal tuff mx + 10-25% cssg | Y | | |
| LX10-2049 | MF18888 | NS | SPSG | in qf xal tuff matrix in OCB | Y | | |
| LX10-2049 | MF18889 | 350.5 | OCB | ad+rh q xal matr | Y | | |
| LX10-2049 | MF18878 | 487.2 | MDST | 5% f.g. pyds | Y | Y | |
| LX10-2049 | MF18879 | 488.5 | MDST | bedded primary sph | Y | Y | |
| LX10-2049 | MF18861 | 658.6 | ADMS | wk ser+qcv | Y | | |
| LX10-2049 | MF18862 | 653.0 | ADMS | | Y | | |
| LX10-2049 | MF18863 | 625.5 | ADMS | ms to fx | Y | | |
| LX10-2049 | MF18864 | 611.5 | ADMS | chl+ser | Y | | |
| LX10-2049 | MF18865 | 588.0 | ADMS | | Y | | |
| LX10-2049 | MF18866 | 570.5 | ADMS | 2% co3 blebs | Y | | |
| LX10-2049 | MF18867 | 563.0 | ADMS | adj fault; wk ser+co3 | Y | | |
| LX10-2049 | MF18868 | 553.0 | AXVC | qs altd clast in axvc | Y | | |
| LX10-2049 | MF18869 | 545.2 | AXVC | qs altd clast in axvc | Y | | |
| LX10-2049 | MF18870 | 536.5 | AXVC | frags | Y | | |
| Abbreviations: | | Code - see Table A2-1 Legend; Comments - see Table A2-1 Legend; HS - hand sample; PTS - polished thin section; EMP - electron microprobe | | | | | |

| DDH | Sample | Depth (m) | Code | Comments | HS | PTS | EMP |
|-----------------------|---------|---|------|---------------------------|----|-----|-----|
| LX10-2035 | MF19879 | 482.0 | ADCT | | Y | | |
| LX10-2035 | MF19880 | 491.5 | ADBX | | Y | | |
| LX10-2035 | MF19881 | 499.6 | RHBX | | Y | | |
| LX10-2035 | MF19882 | 396.0 | MFIV | diorite chilled margin | Y | | |
| LX10-2035 | MF19883 | 400.0 | MFIV | diorite intrn | Y | | |
| LX10-2035 | MF19884 | 416.5 | MFIV | | Y | | |
| LX10-2035 | MF19885 | 502.5 | SPSG | srsc; see racks; bx 90 | Y | | |
| LX10-2035 | MF19886 | 506.5 | SRSC | bx 90; sssg | Y | | |
| LX10-2035 | MF19887 | 511.2 | CHBX | bx 91; sp+pysg | Y | Y | |
| LX10-2035 | MF19888 | 520.0 | AXVC | bx 93; rdbx; tr spds | Y | Y | |
| LX10-2035 | MF19889 | 528.5 | AXVC | FW; qt+ser altn | Y | | |
| LX10-2035 | MF19890 | 543.8 | AXVC | altd fw | Y | | |
| LX10-2035 | MF19891 | 556.0 | AXVC | altd fw | Y | | |
| LX10-2035 | MF19892 | 566.0 | AXVC | altd fw | Y | Y | |
| LX10-2035 | MF19893 | 576.5 | AXVC | altd fw | Y | | |
| LX10-2035 | MF19894 | 586.6 | ADTF | tr pyds | Y | | |
| LX10-2035 | MF19895 | 600.0 | ADMS | tr py+/-cpsg | Y | | |
| LX10-2035 | MF19896 | 609.0 | ADMS | chl+epi+ser altn | Y | | |
| LX10-2035 | MF19897 | 621.5 | ADBX | altd? | Y | | |
| LX10-2035 | MF19898 | 632.5 | AXMS | wk-md ser altn | Y | | |
| LX10-2035 | MF19899 | 646.0 | ADMS | bleached; 7% caco3 dissem | Y | | |
| LX10-2035 | MF19900 | 668.0 | ADMS | str ser altn; wk caco3 | Y | | |
| LX10-2035 | MF19950 | 691.0 | ADMS | | Y | | |
| LX10-2036 | MF19951 | 357.5 | ADBX | sill | Y | | |
| LX10-2036 | MF19952 | 310.5 | MFIV | diorite dyke | Y | | |
| LX10-2036 | MF19953 | 306.5 | MFIV | diorite dyke | Y | | |
| LX10-2036 | MF19956 | 519.7 | AXVC | polymt; leucox??? | Y | | |
| LX10-2036 | MF19958 | 517.0 | AXVC | same as mf19956 | Y | | |
| LX10-2036 | MF19959 | 502.5 | ADMS | patchy epi | Y | | |
| LX10-2036 | MF19960 | 579.0 | RABX | mass flow | Y | | |
| LX10-2036 | MF19954 | 629.0 | ADMS | | Y | | |
| LX10-2036 | MF19955 | 608.5 | ADMS | fw; md caco3 altn | Y | | |
| Abbreviations: | | Code - see Table A2-1 Legend; Comments - see Table A2-1 Legend; HS - hand sample; PTS - polished thin section; EMP - electron microprobe | | | | | |

| Table A2-2.5: Ridge Zone West Sample Catalogue | | | | | | | |
|---|---------|--------------|---------|----------------------|----|-----|-----|
| DDH | SAMPLE | DEPTH (m) | Code | Comments | HS | PTS | EMP |
| LX14-626 | MF19801 | 175.5 | ADVC | dacite clasts | | Y | |
| LX14-626 | MF19806 | 251.5 | AXVC | py+ser+spsg | Y | Y | |
| LX14-626 | MF19808 | 264.0 | CHTF | grey-black chert | Y | Y | |
| LX14-626 | MF19810 | 268.2 | RHTF | cpds+pyds | Y | Y | |
| LX14-626 | MF19811 | 268.5 | SPSG-SM | altered clasts | Y | Y | |
| LX14-626 | MF19812 | 269.0 | SPSM | altered clasts; cpsg | Y | Y | |
| LX14-626 | MF19813 | 271.0 | RHTF | FW to RZW | Y | Y | |
| LX14-626 | MF19815 | 282.8 | CHTF | black siltstone | Y | Y | |
| LX14-626 | MF19817 | 294.5 | RHVC | pyds | Y | Y | |
| LX14-626 | MF19820 | 342.8 | AXVC | py-spsg; ax=se-qt | Y | Y | |
| LX14-626 | MF19822 | 372.7 | ADFL | co3 altered? | Y | Y | |
| LX14-626 | MF19825 | 425.0 | ADFL | | Y | Y | |
| LX14-627 | MF19829 | 185.7 | ADBX | altered clasts | Y | Y | |
| LX14-627 | MF19831 | 235.3 | ADMS | | Y | Y | |
| LX14-627 | MF19834 | 314.0 | SSSG | qt-se-pyds-spsg | Y | Y | |
| LX14-627 | MF19835 | 318.5 | AXVC | spsg;pyds | Y | Y | |
| LX14-627 | MF19836 | 320.6 | AXVC | | Y | Y | |
| LX14-627 | MF19837 | 324.0 | AXVC | pyds+cpds+spsg | Y | Y | |
| LX14-627 | MF19838 | 327.0 | PYMS | 5% cpds | Y | Y | |
| LX14-627 | MF19839 | 330.2 | AXVC | spsg | Y | Y | |
| LX14-627 | MF19840 | 336.7 | RHTF | spsg; ax=si | Y | Y | |
| LX14-627 | MF19845 | 370.0 | RHTF | spsg; ax=si | Y | Y | |
| LX14-627 | MF19853 | 456.0 | ADTF | | Y | Y | |
| LX14-628 | MF19854 | 277.5 | SPSG | ax=qt-se | Y | Y | |
| LX14-628 | MF19856 | 292.0 | SPSG | cpsg+pyds | Y | Y | |
| LX14-628 | MF19857 | 292.1 | SPSG | cpsg+pyds | Y | Y | |
| LX14-628 | MF19858 | 293.5 | RHTF | | Y | Y | |
| LX14-628 | MF19860 | 301.1 | CHTF | spsg | Y | Y | |
| LX14-628 | MF19865 | 317.6 | CHTF | 5% spsg | Y | Y | |
| LX14-628 | MF19867 | 328.9 | CHTF | sp-py-cpsg | Y | Y | |
| LX14-628 | MF19868 | 346.3 | AXVC | py-sp-cpsg; ax=qt-se | Y | Y | |
| LX14-628 | MF19871 | 382.5 | RHTF | py-sp-cpsg; ax=qt-se | Y | Y | |
| LX14-628 | MF19872 | 522.7 | INIV | diorite | Y | Y | |
| Abbreviations: Code - see Table A2-1 Legend; Comments - see Table A2-1 Legend; HS - hand sample; PTS - polished thin section; EMP - electron microprobe | | | | | | | |

| DDH | Sample | Depth (m) | Code | Comments | HS | PTS | EMP |
|-----------------------|---------|---|------|--|----|-----|-----|
| LX10-2060 | MF18895 | 595.2 | ADMS | tr m.g. pyds; 1% qcv; wk bx | Y | | |
| LX10-2060 | MF18896 | 580.5 | ADBX | fresh; autobx or flow-top; tr pyds+CO3 | Y | | |
| LX10-2060 | MF18897 | 562.6 | ADBX | silica altd matrix+frags; tr CO3 | Y | | |
| LX10-2060 | MF18898 | 554.4 | AXMS | bleached coherent unit | Y | | |
| LX10-2060 | MF18899 | 542.1 | AXBX | peperite? | Y | | |
| LX10-2060 | MF18900 | 534.5 | AXMS | yllw grey bleaching; 1-2% pyds | Y | | |
| LX10-2060 | MF18901 | 519.0 | AXVC | qt+ser altd polymt bx | Y | | |
| LX10-2060 | MF18902 | 503.0 | AXVC | qt+ser altd polymt bx | Y | | |
| LX10-2060 | MF18903 | 487.7 | AXVC | qt+ser altd polymt bx | Y | | |
| LX10-2060 | MF18904 | 472.5 | AXVC | white altd cobble+70% qt+ser altd matr | Y | | |
| LX10-2060 | MF18905 | 464.0 | AXVC | fw axvc; qt+ser altd | Y | | |
| LX10-2060 | MF18906 | 460.0 | SSSG | sph+caco3+/-cpy+/-pysg in arms | Y | Y | |
| LX10-2060 | MF18907 | 446.0 | ADBX | | Y | | |
| LX10-2060 | MF18908 | 425.7 | ADTF | mdst bedded fringe to adbx | Y | | |
| LX10-2060 | MF18909 | 423.8 | ADBX | fsp xal + mdst matr+/-py frag | Y | | |
| LX10-2060 | MF18910 | 422.8 | SSSG | sph+caco3+py+cpy vein/frag; rx zone | Y | | |
| LX10-2060 | MF18911 | 415.0 | ADBX | qt+epi+/-py altd matr | Y | | |
| LX10-2060 | MF18912 | 400.0 | ADBX | strong qt+carb+epi altd matr | Y | | |
| LX10-2060 | MF18913 | 385.0 | ADBX | fsp phryic; qt+carb+epi altd matr | Y | | |
| LX10-2060 | MF18914 | 373.0 | ADBX | amph phryic; qt+carb+epi altd matr; 2% qcv | Y | | |
| LX10-2060 | MF18915 | 360.0 | ADMS | amph phryic | Y | | |
| LX10-2060 | MF18916 | 350.0 | ADMS | wk epi patches | Y | | |
| LX10-2060 | MF18917 | 335.0 | ADMS | 1% qcv's; 5% wk epi patches | Y | | |
| LX10-2060 | MF18918 | 320.0 | ADMS | 1-2% qcev's | Y | | |
| LX10-2060 | MF18919 | 310.5 | MFBX | mafic+qt xal tuff bx (silicd) | Y | | |
| LX10-2060 | MF18920 | 305.5 | MFBX | blocky peperite+/-globular(?) | Y | | |
| LX10-2060 | MF18921 | 303.6 | MFBX | qt xal tuff matrix; adbx ct | Y | | |
| LX10-2060 | MF18922 | 301.5 | RGTL | silic'd qt xal tuff; qt+ser+py+qt xal partings | Y | | |
| LX10-2060 | MF18923 | 285.0 | A4V2 | ad+rhyodac+mdst frag; mass flow? | Y | | |
| LX10-2060 | MF18924 | 166.5 | AHTL | polymt vitric lapilli tuff | Y | | |
| LX10-2060 | MF18925 | 147.0 | ACVC | pebbly granulest; tr-2% qcev's | Y | | |
| LX10-2060 | MF18926 | 135.0 | MFMS | ms- polymt bx; tr q+caco3+ep veins | Y | | |
| LX10-2060 | MF18927 | 120.0 | MFMS | | Y | | |
| Abbreviations: | | Code - see Table A2-1 Legend; Comments - see Table A2-1 Legend; HS - hand sample; PTS - polished thin section; EMP - electron microprobe | | | | | |

APPENDIX 3: Electron microprobe analytical conditions and detection limits

Pyrite, chalcopyrite, sphalerite, galena, tennantite-tetrahedrite, barite, and muscovite were analysed by the Cameca SX-50 electron microprobe at the Central Science Laboratory, University of Tasmania. Assistance was by Dr. David Steele of the University of Tasmania.

Table A3-1 lists the analytical conditions. Results and detection limits are included in the main body of the thesis.

| Table A3-1: Microprobe analytical conditions for Ridge Zone West sulphides and sulphosalts | | | | | | | | | |
|--|----------------------|----------------------|--------------|----------|---------|-----------------|------------------|--------------------|--------------------|
| Instrument: Cameca SX50 electronmicroprobe | | | | | | | | | |
| Location: CSL, University of Tasmania | | | | | | | | | |
| Analyses by: Albert Chong, Dr. David Steele | | | | | | | | | |
| File | Beam Current (nA) | Acc. Voltage (kV) | Element line | Standard | Crystal | Pk time secs | Bgd time secs | 95% dl (el wt%) | abs dl (el wt%) |
| chalcopyrite | 50.1 | 20.08 | S Ka | AMARC | PET | 10 | 2*5 | 0.063 | 0.040 |
| | | | Mn Ka | MN | LiF | 40 | 2*20 | 0.027 | 0.018 |
| | | | Fe Ka | AMARC | LiF | 10 | 2*5 | 0.06 | 0.039 |
| | | | Ni Ka | APENT | LiF | 40 | 2*20 | 0.036 | 0.024 |
| | | | Cu Ka | ACUP | LiF | 10 | 2*5 | 0.084 | 0.055 |
| | | | Zn Ka | ASPH | LiF | 10 | 2*5 | 0.13 | 0.08 |
| | | | As La | AGAAS | TAP | 90 | 90 | 0.053 | 0.035 |
| | | | Se La | ABISE | TAP | 60 | 2*30 | 0.057 | 0.038 |
| galena | 50.1 | 20.08 | S Ka | AMARC | PET | 10 | 2*5 | 0.11 | 0.07 |
| | | | Fe Ka | AMARC | LiF | 10 | 2*5 | 0.084 | 0.056 |
| | | | Se La | ABISE | TAP | 60 | 2*30 | 0.047 | 0.032 |
| | | | Ag La | AGAAS | PET | 40 | 2*20 | 0.082 | 0.054 |
| | | | Pb Ma | AGAL | PET | 10 | 2*5 | 0.29 | 0.19 |
| pyrite | 50.1 | 20.08 | S Ka | AMARC | PET | 10 | 2*5 | 0.063 | 0.040 |
| | | | Mn Ka | MN | LiF | 40 | 2*20 | 0.027 | 0.018 |
| | | | Fe Ka | AMARC | LiF | 10 | 2*5 | 0.071 | 0.046 |
| | | | Ni Ka | APENT | LiF | 40 | 2*20 | 0.036 | 0.024 |
| | | | Cu Ka | ACUP | LiF | 10 | 2*5 | 0.084 | 0.055 |
| | | | Zn Ka | ASPH | LiF | 10 | 2*5 | 0.10 | 0.07 |
| | | | As La | AGAAS | TAP | 90 | 90 | 0.053 | 0.035 |
| | | | Se La | ABISE | TAP | 60 | 2*30 | 0.057 | 0.038 |
| sphalerite | 50.1 | 20.08 | S Ka | AMARC | PET | 10 | 2*5 | 0.061 | 0.039 |
| | | | Mn Ka | MN | LiF | 40 | 2*20 | 0.028 | 0.018 |
| | | | Fe Ka | AMARC | LiF | 40 | 2*20 | 0.029 | 0.019 |
| | | | Cu Ka | ACUP | LiF | 10 | 2*5 | 0.084 | 0.055 |
| | | | Zn Ka | ASPH | LiF | 10 | 2*5 | 0.13 | 0.09 |
| | | | Se La | ABISE | TAP | 60 | 2*30 | 0.057 | 0.038 |
| | | | Cd La | CD | PET | 60 | 2*30 | 0.070 | 0.046 |
| | | | Pb Ma | AGAL | PET | 10 | 2*5 | 0.29 | 0.18 |
| tetrahedrite-tenn | 50.1 | 20.08 | S Ka | AMARC | PET | 10 | 2*5 | 0.12 | 0.08 |
| | | | Fe Ka | AMARC | LiF | 40 | 2*20 | 0.028 | 0.019 |
| | | | Ni Ka | APENT | LiF | 40 | 2*20 | 0.035 | 0.023 |
| | | | Cu Ka | ACUP | LiF | 10 | 2*5 | 0.10 | 0.06 |
| | | | Zn Ka | ASPH | LiF | 10 | 2*5 | 0.11 | 0.08 |
| | | | As La | AGAAS | TAP | 10 | 10 | 0.20 | 0.16 |
| | | | Se La | ABISE | TAP | 60 | 2*30 | 0.063 | 0.042 |
| | | | Ag La | AGAAS | PET | 40 | 2*20 | 0.082 | 0.054 |
| | | | Sb La | ASTIB | PET | 30 | 2*15 | 0.072 | 0.048 |

APPENDIX 4: Assay data conditions, block model parameters, and results

A total of 644 samples from 66 drill holes have been analysed for Cu, Pb, Zn, Fe, +/- Au, +/- Ag, +/- Ba. A subset of 258 samples were submitted for Au, Ag, Cu, Pb, Zn, Ba, and Fe analyses by the author with assistance from Alison Hartley. The geological block model and statistics for the Ridge Zone West is based on a total 232 samples.

Appendix 4-1: Assay laboratory methods at Myra Falls.

Appendix 4-2: Assay laboratory quality control program at Myra Falls.

Appendix 4-3: Myra Falls block model parameters.

Appendix 4-4: Assay data results. Not included due to confidentiality.

Available upon request to:

N.V.I. Mining Ltd.,
Geology Department,
Myra Falls Operations,
P.O. Box 8000,
Campbell River, B.C.
Canada
V9W-5E2
1 (250) 287-9271 Extension 312

A4-1 Assay Laboratory Methods at Myra Falls (from Chong and Bakker, 2004)

The following is a brief summary of the methods, standards and checks the lab currently uses.

1. % Cu, Pb, Zn, Fe, Cd.

Samples are digested with hydrochloric/nitric acid combination and read on the atomic absorption spectrophotometer (A.A.) using certified Canmet pulp standards Mp-1a, CCu-1a, CZn-1, and CZn-3.

2. High Zn

Battle-Gap/H-W core >23 % Zn and Zn concentrate samples are titrated with potassium ferrocyanide using CZn-3 as a pulp standard and CZn-1 pulp as a check sample.

3. Au/Ag (g/t)

Samples assayed for gold and silver are run by fire assay using 1/2 assay ton weights (15 g).

4. % As.

Arsenic is determined by digesting the sample with a nitric/sulfuric acid combination then run on the MHS-10 system using the sodium borohydride method. Mp-1a is used as a pulp standard and a pulp sample assayed by S.G.S. Laboratories is used as a check.

5. % Sb.

Antimony is digested with nitric and sulfuric acids and run on the A.A. using a pulp sample assayed by S.G.S. Laboratories as a standard.

6. Au/Ag in Gold Concentrate.

Samples high in metallic gold (ie. Knelson concentrate) are first screened through 100 mesh and then fire assayed. A weighed average of the coarse and fine portions is reported.

7. High Cu.

High copper samples (Cu concentrate, metallurgical float tests) are titrated using the sodium thiosulfate - iodide method. CCu-1a pulp and pure Cu metal are used as standards.

8. Sample Preparation

Sample preparation is accomplished by a drying, jaw crushing, cone crushing, riffle splitting, ring pulverizing and homogenizing. Samples that are >97 % passing (100 mesh) are then analyzed.

9. Barium

Battle-Gap core samples that are greater or equal to 3.0 % Zn, all exploration core and those specifically marked by the Geology department are assayed for barium. The assay consists of a lithium metaborate – potassium carbonate fusion with an atomic absorption finish utilizing a nitrous oxide acetylene flame. Standards consist of pulp samples from the mine that have been assayed by the Kamloops Research and Assay Laboratory Ltd.

A4-2 Assay Lab Quality Control Program

(from Chong and Bakker, 2004)

Introduction

The Assay Lab quality control program consists of quarterly; provisional shipment and spot check sample assay comparisons with outside certified labs. Certified standards, control samples and special laboratory techniques are also used to maintain the quality control program.

Quarterly Samples

Copper and zinc quarterly composite samples are assayed by all assayers. The results are tabulated and compared to the outside lab assays (S.G.S). An average of differences for each assayer and the lab as a whole is calculated and is used to track accuracy and precision. The standard deviation for the assay lab has been calculated as well. The quarterly samples are integrated with the assayer's normal work routine.

Spot check samples

On occasion, samples assayed by our lab are sent to certified outside laboratories. A comparison between our lab and two independent outside labs is made. The Geology and Metallurgy departments usually make this request.

Laboratory techniques

Canmet certified pulp standards are used for the determination of % Cu, Pb, Zn, Fe, and As. Samples previously analyzed by a certified lab are used for the determination of % Cd, Sb. All pulp standards are prepared in duplicate and are crosschecked with the standards in use prior to introduction. Determination of high % Zn by titration and % As by MHS-10 method include control samples. The determination of % Cu by titration includes the use of two certified standards, which are compared and averaged. As a cross check, the % Cu (titration) value is compared to the % Cu determined by atomic absorption.

A4-3 Myra Falls Block Model Parameters

Compass/Minesight is a commercial 3-D Block Modeling program available from Mintec Inc. which is based out of Tucson Arizona USA, with branch offices in Canada, Peru, Chile, South Africa and affiliates in Australia. Compass has been used in various stages at MFO since 1988 and has been verified by a number of in-house tests as well as through outside consultants such as MRDI, CESL Engineering, Noranda, Wrigglesworth and Assoc., Winters Group, Derry, Michener, Booth and Wahl.

Compass employs a search ellipse of 25 metres N and S, 50 metres E and W, and 15 metres vertically up and down. This search ellipse is not varied to accommodate different structural controls of the various ore bodies. Inverse cubed is the weighting factor for drill holes. Kriging is not used. Compass honors the geological lens code and does not expand the model beyond those determined by the geologist. It also will not use material from one lens code to calculate grades for another, unless specifically requested to do so.

The Block Model is based on a 5m x 5m x 4m (vertical) block size. Each block contains the calculated metal value for that block, density, percentage of the block that is ore, percentage that has been mined out and the percentage that has been “removed” from reserves. It also contains the “r-type”, or reserve type (e.g. proven, probable etc.), classification of the ore. In cases where two lenses overlap, it carries the values of the material, which is in majority.

Compass calculates reserves based on proximity to the nearest diamond drill hole. Measured (proven) is material within 15 m, probable (indicated) is material between 15 and 30 m, possible (inferred) is material between 30 and 50 m and potential is material greater than 50 m from the nearest drill hole. These results are then tabulated by lens, zone or area. These categories are then often downgraded to more closely reflect the various resource categories as outlined in MFO standards that are based on National Policy 2A and the new TSE standards. Areas that do not have access or are not currently being mined are downgraded to the indicated-probable category. Depending on the degree of confidence in the area, indicated-probable resources may then also be downgraded to the inferred category and so on.

A4-4 Assay Results

Available upon request to:

Geology Department,
Myra Falls Operations,
N.V.I. Mining Ltd.,
P.O. Box 8000,
Campbell River, B.C.
V9W-5E2
1 (250) 287-9271